CONTROL OF MOLECULAR GEOMETRIES USING NEW PHOTO-ELECTRO-SWITCHABLE AZOBENZENES

by

CARL JACKY SAINT-LOUIS

SILAS C. BLACKSTOCK, COMMITTEE CHAIR

MICHAEL P. JENNINGS
PATRICK R. LECLAIR
KEVIN H. SHAUGHNESSY
TIMOTHY S. SNOWDEN

A DISSERTATION

Submitted in partial fulfillment of the requirements
for the degree of Doctor of Philosophy
in the Department of Chemistry
in the Graduate School of
The University of Alabama

TUSCALOOSA, ALABAMA

2015

Copyright Carl Jacky Saint-Louis 2015
ALL RIGHTS RESERVED

ABSTRACT

There has been a recent growing interest in azobenzene derivatives because of their ability to isomerize when visible light is absorbed. This unique property allows azobenzenes to undergo reversible conformation change between the *trans* and *cis* forms upon absorbing light and slowly thermally relaxing from the *cis* to the *trans* form.

By adding a redox-active (RA) group to the azobenzene skeleton, we have developed a series of new redox appended azo switches capable of efficient photo "folding" and catalytic electron transfer mediated "opening" on exposure to an oxidant or a small amount of voltage as an electrical trigger.

We utilized an aryl amino group as our redox auxiliary moiety because of its excellent redox properties- it is chemically stable in both neutral and radical cation forms. The basic premise of our work is that the cationic state of the RA-azo will be much more reactive toward azo isomerization (*cis*-to-*trans*) than its neutral form. Thus, upon one electron removal from the *cis*-RA-azo to make *cis*-$RA^{\bullet+}$-azo, the azo group will immediately unfold. How well the redox activation of azo unfolding works may depend on where the RA group is located. Thus, we have prepared RA-azo substrates with the RA group linked at the *para* and *meta* positions of the azobenzene ring to test their relative abilities to support redox activation of azo unfolding.

Because the oxidized radical cation state of the RA group ($RA^{\bullet+}$) is so chemically stable, it should be able to exchange an electron with other neutral *cis*-RA-azo molecules thereby generating a catalytic cycle for azo unfolding. Based on this study, we hypothesized a new photo-electro isomerization catalysis mechanism that accounts for the fast relaxation from

"folded" *cis* to "open" *trans*.

To date, we have successfully synthesized six different RA-azo in which the placement of the RA moiety is varied on the azobenzene ring and we observed that redox activation of the RA-azo unfolding process works catalytically with rate increases relative to thermal azobenzene unfolding of $\geq 10^5$ and turnover numbers in the 100-1000 range.

LIST OF ABBREVIATIONS AND SYMBOLS

AA	arylamino
AB	azobenzene
aAB	amino azobenzene
anhyd	anhydrous
BINAP	2,2’-bis(diphenylphosphino)-1,1’-binaphthyl
br	broad (spectral)
°C	degree Celsius
calc	calculated
cm	centimeter(s)
conc	concentrated
CV	cyclic voltammetry
Δ	heat
δ	chemical shift
d	doublet (spectral)
DCM	dichloromethane
dd	doublet of doublets (spectral)
DI	deionized
DMSO-*d*6	deuterated dimethylsulfoxide
E°′	formal oxidation potential

g	gram(s)
h	hour(s)
HOMO	highest occupied molecular orbital
HRMS	high resolution mass spectroscopy
Hz	Hertz
I	electrical current
J	coupling constant (NMR)
LUMO	lowest unoccupied molecular orbital
LED	light-emitting diode
m	multiplet (spectral)
mg	milligram(s)
MHz	megahertz
min	minute(s)
mL	milliliter(s)
mmol	millimole(s)
mp	melting point
mV	millivolt(s)
μA	microamperes
nm	nanometer(s)
NMR	nuclear magnetic resonance
ORTEP	Oak Ridge Thermal Ellipsoid Plot
$Pd(dba)_2$	bis-(dibenzylideneacetone)palladium(0)
$Pd_2(dba)_3$	Tris-(dibenzylideneacetone)dipalladium(0)

Ph	phenyl
ppm	part(s) per million
RA	Redox Auxiliary
rb	round bottom
rt	room temperature
s	second(s); singlet (spectral)
SCE	saturated calomel electrode
$TBABF_4$	*n*-tetrabutylammonium tetrafluoroborate
TLC	thin-layer chromatography
TMS	tetramethylsilane
V	volt(s)

ACKNOWLEDGMENTS

Nelson Mandela once said, “Difficulties break some men but make others. No axe is sharp enough to cut the soul of a sinner who keeps on trying, one armed with the hope that he will rise even in the end.”

Perseverance is key to making it though this journey, however I could not complete this journey on my own. This great achievement would not be possible without the help and blessings of my creator, God.

I would like to give great thanks to my advisor, Professor Silas Blackstock, for believing in me and giving me a chance to grow into the scientist that I am today. I am thankful for his guidance, and his ability to encourage me to accomplish my goals.

I would like to thank my parents, Claude Jacky Saint-Louis and Anne Remonde Beaugé, for all their hard work and all their sacrifices. My full gratitude goes to my mother and my role model. She is the hardest working woman I have ever known and I owe my life to her as she dedicated her life to raise me. I would like to thank my best friend, Takenya Moore, for her words of encouragement.

Frequently people ask me if I had the chance to do it all over, would I take the same route? I would like to end with this quote from Nelson Mandela to answer this question. “If I had my time over I would do the same again. So would any man who dares call himself a man.”

CONTENTS

ABSTRACT ii

LIST OF ABBREVIATIONS AND SYMBOLS iv

ACKNOWLEDGMENTS vii

LIST OF TABLES xi

LIST OF FIGURES xii

LIST OF SCHEMES xix

COMPOUND STRUCTURE LEGEND xx

CHAPTER 1 - GENERAL OVERVIEW OF DIFFERENT CLASSES OF AZOBENZENES 1

1.1 Introduction 1

1.2 Electronic Structure of Azobenzene 2

1.3 Absorption Spectroscopy of Azobenzene 4

1.4 Photochemistry of Azobenzene 6

1.5 Thermal Isomerization of Azobenzene 7

1.6 Categories of Azo Aromatic Compounds 10

1.7 Applications of Azo Compounds 16

CHAPTER 2 - MONO(AMINO)AZOBENZENES AS PHOTO-ELECTRO SWITCHES 21

2.1 Introduction 21

2.2 *para*- arylaminoazobenzenes: *p*AA-Ph-N=N-Ph **4a** and *p*AA-Ph-N=N-An **5a** 22

2.2.1 Photochemistry and Optical Absorption of **4a** and **5a** 24

2.2.2 Thermal *cis*-to-*trans* isomerization of **4a** and **5a** 33

2.2.3 Electron Transfer Catalysis of *cis*-to-*trans* isomerization 46

2.2.4 Thin Cell Photo-Electro Device (PED 55

2.2.5 Conclusions 58

2.3 *meta-arylaminoazobenzene: m*AA-Ph-N=N-An **19a** 61

2.3.1 Photochemistry and Optical Absorption of **19a** 62

2.3.2 Thermal *cis*-to-*trans* isomerization of **19a** 68

2.3.3 Electron Transfer Catalysis of *cis*-to-*trans* isomerization 75

2.3.4 Conclusions 80

2.4 Synthesis experimental details for chapter 2 83

CHAPTER 3 - BIS(AMINO)AZOBENZENES AS PHOTO-ELECTRO SWITCHES 96

3.1 Introduction 96

3.2 *bis*(arylamino)azobenzenes: *p*AA-Ph-N_2-Ph-*p*AA **27a** and *p*AA-Ph-N_2-Ph- *m*AA **28a** 97

3.2.1 Photochemistry and Optical Absorption of **27a** and **28a** 100

3.2.2 Thermal *cis*-to-*trans* isomerization of **27a** and **28a** 111

3.2.3 Electron Transfer Catalysis of *cis*-to-*trans* isomerization 121

3.2.4 Conclusions 129

3.3 Synthesis experimental details for chapter 3 133

CHAPTER 4 - BIS(AZOBENZENE) DERIVATIVE AS PHOTO-ELECTRO SWITCH 137

4.1 Introduction.....137

4.1.1 Photochemistry and Optical Absorption of **33a**.....140

4.1.2 Thermal *cis*-to-*trans* isomerization of **33a** 143

4.1.3 Electron Transfer Catalysis of *cis*-to-*trans* isomerization 145

4.1.4 Conclusions.....149

4.2 Synthesis experimental details for chapter 4 150

CHAPTER 5 - TRIS(AZOBENZENE) DERIVATIVE AS PHOTO-ELECTRO SWITCH.....154

5.1 Introduction.....154

5.2 Synthesis experimental details for chapter 5 154

REFERENCES 158

APPENDIX A – NMR Spectra.....165

APPENDIX B – Crystallographic Data For **4a** 211

APPENDIX C – Crystallographic Data For **5a** 219

APPENDIX D – Crystallographic Data For **19a** 225

APPENDIX E – Crystallographic Data For **18a**.....233

APPENDIX F – Crystallographic Data For **27a**.....240

APPENDIX G – Crystallographic Data For **37** 251

LIST OF TABLES

1.1 Differences in Categories of Substituted-AB 13

2.2.1 Isomrizaion properties of *p*AA-Ph-N=N-Ph **4a** and *p*AA-Ph-N=N-An **5a**. 59

2.2.2 Experimental Details for the Crystal Structures of *p*AA-Ph-N=N-Ph **4a** and *p*AA-Ph-N=N-An **5a**. 60

2.3.1 Comparison of the physical properties of *p*AA-Ph-N=N-Ph **4a**, *p*AA-Ph-N=N-An **5a** and *m*AA-Ph-N=N-An **19a**.....81

2.3.2 Experimental Details for the Crystal Structure of *m*AA-Ph-N=N-Ph **18a** and *m*AA-Ph-N=N-An **19a**.....82

3.2.1 Comparisons of the physical properties between *p*AA-Ph-N=N-Ph **4a**, *p*AA-Ph-N=N-Ph-*p*AA **27a**, *m*AA-Ph-N=N-An **19a** and *p*AA-Ph-N=N-Ph-*m*AA **28a**.....131

3.2.2 Experimental Details for the Crystal Structures of *p*AA-Ph-N=N-Ph-pAA **27a**.....132

LIST OF FIGURES

1.1. Isomeric configurations of azobenzene. 1

1.2. Molecular orbital energy diagram for the azobenzene system 3

1.3. Schematic illustration of the energy state diagram for photoisomerization of azobenzene 4

1.4. Absorption spectra of *cis* and *trans*- azobenzene in an ethanol solution.....5

1.5. Potential energy diagram showing of *trans* and *cis*- azobenzene 8

1.6. Potential energy diagrams of stilbene and azobenzene 9

1.7. Absorption spectra of *trans*- azobenzene (red line), 4-aminoazobenzene (green line) and 4-nitro-4′-aminoazobenzene (blue line) in ethanol.....12

1.8. Visible absorption Spectra of dimethyl-aminoazobenzene in different solvents..... 15

1.9. Rate Enhancement (*ca.* 10^5) of the thermal isomerization of 4-(dimethylamino)-4′-nitroazobenzene on changing the solvent from n-hexane to formamide. 16

1.10. Molecular scissors based on azobenzene. 18

1.11. Photo control of the structure of the α-helix in the polypeptide azo derivative..... 19

1.12. Representation of the photo control of a K^+ channel membrane 20

2.1.1 Model of the mono-aAB photo-electro switch. The *trans*- isomer (blue) isomerizes to the *cis*- isomer (red) by photo-absorption, and the *cis*- isomer (red) then rapidly isomerizes to the *trans*- isomer (blue) upon removal of an electron 22

2.2.1. Optical spectrum of **4a** (6.35×10^{-4} M in C_6D_6) irradiated with a 430 nm LED at room temperature in 0.1 cm quartz UV-Vis cell.....25

2.2.2. Optical spectrum of **5a** (6.37×10^{-4} M in C_6D_6) irradiated with a 430 nm LED at room temperature in 0.1 cm quartz UV-Vis cell. 26

2.2.3. Absorption intensity monitored at 438 nm and shows the establishment of a PSS for **4a** (6.35×10^{-4} M in deaerated C_6D_6) using 0.1 cm quartz UV-Vis cell at room temperature. 27

2.2.4. Absorption intensity monitored at 436 nm and shows the establishment of a PSS for **5a** (6.37×10^{-4} M in deaerated C_6D_6) using 0.1 cm quartz UV-Vis cell at room temperature. 28

2.2.5. Full ^{1}H NMR spectrum of completely **4a** (1.67×10^{-2} M in C_6D_6) before irradiation. 29

2.2.6. Full ^{1}H NMR spectrum of completely **5a** (1.63×10^{-2} M in C_6D_6) before irradiation 30

2.2.7. Expanded view of the aromatic section in the ^{1}H NMR spectrum of **4a** (1.67×10^{-2} M in C_6D_6). **a**) Spectrum before irradiation **b**) PSS spectrum after irradiation with 430 nm LED light. PSS is established at a 29:71 **4a**:**4b** ratio at room temperature.....31

2.2.8. Expanded view of the aromatic section in the ^{1}H NMR spectrum of **5a** (1.63×10^{-2} M in C_6D_6). **a**) Spectrum before irradiation **b**) PSS spectrum after irradiation with 430 nm LED light. PSS is established at a 32:68 **5a**:**5b** ratio at room temperature.....31

2.2.9. Expanded view of the alkyl section in the ^{1}H NMR spectrum of **4a** (1.67×10^{-2} M in C_6D_6) **a**) Spectrum before irradiation **b**) PSS spectrum after irradiation with 430 nm LED light. A PSS is established at a 29:71 **4a**:**4b** ratio at room temperature.....32

2.2.10. Expanded view of the alkyl section in the ^{1}H NMR spectrum of **5a** (1.63×10^{-2} M in C_6D_6) **a**) Spectrum before irradiation **b**) PSS spectrum after irradiation with 430 nm LED light. A PSS is established at a 32:68 **5a**:**5b** ratio at room temperature.....33

2.2.11. Optical spectrum of the thermal isomerization of **4b** to **4a** (6.35×10^{-4} M in C_6D_6) recorded every 30 minutes in the dark at room temperature in a 0.1 cm quartz cell after irradiating with a 430 nm LED to PSS (71:29 **4b:4a** ratio).....34

2.2.12. Optical spectrum of the thermal isomerization of **5b** to **5a** (6.37×10^{-4} M in C_6D_6) recorded every 10 minutes in the dark at room temperature in a 0.1 cm quartz cell after irradiating with a 430 nm LED to a PSS (68:32 **5b:5a** ratio).....35

2.2.13. Determination of the thermal isomerization rate of **4b** to **4a** over 24 hour using a plot of ln[C] vs. Time where C is the ratio of *cis*- to *trans*-.....36

2.2.14. Determination of the thermal isomerization rate of **5b** to **5a** over a 12-hour timeframe using plot of ln[C] vs. Time where C is the ratio of *cis*- to *trans*-.....37

2.2.15. A potential energy diagram of **1** (left) and **4** (right) that illustrates the effects of **3** on the $\Delta G^{\neq}$ of **4b** to **4a.** 38

2.2.16. Crystal structure of triphenylamine illustrating a three-bladed propeller structure 39

2.2.17. Crystal structure of **4a** illustrating loss of propeller-shaped geometry 40

2.2.18. Cap and stick diagram of the crystal structure of **4a**. 41

2.2.19. Figure showing planarity of the AB in 4a 42

2.2.20. Potential energy diagram of 4 and 5 43

2.2.21. Crystal structure of 5a illustrating loss of the propeller-shaped structure 44

2.2.22. Cap and stick diagram of the crystal structure of **5a** 45

2.2.23. The planarity of the azobenzene core helps stabilize **5a** 46

2.2.24. Cyclic voltammogram of **4a** 47

2.2.25. Cyclic voltammogram of **5a** 48

2.2.26. Cyclic voltammogram of **6** 49

2.2.27. B3LYP/6-31G** molecular orbital calculations of **4b** 50

2.2.28. B3LYP/6-31G** molecular orbital calculations of **5b** 51

2.2.29. Optical spectrum of **4a** (6.35×10^{-4} M in C_6D_6) irradiated with a 430 nm LED and CRET injection 52

2.2.30. Optical spectrum of **5a** (6.37×10^{-4} M in C_6D_6) irradiated with a 430 nm LED and CRET injection 53

2.2.31. Mechanism of the *cis* to *trans* electro isomerization 55

2.2.32. Photo-electro cell device 56

2.2.33. Tracking the absorbance at maximum (436 nm) of **4a** through multiple isomerization cycles reveals no signs of degradation 57

2.2.34. Expanded view of the changes in maximum absorbance intensity peak for **4** through multiple isomerization cycles 57

2.3.1 Model of the mono *meta*-d-AB photo-electro switch 61

2.3.2. Optical spectrum of **19a** 63

2.3.3 Absorption intensity was monitored at 344 nm and shows the establishment of a PSS for **19a** (6.55×10^{-4} M in deaerated C_6D_6) using 0.1 cm quartz UV-Vis cell at room temperature 64

2.3.4. Full ^{1}H NMR spectrum of **19a** (1.67×10^{-2} M in C_6D_6) before irradiation 65

2.3.5. Full ^{1}H NMR of **19** (1.67×10^{-2} M) *m*AA-Ph-N=N-An in C_6D_6 irradiated with 365 nm light. A PSS with an 80:20 ratio of **19b**:**19a** at room temperature 66

2.3.6 Expanded view of the aromatic section in the ^{1}H NMR spectrum of **19a** (1.67×10^{-2} M in C_6D_6) **a**) Spectrum before irradiation **b**) PSS after irradiation with 365 nm light. PSS is established at a 20:80 **19a**:**19b** ratio at room temperature. Blue arrows indicate **19a** and red arrows indicate **19b**. 67

2.3.7. Expanded view of the alkyl section of the ^{1}H NMR spectrum of **19** (1.67×10^{-2} M in C_6D_6) **a**) Before irradiation **b**) PSS after irradiation with 365 nm light. A PSS is established at a 20:80 **19a**:**19b** ratio at room temperature. Blue arrows indicate **19a** and red arrows indicate **19b**... 68

2.3.8. Optical spectrum of the thermal isomerization of **19b** to **19a** (6.55×10^{-4} M in C_6D_6) recorded every 60 minutes in the dark at room temperature in a 0.1 cm quartz cell after irradiating with 365 nm light to a PSS (80:20 **19b**:**19a** ratio 69

2.3.9. Optical spectrum of the thermal isomerization of **19b** showing the max absorbance at 344 nm. 70

2.3.10. ln[C] vs. Time plot to determine the rate at which **19b** thermally converts to **19a** over 250 hours 71

2.3.11. Potential energy diagram of azobenzene and **19a** 72

2.3.12. Crystal structure of **19a** 73

2.3.13. Spatial arrangement of **19a** in the *cis*- and *trans*- form 74

2.3.14. B3LYP/6-31G** molecular orbital calculations of **19a** 75

2.3.15. Cyclic voltammogram of **19a** 76

2.3.16. B3LYP/6-31G** molecular orbital calculations of **19b**. 77

2.3.17. Optical spectrum of **19a** (6.19×10^{-4} M in C_6D_6) irradiated with 365 nm light and CRET injection 78

3.1.1 Model of the bis(amino)azobenzene photo-electro switch 97
3.2.1. Optical spectrum of **27a** (4.89 x 10^{-4} M in C_6D_6) irradiated with a 450 nm LED at room temperature in 0.1 cm quartz UV-Vis cell 101

3.2.2. Optical spectrum of **28a** (6.01 x 10^{-4} M in C_6D_6) irradiated with a 450 nm LED at room temperature in 0.1 cm quartz UV-Vis cell 102

3.2.3. Absorption intensity was monitored at 480 nm and shows the establishment of a PSS for **27a** (4.89 x 10^{-4} M in deaerated C_6D_6) using 0.1 cm quartz UV-Vis cell at room temperature 103

3.2.4. Absorption intensity was monitored at 446 nm and shows the establishment of a PSS for **28a** (6.01 x 10^{-4} M in deaerated C_6D_6) using 0.1 cm quartz UV-Vis cell at room temperature. 104

3.2.5. Full ^{1}H NMR spectrum of completely **27a** before irradiation 105

3.2.6. Full ^{1}H NMR spectrum of completely **28a** before irradiation 106

3.2.7. Expanded view of the aromatic section in the ^{1}H NMR spectrum of **27a** (1.17 x 10^{-2} M in C_6D_6) **a**) Spectrum before irradiation **b**) PSS spectrum after irradiation with a 450 nm LED light. The PSS is established at a 69:31 **27a**:**27b** ratio at room temperature. Blue arrows indicate **27a** and red arrows indicate **27b**. 107

3.2.8. Expanded view of the aromatic section in the ^{1}H NMR spectrum of **28a** (9.63 x 10^{-3} M in C_6D_6). **a**) Spectrum before irradiation. **b**) PSS spectrum after irradiation with 450 nm LED light. PSS is established at a 49:51 **28a**:**28b** ratio at room temperature. Blue arrows indicate **28a** and red arrows indicate **28b**.....108

3.2.9. Expanded view of the alkyl section in the ^{1}H NMR spectrum of **27a** (1.17 x 10^{-2} M in C_6D_6) **a**) Spectrum before irradiation **b**) PSS spectrum after irradiation with 450 nm LED light. A PSS is established at a 69:31 **27a**:**27b** ratio at room temperature. Blue arrows indicate **27a** and red arrows indicate **27b**.....109

3.2.10. Expanded view of the alkyl section in the ^{1}H NMR spectrum of **28a** (9.63 x 10^{-3} M in C_6D_6). **a**) Spectrum before irradiation. **b**) PSS spectrum after irradiation with 430 nm LED light. A PSS is established at a 49:51 **28a**:**28b** ratio at room temperature. Blue arrows indicate **28a** and red arrows indicate **28b**.....110

3.2.11. Optical spectrum of the thermal isomerization of **27b** to **27a** 111

3.2.12. Optical spectrum of the thermal isomerization of **28b** to **28a** (6.01 x 10^{-4} M in C_6D_6) recorded every 30 minutes in the dark at room temperature in a 0.1 cm quartz cell after irradiating with a 450 nm LED to a PSS.....112

3.2.13. Determination of the thermal isomerization rate of **27b** to **27a** over 12 hours using a plot of ln[C] vs. Time where C is the ratio of *cis*- to *trans*-.....113

3.2.14. Determination of the thermal isomerization rate of **28b** to **28a** over 27 hours using a plot of ln[C] vs. Time where C is the ratio of *cis*- to *trans*-.....114

3.2.15. A potential energy diagram of **4a** (left) and **27a** (right) that illustrates the effects of **3** on the thermal isomerization $\Delta G^{\neq}$ for isomerization from **27b** to **27a** 115

3.2.16. A potential energy diagram of **19a** (left) and **28a** (right) that illustrates the effects of **3** on the thermal isomerization $\Delta G^{\neq}$ for isomerization from **28b** to **28a** 116

3.2.17. Ellipsoid diagram of the crystal structure of **27a**. It shows twisting in both RA groups. The pi orbitals of the AB's phenyl groups are twisted out of conjugation with the lone pair of the nitrogen atoms on the RA groups and the pi orbitals of the -N=N- group .....
.....116

3.2.18. Cap and stick diagram of the crystal structure of **27a**. 118

3.2.19. Showing the extended pi system in **27b** and **27a**.....119

3.2.20. Showing the extended pi system in **28b** and **28a**.....120

3.2.21. Cyclic voltammogram of **27a** 122

3.2.22. Cyclic voltammogram of **28a** 123

3.2.23. Cyclic voltammogram of **6** 124

3.2.24. B3LYP/6-31G** molecular orbital calculations of **27b**.....125

3.2.25. B3LYP/6-31G** molecular orbital calculations of **28b**.....126

3.2.26. Optical spectrum of **27a** (4.89×10^{-4} M in C_6D_6) irradiated with a 450 nm LED and CRET injection 127

3.2.27. Optical spectrum of **27a** (6.01×10^{-4} M in C_6D_6) irradiated with a 450 nm LED and CRET injection 128

4.1.1. Model of the bis(azobenzene) photo-electro switch 138

4.1.2. Optical spectrum of **33a** (black), **4a** (red) and azoanisole (blue) 140

4.1.3. Optical spectrum of **33a**.....141

4.1.4. Optical spectrum of **33a** irradiated with 450 nm LED 142

4.1.5. Optical spectrum of **33a** irradiated with 365 nm light.....143

4.1.6. Optical spectrum of thermal isomerization of **33b** to **33a** 144

4.1.7. Optical spectrum of thermal isomerization of **33c** to **33a**.....145

4.1.8. B3LYP/6-31G** molecular orbital of **33d** 146

4.1.9. Optical spectrum of **33a** irradiated with 365 nm and 450 nm light and CRET injection 147

4.1.10. Optical spectrum of **33a** irradiated with 365 nm and 450 nm light and CRET injection at PSS with prolonged irradiation.....149

LIST OF SCHEMES

1.1. Photoisomerization of azobenzenes 6

1.2. Rotation and Inversion mechanism for *cis*-to-*trans* isomerization of azobenzene 10

2.2.1. Synthetic route to obtain *p*AA-Ph-N=N-Ph **4a** 23

2.2.2. Synthetic route to obtain *p*AA-Ph-N=N-An **5a**. 24

2.2.3. Postulated photo-electro catalysis mechanism of **4a** and **5a** 54

2.3.1. Synthetic route to obtain *m*AA-Ph-N=N-An **19a**. 62

2.3.2. Postulated photo-electro catalysis mechanism of **19a** 79

3.2.1 Synthetic route to obtain *p*AA-Ph-N=N-Ph-*p*AA **27a** 98

3.2.2. Synthetic route to obtain *p*AA-Ph-N=N-Ph-*m*AA **28a** 99

3.2.3. Postulated photo-electro catalysis mechanism of **27a** and **28a** 129

4.1.1. Synthetic route to obtain **33a** 139

4.1.2. Postulated photo-electro catalysis mechanism of **33a** 147

COMPOUND STRUCTURE LEGEND

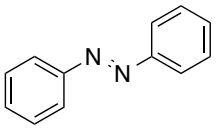

1a

***trans*-Ph-N=N-Ph**

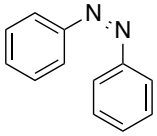

1b

***trans*-Ph-N=N-Ph**

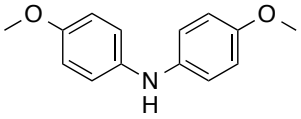

3

Redox Auxiliary

AA

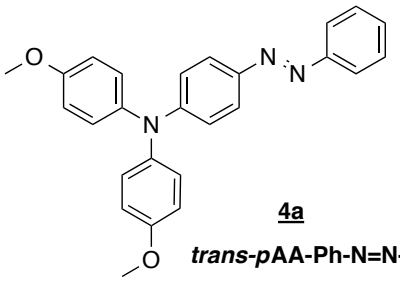

4a

***trans-p*AA-Ph-N=N-Ph**

(b) E^{o} (1) = 0.94 V (vs. SCE))

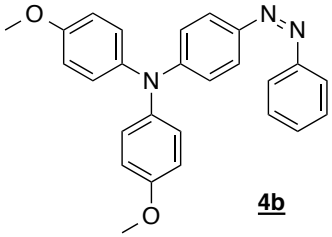

4b

***cis-p*AA-Ph-N=N-Ph**

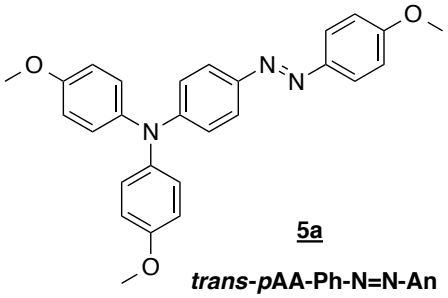

5a

***trans-p*AA-Ph-N=N-An**

(b) E^{o} (1) = 0.85 V (vs. SCE)

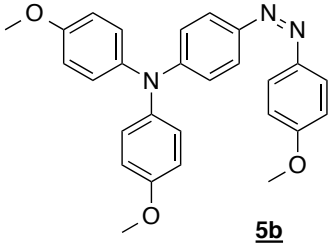

5b

***cis-p*AA-Ph-N=N-An**

(a) Previously unknown substrates are underlined.
(b) Oxidation potentials (E°) reported are in V vs. SCE at Pt electrode in 0.1 M Bu_4NBF_4/CH_2Cl_2

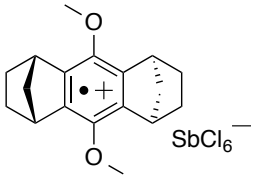

6

CRET

(b) E^o (1) = 1.25 V (vs. SCE)

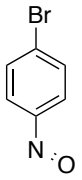

8

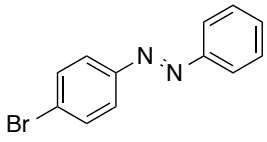

10

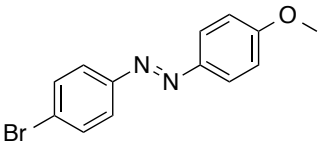

13

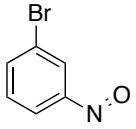

15

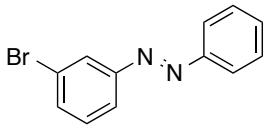

16

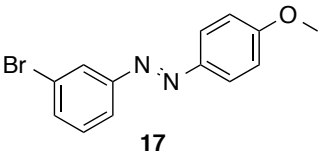

17

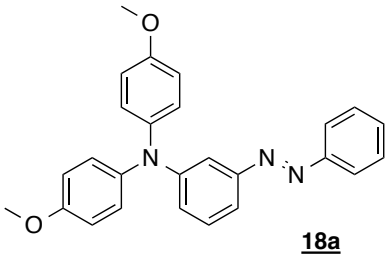

18a

***trans-m*AA-Ph-N=N-Ph**

(b) E^o (1) = 0.87 V (vs. SCE))

(a) Previously unknown substrates are underlined.
(b) Oxidation potentials (E°) reported are in V vs. SCE at Pt electrode in 0.1 M Bu_4NBF_4/CH_2Cl_2

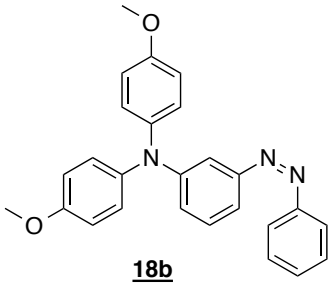

18b

***cis-m*AA-Ph-N=N-Ph**

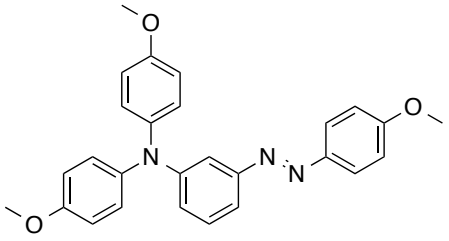

19a

***trans-m*AA-Ph-N=N-An**

(b) E^{o} (1) = 0.84 V (vs. SCE))

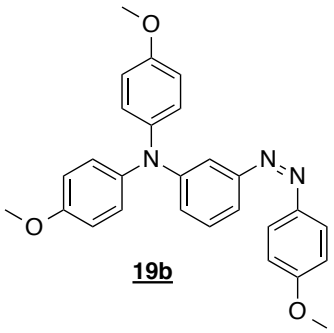

19b

***cis-m*AA-Ph-N=N-An**

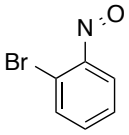

20

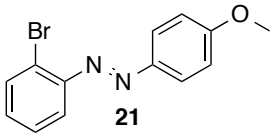

21

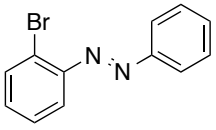

22

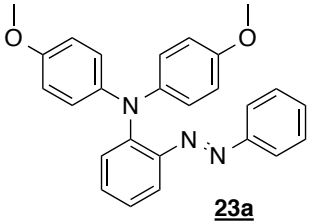

23a

***trans-o*AA-Ph-N=N-Ph**

(b) E^{o} (1) = V (vs. SCE))

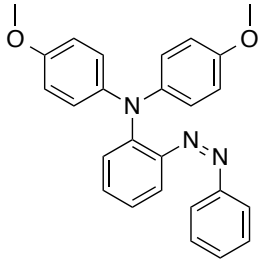

23b

***cis-o*AA-Ph-N=N-Ph**

(a) Previously unknown substrates are underlined.
(b) Oxidation potentials (E^{o}) reported are in V vs. SCE at Pt electrode in 0.1 M Bu_4NBF_4/CH_2Cl_2

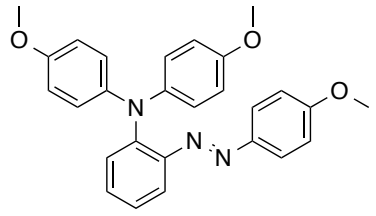

24a

***trans*-*o*AA-Ph-N=N-An**

(b) E^o (1) = V (vs. SCE))

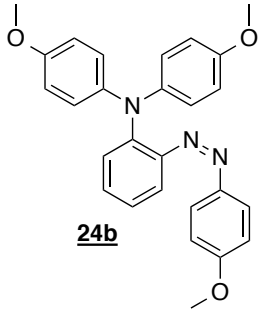

24b

***cis*-*o*AA-Ph-N=N-An**

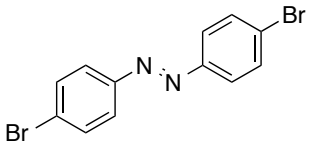

25

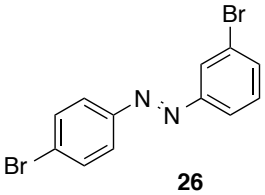

26

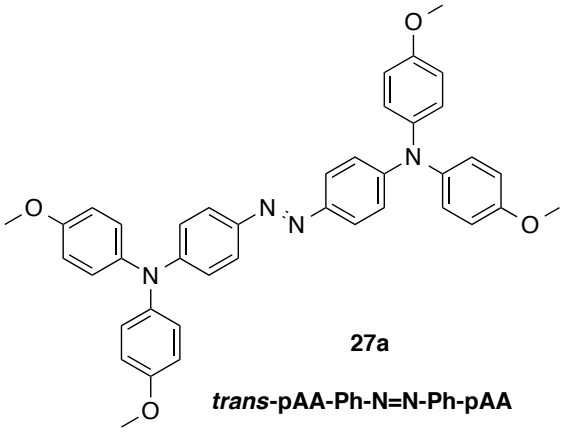

27a

***trans*-pAA-Ph-N=N-Ph-pAA**

(b) E^o (1) = 0.78 V (vs. SCE)
E^o (2) = 0.94 V (vs. SCE)

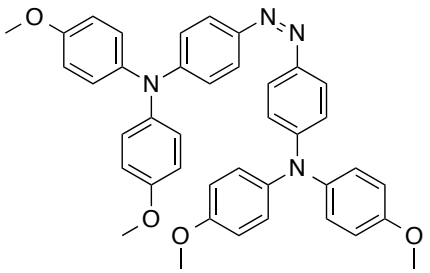

27b

***cis*-*p*AA-Ph-N=N-Ph-*p*AA**

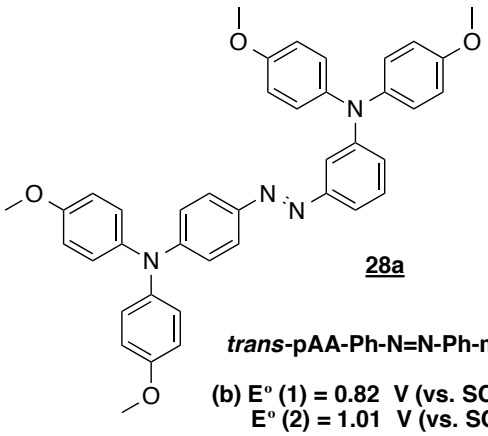

28a

***trans*-pAA-Ph-N=N-Ph-mAA**

(b) E^o (1) = 0.82 V (vs. SCE)
E^o (2) = 1.01 V (vs. SCE)

(a) Previously unknown substrates are underlined.
(b) Oxidation potentials (E°) reported are in V vs. SCE at Pt electrode in 0.1 M Bu_4NBF_4/CH_2Cl_2

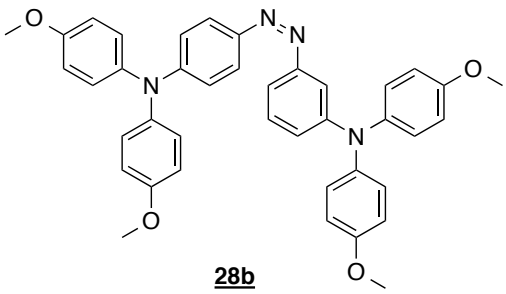

28b

***cis-p*AA-Ph-N=N-Ph-*m*AA**

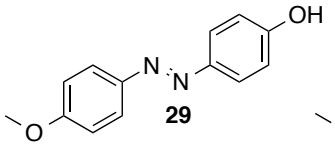

29

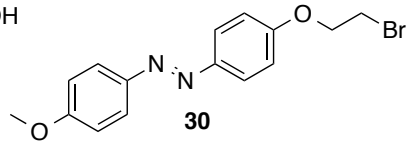

30

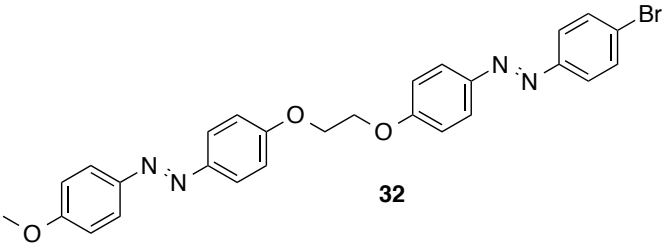

32

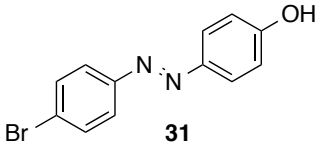

31

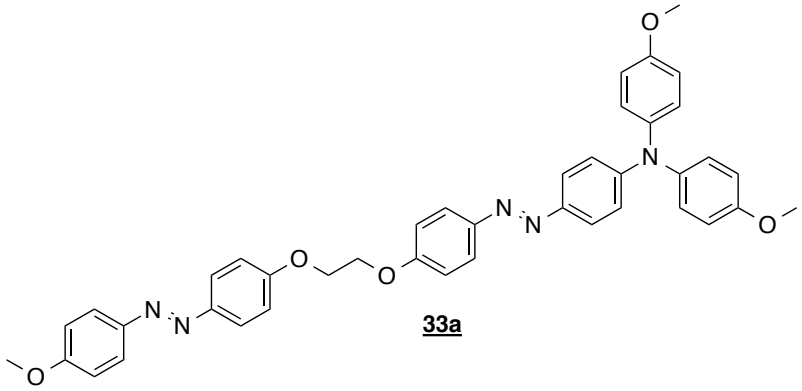

33a

(a) Previously unknown substrates are underlined.
(b) Oxidation potentials (E°) reported are in V vs. SCE at Pt electrode in 0.1 M Bu_4NBF_4/CH_2Cl_2

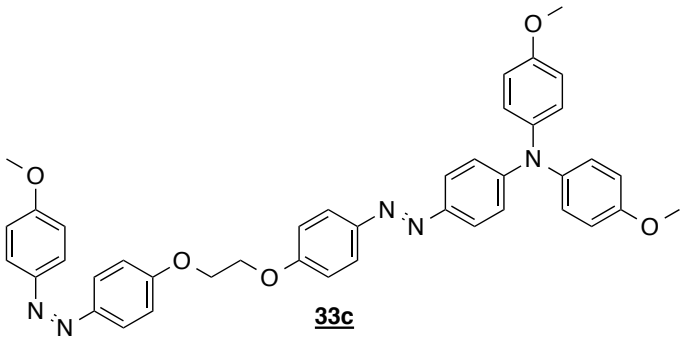

33c

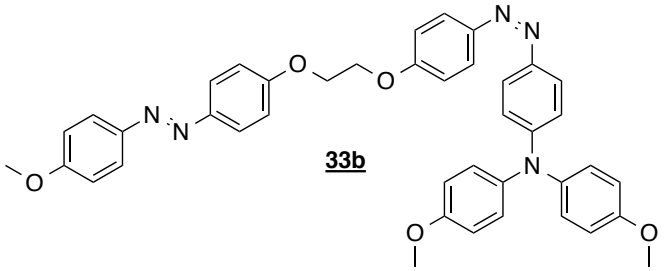

33b

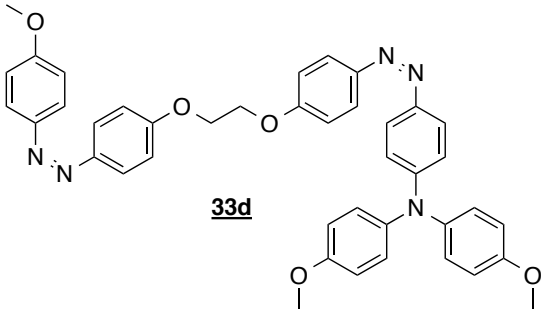

33d

(a) Previously unknown substrates are underlined.
(b) Oxidation potentials (E°) reported are in V vs. SCE at Pt electrode in 0.1 M Bu_4NBF_4/CH_2Cl_2

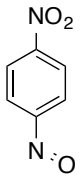

34

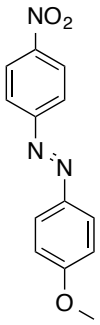

35

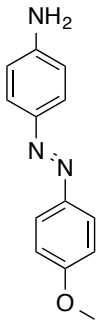

36

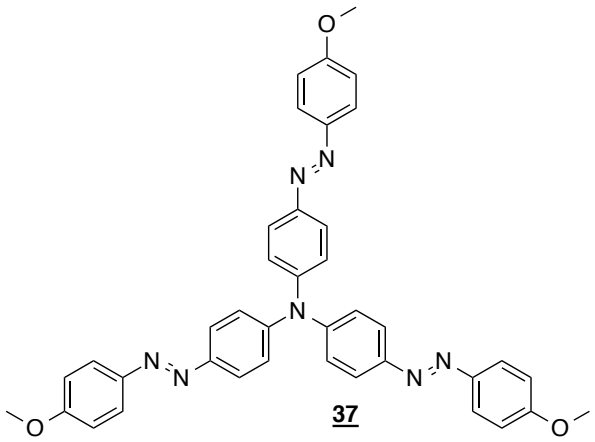

37

CHAPTER 1

GENERAL OVERVIEW OF DIFFERENT CLASSES OF AZOBENZENES

1.1 Introduction

Aromatic azo compounds are diazene (H-N=N-H) derivatives in which the hydrogen atoms are replaced by aromatic rings. The term azobenzene and the prefix azo are frequently used to refer to a large class of compounds that share the core azobenzene structure (Figure 1.1). This azobenzene structure can be incorporated into organic,[1] inorganic,[2] and organometallic[3] frameworks, but here the focus will be limited to organic azo compounds.

trans- azobenzene *cis*- azobenzene

Figure 1.1. Isomeric configurations of azobenzene.

Eilhard Mitscherlich first described azobenzenes in 1834.[4,5] Over a century later, in 1937, Hartley G. S. published studies on the discovery of the *cis* isomer formed when he exposed an acetone solution of a *trans*- azobenzene to light. In the *Nature* publication, Hartley described the influence of light on the configuration of the -N=N- bond and how the azo (-N=N-) linkage

[1] Zollinger, H. Azo and Diazo Chemistry: Aliphatic and Aromatic Compounds, Interscience Publishers, New York and London, 1961; Zollinger, H. Colour Chemistry: Synthesis, Properties and Applications of Organic Dyes. 3rd Ed. Wiley-VCH, Weinheim 1987.
[2] Bock, H.; Rudolph, G.; Baltin, E.; Kroner, J. Farbe und Konstitution bel Azoverbindungen. *Angew. Chem.,* **1965,** *77*, 469-516; Color and Constitution of Azo Compounds *Angew. Chem. Intl. Ed. Engl.*, **1965,** *4*, 457-541.
[3] Bruce, M.I. Cyclometalation Reactions. *Angew.Chem. Int.Ed. Engl.,* **1977**, *16*, 73-86.
[4] Mitscherlich, E. Ueber das Stickstoffbenzid. *Ann. Pharm.*, **1834**, *12*, 311-314.
[5] Merino, E.; Ribagorda, M. Control over Molecular Motion Using the *Cis-Trans* Photoisomerization of the Azo Group. *Beilstein J. Org. Chem.*, **2012**, *8*, 1071-1090.

can exist as two isomeric configurations, *trans* and *cis* isomers (Figure 1.1).[6] The photoisomerization process of azobenzene has become one the most well-known and studied process since Hartley's discovery.

1.2 Electronic Structure of Azobenzene

Cis and *trans* azobenzene have three available excited singlet states corresponding to the three absorption bands in the visible region and near the UV region.[7] The orbital diagram in Figure 1.2 will be utilized as a reference to discuss the three excited states. The ground state (S_0) of azobenzene is a singlet state. The two orbitals, $\mathbf{n}_+$ and $\mathbf{n}_-$, represent the atomic orbitals of the azo-nitrogen atoms when in the highly conjugated *trans* form. The lowest energy transition, S_1 ($\mathbf{n}_- \rightarrow \pi^*$), occurs at 440 nm and 430 nm in *trans* and *cis* azobenzene, respectively. The second transition, S_2 ($\pi \rightarrow \pi^*$), is responsible for absorption bands in the UV region at 314 nm and 280 nm for *trans* and *cis* isomers, respectively.[8] The highest energy transition, $\sigma \rightarrow \sigma^*$, involves electrons delocalized within the closely associated aromatic σ-orbitals. The absorption band for this high energy transition, $\sigma \rightarrow \sigma^*$, occur in the region of 230-240 nm for both *cis* and *trans* isomers. This high energy transition state is unlikely to be involved in the solution phase reactions of azobenzene.[7] Changing the ordering of the orbitals can alter the transition energies in Figure 1.2. Substitution of an electron-rich moiety at the *ortho*- or *para*- positions of an azobenzene ring increases the π orbital's energy (shown in blue) (Figure 1.2). This re-ordering of the orbitals results in a lowered S_2 energy and an altered absorption profile.

[6] Hartley, G. S. The *Cis*-form of Azobenzene. *Nature,* **1937**, 140, 281-282.
[7] Griffiths, J. Photochemistry of Azobenzene and Its Derivatives. *Chemical Society Reviews,* **1972**, *1*, 481-493.
[8] Dhammika Bandara, H. M.; Burdette, S.C. Photoisomerization in Different Classes of Azobenzene. *Chem. Soc. Rev.,* **2012**, *41*, 1809-1825.

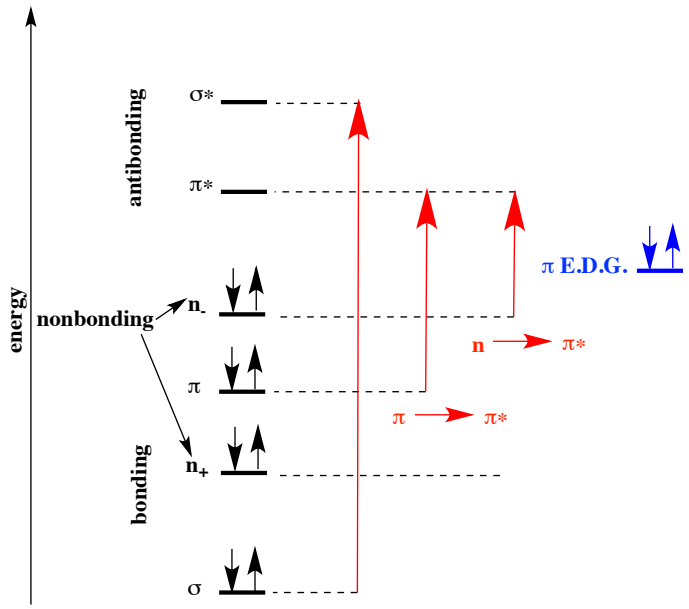

Figure 1.2. Molecular orbital energy diagram for the azobenzene system. Figure reproduced from reference).[7]

The irradiation process of *trans*- azobenzene at 320-350 nm causes photo-excitation of the *trans* isomer from $S_2 \leftarrow S_0$ followed by non-irradiative decay to the ground state (S_0) to either the *trans* or *cis* geometry (Figure 1.3). Similarly, the irradiation process of *cis* azobenzene at 400-450 nm causes photo-excitation of the *cis* isomer from $S_1 \leftarrow S_0$ followed by non-irradiative decay to the ground state (S_0) to either the *trans* or *cis* geometry. A photo stationary state (PSS) can be generated when a dynamic equilibrium between the photochemical reactions is reached. Under constant irradiation, the rate of the *cis*-to-*trans* photo conversion becomes equal to the rate of *trans*-to-*cis* conversion.

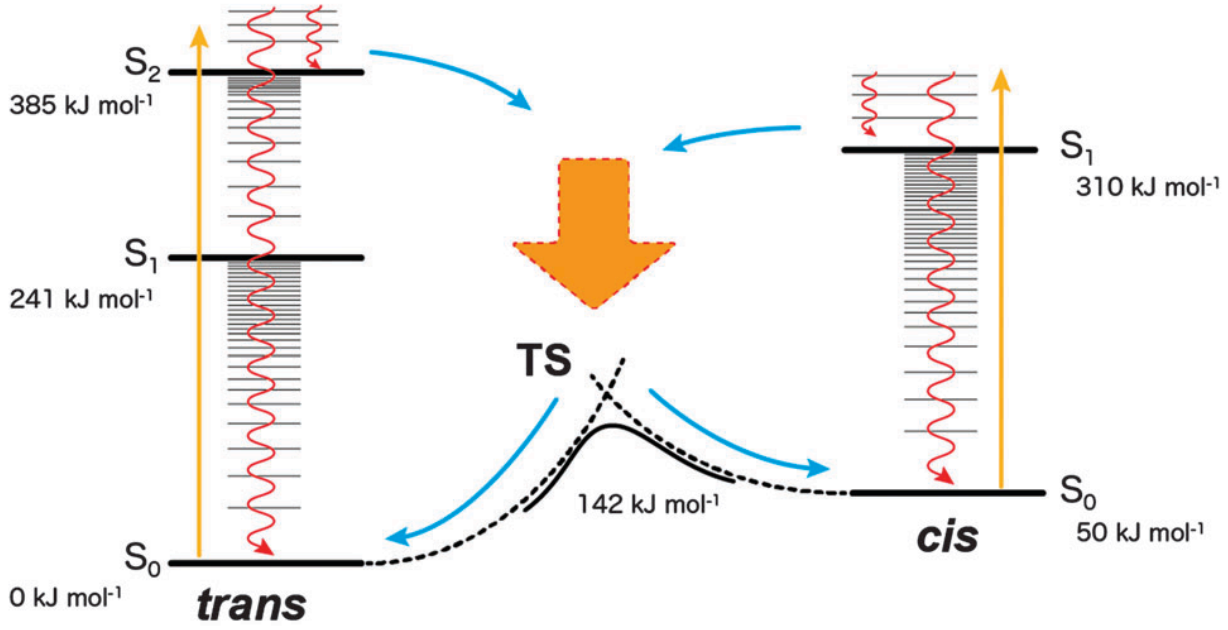

Figure 1.3. Schematic illustration of energy state diagram for photoisomerization of azobenzene. Reproduced and adapted from reference.[9]

1.3 Absorption Spectroscopy of Azobenzene

The *trans/cis* configuration of azobenzene alters the absorption spectrum from that of the *trans* isomer to the *cis* isomer as shown in Figure 1.4. The *trans* isomer absorption spectrum consists of two separated bands in the UV visible region (Figure 1.4).[10,11] The intense primary absorption peak (λ_{max} ~ 320 nm, ε ~ 2200 L mol^{-1} cm^{-1}) corresponds to a $\pi \rightarrow \pi^*$ transition.[12] The absorption of the $\pi \rightarrow \pi^*$ band for the *trans* isomer is due to the planar C_{2h} symmetry of the *trans* isomer. The weaker absorption peak (λ_{max} ~ 450 nm, ε ~ 400 L mol^{-1} cm^{-1}) corresponds to

[9] Ramakrishnan, V.; Yamamoto, D.; Sasamoto, S.; Shimada, T.; Nabetani, Y.; Tachibana, H.; Inoue, H. Remarkable Enhancement of the Photoreactivity of a Polyfluoroalkyl Azobenzene Derivative in an Organic-Inorganic Nano-layered Microenvironment. *Phys. Chem. Chem. Phys.* **2014**, *16*, 23663-23670.
[10] Hamm, P.; Ohline, S.M.; Zinth, W. Vibrational Cooling After Ultrafast Photoisomerization of Azobenzene Measured by Femtosecond Infrared Spectroscopy. *J. Chem. Phys.*, **1997,** *106*, 519-529**.**
[11] Lednev, I.K.; Ye, T.Q.; Matousek, P.; Towrie, M.; Foggi, P.; Newahl, F.V.R.; Umapathy, S.; Hester, R.E.; Moore, J.N. Femtosecond Time-Resolved UV-visible Absorption Spectroscopy of *Trans*-azobenzene: Dependence on Excitation Wavelength. *Chem. Phys. Lett.,* **1998**, *290*, 68-74.
[12] Forber, C.L.; Kelusky, E. C.; Bunce, N. J.; Zerner, M. C. Electronic spectra of cis- and trans-azobenzenes: consequences of ortho substitution. *J. Am. Chem. Soc.*, **1985**, *107*, 5884-5890.

a weak forbidden n → π* transition (Figure 1.4).[13] The *cis* isomer absorption spectrum consist of two π → π* and a n → π* absorption bands. The *cis* isomer has a non-planar geometry in which conjugation is partially disrupted causing the intensity of the π → π* transitions (λ_{max} ~ 270 nm, ε ~ 5000 L mol^{-1} cm^{-1}; λ_{max} ~ 250 nm, ε ~ 11 000 L mol^{-1} cm^{-1}) to be less intense. The n → π* transition (λ_{max} ~ 450 nm, ε ~ 1500 L mol^{-1} cm^{-1}) of *cis* azobenzene absorbs more strongly than that of *trans* azobenzene because it is more "allowed" for the *cis* isomer (Figure 1.4). [12,13]

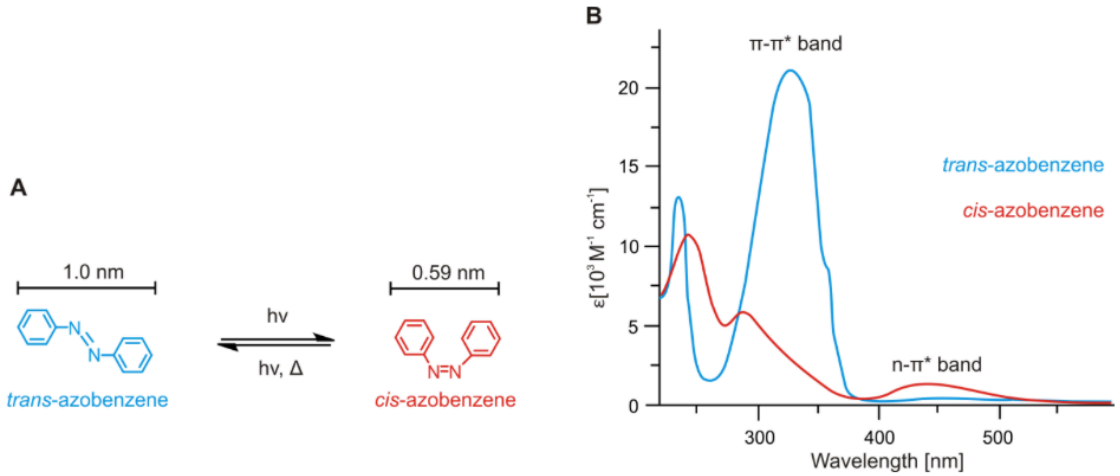

Figure 1.4. (**A**) The trans *cis* isomerization of azobenzene, with the diameter of each configuration. (**B**) Absorption spectra of *cis* and *trans*- azobenzene in an ethanol solution. Reprinted and adapted from reference[14]

Many applications of azobenzenes rely on the photo control of their molecular dynamics. Azo compounds exhibit a photomechanical effect upon exposure to UV or visible light.[15] A photomechanical effect is defined as a reversible photo-transformation of a chemical species

[13] Cusati, T.; Granicciu, G.; Persico, M.; Spighi, G. Oscillator Strength and Polarization of the Forbidden n→pi* Band of *Trans*- azobenzene: A Computational Study. *J. Chem. Phys.* **2008**, *128, 19*, 194312/194311-194312/194319.
[14] Rau, H. in Photoreactive Organic Thin Films, Academic Press, San Diego, 2002, S. 3-47.
[15] Zhang, Q.M.; Li, X.; Islam, M.R.; Wei, M.; Serpe, M.J. Light Switchable Optical Materials from Azobenzene Crosslinked Poly(*N*-isopropylacrylamide)-based Microgels. *J. Mater. Chem. C.,* **2014**, *2*, 6961-6965.

yielding two different geometries with two distinct absorption spectra.[16] Azobenzenes can reversibly photoisomerize between the *trans* and *cis* isomers as shown in Scheme 1.1.

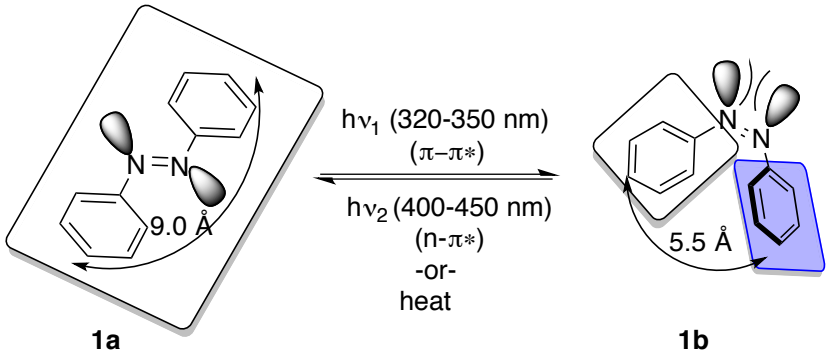

Scheme 1.1. Photoisomerization of azobenzenes. *Trans* **1a** can be converted to *cis* **1b** using wavelengths from 320-350 nm and *cis*-to-*trans* using wavelengths 400-450 nm or thermally. Reproduced and adapted from reference.[5]

Absorption of a photon (320-350 nm) by the *trans* isomer can stimulate isomerization to the *cis* isomer. The *cis*-to-*trans* isomerization occurs upon excitation of the n → π* band at 400-450 nm (2.95 eV)[17] (Scheme 1.1). The conformational change results in a change in distance between the 4- and 4′- positions of the aromatic rings from 9.0 Å (*trans*) to 5.5 Å (*cis*) as shown in Scheme 1.1 and can be thus be utilized to move an attached payload in space accordingly.

1.4 Photochemistry of Azobenzene

The photoisomerization of azobenzene has been thoroughly studied. *Cis* ←→ *trans* photoisomerization of azobenzene can be controlled by irradiating at either transitions. *Trans* azobenzene undergoes *trans*-to-*cis* isomerization following both $S_1 \leftarrow S_0$ and $S_2 \leftarrow S_0$ excitation.[18] *Cis*- azobenzene can also be converted to *trans*- azobenzene by excitation to the S_1 and S_2 state.[18] Quantum yields of the *trans*-to-*cis* and *cis*-to-*trans* photoisomerization of azobenzenes

[16] Mahimwalla Z.; Yager K.; Mamiya J.-i.; Shishido A.; Priimagi A.; Barrett C. Azobenzene Photomechanics: Prospects and Potential Applications. *Polymer Bulletin*, **2012**, *69*, 967-1006.
[17] Rau, H. Azo compounds. *In Photochromism: Molecules and Systems*; Durr, H., Bouas-Laurent, H., Eds.; Elsevier: *Amsterdam*, 1990, p. 165.
[18] Bortolus, P.; Monti, S. Cis-Trans Phtoisomerization of Azobenzene- Solvent and Triplet Donor Effects. *J. Phys. Chem.*, **1979**, *83*, 648-652.

can be determined by steady irradiation and monitoring the absorbance while approaching PSS. Average quantum yields for azobenzene are $\Phi_E = 0.25$ and $\Phi_Z = 0.52$ for excitation at 436 nm, and $\Phi_E = 0.11$and $\Phi_Z = 0.44$ for excitation at 313 nm in n-hexane.[18] The two isomerization reactions do not occur on the same potential surface and as a result the sum of the quantum yields does not equal unity.[18]

1.5 Thermal Isomerization of Azobenzene

Azobenzene and a large number of its derivatives exist mainly in the *trans* form at room temperature. The *trans* isomer **1a** is the thermodynamically favored species and is approximately ~ 0.60 eV (~15.2 kcal mol^{-1}) lower in energy than the *cis* isomer as shown in Figure 1.5.[19] As a result, the thermal *cis*-to-*trans* isomerization of azobenzene can also occur spontaneously in the dark at room temperature. [7, 17,20,21,]

[19] Schulze, F. W.; Petrick, H. J.; Cammenga, H. K.; Klinge, H. Hermodynamic Properties of the Structural Analogues Benzo[c]-cinnoline, Trans-Azobenzene and Cis-Azobenzene. *Z. Phys. Chem. Neue. Fol.,* **1977**, *1*, 107.
[20] Knoll, H., Handbook of Organic Photochemistry and Photobiology, 2nd Ed. CRC Press, Boca Raton, FL, 2004, page 89/81–89/16.
[21] Rau, H.; Lueddecke, E. On the Rotation-Inversion Controversy on Photoisomerization of Azobenzenes. Experimental Proof of Inversion. *J. Am. Chem. Soc.,* **1982**, *104*, 1616–1620.

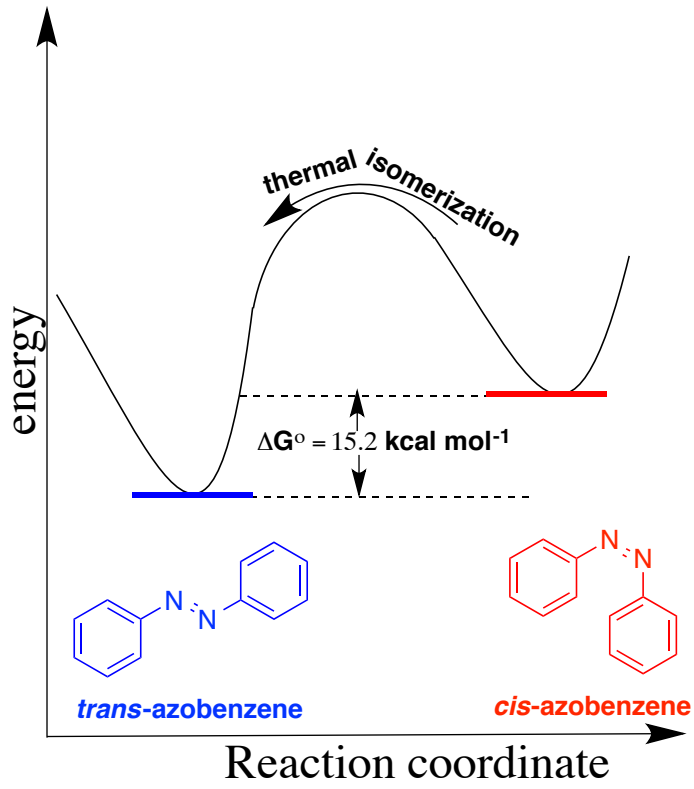

Figure 1.5. Potential energy diagram showing *trans*- azobenzene is thermodynamically more stable than *cis*- azobenzene by 15.2 kcal mol^{-1}.

Unlike stilbene, which has a 1.9 eV (43.82 kcal mol^{-1}) thermal isomerization barrier,[22,23,24] the activation barrier of the thermal back-reaction for azobenzene is ~1.1 eV (~25.8 kcal mol^{-1}) as shown in Figure 1.6.[25,26,27] In the *cis* form, the nonbonding lone pair of the nitrogen atoms are in close proximity and repulsing each other. This in turn increased the steric interaction of the rings in *cis*- azobenzene resulting in a lower activation barrier for the *cis*-to-*trans* thermal isomerization. It is low enough to allow the less stable *cis*- azobenzene to thermally re-

[22]Durr, H.; Bouas-Laurent, H. *Photochromism: Molecules and Systems.* 1st Ed., Elsevier: *Amsterdam*, 2003, p.68.
[23] Waldeck, D. H. Photoisomerization Dynamics of Stilbenes. *Chem. Rev.,* **1991**, *91*, 415-436.
[24] Meier, H. The Photochemistry of Stilbenoid Compounds and Their Role in Materials Technology. *Angew. Chem. Int. Edn.,* **1992**, *31*, 1399-1420.
[25] Tamai, N.; Miyasaka, H. Ultrafast Dynamics of Photochromic Systems. *Chem. Rev.,* **2000**, *100*, 1875–1890.
[26] Fangha¨nel, D.; Timpe, G.; Orthman, V. In *Organic Photochromes*; El'tsov, A. V., Ed.; Consultants Bureau: New York, 1990; p 105.
[27] Blevins, A. A.; Blanchard, G. J. Effect of Positional Substitution on The Optical Response of Symmetrical Disubstituted Azobenzene Derivatives. *J. Phys. Chem. B*., **2004**, *108*, 4962-4968.

isomerized back to the lower energy *trans*- azobenzene.

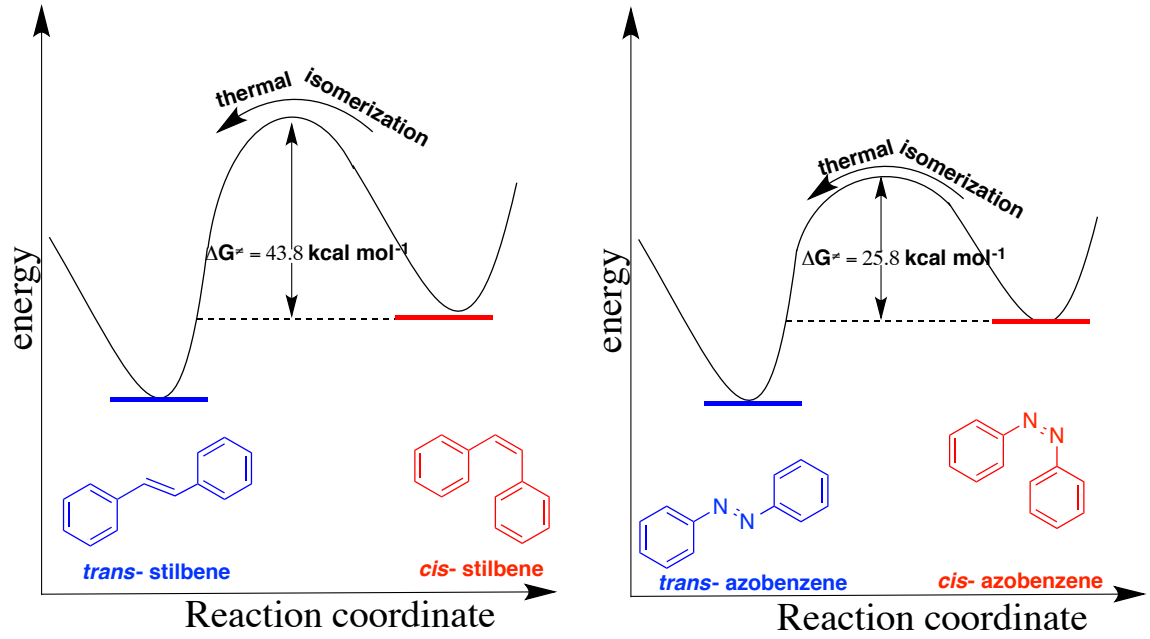

Figure 1.6. Potential energy diagrams of stilbene (**left**) and azobenzene (**right**) that illustrates the difference in the activation barrier of the thermal back-reaction.

Since the discovery of *trans*- azobenzene by Eilhard Mitscherlich in 1834 and the discovery of the *cis* isomer by Hartley G. S. in 1937, the mechanism at which the thermal isomerization of azobenzene occurs was always a dispute. Two major pathways, rotation[28] and inversion[29], have been proposed over the years as shown in Scheme 1.2. The rotational pathway involves rotation around the -N=N- bond and include rupture of the π–bond as shown in Scheme 1.2. In the inversion pathway, the π–bond remain unbroken where one of the nitrogen atoms is sp-hybridized ($sp^2 \rightarrow sp$) in the linear transition state and then interconverts to the corresponding isomer as shown in Scheme 1.2. Previously, it was suggested that the thermal isomerization mechanism of azobenzene might follow the rotational pathway because of its similarity to

[28] Cembran, A.; Bernadi, F.; Garavelli, M.; Gagliari, L.; Orlandi, G. On the Mechanism of the cis−trans Isomerization in the Lowest Electronic States of Azobenzene: S_0, S_1, and T_1. *J. Am. Chem. Soc.*, **2004**, *126*, 3234-3243.

[29] Cattaneo, P.; Persico, M. An ab initio study of the photochemistry of azobenzene. *Phys. Chem. Chem. Phys.*, **1999**, *1*, 4739-4743.

stilbene. However, in 1980, a different mechanism was proposed for the thermal isomerization of *cis*-to-*trans* azobenzene. Rau, Luddecke, and Tamaoki presented proof that the inversion pathway is the dominant pathway in the *cis*-to-*trans* thermal isomerization of azobenzene by showing that azobenzenophanes that cannot thermally isomerized by rotation still thermally isomerized from *cis*-to-*trans* in the dark after irradiation. [30]

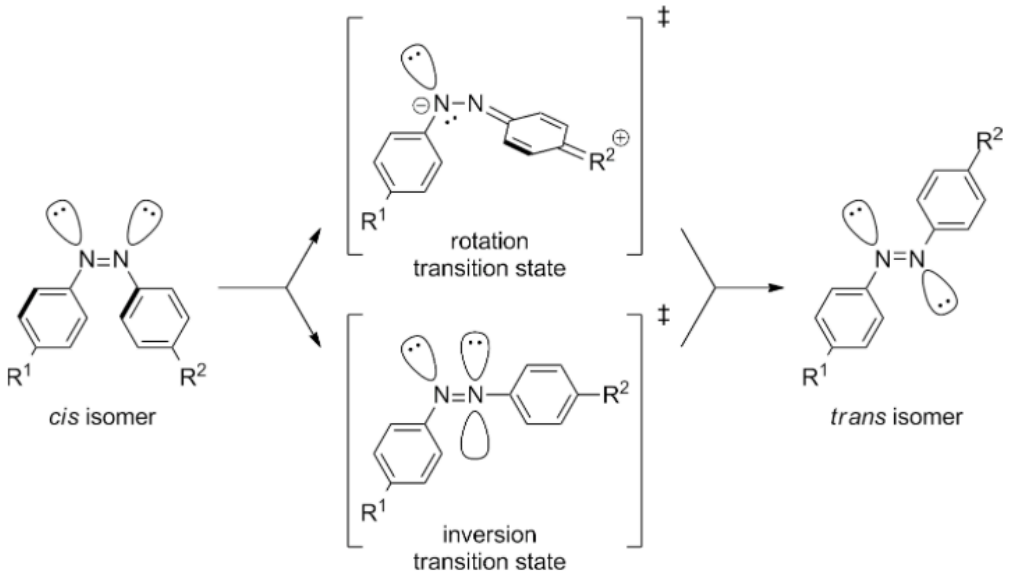

Scheme 1.2. Rotation and inversion mechanism proposed for the thermal cis-to-trans isomerization processes of azobenzene. Reprinted and adapted from reference[31]

1.6 Categories of Azo Aromatic Compounds

Traditionally, Rau H. classified aromatic azo compounds based on the relative energies of their $\pi \rightarrow \pi^*$ and $n \rightarrow \pi^*$ transitions.[17] Three categories of aromatic azo compounds have been formulated: azobenzenes (ABs), donor-substituted azobenzenes (d-ABs), and donor/acceptor-substituted azobenzenes (da-ABs).[17]

[30] Tamaoki, N.; Ogata, K.; Koseki, K.; Yamaoka, T. (4,4′) Azobenzene. Synthesis, structure, and Cis-Trans Isomerization. *Tetrahedron,* **1990**, *46*, 5931-5942.
[31] Garcia-Amoros, J.; Velasco, D. Recent Advances towards Azobenzene-based light-Driven Real-Time Information-Transmitting materials. *Beilstein J. Org. Chem*., **2012**, *8*, 1003-1007.

ABs includes unsubstituted-AB and derivatives with an AB core that are substituted with alkyl,[32, 33] aryl,[34] halide,[34] carbonyl,[35] amide,[36] nitrile,[35] ester,[37] and carboxylic acid [38] moieties as shown in Table 1.1. They have absorption spectra very similar to unsubstituted-AB and their high intensity $\pi \rightarrow \pi^*$ transition occurs at the UV region and is separated from their low intensity $n \rightarrow \pi^*$ band as shown in Figure 1.7.[14] ABs possess photoisomerization quantum yields similar to unsubstituted-AB but possess higher rates of thermal isomerization than unsubstituted-AB due to steric effects in the *cis* form and electronic effects of the substituents as shown in Table 1.1.

[32] Gegiou, D.; Muszkat, K. A.; Fischer, E. Temperature Dependence of Photoisomerization. V. Effect of Substituents on the Photoisomerization of Stilbenes and Azobenzenes. *J. Am. Chem. Soc.,* **1968**, *90*, 3907–3918.
[33] Tamai, N.; Miyasaka, H. Ultrafast Dynamics of Photochromic Systems. *Chem. Rev.*, **2000**, *100*, 1875-1890
[34] Brode, W. R.; Gould, J. H.; Wyman, G. M. The Relation between the Absorption Spectra and the Chemical Constitution of Dyes. XXV. Phototropism and Cis-trans Isomerism in Aromatic Azo Compounds *J. Am. Chem. Soc.,* **1952**, *74*, 4641–4646.
[35] Tang, Z.; Johal, M. S.; Scudder, P.; Caculitan, N.; Magyar, R. J.; Tretiak, S.; Wang, H.-L. Control Formation of Functional Nanoscaled using Langmuir-Blodgett Method: Interplay between p-p and Dipole-dipole Interactions. *Thin Solid Films,* **2007**, *516*, 58–66.
[36] Lednev, I. K.; Ye, T.-Q.; Abbott, L. C.; Hester, R. E.; Moore, J. N. Photoisomerization of a Caped Azobenzene in Solution Probed by Ultrafast Time-Resolved Electronic Absorption Spectroscopy. *J. Phys. Chem. A,* **1998**, *102*, 9161–9166.
[37] Zacharias, P. S.; Ameerunisha, S.; Korupoju, S. R. Photoinduced Fluorescence changes on E-Z Isomerization in Azobenzene Derivatives. *J. Chem. Soc., Perkin Trans. 2,* **1998**, 2055–2060.
[38] Ohtani, O.; Furukawa, T.; Sasai, R.; Hayashi, E.; Shichi, T.; Yui, T.; Takagi, K. Effect of Fluorinated Ammonium Counterions upon the Reversibility in E-Z Photoisomerization of Azobenzene Ion Pair Films *J. Mater. Chem.,* **2004**, *14*, 196–200.

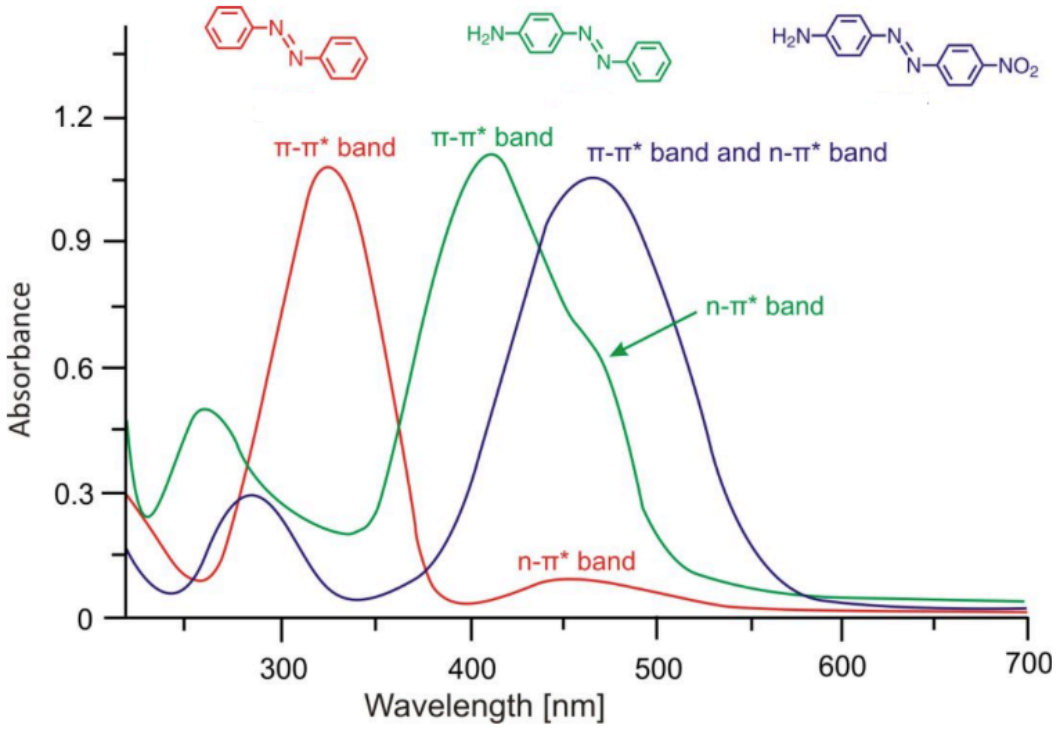

Figure 1.7. Absorption spectra of *trans*- azobenzene (red line), 4-aminoazobenzene (green line) and 4-nitro-4´-aminoazobenzene (blue line) in ethanol. Reprinted and adapted from reference.[14]

[39]Table 1.1. Differences in Categories of Substituted-AB

Type Compound	Solvent	λ_{max} (π-π^*)	$\Phi_{trans \rightarrow cis}$	k_{-1} (Δ)
AB				
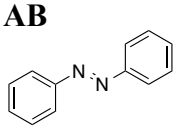	n-hexane	320 nm	0.11	0.3 x 10^{-5} s^{-1}
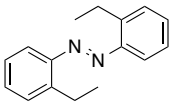	toluene	334 nm	0.09	
dAB				
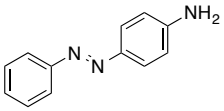	benzene	352 nm	0.04	5.1 x 10^{-5} s^{-1}
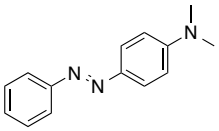	benzene	405 nm	0.12	9.8 x 10^{-5} s^{-1}
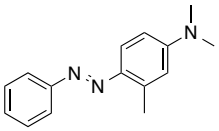	benzene	420 nm	0.28	958.5 x 10^{-5} s^{-1}
daAB				
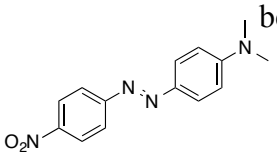	benzene	478 nm	0.68	1149.3 x 10^{-5} s^{-1}
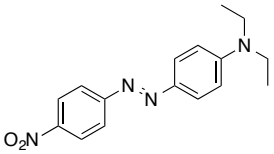	benzene	460 nm	1	2757.4 x 10^{-5} s^{-1}

[39] Wazzan, N. *Cis-Trans* Isomerisation of Azobenzenes Studied by NMR Spectroscopy with *In situ* Laser Irradiation and DFT Calculations. Ph.D. Thesis, The University of Edinburgh, Edinburgh, Scotland, 2009.

Donor-substituted azobenzenes (d-ABs) are compounds with an azobenzene core that contains *ortho*- and/or *para*- positioned electron-donating substituents such as amino, hydroxyl, and alkoxy.[8] These functional groups contain a lone pair of electrons in conjugation with the corresponding azobenzene π-system. This is a very high energy π-system orbital and consequently the $\pi \rightarrow \pi^*$ transition will be much lower energy than in AB. This lower energy transition results in a redshifted $\pi \rightarrow \pi^*$ absorption band (to longer wavelengths), and typically leads to overlap of the $\pi \rightarrow \pi^*$ and the $n \rightarrow \pi^*$ absorption bands as illustrated in Figure 1.7.[14] The overlap of the $\pi \rightarrow \pi^*$ and the $n \rightarrow \pi^*$ absorption bands in d-ABs depends on the nature of the donor group (e.g. number of amino substituents,[27] degree of amine alkylation)[40] as shown in Table 1.1. The more electron-donating a substituent is, the greater the redshift of the $\pi \rightarrow \pi^*$ absorption band. S_1 and S_2 overlap present difficulties in assigning quantum yields to each different excitation.[8] Higher thermal isomerization rates are observed for d-ABs than ABs[41] as shown in Table 1.1.

The photophysical behavior of d-ABs depends on its surrounding and on the interactions with the solvent. A red shift of the λ_{max} of the $\pi \rightarrow \pi^*$ absorption band is observed for the d-ABs when dissolved in polar solvents compared to a non-polar solvent as shown in Figure 1.8. The shift of an absorption wavelength due to the presence of a solvent with different polarity is called the solvatochromic.[42] The strong solvatochrmoinc behavior is observed for d-ABs because they possess a large dipole moment change during transitions between the two electronic states. Figure 1.8 illustrates a red shift of the $\pi \rightarrow \pi^*$ absorption band in DMSO solution compared to

[40] Cilento, G.; Miller, E. C.; Miller, J. A. On The Addition of Protons to Derivatives of 4-Aminoazobenzene *J. Am. Chem. Soc*., **1956**, *78*, 1718-1722.
[41] YA, Q.; Dong, X.-Z.; Chen, W.-Q.; Duan, X.-M. The Synthesis of Aminoazobenzenes and The Effect of Intermolecular Hydrogen Bonding on Their Photoisomerization *Dyes Pigm*., **2008**, *79*, 159-165.
[42] Zakerhamidi, M.S.; Ghanadzadeh, A.; Moghadam, M. Solvent Effects on the UV/Visble Absorption Spectra of Some Aminoazobenzene. *Chem. Sci. Trans*., **2012**, *1*, 1-8.

the solution of cyclohexane. This feature can be correlated to the stabilization of the electronic state of the dAB relative to the ground state.[42]

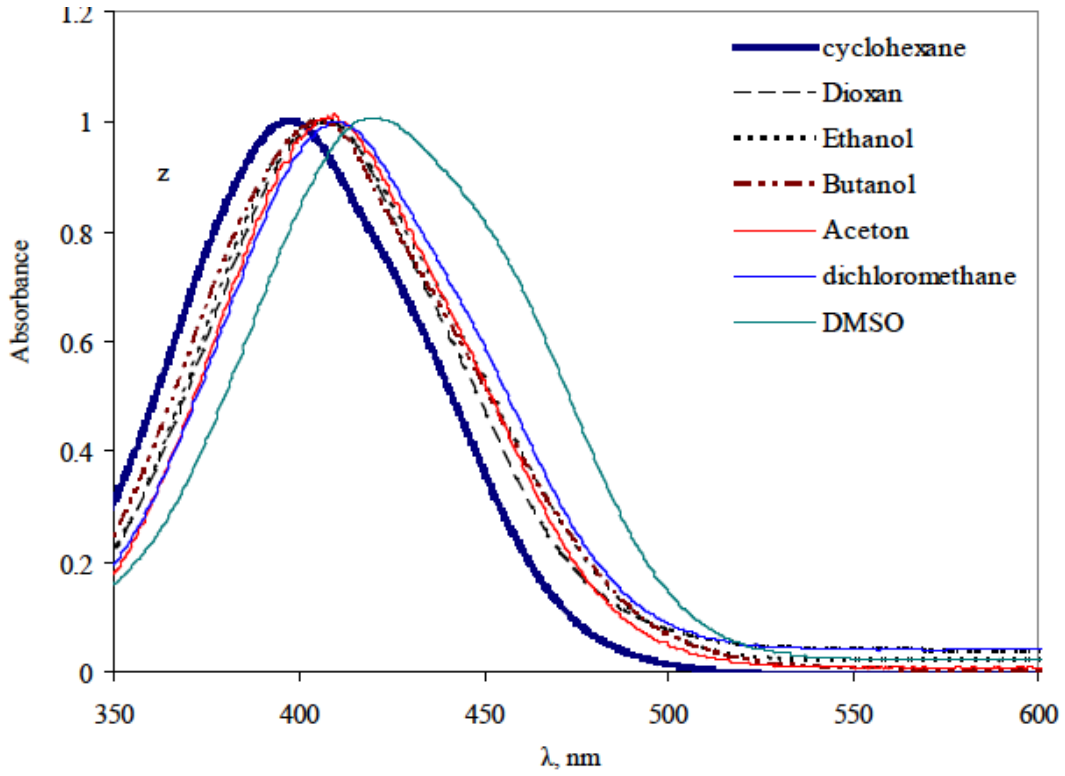

Figure 1.8. Visible absorption Spectra of dimethyl-aminoazobenzene in different solvents. Reprinted and adapted from reference.[42]

Donor/acceptor-substituted azobenzenes (da-AB) are compounds with an AB core that is substituted on a phenyl ring by a strong electron donor at the 4- position and on the other phenyl ring by a strong electron acceptor at the 4′- position in what is called a donor-acceptor system.[8] In da-AB, the $\pi \rightarrow \pi^*$ and $n \rightarrow \pi^*$ transitions both occur in the visible region as shown in Figure 1.7. They exhibit extremely fast thermal isomerization rates on the order of milliseconds to seconds as shown in Table 1.1. The thermal isomerization rate also strongly depends on solvent polarity.[43] Changing from a nonpolar solvent to a polar solvent increases the isomerization rate by roughly 100,000-fold. *Ab inito* calculations of the transition state of 4-(dimethylamino)-4′-

nitroazobenzene showed that polar solvent stabilized the transition state structure of the rotation path[43] as shown in Figure 1.9. This solvent effect was interpreted as an indication of the dipolar character of the activated complex.

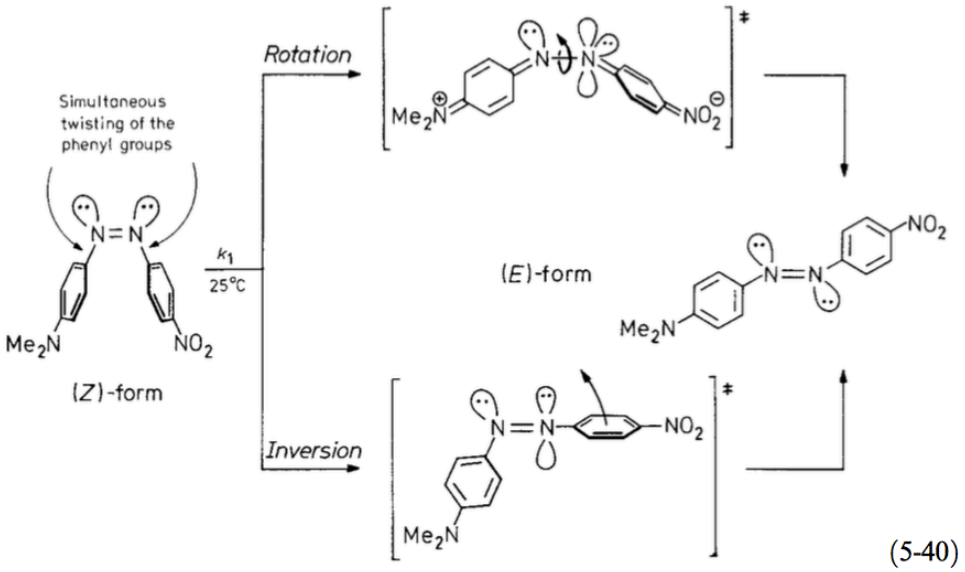

Solvent	n-C_6H_{14}	C_6H_6	CH_2Cl_2	CH_3COCH_3	CH_3OH	$HCONH_2$
k_1^{rel}	1	5	450	4760	$2.5 \cdot 10^4$	$8.2 \cdot 10^5$
$\Delta V^{\neq}/(cm^3 \cdot mol^{-1})$	$-3^{a)}$	$-22^{a)}$	−29	−30	−27	

a) At 40 °C.

Figure 1.9. Rate Enhancement (*ca.* 10^5) of the thermal isomerization of 4-(dimethylamino)-4′-nitroazobenzene on changing the solvent from n-hexane to formamide. Polar solvent stabilized the transition state structure of the rotation pathway. Reprinted and adapted from reference[43]

1.7 Applications of Azo Compounds

Azo molecules gained early industrial significance from their applications in textile dyeing and as colorants in ink and more recently from their applications as optical switches, optical data storage devices,[44,45] molecular machines,[46,47] and manipulators.[48,49] The thermal

[43] Reichardt, C. Solvent and Solvent Effects in Organic Chemistry, 3rd ed.; Wiley-VCH: Weinheim/Germany, 2002, p. 184.
[44] Yager, K. G.; Barrett, C. J. Novel Photo-Switching Using Azobenzene Functional Materials. *Journal of Photochemistry and Photobiology A: Chemistry,* **2006,** *182*, 250-261.
[45] Irie, M. Photochromism: Memories and Switches – Introduction. *Chem. Rev.,* **2000**, 100(5), 1683–1684.

lifetime of the *cis* isomer of azo molecules plays a critical role in both traditional and new applications.[8] For instance, in dyeing and printing, a long-lived *cis* isomer is disadvantageous because it results in a pronounced photochromic effect and weakened consistency of the color. Conversely, azo molecules with long-lived *cis* isomer states can be advantageous for the construction of devices that are capable of carrying out mechanical work at the molecular level, [50,51] such as: molecular switches,[52] which can be utilized for optical data storage, molecular actuation,[53] and molecular scissors.[54]

In 2003, Aida and co-workers published studies on a molecular scissor composed of different types of organic systems connected with an azobenzene unit as the epicenter of motion.[55] Figure 1.10 illustrates the molecular scissor that is composed of a ferrocene as the central unit, two phenyl groups as scissor blades, and two phenylethylene groups as handles linked through an azobezene. Irradiation of the *trans* isomer with 350 nm light leads to formation of the *cis* isomer, consequently opening the scissor blades. Subsequent exposure to visible light (> 400 nm) triggers the back reaction to *trans* isomer, thus closing the scissor blades.

---

[46] Norikane, Y.; Tamaoki, N. Light-Driven Molecular Hinge: A New Molecular Machine Showing a Light-Intensity-Dependent Photoresponse that Utilizes the *Trans−Cis* Isomerization of Azobenzene *Org. Lett.* **2004**, *6*, 2595-2598.
[47] Muraoka, T.; Kinbara, K.; Aida, T. Mechanical Twisting of a Guest by a Photoresponsive Host *Nature* **2006**, *440*, 512-515.
[48] Feringa, B. L., *Molecular switches.* 2nd Ed.; Wiley-VCH: Weinheim, 2001; page 281.
[49] Balzani V.; Credi, A.; Venturi, M. *Molecular Devices and Machines*; Wiley-VCH: Weinheim, 2008; page 308.
[50] Hugel, T.; Holland, N. B.; Cattani, A.; Moroder, L.; Seitz, M.; Gaub, H. E. Single-Molecule Optomechanical Cycle *Science* **2002***, 296*, 1103-1106.
[51] Jiang, C.-W.; Xie, R.-H.; Li, F.-L.; Allen, R. E. Comparative Studies of the *Trans*−C*is* Photoisomerizations of Azobenzene and a Bridged Azobenzene *J. Phys. Chem. A* **2011**, *115* (3), 244–249.
[52] Feringa, B. L., *Molecular switches.* 2nd Ed.; Wiley-VCH: Weinheim, 2001; page 67.
[53] Zhang, L.; Wang, D.; Hu, P.; Zha, J-W.; You, F.; Li, S-T.; Dang, Z-M Highly improved Electro-Actuation of Dielectric Elastomers by Molecular Grafting of Azobenzenes to Silicon Rubber. *J. Mater. Chem. C.* **2015**, *3*, 4883-4889.
[54] Takuzo, M.; Kazushi, K.; Yuka, K.; Takahiro, M. Light-Driven Open-Close Motion of Chiral Molecular Scissors *J. Am. Chem. Soc*. **2003**, *125*, 5612-5613.
[55] Muraoka, T.; Kinbara, K.; Aida, T. Reversible Operation of Chiral Molecular Scissors by Redox and UV light *Chem. Commun.* **2007**, 1441-1443.

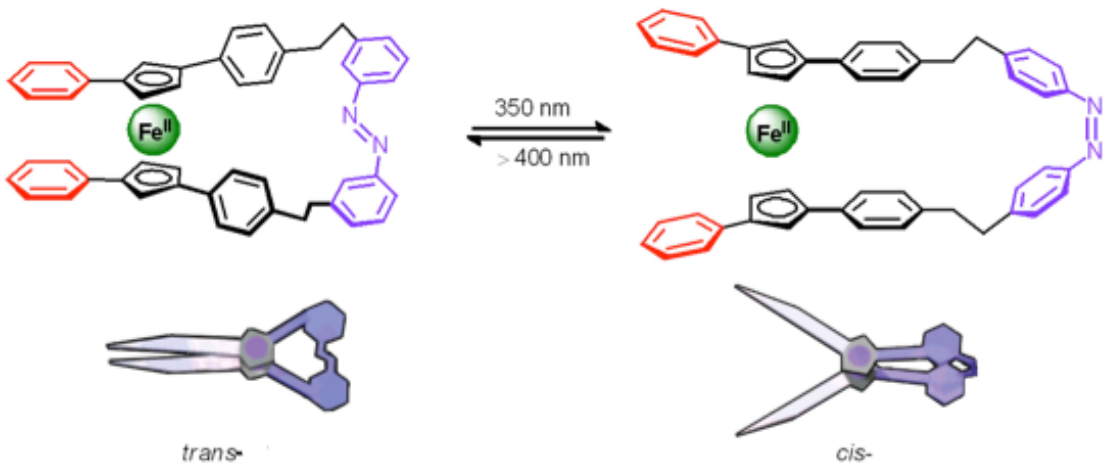

Figure 1.10. Molecular scissors based on azobenzene. Reprinted and adapted from reference.[54,55]

Azobenzenes can also be utilized *in vivo* where they act as conformational photo-switches in peptides, proteins,[56] nucleic acids,[57] or ion channels.[58,59,60] In 2005, Woolley and co-workers published studies on a photoswitchable peptide.[61,62] In the publication, they described the introduction of an azobenzene moiety to control the α-helical conformation of the peptide.

[56] Zhang, Z.; Burns, D.C.; Kumita, J.R.; Smart, O.S.; Woolley, G.A. A Water-Soluble Azobenzene Cross-linker for Photocontrol of Peptide Conformation *Bioconjug Chem.* **2003**, *4*, 824-829.
[57] **(a)**Woolley, G. A.; Jaikaran, A. S. I.; Berezovski, M.; Calarco, J. P.; Krylov, S. N.; Smart, O. S.; Kumita, J. R. Reversible Photocontrol of DNA Binding by a Designed GCN4-bZIP Protein. *Biochemistry,* **2006**, *45*, 6075–6084. **(b)** Renner, C.; Kusebauch, U.; Löweneck, M.; Milbradt, A. G.; Moroder, L. J. Azobenzene as Photoresponsive Conformational Switch in Cyclic Peptides. *Pept. Res*., **2005**, *65*, 4–14. **(c)** Pieroni, O.; Fissi, A.; Angelini, N.; Lenci, F. Photoresponsive Polypeptides. *Acc. Chem. Res.,* **2001**, *34*, 9–17. **(d)** Renner, C.; Moroder, L. Azobenzene as Conformational Switch in Model Peptides. *ChemBioChem,* **2006**, *7*, 868–878. **(e)** Aaemissegger, A.; Kräutler, V.; van Gunsteren, W. F.; Hilvert, D. A Photoinduced β-Hairpin. *J. Am. Chem. Soc*., **2005**, *127*, 2929–2936**. (f)** Beharry, A. A.; Woolley, G. A. Azobenzene Photoswitches for Biomolecules. *Chem. Soc. Rev.* **2011**, *40*, 4422–4437. **(g)** Sadovski, O.; Beharry, A. A.; Zhang, F.; Woolley, G. A. Spectral Tuning of Azobenzene Photoswitches for Biological Applications. *Angew. Chem., Int. Ed.,* **2009**, *48*, 1484–1486. **(h)** Beharry, A. A.; Sadovski, O.; Woolley, G. A. Azobenzene Photoswitching Without Ultraviolet Light *J. Am. Chem. Soc*., **2011**, *133*, 19684–19687.
[58] Lien, L.; D. Jaikaran, C. J.; Zhang, Z.; Woolley, G. A. Photomodulated Blocking of Gramicidin Ion Channels, *J. Am. Chem. Soc.* **1996**, *118*, 12222–12223.
[59] Mourot, A.; Kienzler, M. A.; Banghart, M. R.; Fehrentz, T.; Huber, F. M. E.; Stein, M.; Kramer, Trauner, R. H. D.Tuning Photochromic Ion Channel Blockers *ACS Chem. Neurosci*., **2011**, *2*, 536–543.
[60] Hilf, R. J. C.; Bertozzi, C.; Zimmermann, I.; Reiter, A.; Trauner, D.; Dutzler, R. Structural Basis of Open Channel Block in a Prokaryotic Pentameric Ligand-gated Ion Channel. *Nat. Struct. Mol. Biol*., **2010**, *17*, 1330–1336.
[61] Bredenbeck, J. ; Helbing, J. ; Kumita, J. R. ; Woolley, G. A. ; Hamm, P. α-Helix Formation in a Photoswitchable Peptide Tracked from Picoseconds to Microseconds by Time-resolved IR Spectroscopy. *Proc. Natl. Acad. Sci. U. S. A*., **2005**, *102*, 2379–2384.
[62] Guerrero, L.; Smart, O. S.; Woolley, G. A.; Allemann, R. K. Photocontrol of DNA Binding Specificity of a Miniature Engrailed Homeodomain. *J. Am. Chem. Soc.,* **2005**, *127*, 15624–15629.

Peptides containing pairs of cysteine residues were covalently cross-linked with an azobenzene moiety that contains two iodine as end groups to yield the photoswitchable peptide. The conformation of the peptide depends on the photosiomerization of the azobenzene moiety. When the azo group is in the *trans* form, it preserves the affinity for its α-helical conformation as shown in Figure 1.11. However, the affinity for the α-helical conformation is disrupted once it is photoisomerized to the *cis* isomer as shown in Figure 1.11.

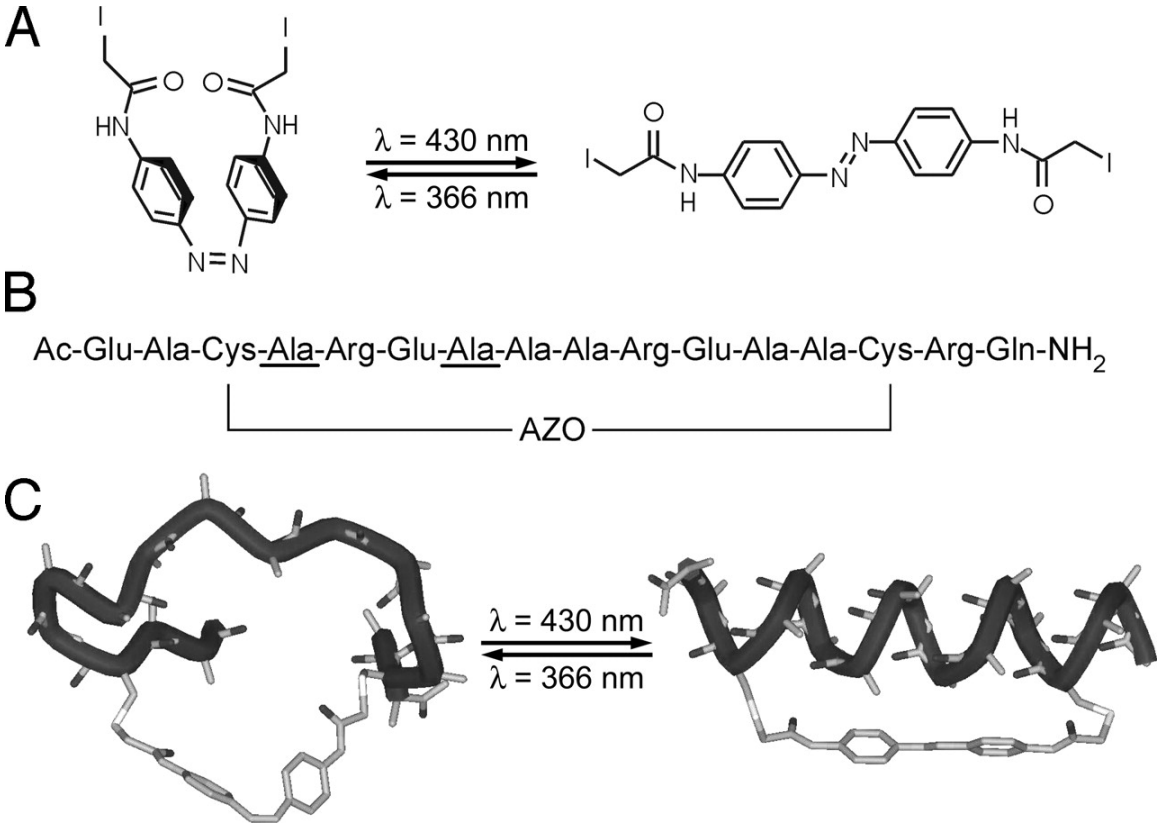

Figure 1.11. Photocontrol of the structure of the α-helix in the polypeptide azo derivative. Reprinted and adapted from ref.[61,62]

In 2004, Trauner and co-workers published studies on tuning ion channel blockers.[63] In the publication, they described the use of azo isomerization to control the opening and closing of pores in cellular membranes for the transport of ions. The azobenzene contained a terminal

[63] Banghart, M.; Borges, K.; Isacoff, E.; Trauner, D.; Kramer, R. H. Light-Activated Ion Channels for Remote Control of Neuronal Firing. *Nat. Neurosci.*, **2004**, *7*, 1381–1386.

quaternary ammonium salt that acts as a K^+ blocker when in the *trans* form (Figure 1.12). Conversion to the *cis* isomer upon irradiation with a 380 nm light brings the aromatic rings closer, which leads to a retraction of the ammonium arm and opening of the K^+ channel, allowing the passage of K^+ ions.

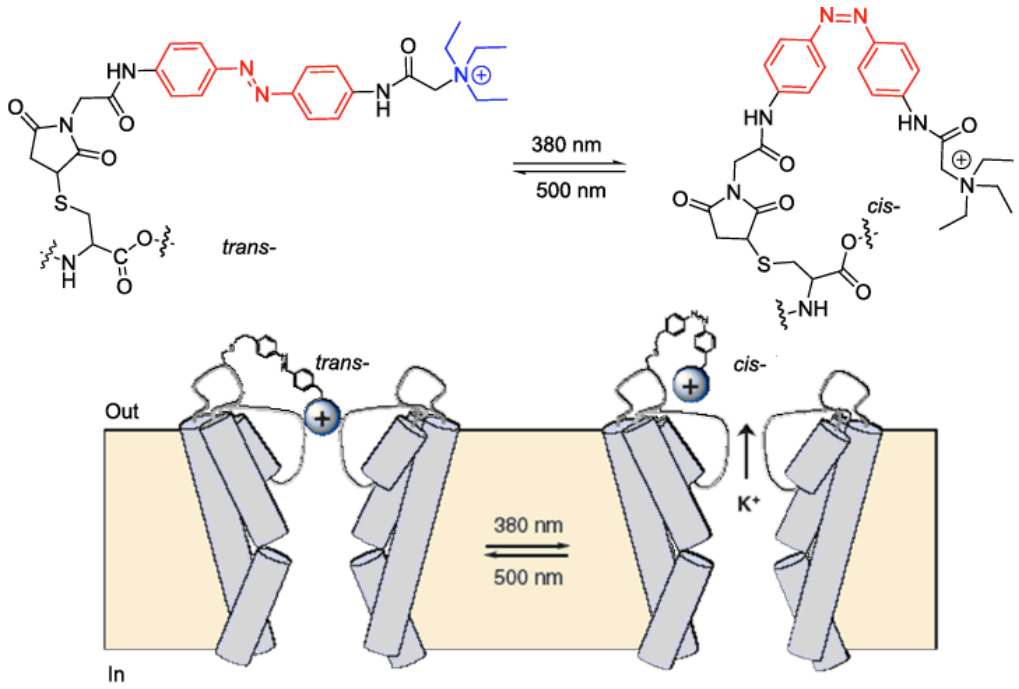

Figure 1.12. Representation of the photocontrol of a K^+ channel membrane based on the isomerization of azo compound. Reprinted and adapted from reference.[63]

CHAPTER 2

MONO(AMINO)AZOBENZENES AS PHOTO-ELECTRO SWITCHES

2.1. Introduction

As stated in the introduction chapter, changing the ring substituents can drastically alter the photochemical properties of AB. Generally, d-ABs exhibit higher isomerization quantum yields than AB, and can easily be photoisomerized in picoseconds from the *trans* to the *cis* isomer by irradiation with visible light that is paramount for biology applications. However, because the $\pi \rightarrow \pi^*$ and the $n \rightarrow \pi^*$ absorption bands overlap; the isomerization from the *cis* to the *trans* isomer via irradiation is impossible. In d-AB, the *cis to-trans* isomerization can only occur via thermal relaxation, which is much slower (milliseconds to days) than the photoisomerization of the *cis*-to-*trans*-AB isomer.

Incorporating an electron rich redox-active (RA) arylamino moiety into the overall structure of AB will result in a redshift of the $\pi \rightarrow \pi^*$ absorption band (to longer wavelengths), and as a result it will lead to overlap of the $\pi \rightarrow \pi^*$ and the $n \rightarrow \pi^*$ absorption bands. The incorporation of a RA into the overall structure of AB can also decrease the relaxation time of *cis*-to-*trans* isomerization. These new redox-appended azo switches are capable of efficient "photo-closing" to the *cis* isomer and rapid isomerization to the *trans* isomer (within picoseconds) via a catalytic electron transfer cycle. This electron transfer is mediated by "oxidative-opening" to *trans* on exposure to an oxidant or a voltage. Figure 2.1.1 illustrates a model of the mono(RA)AB photo-electro switch. The *trans* isomer (blue) isomerizes to the *cis*

isomer (red) by photo-absorption, and the *cis* isomer (red) then rapidly isomerizes to the *trans* isomer (blue) upon one electron removal.

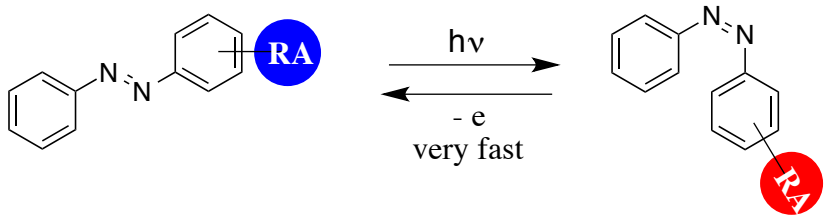

Figure 2.1.1 Model of the mono(amino) azobenzene photo-electro switch. The *trans* isomer (blue) isomerizes to the *cis* isomer (red) by photo-absorption, and the *cis* isomer (red) then rapidly isomerizes to the *trans* isomer (blue) upon removal of an electron.

2.2 *para*-arylaminoazobenzenes: *p*AA-Ph-N=N-Ph 4a and *p*AA-Ph-N=N-An 5a

The first redox-appended azo switches to be discussed in this manuscript are the *para*-arylamino-substituted azobenzenes, *p*AA-Ph-N=N-Ph **4a** and *p*AA-Ph-N=N-An **5a**. Scheme 2.2.1 and Scheme 2.2.2 depict their synthetic routes, respectively. We used arylamine **3** as our redox auxiliary (RA) because of its excellent redox properties; it is chemically stable in both neutral and radical cation forms. The basic premise of our work is that the radical cation, *cis*-$AA^{\bullet+}$-azo, will be much more reactive toward *cis*-to-*trans* isomerization than its neutral form. Thus, removal of one electron from *cis*-AA-azo to make *cis*-$AA^{\bullet+}$-azo induces rapid *cis*-to-*trans* isomerization in the azo moiety. The azo group immediately isomerizes back to the *trans* isomer. The efficiency of redox activation on azo opening may depend upon the placement of the RA moiety on the AB skeleton.

Synthesis:

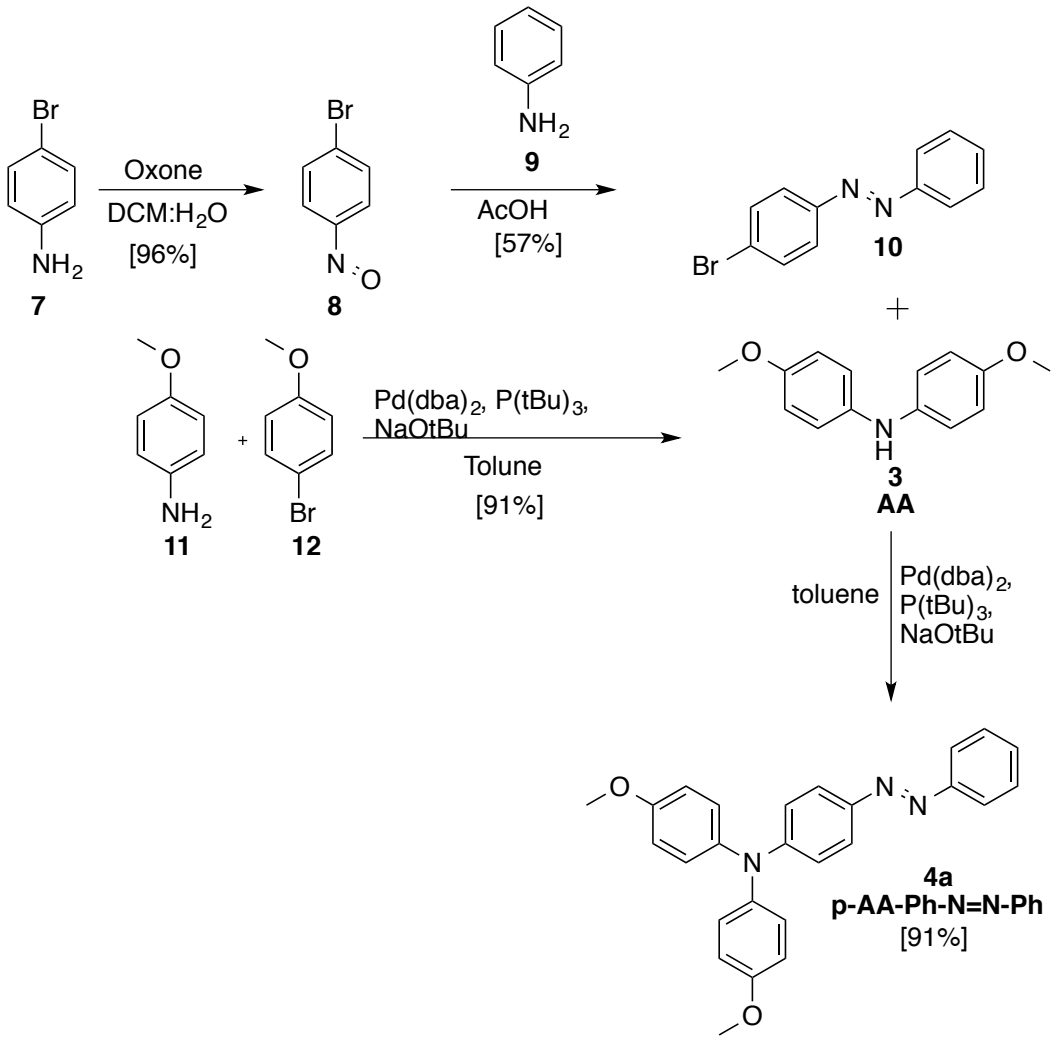

Scheme 2.2.1 Synthetic route to obtain *p*AA-Ph-N=N-Ph **4a**.

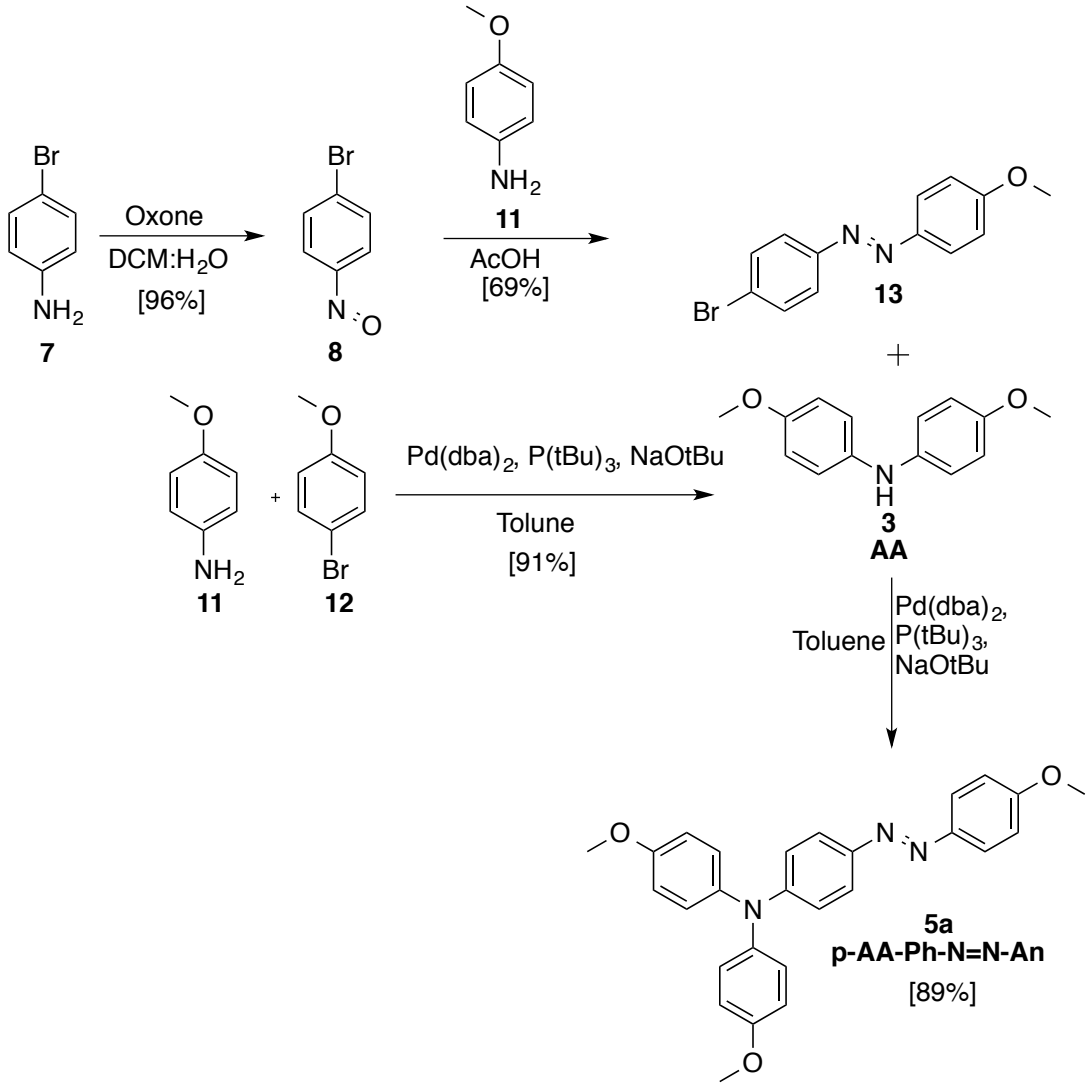

Scheme 2.2.2. Synthetic route to obtain *p*AA-Ph-N=N-An **5a**.

2.2.1 Photochemistry and optical absorption of 4a and 5a

We predicted that placing **3** at the 4- position of AB would result in a bathochromic shift of the $\pi \rightarrow \pi^*$ absorption band in the absorption spectrum. It is also expected that the $\pi \rightarrow \pi^*$ and the $n \rightarrow \pi^*$ absorption bands would overlap for both **4a** and **5a**. This bathochromic shift is beneficial because it positions the $\pi \rightarrow \pi^*$ absorption band in the visible region of the spectrum where visible light can be applied to isomerize both **4a** and **5a** to their respective *cis* isomers, **4b** and **5b**. However, in these two systems, return to the *trans* isomer via "photo-opening" is not

possible due to the overlap of the two transitions. The isomerization of **4b** and **5b** to their corresponding *trans* isomers can only occur by allowing the *cis* isomers to thermally relax to their respective *trans* isomers, which poses a problem when using AB derivatives as molecular switches because it cannot be turn on and off on demand.

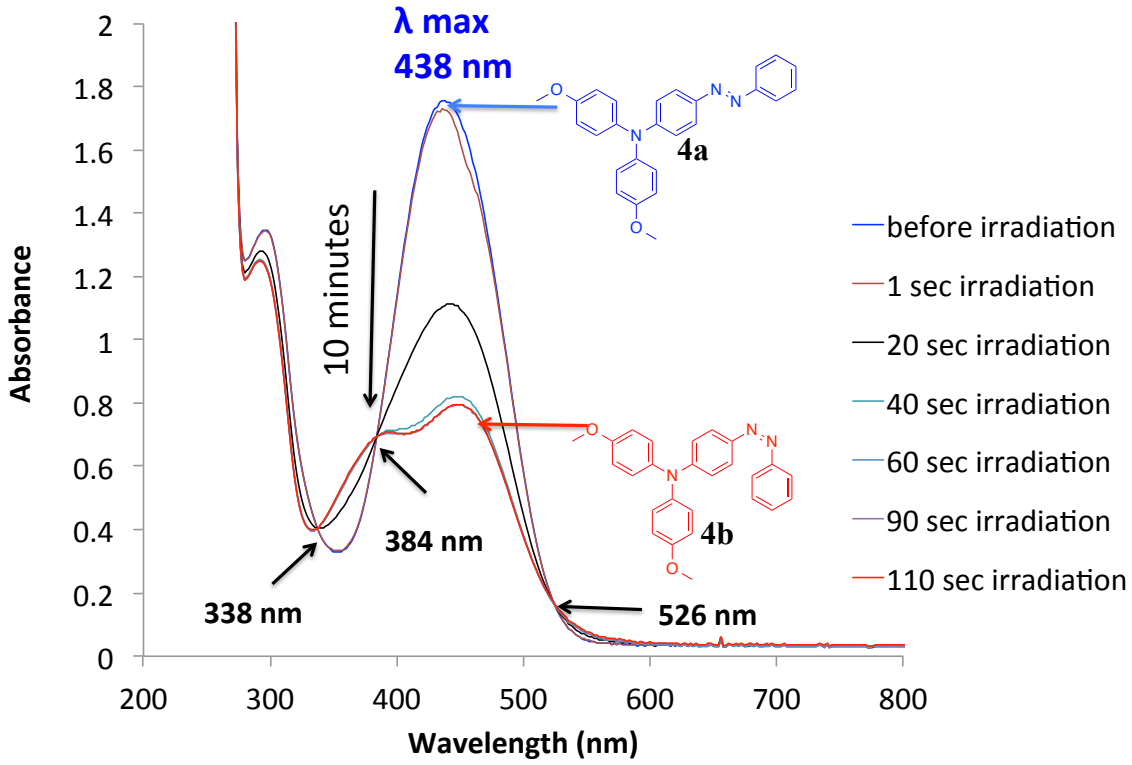

Figure 2.2.1. Optical spectrum of **4a** (6.35 x 10^{-4} M in C_6D_6) irradiated with a 430 nm LED at room temperature in 0.1 cm quartz UV-Vis cell.

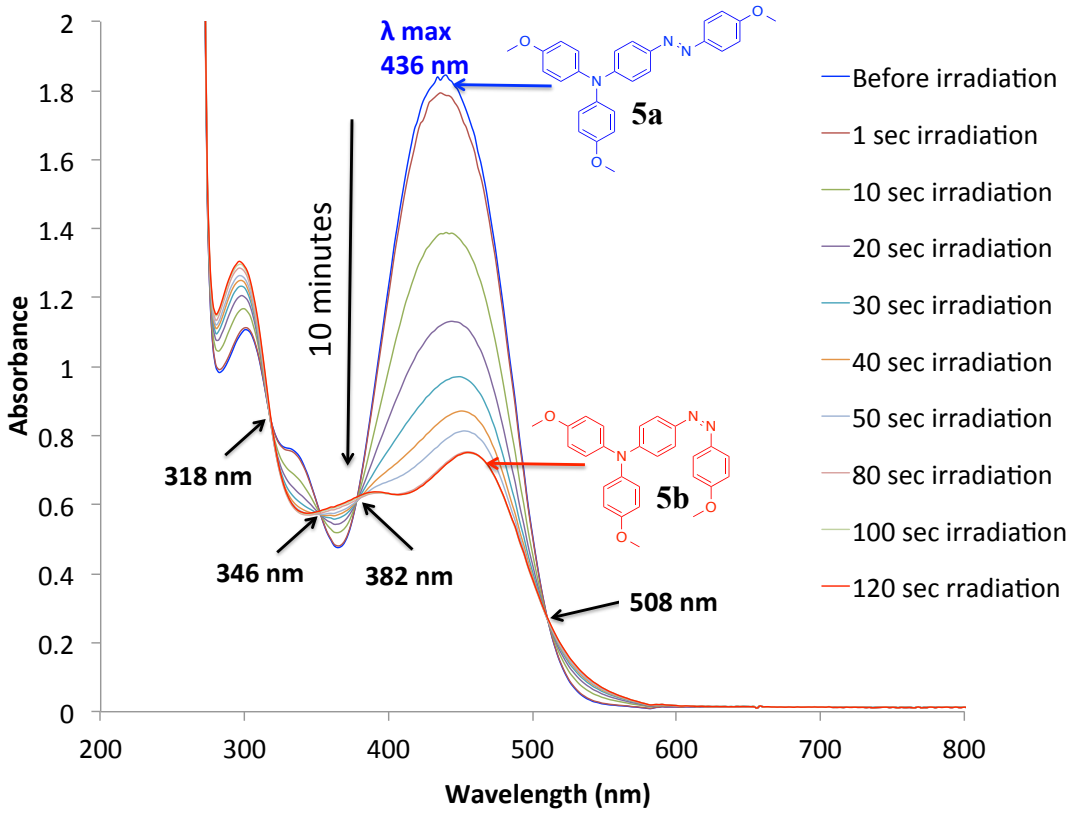

Figure 2.2.2. Optical spectrum of **5a** (6.37×10^{-4} M in C_6D_6) irradiated with a 430 nm LED at room temperature in 0.1 cm quartz UV-Vis cell.

Ultraviolet-visible spectroscopy is a valuable tool in determining the light source needed to isomerize **4a** and **5a** to their corresponding *cis* isomers. Figure 2.2.1 and Figure 2.2.2 illustrate the *trans*-to-*cis* photoisomerization of **4a** and **5a**, respectively. In **4a** and **5a**, the *trans*-to-*cis* isomerization occurs upon excitation of the $\pi \rightarrow \pi^*$ absorption band at 400-515 nm (2.41 eV), while the *cis*-to-*trans* isomerization cannot occur via photo excitation of the $n \rightarrow \pi^*$ absorption band because the two transitions overlap. *Cis-to-trans* isomerization can only occur thermally.

The optical spectra in Figure 2.2.1 and Figure 2.2.2 exhibit a strong π → π* absorption maximum at 438 nm and 436 nm for **4a** and **5a**, respectively. The n → π* absorption bands for both **4a** and **5a** cannot be resolved until the lowering of the absorbance due to π → π* transition band. However, after irradiating the π → π* absorption band with a 430 nm LED light source and reaching PSS, the n → π* absorption band becomes visible with a weak absorption maximum at 448 nm for **4a** to **4b** with three isosbestic points at 338 nm, 384 nm and 526 nm and a weak absorption maximum at 452 nm for **5a** to **5b** with four isosbestic points at 318 nm, 346 nm, 382 nm and 508 nm.

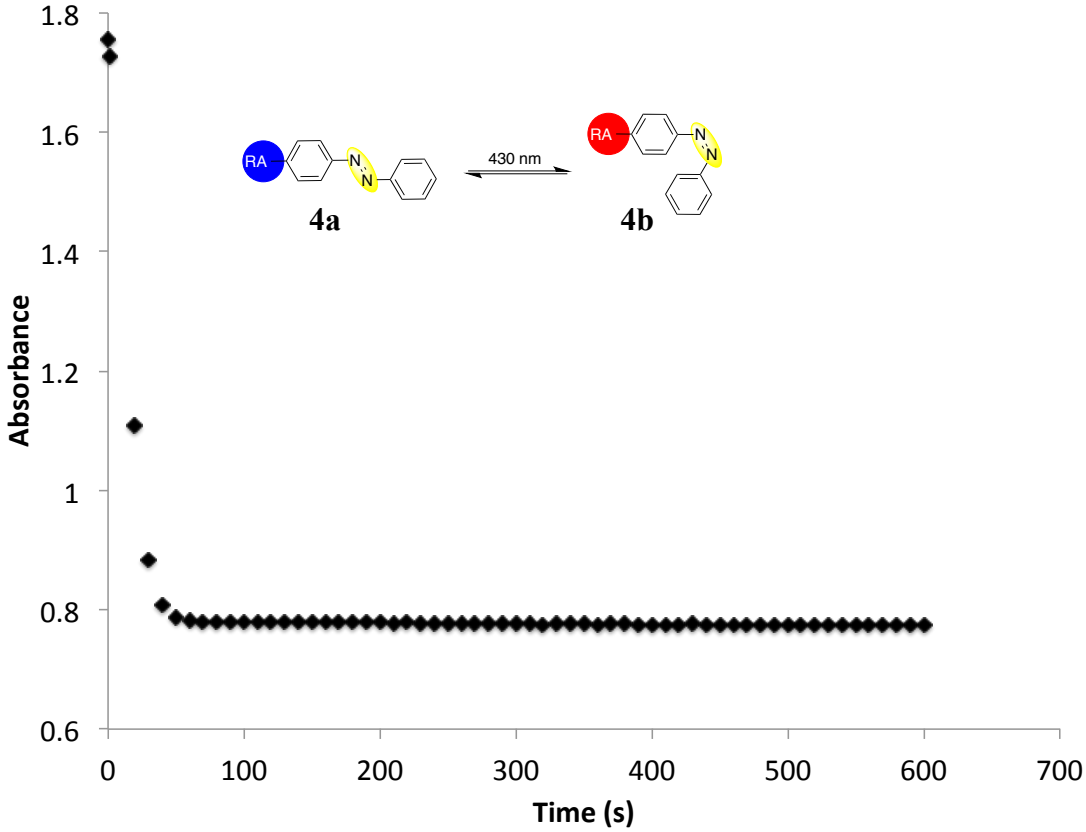

Figure 2.2.3. Absorption intensity was monitored at 438 nm and shows the establishment of a PSS for **4a** (6.35 x 10^{-4} M in deaerated C_6D_6) using 0.1 cm quartz UV-Vis cell at room temperature.

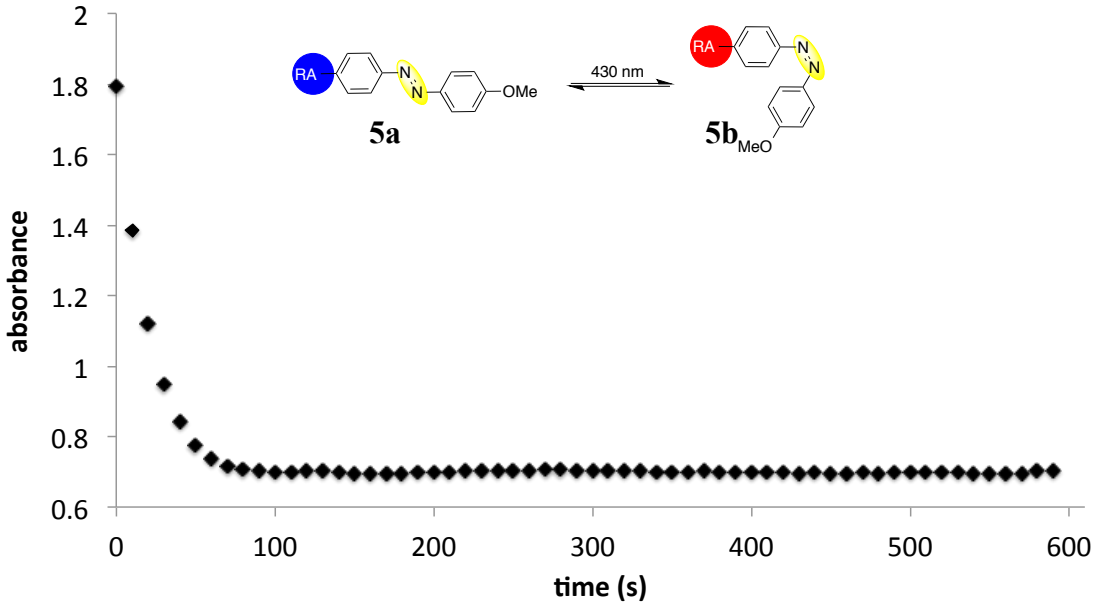

Figure 2.2.4. Absorption intensity was monitored at 436 nm and shows the establishment of a PSS for **5a** (6.37×10^{-4} M in deaerated C_6D_6) using 0.1 cm quartz UV-Vis cell at room temperature.

The time to reach PSS was determined by following the absorption maximum at 438 nm and 436 nm for **4a** and **5a** during irradiation, respectively as illustrated in Figures 2.2.3 and 2.2.4. After about 1 minute of irradiation, no changes in absorbance were observed. Figures 2.2.3 and 2.2.4 demonstrate the PSS was established for both systems as shown by the plateau of the absorbance.

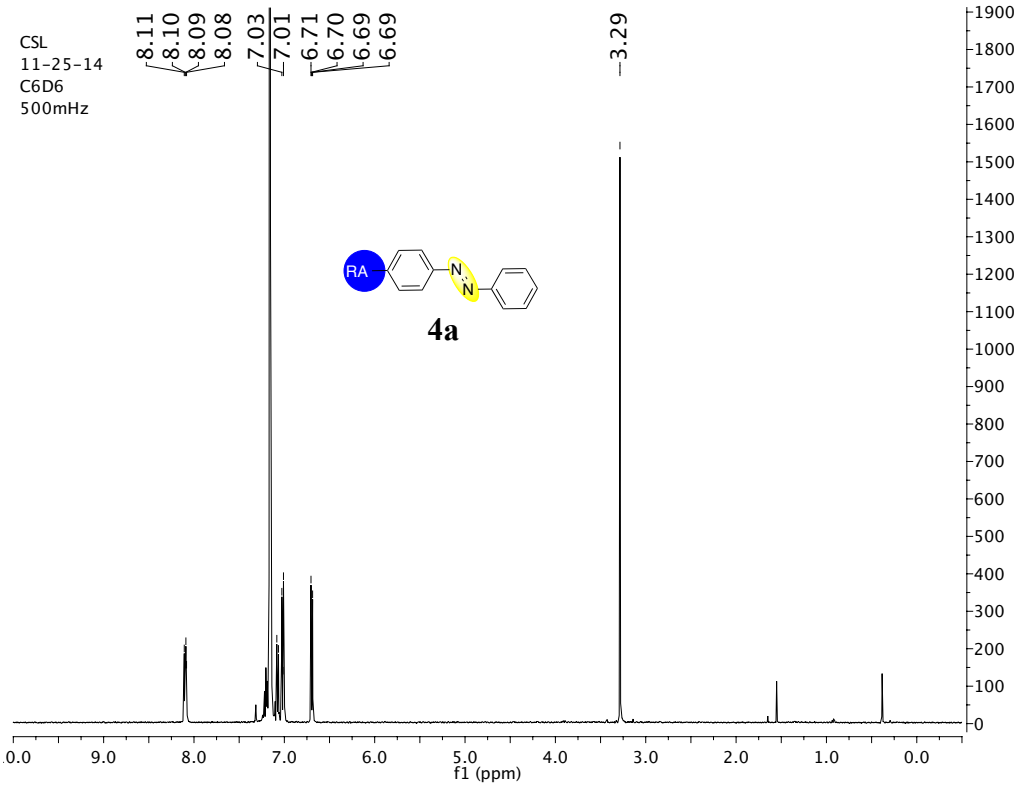

Figure 2.2.5. Full ^{1}H NMR spectrum of completely **4a** (1.67 x 10^{-2} M in C_6D_6) before irradiation.

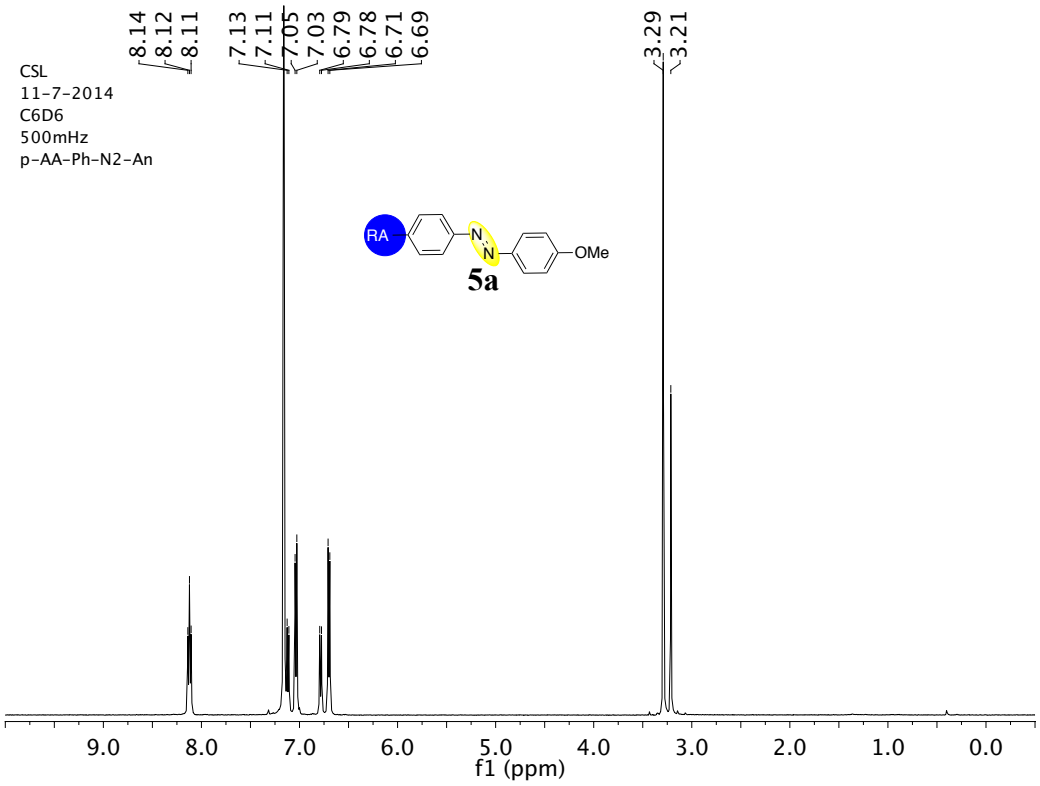

Figure 2.2.6. Full ^{1}H NMR spectrum of completely **5a** (1.63 x 10^{-2} M in C_6D_6) before irradiation.

The isomeric ratios of **4a:4b** and **5a:5b** at PSS were determined via ^{1}H NMR spectroscopy in C_6D_6 at room temperature. Figure 2.2.5 and Figure 2.2.6 demonstrate the full spectra for **4a** and **5a** in C_6D_6 before irradiation, respectively.

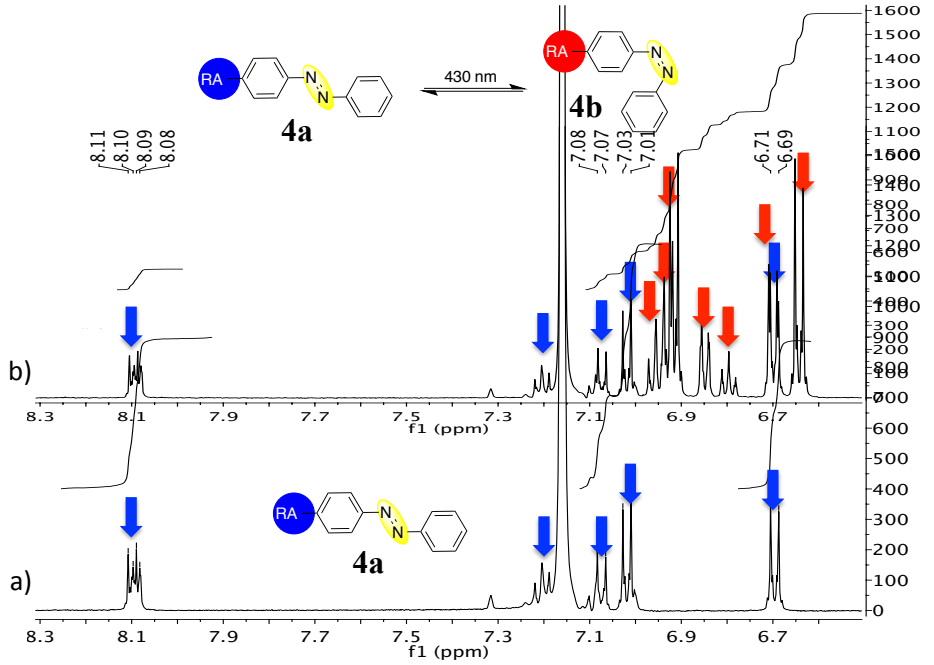

Figure 2.2.7. Expanded view of the aromatic section in the ^{1}H NMR spectrum of **4a** (1.67 x 10^{-2} M in C_6D_6). **a**) Spectrum before irradiation **b**) PSS spectrum after irradiation with 430 nm LED light. PSS is established at a 29:71 **4a**:**4b** ratio at room temperature. Blue arrows indicate **4a** and red arrows indicate **4b**.

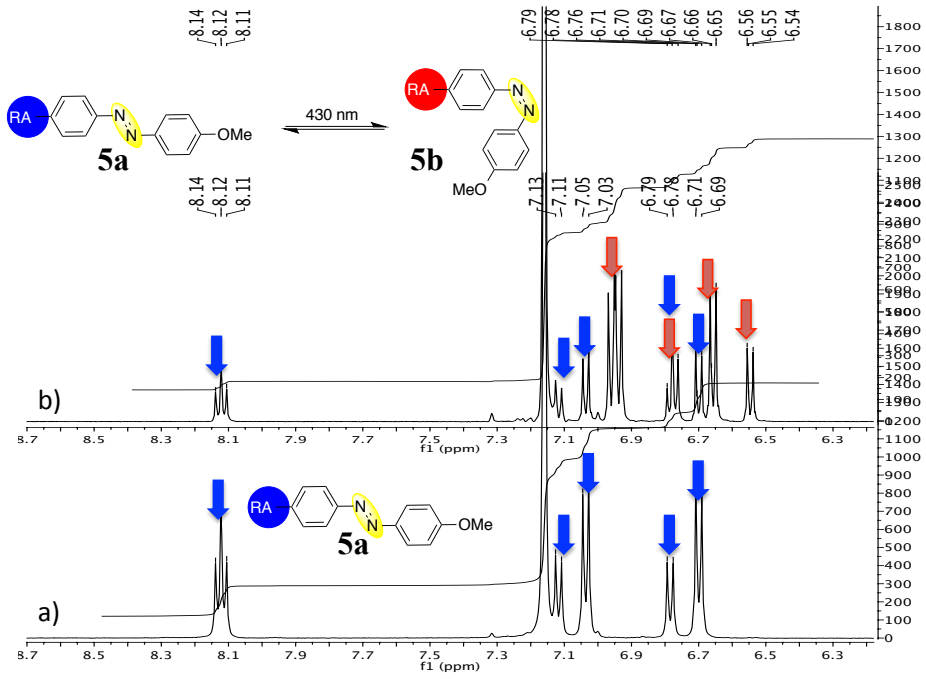

Figure 2.2.8. Expanded view of the aromatic section in the ^{1}H NMR spectrum of **5a** (1.63 x 10^{-2} M in C_6D_6). **a**) Spectrum before irradiation **b**) PSS spectrum after irradiation with 430 nm LED

light. PSS is established at a 32:68 **5a**:**5b** ratio at room temperature. Blue arrows indicate **5a** and red arrows indicate **5b**.

Expanded views of the aromatic sections of in the ^{1}H NMR spectra of **4a** and **5a** before irradiation and at the PSS are illustrated in Figure 2.2.7 and Figure 2.2.8, respectively. The spectra of the aromatic sections confirm there are mixtures of *cis* and *trans* isomers at the PSS in both cases. The two isomers can be easily detected via ^{1}H NMR spectroscopy experiment since the isomers have different structural orientations. As a result, each isomer will possess different aromatic signals.

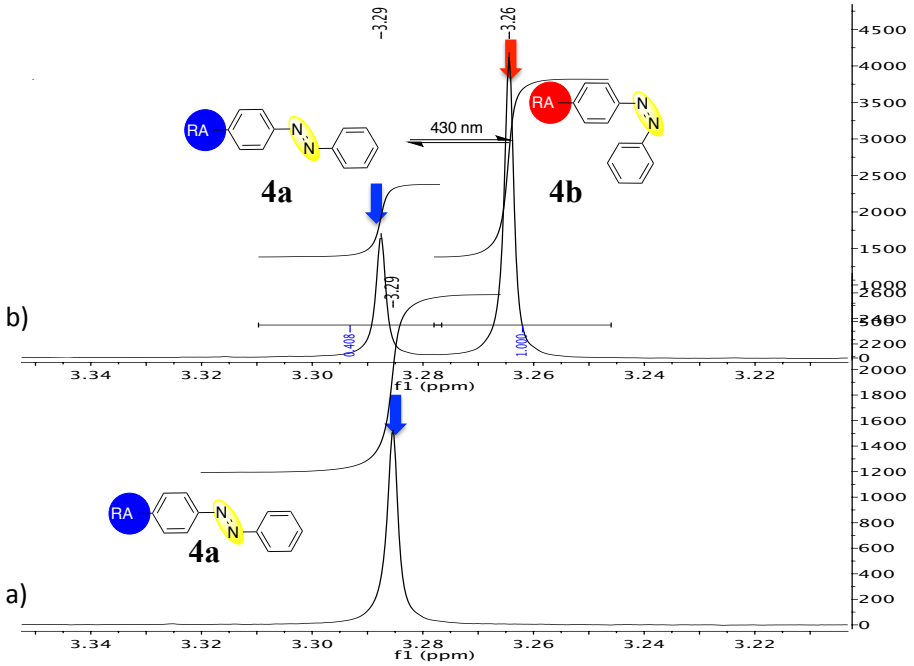

Figure 2.2.9. Expanded view of the alkyl section in the ^{1}H NMR spectrum of **4a** (1.67×10^{-2} M in C_6D_6) **a**) Spectrum before irradiation **b**) PSS spectrum after irradiation with 430 nm LED light. A PSS is established at a 29:71 **4a**:**4b** ratio at room temperature. Blue arrows indicate **4a** and red arrows indicate **4b**.

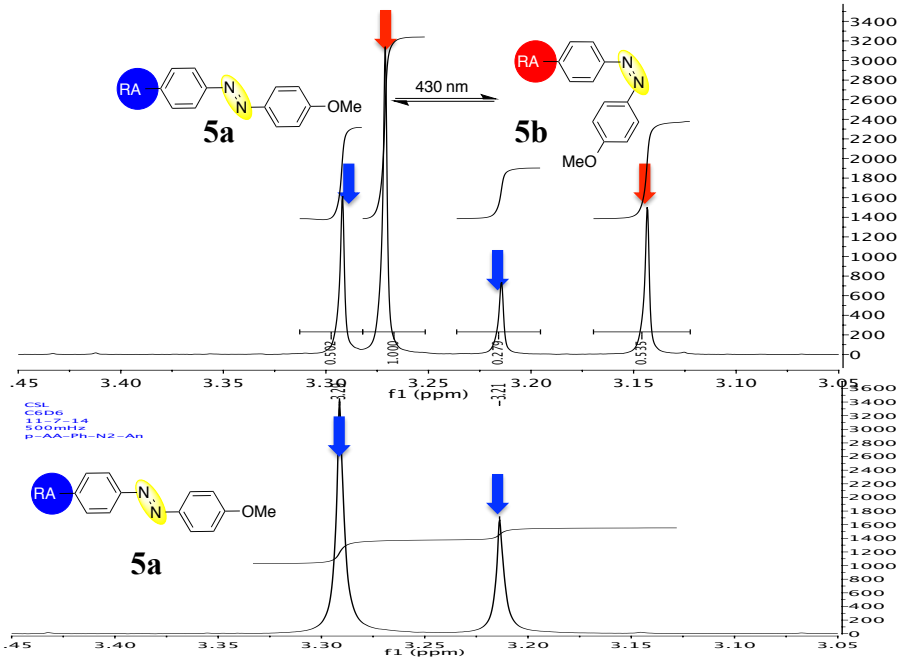

Figure 2.2.10. Expanded view of the alkyl section in the ^{1}H NMR spectrum of **5a** (1.63 x 10^{-2} M in C_6D_6) **a**) Spectrum before irradiation **b**) PSS spectrum after irradiation with 430 nm LED light. A PSS is established at a 32:68 **5a**:**5b** ratio at room temperature. Blue arrows indicate **5a** and red arrows indicate **5b**.

Similarly, the alkyl section of **4b** and **5b** should be distinct from the alkyl sections of their corresponding *trans* isomers, as illustrated in Figure 2.2.9 and Figure 2.2.10, respectively. Integration of the methoxy peaks in the alkoxy section of the ^{1}H NMR spectra in Figure 2.2.9 and Figure 2.2.10 were used to evaluate the isomeric ratio of **4a**:**4b** (29:71) and ratio of **5a**:**5b** (32:68) in the mixtures at the PSS.

2.2.2 Thermal *cis*-to-*trans* isomerization of 4a and 5a

After obtaining the isomeric ratio of **4a**:**4b** and **5a**:**5b** at the PSS**,** the stability of **4b** and **5b** at room temperature were examined to understand the effect of the RA moiety on the thermal isomerization process. The thermal reversibility from **4b** to **4a** and from **5b** to **5a** was monitored over a period of 24 hours via a UV-Vis spectroscopy experiment. After establishing a PSS for

4a and **5a**, spectra were taken at room temperature in the dark until there were no changes in the maximum absorbance.

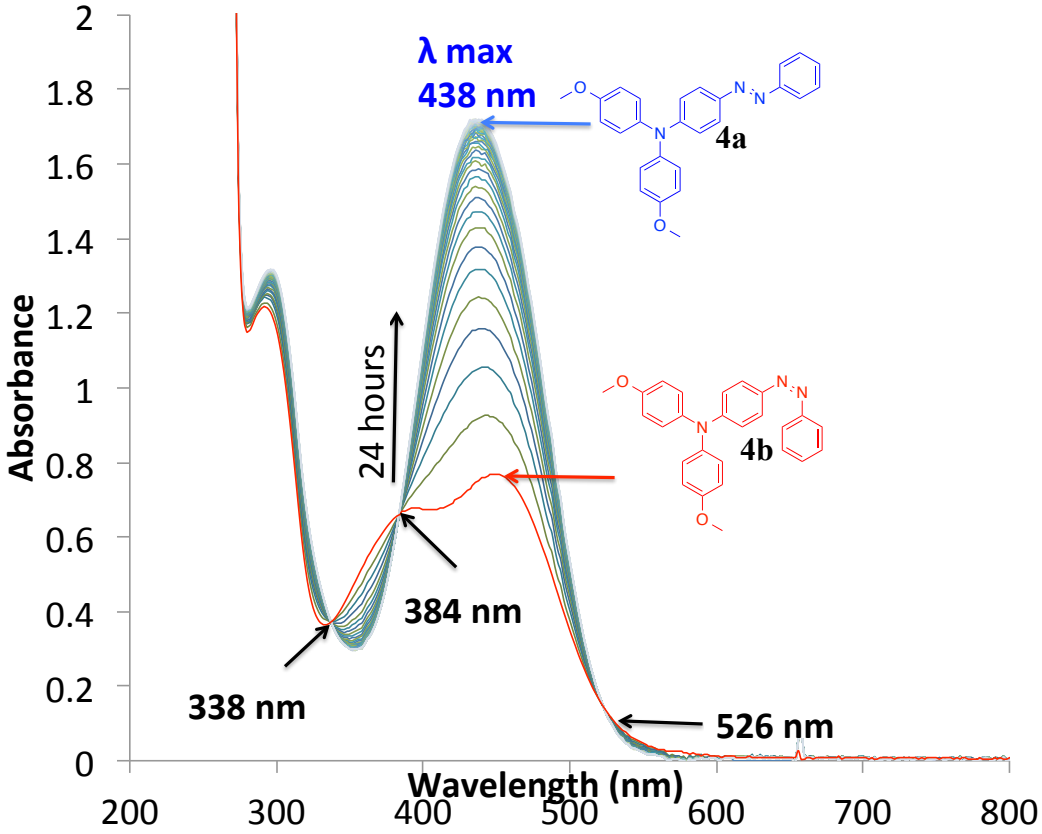

Figure 2.2.11. Optical spectrum of the thermal isomerization of **4b** to **4a** (6.35×10^{-4} M in C_6D_6) recorded every 30 minutes in the dark at room temperature in a 0.1 cm quartz cell after irradiating with a 430 nm LED to PSS (71:29 **4b:4a** ratio).

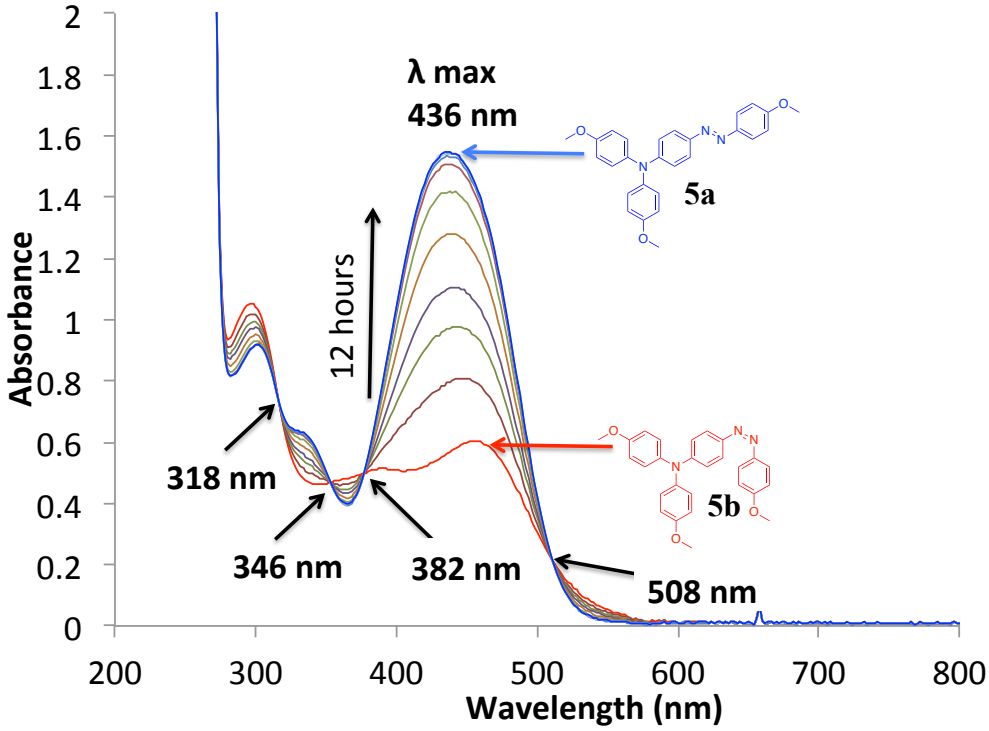

Figure 2.2.12. Optical spectrum of the thermal isomerization of **5b** to **5a** (6.37 x 10^{-4} M in C_6D_6) recorded every 10 minutes in the dark at room temperature in a 0.1 cm quartz cell after irradiating with a 430 nm LED to a PSS (68:32 **5b:5a** ratio).

The absorbance maximum was also utilized to monitor the thermal recovery of **4a** from **4b** and of **5a** from **5b** in the dark until no *cis* isomers were present. Figure 2.2.11 and Figure 2.2.12 demonstrate the decaying of the *cis* isomers and the recovery of the *trans* isomers over time in the dark until there were no changes in the spectra. The thermal isomerization process of **4b** was compared to the thermal isomerization process of **1b**. The thermal half-life of **1b** in solution at room temperature was experimentally measured to be approximately ~2 days.[64,65]

[64] Blevins, A. A.; Blanchard, G. J. Effect of Positional Substitution on The Optical Response of Symmetrical Disubstituted Azobenzene Derivatives" *J. Phys. Chem. B*. ,**2004**, *108*, 4962-4968.
[65] Crecca, R. C.; Roitberg, A.E. Theoretical Study of the Isomerization Mechanism of Azobenzene and Disubstituted Azobenzene Derivatives. *J. Phys. Chem. A.,* **2006**, *110*, 8188-8203.

Whereas, **4b** thermally isomerized back to **4a** at a rate of 8.4 x 10^{-5} ± 8.6 x 10^{-7} s^{-1} with a half-life of approximately 2.5 hours, as shown in Figure 2.2.13. As predicted, **4b** behaves as an da-AB and thermally isomerized to **4a** at a faster rate than **1b** thermally isomerized to **1a**.

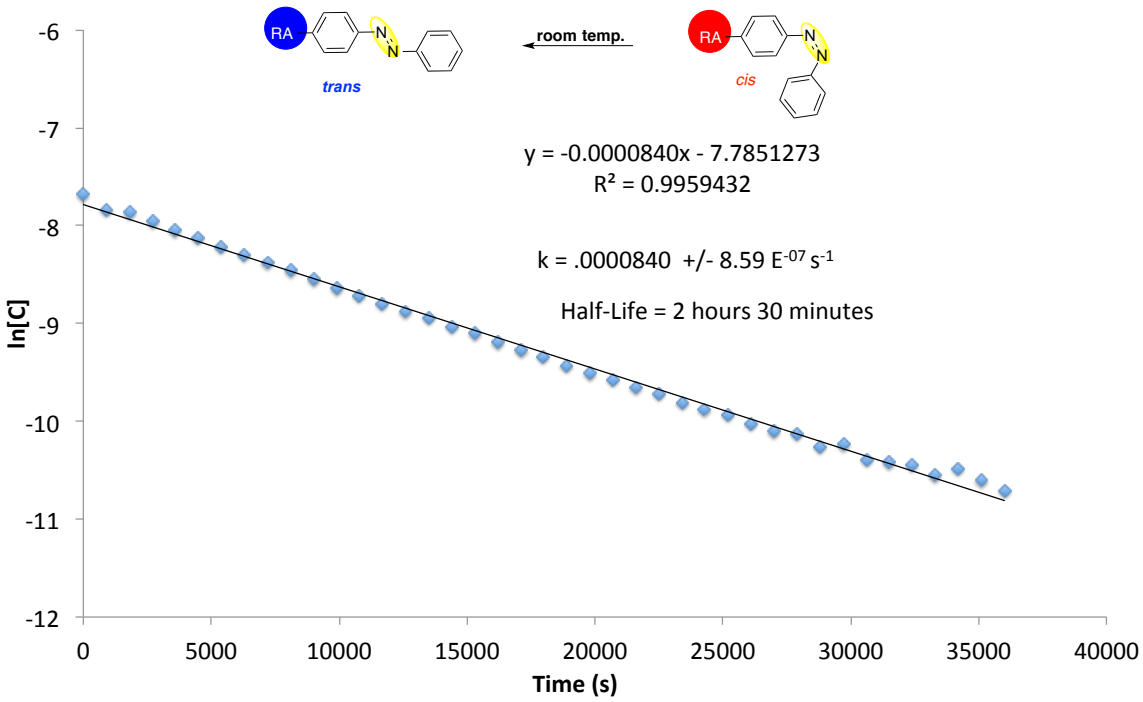

Figure 2.2.13. Determination of the thermal isomerization rate of **4b** to **4a** over 24 hour using a plot of ln[C] vs. Time where C is the ratio of *cis*- to *trans*.

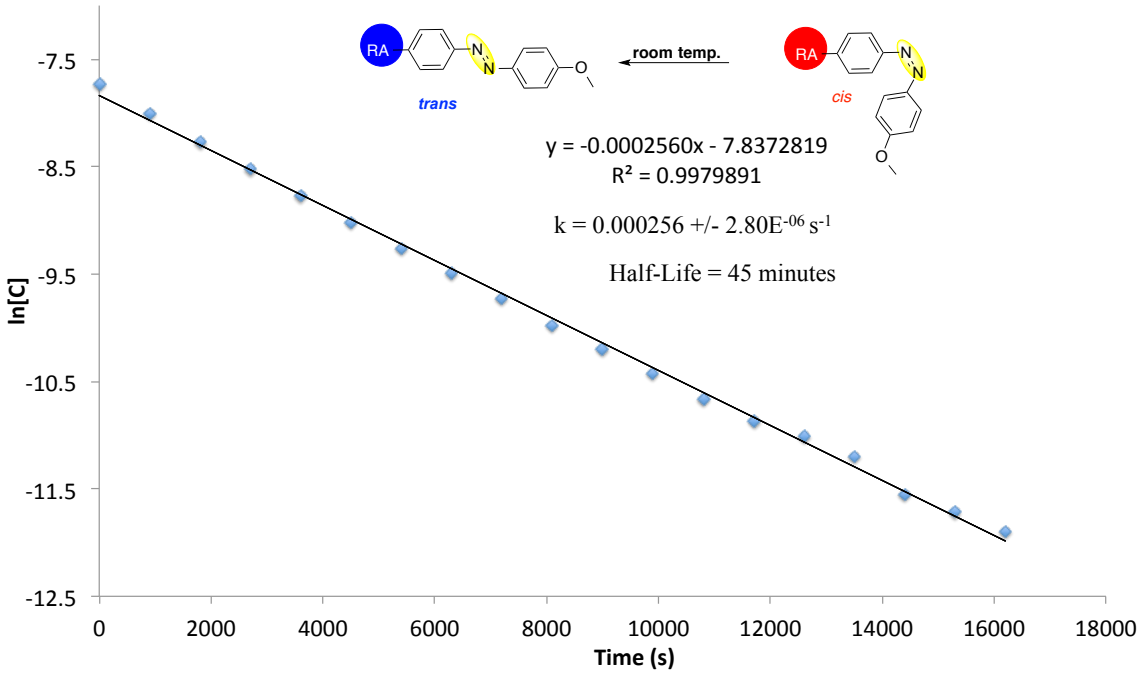

Figure 2.2.14. Determination of the thermal isomerization rate of **5b** to **5a** over a 12-hour time frame using plot of ln[C] vs. Time where C is the ratio of *cis*- to *trans*.

The thermal half-life of **5b** was also measured and it was found to thermally isomerize back to **5a** at a rate of 2.6 x 10^{-4} ± 2.8 x 10^{-6} s^{-1} that is a faster rate than **4b**. As expected, introducing an additional electron rich moiety, -OCH_3 at the 4′- position of the -N=N- group should increase the thermal isomerization rate from **5b** to **5a**. The **5b** isomer has a half-life of approximately 45 minutes, as shown in Figure 2.2.14.

To understand the thermodynamic effect of the RA group on **4b** and **5b,** it was necessary to experimentally measure the $\Delta G^{\neq}$ for their thermal isomerization in relation to their rates. The $\Delta G^{\neq}$ for the thermal isomerization for **4b** to **4a** was experimentally measured to be approximately 23.0 kcal mol^{-1}, which is lower than that for **1b** to **1a** known to be approximately 25.8 kcal mol^{-1}. Figure 2.2.15 displays the effect of the RA group on the $\Delta G^{\neq}$ for the thermal isomerization of **4b** at room temperature.

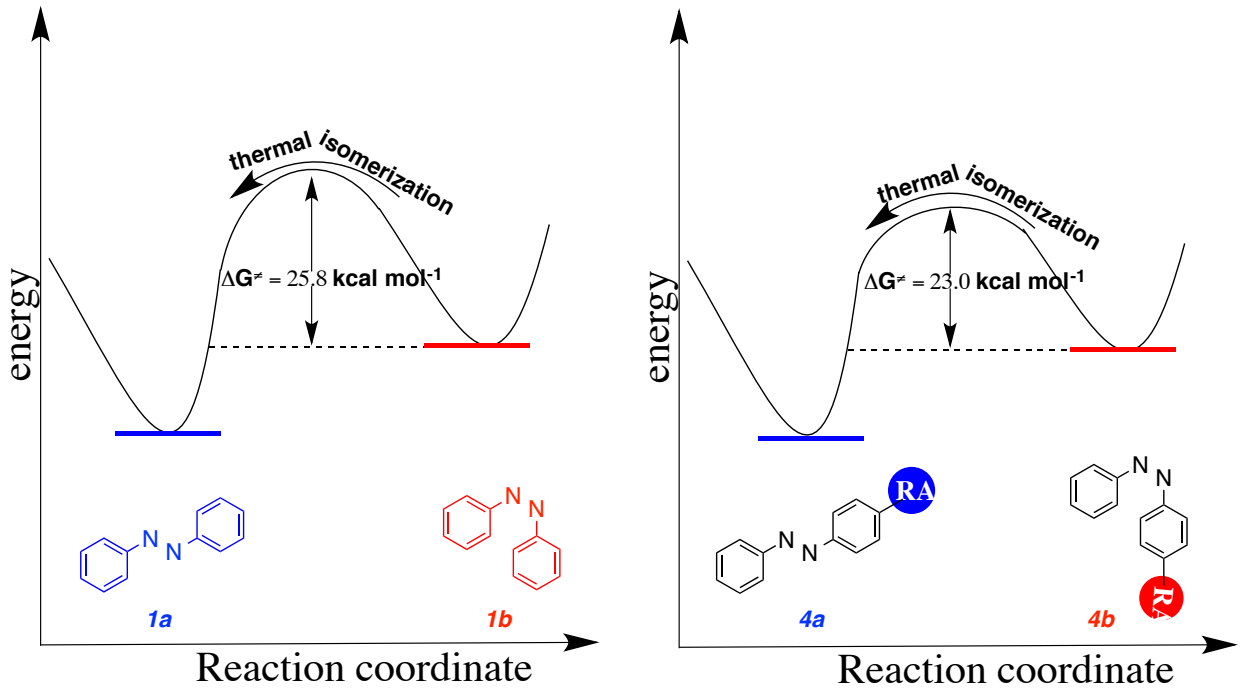

Figure 2.2.15. A potential energy diagram of **1** (left) and **4** (right) that illustrates the effects of **3** on the $\Delta G^{\neq}$ of **4b** to **4a.**

Examining the crystal structure of **4a** and comparing it to the crystal structure of triphenylamine can clarify the reasoning in difference of Gibbs free energy of activation. Figure 2.2.16 depicts the X-ray structure of triphenylamine

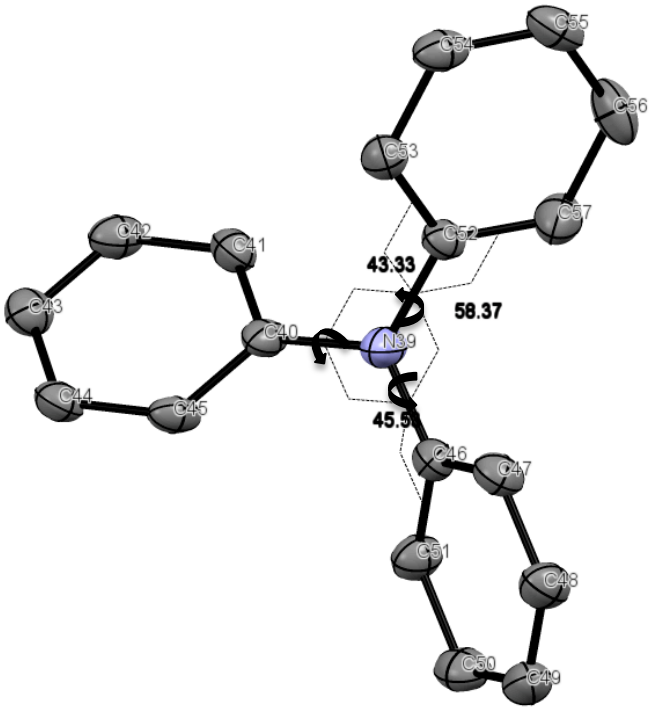

Figure 2.2.16. Crystal structure of triphenylamine illustrating a three-bladed propeller shape where all the aromatic rings are twisted.

Figure 2.2.16 shows that triphenylamine has a three-bladed propeller shape where all the aromatic rings are twisted almost equally with dihedral angles ∠C57C52N39C46 (58.37°), ∠C53C52N39C40 (43.33°), and ∠C51C46N39C40 (45.53°). This twisting in triphenylamine is necessary because it allows the lone pair on the nitrogen atom to be almost equally shared between the three phenyl rings.

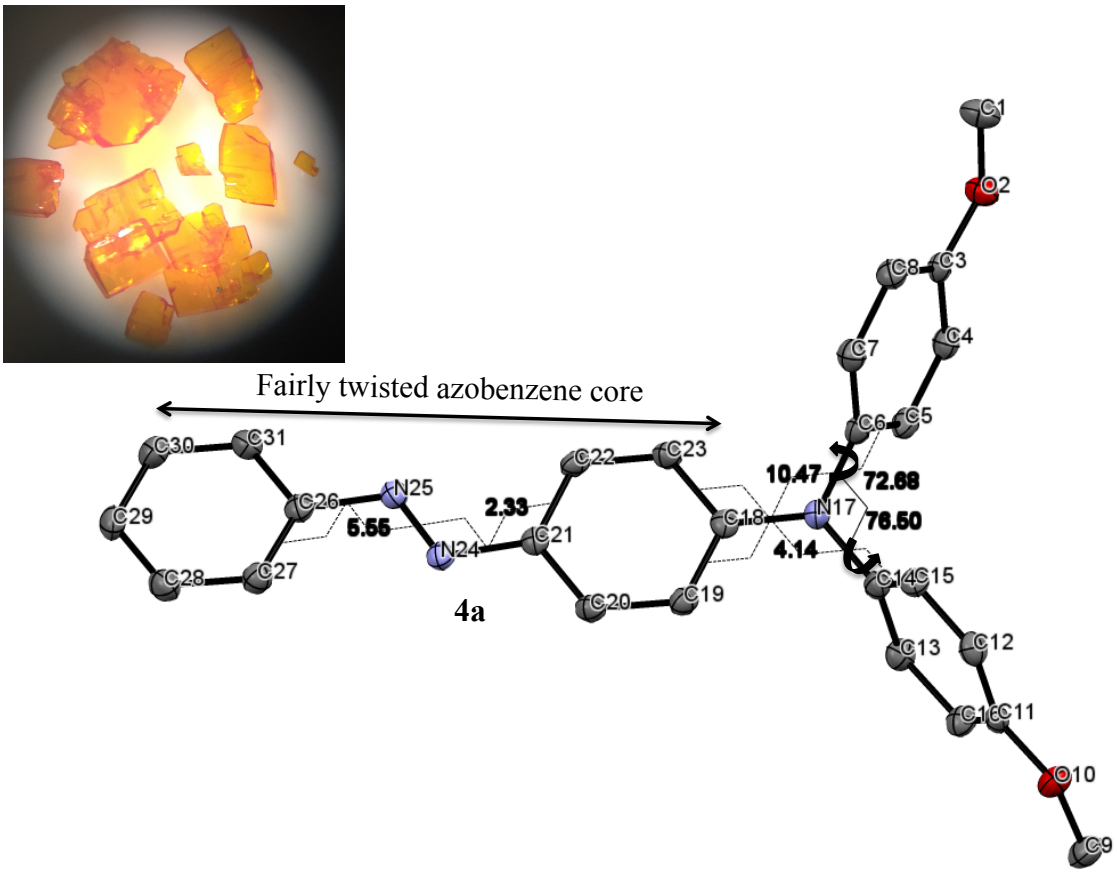

Figure 2.2.17. Crystal structure of **4a** illustrating the loss of propeller-shaped geometry. Twisting is increased in the phenyl rings of the RA group compare to triphenylamine. The AB core is planar to help create an extended pi system between the electron-withdrawing moiety, -N=N-, and the lone pair of the central nitrogen of RA group.

The crystal structure of **4a** is shown in Figure 2.2.17. The three-bladed propeller-shaped is lost as the azo group is added. The phenyl groups of the RA moiety are more twisted than that of triphenylamine with dihedral angles ∠C5C6N17C14 (72.68°), ∠C15C14N17C6 (76.50°) while the phenyl group of the AB core that is attached to the RA group is fairly planar to the RA group with dihedral angles ∠C19C18N17C14 (4.14°) and ∠C23C18N17C6 (10.47°) as illustrated in Figure 2.2.17.

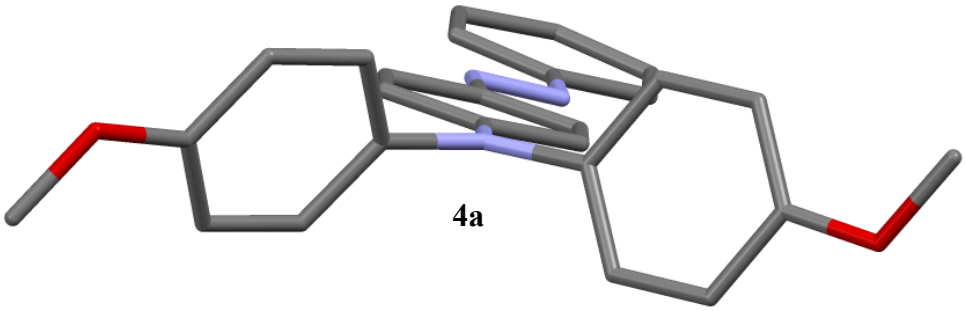

Figure 2.2.18. Cap and stick diagram of the crystal structure of **4a**. It illustrates that the AB core is planar to help align the pi orbitals of the AB phenyl group to the lone pair of the nitrogen atoms on the RA groups and the pi orbitals of the -N=N- group.

The decrease in twisting of the phenyl group attached to the RA moiety is necessary because it helps align its pi orbitals with the pi orbitals of the -N=N- group and the lone pair of the nitrogen atom of the RA group and as a result the AB core is nearly planar with dihedral angles of ∠C27C26N25N24 (5.55°) and C22C21N24N25 ∠ (2.33°) as illustrated in Figure 2.2.18.

The planarity of the AB core is essential because it helps stabilize **4a** by creating an extended pi system between the phenyl ring attach to the RA group, the electron withdrawing moiety, -N=N-, and the lone pair of the nitrogen atom of the RA group as illustrated in Figure 2.2.18. This spatial arrangement of **4a** allows for a donor-acceptor interaction through the extended pi system as illustrated in Figure 2.2.19a. However, due to a change in 3-D

conformation resulting from isomerization from **4a** to **4b**, the planarity of the extended pi system is disrupted, thus the conjugation that had extended from the -N=N- group to the lone pair of the nitrogen of RA group in **4a** is broken upon isomerization to **4b**. This effect in turn increased the energy of **4b** and decreased its stability compared to the **4a** as demonstrated in Figure 2.2.19b.

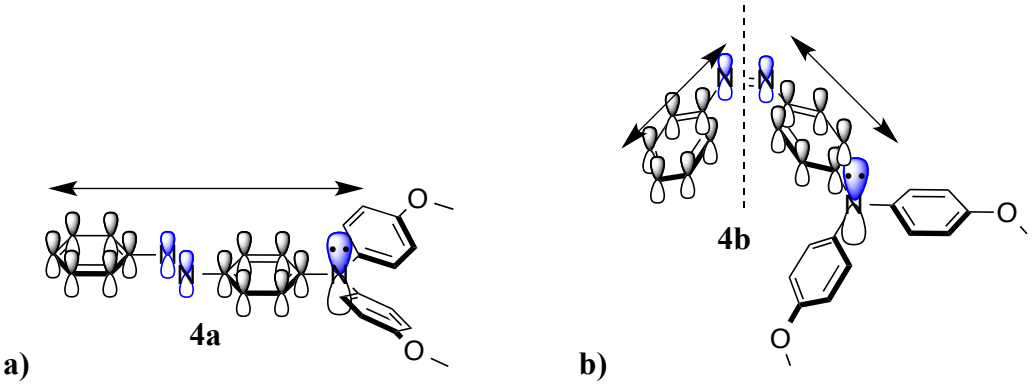

Figure 2.2.19. a) The planarity of the AB core helps stabilize **4a** by forming an extended pi system between the phenyl ring attach to the RA group, the electron-withdrawing group, -N=N-, and the electron rich group, the lone pair of the nitrogen of RA moiety **b**) The extended pi system is broken thus increasing the energy of **4b**.

Two major factors contribute to the destabilization of **1b**. The first factor is the steric interaction of the two phenyl rings in the *cis* conformation as illustrated in Scheme 1.1, and the second factor is the close proximity of the two lone pairs on the azo nitrogen atoms in the *cis* conformation that results in lone-pair - lone pair repulsion, as illustrated in Scheme 1.1. In comparison to **1b**, **4b** has more factors contributing to its destabilization. The first factor is the steric interaction of the two benzene rings in the *cis*- conformation, just as in **1b**. The second factor is the close proximity of the two lone pairs on the azo nitrogen atoms that results in repulsion, just as in **1b**. The third factor is the loss of the extended pi system throughout the molecule that results in the loss of the donor-acceptor interaction between the -N=N- group and the lone pair of the central nitrogen of RA group as shown in Figure 2.2.19. This third additional

factor results in a supplementary destabilization of **4b** by raising its energy relative to that of **1b**. As a result, the $\Delta G^{\neq}$ for the thermal isomerization from **4b** to **4a** is lower than that from **1b** to **1a** as shown in Figure 2.2.15, and this decreased $\Delta G^{\neq}$ leads to a decreased half-life of **4b** from ~2 days to 2.5 hours.

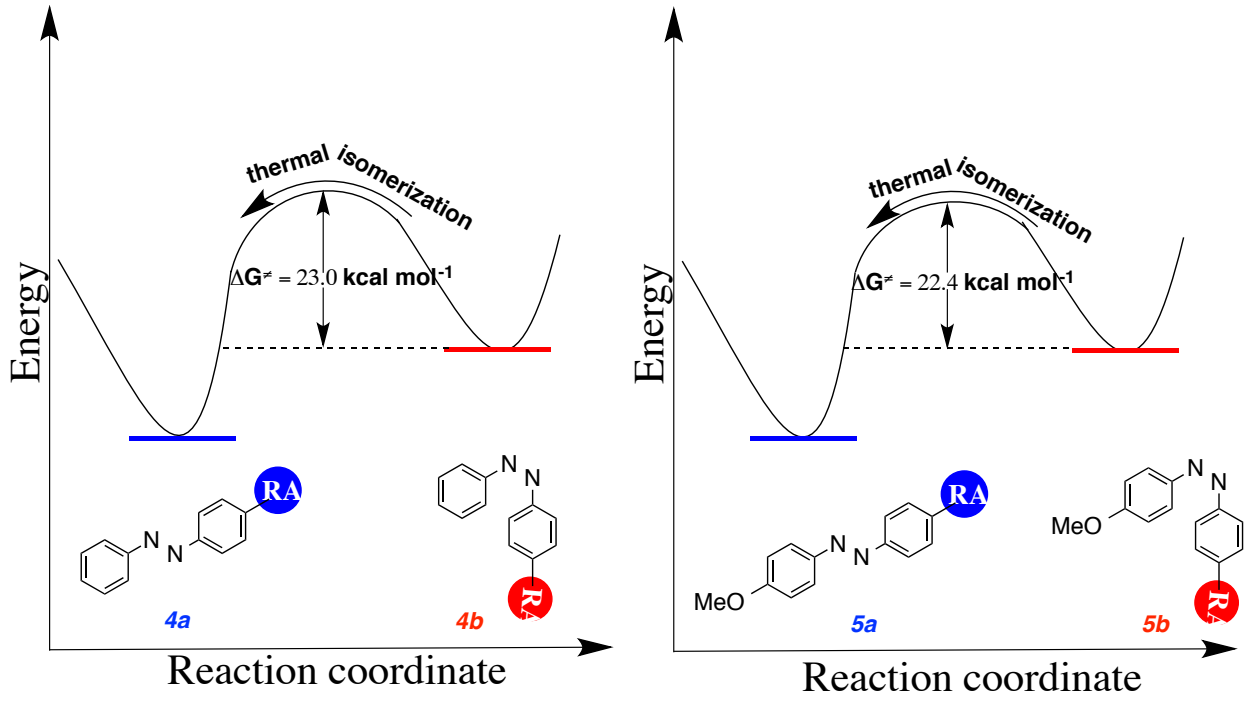

Figure 2.2.20. Potential energy diagram of **4** (left) and **5** (right). It illustrates the effects of an additional electron donating moiety on the $\Delta G^{\neq}$ of **5b** to **5a.**

The $\Delta G^{\neq}$ for the thermal isomerization from **5b** to **5a** was also experimentally measured to be approximately 22.4 kcal mol^{-1}, which is marginally lower than the 23.0 kcal mol^{-1} for the $\Delta G^{\neq}$ for the thermal isomerization **4b** to **4a** as shown in Figure 2.2.20. This slight difference in $\Delta G^{\neq}$ can explain the faster thermal isomerization time of **5b** in comparison to that of **4b.**

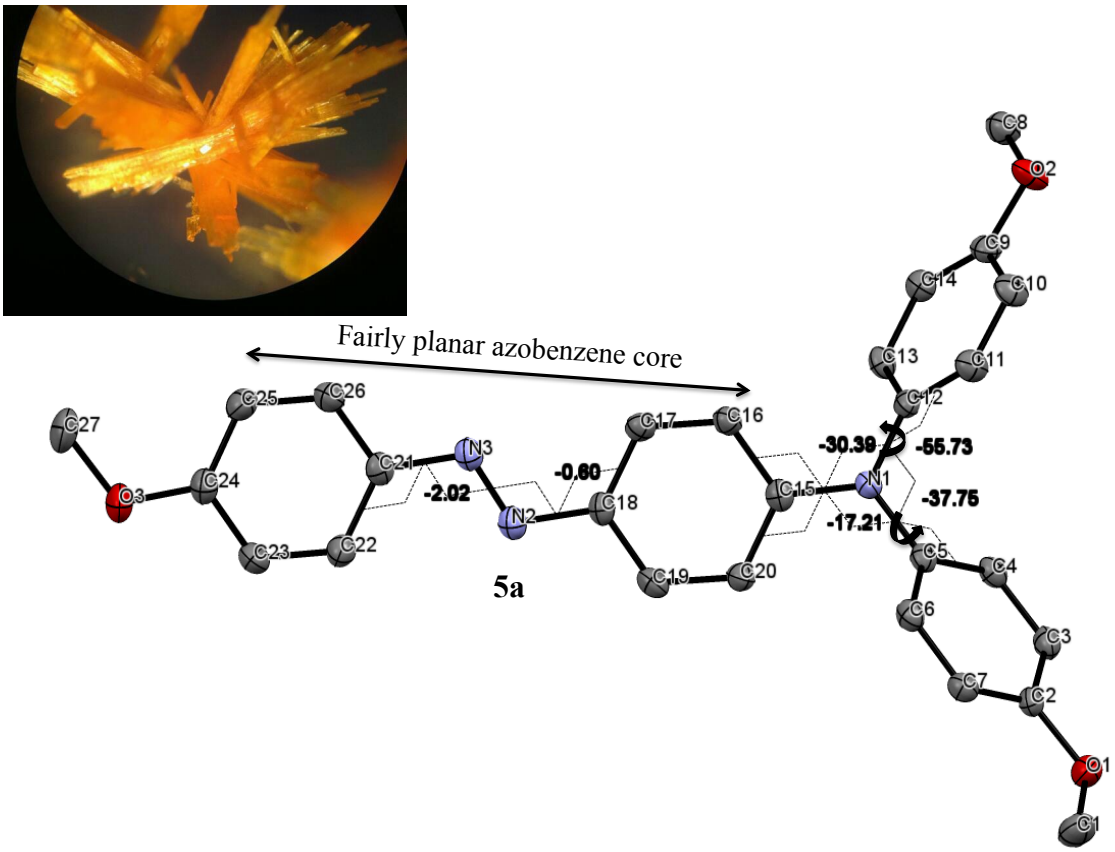

Figure 2.2.21. Crystal structure of **5a** illustrating loss of the propeller-shaped structure. Twisting is only observed in the two anisyl rings whereas the aromatic rings attached to the azo group are planar.

The crystal structure of **5a** is given in Figure 2.2.21. It also demonstrates the loss of the three-bladed propeller shape in **5a** as the azo group is added. As in **4a**, the phenyl groups of the RA moiety of **5a** are also twisted. However, they are less twisted than the phenyl groups of **4a** with dihedral angles of ∠C11C12N1C5 (55.73°) and C4C5N1C12 ∠ (37.75°). This difference can be explained by the addition of the -OCH_3 moiety at the 4′- position of the -N=N- group. This extra -OCH_3 acts as a secondary electron-donating substituent in conjugation with the -N=N- group, as a result the -N=N- group is in conjugation with two moieties, the -OCH_3 at the 4'-position and the RA group at the 4- position.

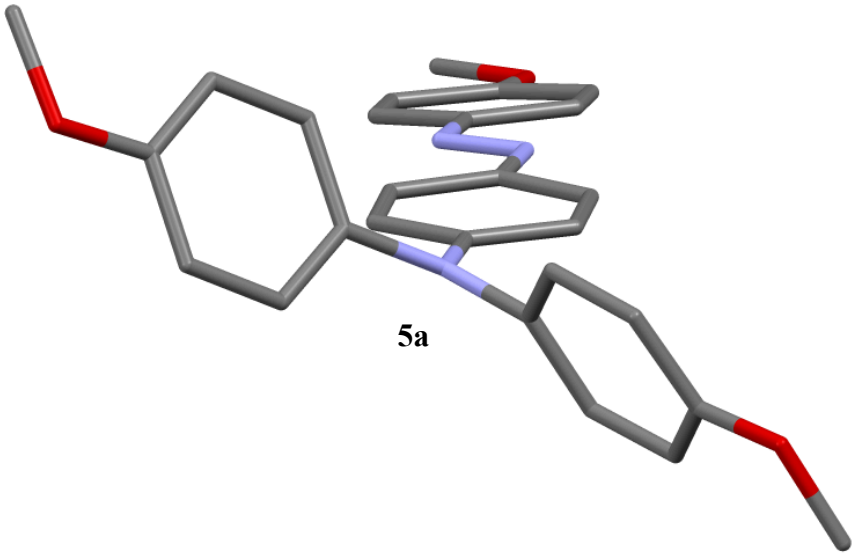

Figure 2.2.22. Cap and stick diagram of the crystal structure of **5a.** It illustrates that the AB core is planar to help create a donor-acceptor-donor interaction through an extended pi system by aligning the pi orbitals of the AB phenyl groups to the electron-withdrawing group, -N=N-, and the two electron rich groups, nitrogen (blue) and -OCH_3 (red).

As illustrated in Figure 2.2.22, the AB core of **5a** has an additional planarity with dihedral angles of ∠C22C24N3N2 (2.02°) and ∠C17C18N2N3 (0.60°). This increase in planarity of the AB core can be explained by the spatial arrangement of **5a** that allows for a donor-acceptor-donor interaction through an extended pi system between the electron-withdrawing group, -N=N-, and the two electron rich groups, RA and -OCH_3 as illustrated in Figure 2.2.22. However, once **5a** is isomerized to **5b**, the extended pi system between the -N=N- group and the two electron rich moieties, the -OCH_3 moiety and the electron pair on the nitrogen atom of the RA moiety, is broken and the energy of **5b** relative to **4b** increases as demonstrated in Figure 2.2.23b.

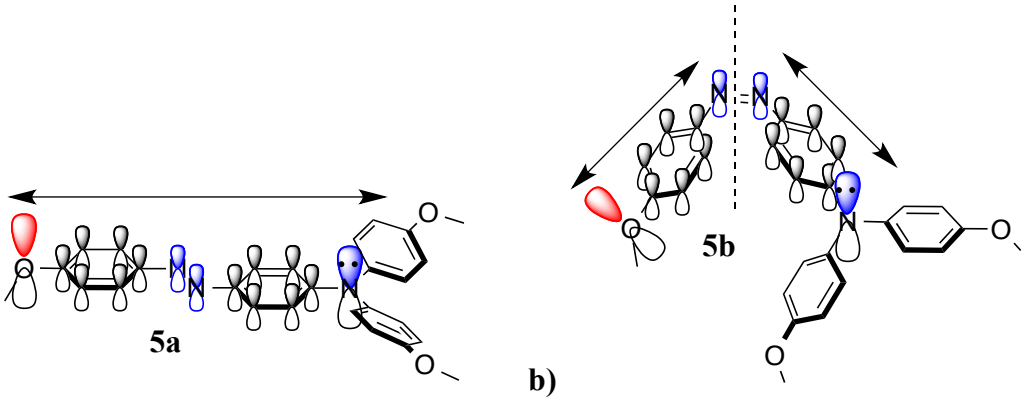

Figure 2.2.23. a) The planarity of the azobenzene core helps stabilize **5a** by forming an extended pi system between the electron-withdrawing group, -N=N-, and the two electron rich groups, nitrogen (blue) and -OCH_3 (red) **b**) The extended pi system is broken between the -N=N- group and the lone pairs on both of the electron rich nitrogen (blue) and -OCH_3 (red) thus increasing the energy of **5b**.

2.2.3 Electron Transfer Catalysis of *cis*-to-*trans* isomerization

In order to test whether the isomerization time of *cis*-to-*trans* isomerization for **4a** and **5a** could be exponentially decreased via a catalytic electron transfer cycle, it was necessary to select an oxidant with an oxidation potential greater than the oxidation potential of **4a** and **5a**. The cyclic voltammograms of **4a** and **5a**, shown in Figure 2.2.24 and Figure 2.2.25, provide the reversible oxidation potentials of **4a** as E° = 0.94 V (vs. SCE) and **5a** as E° = 0.85 V (vs. SCE), respectively.

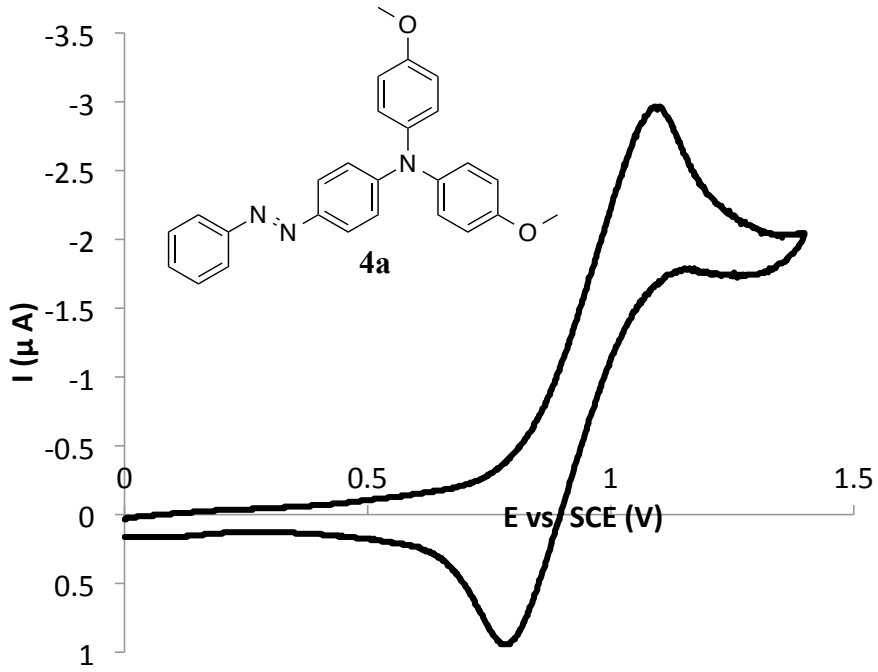

Figure 2.2.24. Cyclic voltammogram of **4a** (1.0 mM in dichloromethane with 0.1 M $TBABF_4$) at 20 mV/s scan rate with an $E^{\circ} = 0.94$ V (vs. SCE).

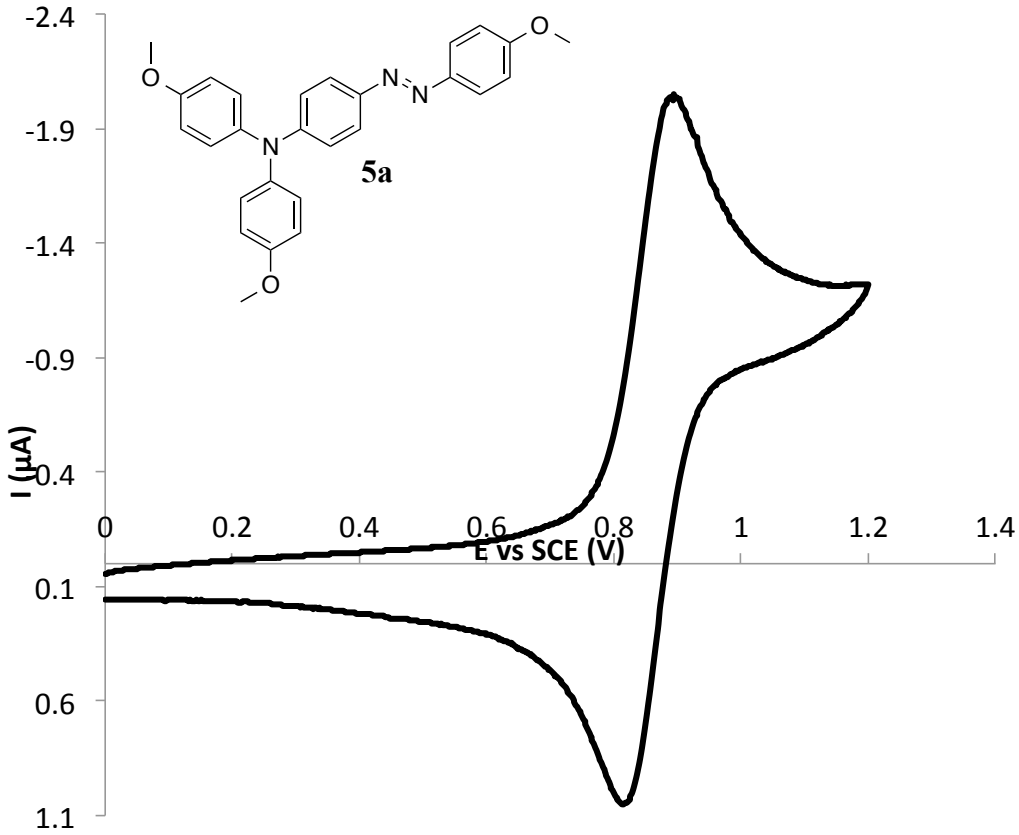

Figure 2.2.25. Cyclic voltammogram of **5a** (1.0 mM in DCM with 0.1 M $TBABF_4$) at 20 mV/s scan rate with an E° = 0.85 V (vs. SCE).

Figure 2.2.26 shows the cyclic voltammetry of the chosen oxidant, **6**. The oxidant, **6**, was chosen because of its stability at room temperature and its potent oxidation potential of 1.25 V (vs. SCE) that is higher than the oxidation potential of **4a** and **5a**.

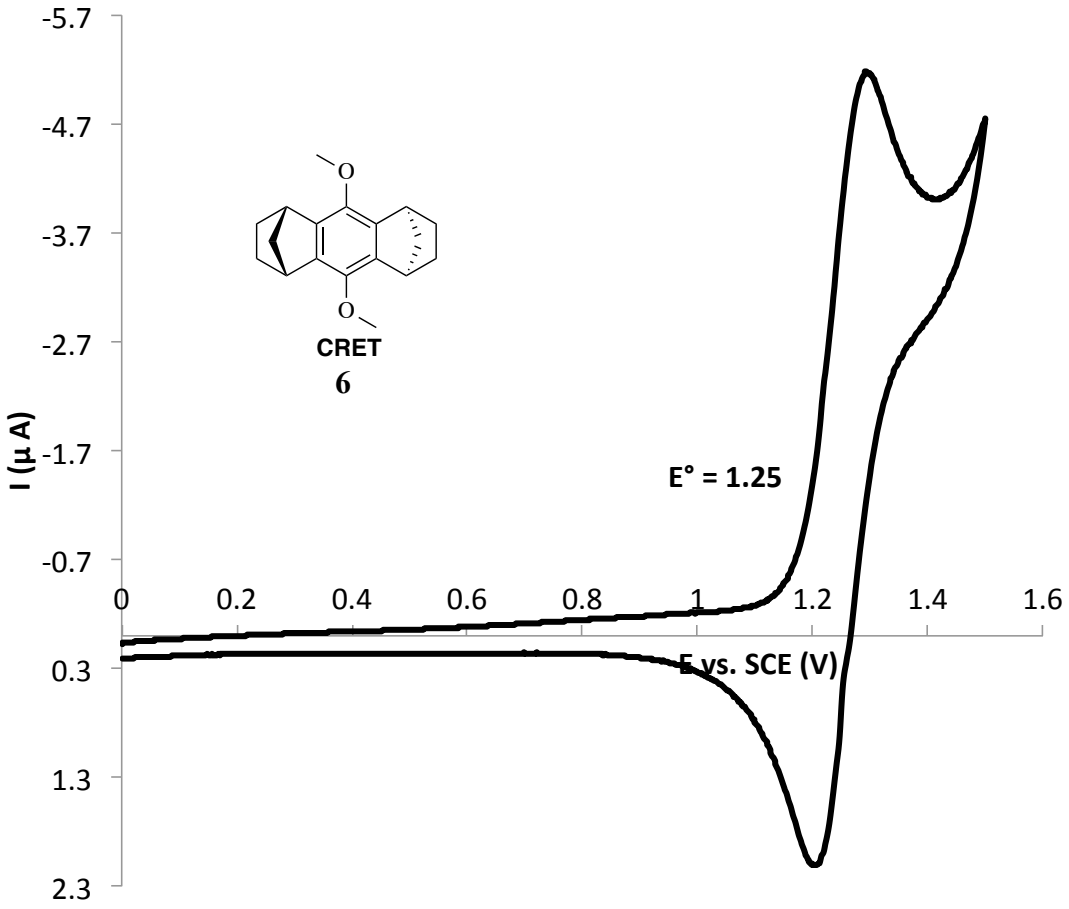

Figure 2.2.26. Cyclic voltammogram of **6** (1.0 mM in DCM with 0.1 M $TBABF_4$) at 20 mV/s scan rate with an E° = 1.25 V (vs. SCE).

Before attempting to oxidized **4b** and **5b**, the molecular orbital of the *cis* isomers were computed using density-functional theory with the B3LYP/6-31G** basis set to locate the energy level of the HOMO for each molecule and to confirm that the RA group would be the moiety interacting with the oxidant. Figure 2.2.27 illustrates the molecular orbitals in the HOMO of **4b**. It shows that the HOMO is predominantly located around and at the central nitrogen atom of the RA moiety. It also illustrates that the phenyl ring attached to the RA group possesses some amount of electron density, whereas the phenyl ring without the RA group was not as electron rich. It also indicates that the electron-dense rich phenyl ring is planar to the -

N=N- group in the *cis* form, whereas the phenyl ring lacking in electron density is twisted out of conjugation with the -N=N- group. This spatial arrangement of **4b** indicates that the lone pair of the central nitrogen atom of the RA group is in conjugation with the electron acceptor, -N=N- group, thus forming a donor-acceptor interaction in the *cis* form. This spatial arrangement also signifies that the removal of an electron from **4b** should disturb the -N=N- group by resonance. As a result, it would cause the -N=N- bond to break and convert into -N-N- then isomerize back to **4a**. Based on this result, it was safe to continue testing our electron transfer catalysis of *cis*-to-*trans* isomerization on **4b**.

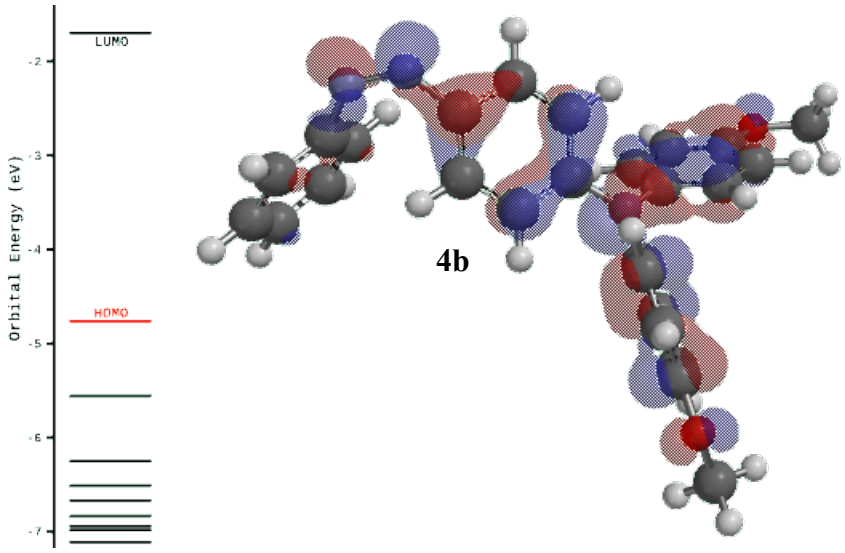

Figure 2.2.27. Density-functional theory calculations of **4b** with the B3LYP/6-31G** basis set. The HOMO is predominantly located at and around the central nitrogen atom of the RA group. The blue and red lobes indicate the orbital phases of the HOMO.

The molecular orbital of the *cis* isomer of **5b** were also computed using density-functional theory with the B3LYP/6-31G** basis set. Figure 2.2.28 illustrates that the HOMO is predominantly located around and at the central nitrogen atom of the RA moiety. It also illustrates that the phenyl ring attached to the RA group possesses a large amount of the electron density, whereas the phenyl ring deprived of the RA group possess a minimal amount of electron

density. As a consequence, the phenyl ring attached to the RA group is slightly twisted compared to the electron density rich phenyl ring of **4b** in the *cis*- form. Furthermore, the phenyl ring with the -OCH_3 group attached is also not planar to the -N=N- group. Similarly to **4b,** as a result of the planarity of the phenyl ring attached to the RA group, we can conclude that the spatial arrangement of **5b** positions the lone pair of the central nitrogen atom of the RA group into conjugation with the -N=N- group, thus forming a donor-acceptor interaction. Based on this result, it was safe to continue testing our electron transfer catalysis of *cis*- to *trans*- isomerization on **5b**.

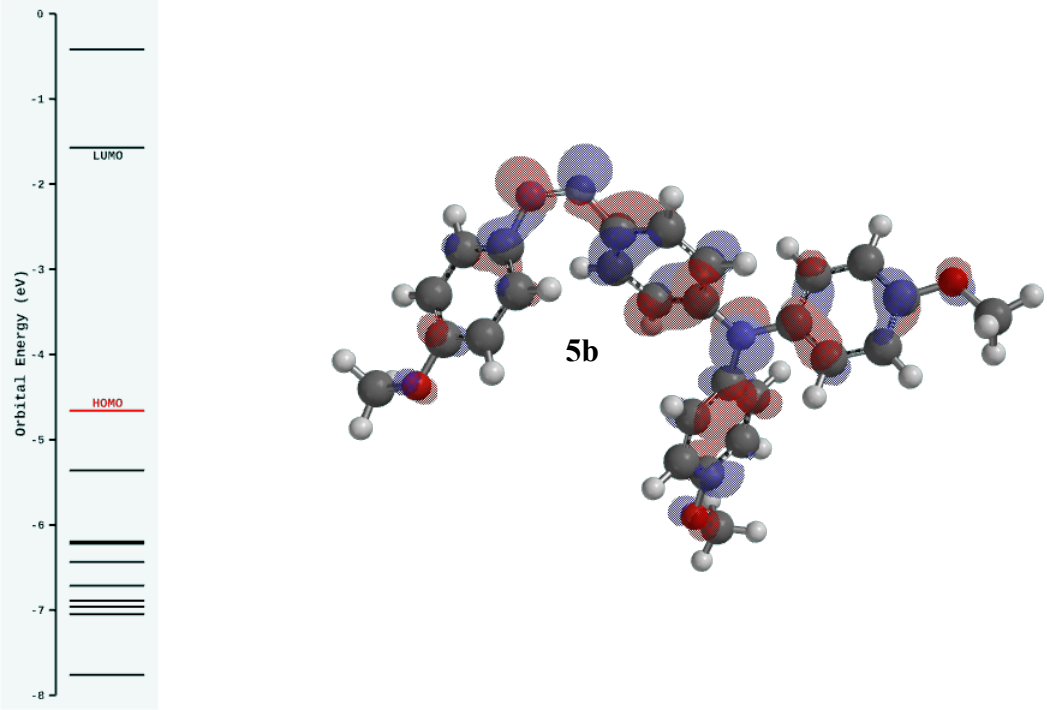

Figure 2.2.28. Density-functional theory calculations of **5b** with the B3LYP/6-31G** basis set. The HOMO is predominantly located at and around the central nitrogen atom of the RA group. The blue and red lobes indicate the orbital phases of the HOMO.

To test our hypothesis, 1% mole of **6** was injected into a solution of **4b** and a solution of **5b** in deaerated benzene at the PSS. Upon injection and mixing, both isomers, **4b** and **5b**

isomerized back to their corresponding *trans* isomers in less than 2 seconds as judged by optical spectra analysis illustrated in Figure 2.2.29 and Figure 2.2.30, respectively. Based on these results, it was concluded that a catalytic amount (1% mole) of **6** was sufficient to oxidize **4b** to **4b**$^{+}$ and **5b** to **5b**$^{+}$, thus initiating and forming the electrical catalysis cycle shown in Scheme 2.1.3.

To test the dependability of our photo-electro catalysis cycle, the new sample of **4a** and **5a** were irradiated for a total of 12 minutes in order to re-form their respective *cis* isomers. After this prolonged irradiation the *cis* isomers were not observed as displayed in Figures 2.2.29 and 2.2.30.

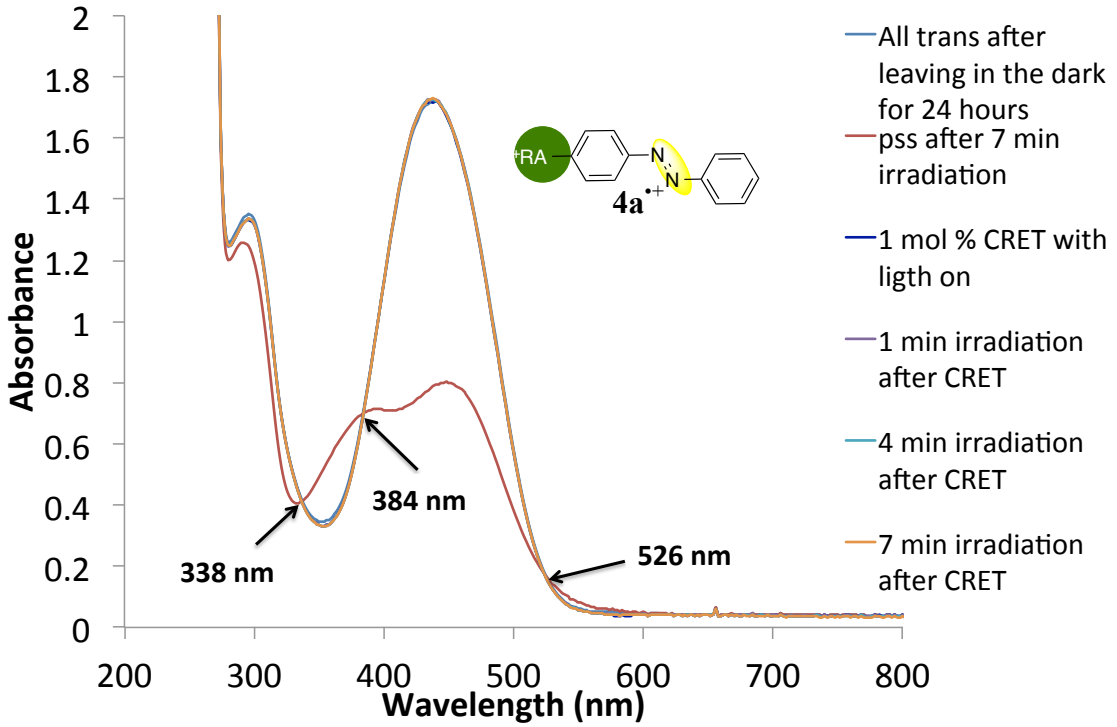

Figure 2.2.29. Optical spectrum of **4a** (6.35 x 10^{-4} M in C_6D_6) irradiated with a 430 nm LED and CRET injection (1% mole in DCM) at room temperature in 0.1 cm quartz UV-Vis cell.

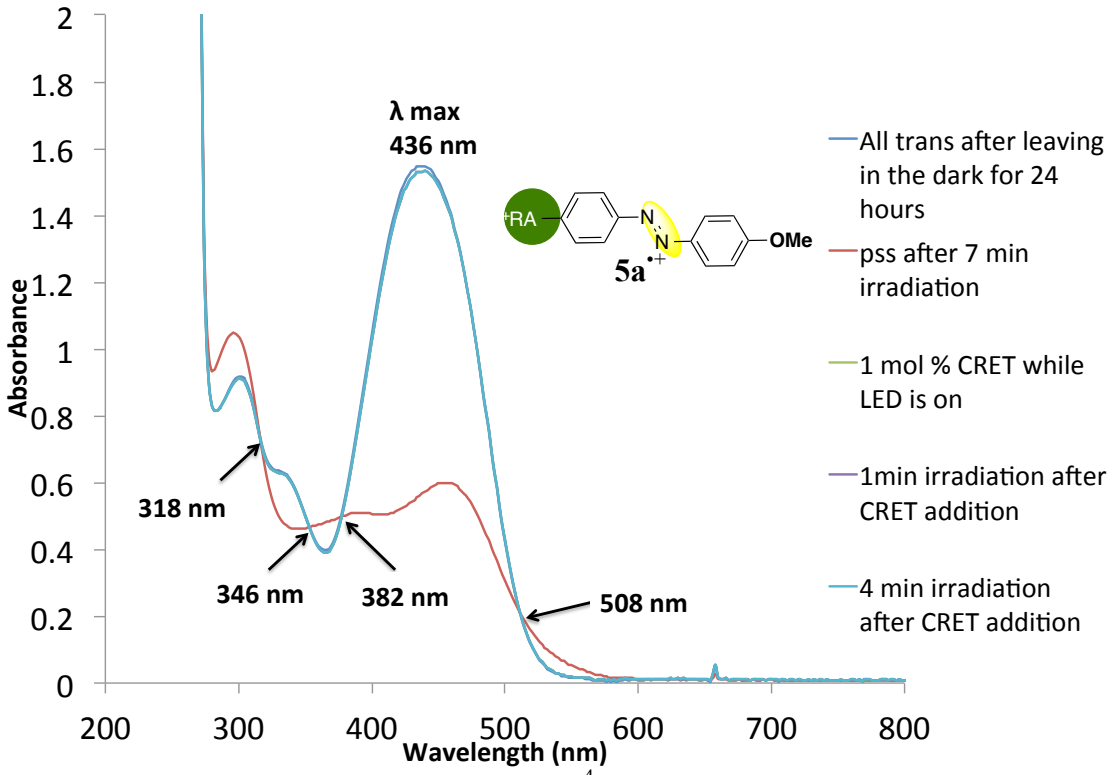

Figure 2.2.30. Optical spectrum of **5a** (6.37×10^{-4} M in C_6D_6) irradiated with a 430 nm LED and CRET injection (1% mole in DCM) at room temperature in 0.1 cm quartz UV-Vis cell.

Because the *trans*-RA$^{\bullet+}$ is exceptionally chemically stable, it is able to exchange an electron with other neutral *cis* isomers thereby generating a catalytic cycle for azo-unfolding as shown in Scheme 2.2.3. Grounded on this result, we postulated a new photo-electro isomerization catalysis mechanism that accounts for the fast relaxation of *cis*-to-*trans*. The photo-electro catalysis mechanism cycle in Scheme 2.2.3 demonstrates that a 430 nm LED can be used to isomerize **4a** and **5a** to their corresponding *cis* isomers. Subsequent addition of a catalytic amount of oxidant will regenerate the *trans* isomers, thus exponentially increasing the rate at which the *cis* isomer relaxes back to the *trans* isomer.

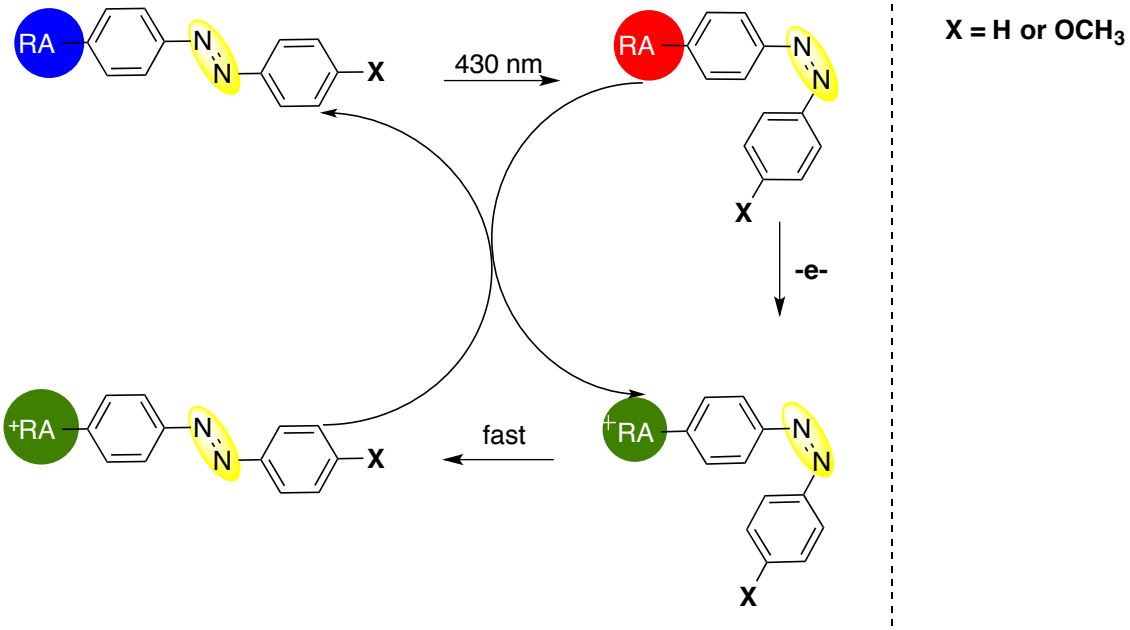

Scheme 2.2.3. Postulated photo-electro catalysis mechanism of **4a** and **5a.**

To better understand the effect of the $RA^{\bullet+}$ group on the *cis* to *trans* isomerization rate, the molecular orbitals of methyl yellow radical cation were computed using density-functional theory with the B3LYP/6-31G** basis set. Figure 2.2.31 shows the molecular orbital of methyl yellow radical cation at the transition state after oxidizing the *cis* isomer and isomerizing to the *trans* isomer. It shows that the radical cation species of the *cis* isomer has a transition state that prefers to align the half-filled p orbital of the oxidized nitrogen to the filled p orbital of one the azo nitrogen via an N-inverson mechanism. This spatial arrangement allows for a filled-unfiled stabilization of the radical cation, thus exponentially accelerates the the electro isomerization compare to the thermal

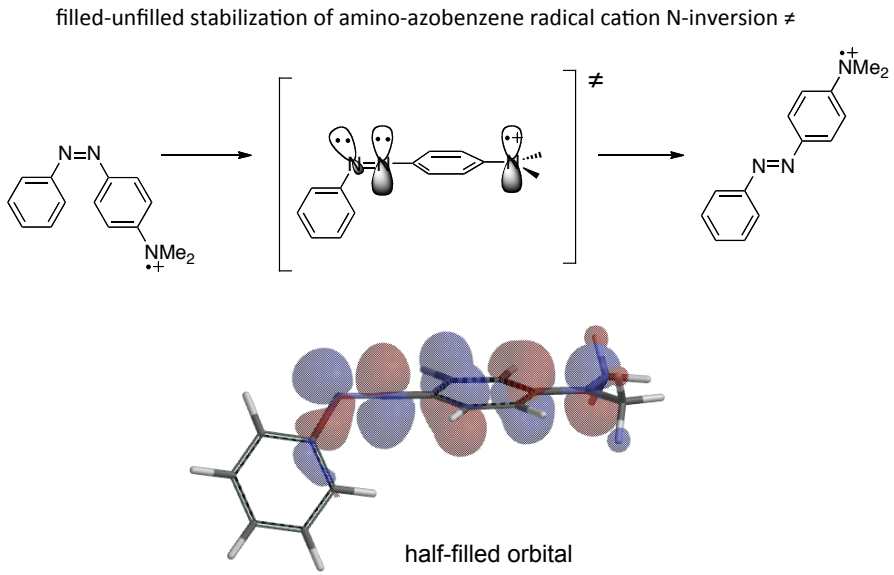

Figure 2.2.31. Mechanism of the *cis* to *trans* electro isomerization.

2.2.4 Thin cell Photo-Electro Device (PED)

After demonstrating that we can exponentially increase the isomerization rate of *cis*-to-*trans* in the *para*-arylamine azobenzene systems via catalytic electron transfer cycle with a chemical oxidant, it was necessary to attempt to reproduce the results using a different oxidation method. We anticipated that applying 1.5 V would oxidize the *cis* isomer and cause rapid isomerization to the *trans* isomer (within picoseconds) via a catalytic electron transfer cycle similar to that of Scheme 2.2.3. Figure 2.2.32 illustrates the design of the photo-electro cell device used to test the effect of electricity on the *cis* isomers.

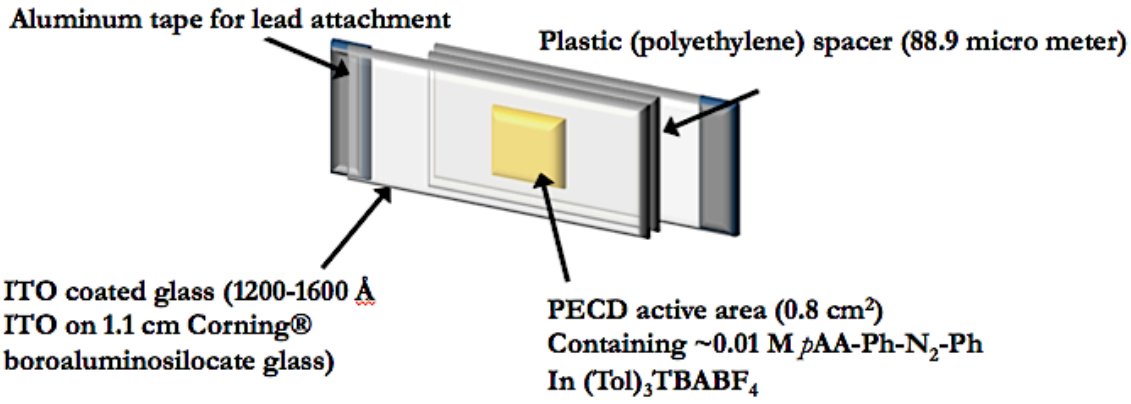

Figure 2.2.32. Photo-electro cell device designed to test the effect of electricity on the *cis* isomers of *para*-arylaminoazobenzene.

In order to complete the experiment, compound **4a** was chosen in favor of **5a** because it has a longer half-life and has a more thermodynamically stable *cis* isomer. Isomerization of **4a** to **4b** was achieved by irradiating the **4a** sample with 430 nm LED for 30 seconds, and then 1.5 V was immediately applied to the sample for 30 seconds to regenerate the **4a** isomer. The photo-electro equilibrium is repeatable for many cycles with no evidence of degradation as illustrated in Figure 2.2.33.

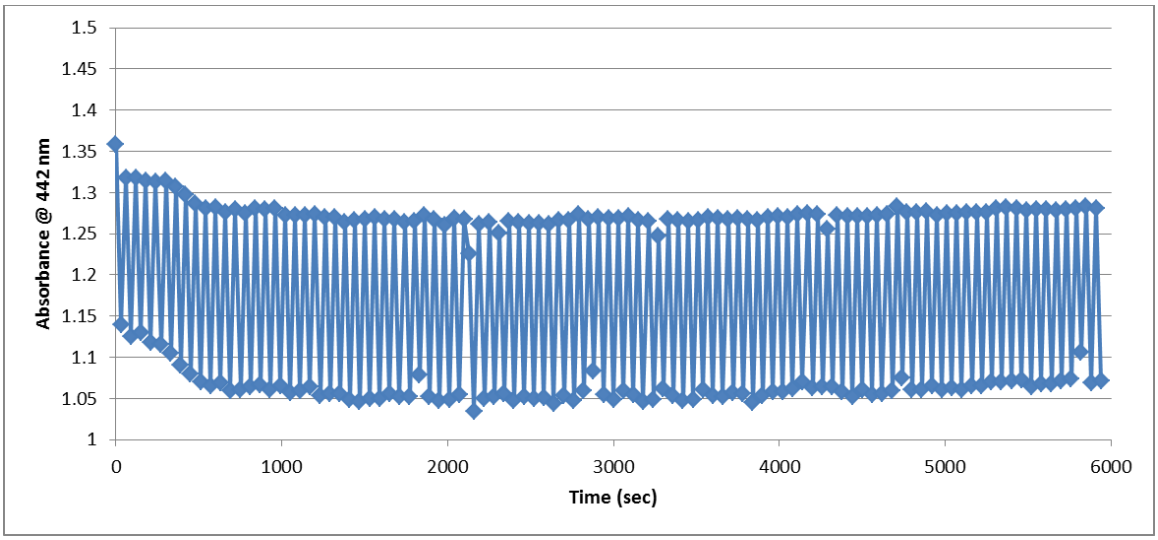

Figure 2.2.33. Tracking the absorbance at maximum (438 nm) of **4a** through multiple isomerization cycles reveals no signs of degradation. Irradiation for 30 seconds with 430 nm LED corresponds to the decreases in absorbance. Application of 1.5 V for 30 seconds corresponds to the increases in absorbance.

Figure 2.2.34 shows an expanded view of the photo-electro isomerization cycles of **4a** to **4b** and vice versa. It illustrates that isomerization from **4a** to **4b** is generated by irradiating with 430 nm light, therefore turning "OFF" the switch. The switch is then turned back "ON" by applying a 1.5 V to the **4b** isomer, thus regenerating the **4a** isomer.

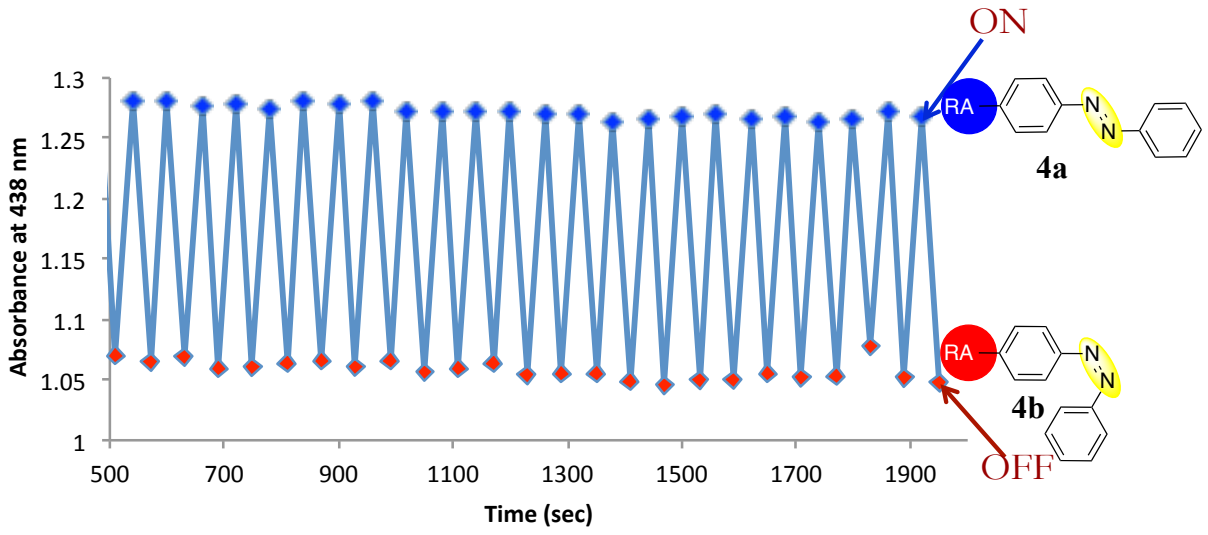

Figure 2.2.34. Expanded view of the changes in maximum absorbance intensity peak for **4**

through multiple isomerization cycles. Irradiated for 30 seconds with 430 nm LED to turn off the switch. Application of 1.5 V for 30 seconds corresponds to turn on the switch.

2.2.5 Conclusions

We have synthesized two mono *para*-amino azobenzene photo-electro switches. We have demonstrated that placing an electron rich moiety at the 4- position to the -N=N- group results in a redshift of the $\pi \rightarrow \pi^*$ absorption band for both **4a** and **5a**. As a result, both the $\pi \rightarrow \pi^*$ and the $n \rightarrow \pi^*$ absorption bands overlapped.

As a result of the overlap between the $\pi \rightarrow \pi^*$ and the $n \rightarrow \pi^*$ absorption bands, **4a** and **5a** can easily be isomerized to their respective *cis* isomers by light irradiation but can only be thermally isomerized back to the *trans* isomers. The addition of the RA group also destabilizes both *cis* isomers and decreased their half-lives compared to **1b**. The addition of the RA moiety to the AB core creates a new route to chemically control the isomerization from the *cis* to the *trans* isomer by assisting as a trigger in the oxidizing state. This oxidation can either be chemically induced or electrically induced by the removal of an electron from the RA moiety.

It was also demonstrated the photo-electrical switching for **4a** and **5a** can be executed for many cycles with no sign of molecular degradation as shown in Figure 2.2.33. Table 2.2.1 illustrates a detailed, tabulated comparison between **4a** and **5a.**

Table 2.2.1. Comparisons of the physical properties between *p*AA-Ph-N=N-Ph **4a** and *p*AA-Ph-N=N-An **5a**.

Compounds	*p*AA-Ph-N_2-Ph **4a**	*p*AA-Ph-N_2-An **5a**
PSS (*trans* : *cis*)[a]	29 : 71	32 : 68
Half-life[b]	2.5 hours	45 minutes
Thermal *cis*-to-*trans* isomerization rate[b]	8.4×10^{-5} $\pm 8.6 \times 10^{-7}$ s^{-1}	2.6×10^{-4} $\pm 2.8 \times 10^{-6}$ s^{-1}
$\Delta G^{\neq}$	23.0 kcal mol^{-1}	22.4 kcal mol^{-1}
E° [c]	0.94 V (vs. SCE)	0.85 V (vs. SCE)
***cis*- HOMO energy[d]**	- 4.8 eV	- 4.7 eV
Photo-electro catalysis[e]	Yes	Yes

[a]Deaerated C_6D_6 at room temperature after irradiating with a 430 nm LED. ^{1}H NMR spectra were recorded on Bruker AM-500 instrument.
[b] Deaerated C_6D_6 at room temperature in a 0.1 cm quartz cell in the dark.
[c] 1.0 mM in DCM with 0.1 M $TBABF_4$ at 20 mV/s scan rate.
[d] MacSPARTAN ´10 Quantum Mechanics Program: (x86/Darwin) build 1.1.0v4.
[e] 0.0021 mmol dissolved in 0.25 mL Tol_3TBABF_4 gel. The gel solution was applied to ITO glass anode. Cycling conditions were: 30 seconds irradiation with 430 nm LED and 0.0 V, then 1.5 V for 30 s with no irradiation (Cyclic Voltammetry Scan Rate: 2 V/s). Spectrophotometer Reading- 30 s intervals.

Table 2.2.2 . Experimental Details for the Crystal Structures of *p*AA-Ph-N=N-Ph **4a**, and *p*AA-Ph-N=N-An **5a**.

Structure	***p*AA-Ph-N=N-Ph**	***p*AA-Ph-N=N-An**
Reference code	scb260b	scb261
Empirical Formula	$C_{26}H_{23}N_3O_2$	$C_{27}H_{25}N_3O_3$
Formula Weight	409.48	439.51
Crystal Dimensions (mm)	0.04 x 0.11 x 0.70	0.05 x 0.09 x 0.07
Crystal System, Space Group	Triclinic, P-1	Orthorhombic, Pbca
Lattice Parameters: a	9.891(2)	20.703(4)
b	12.208(2)	8.2765(17)
c	17.885(4)	26.773(5)
α	88.65(3)	90
β	78.18(3)	90
γ	82.58(3)	90
Volume ($Å^3$), Z	2096.1(7), 4	4587.3(16), 8
D_{calc} (g/cm^3)	1.298	1.273
F_{000}, μ(MoKα) (mm^{-1})	864, 0.083	1856, 0.084
Diffractometer	Siemens SMART	Siemens SMART
Wavelength (Å), Temperature	0.71073, 20 °C	0.71073, 20 °C
θ range for data collection	1.16 to 26.91 °C	1.52 to 26.83 °C
Limiting indices	-12<=h<=12	-26<=h<=26
	-15<=k<=15	-10<=k<=10
	-22<=l<=21	-34<=l<=33
Reflections Measured-Total	25598	51135
Unique	8769 (R_{int} 0.0577)	4918 (R_{int} 0.1238)
Corrections: Decay	No	No
Absorption	No	No
Secondary Extinction	coeff: 0.0011(9)	coeff: 0.0016(6)
Structure Solution	Direct	Direct
Data/restraints/parameters	8769/0/564	4918/0/299
GOF on F^2	0.715	0.698
Final R indices [I>2σ(I)] (R_1, wR_2)	0.0619, 0.1732	0.0550, 0.1462
R indices (all data) (R_1, wR_2)	0.1186, 0.222	0.1118, 0.1989
Largest diff. peak and hole ($e^-Å^{-3}$)	0.299, -0.258	0.257, -0.224

2.3 *meta*-arylaminoazobenzene: *m*AA-Ph-N=N-An 19a

As discussed in section 2.2, positioning the RA group at the 4- position in reference to the -N=N- group increases the *cis*-to-*trans* thermal isomerization rate. Furthermore, positioning the RA group at the 4- position (to the -N=N- group) exponentially increases the rate for *cis*-to-*trans* isomerization via the catalytic electron transfer cycle.

To better understand such systems, it is essential to elucidate the effects of relocating the RA moiety from the 4- position to the 3- position in reference to the -N=N- group as illustrated in Figure 2.3.1. In this section, we will investigate how the location of the RA group affects the rate of the thermal *cis*-to-*trans* isomerization. We will also determine if the relocation of the RA group to the 3- position will interfere with the redox-induced *cis*-to-*trans* isomerization.

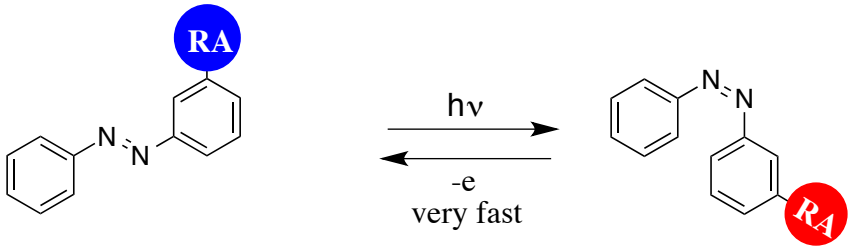

Figure 2.3.1 Model of the mono *meta*-amino-AB photo-electro switch. The *trans* isomer (blue) isomerizes to the *cis* isomer (red) by utilizing light, and the *cis* isomer (red) then rapidly isomerizes to the *trans* isomer (blue) upon removal of an electron.

To investigate the effects of relocating the RA group, we've synthesized a new *meta*- substituted arylamino azobenzene, *m*AA-Ph-N=N-An, **19a**. The synthetic route to obtain **19a** is shown in Scheme 2.3.1. We hypothesized that relocating the RA group to the 3- position to the -N=N- group will disrupt the extended pi-system that exists in the *para*- substituted arylamino azobenzenes. As a result, the disruption of the extended pi-system will cause the *meta*- arylamino azobenzene, **19a**, to exhibit absorption spectra similar to unsubstituted-AB and

behave analogously. Furthermore, we predict a decrease in the thermal isomerization rate of *cis*-to-*trans* for **19b** in comparison to **4b** and **5b**.

Synthesis:

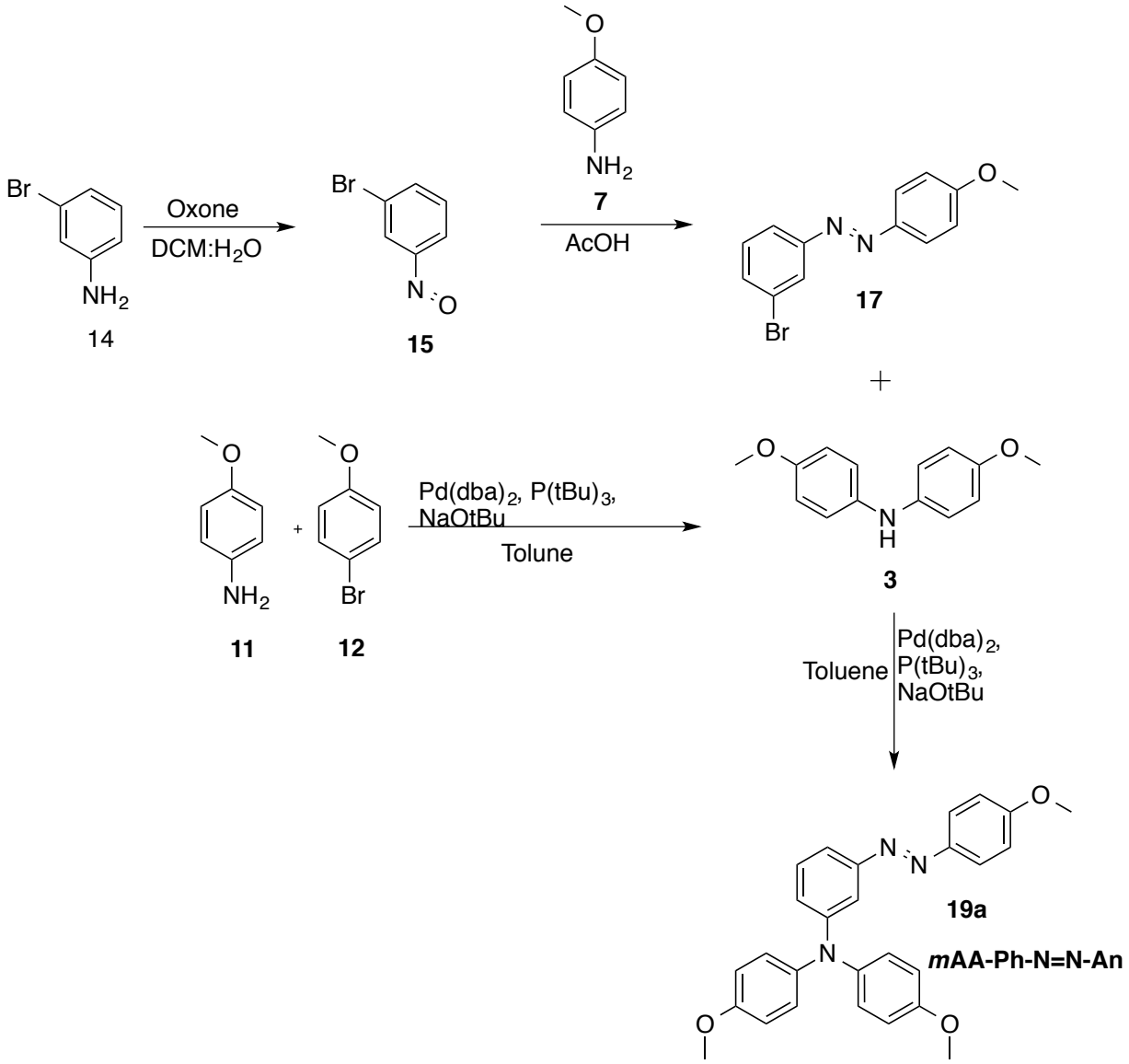

Scheme 2.3.1. Synthetic route to obtain *m*AA-Ph-N=N-An **19a**.

2.3.1 Photochemistry and optical absorption of 19a

A hypsochromic shift of the $\pi \rightarrow \pi^*$ absorption band is observed for **19a** compared to the optical spectra of **4a** and **5a**. This hypsochromic shift positions the $\pi \rightarrow \pi^*$ absorption band in

the UV region of the spectrum where a light source with less than 400 nm wavelength could be utilized to isomerize the *meta*- substituted arylamino azobenzene from *trans*-to-*cis* isomer. Figure 2.3.2 illustrates the optical spectrum of **19a**, which features a strong π → π* absorption band having an absorption maximum at 344 nm. Unlike the π → π* absorption bands of **4a** and **5a**, the π → π* absorption band of **19a** does not overlap with its n → π* absorption band, as a result a weak absorption maximum corresponding to the n → π* absorption band is displayed at 428 nm for **19a**.

The separation of the π → π* and n → π* absorption bands makes it possible to exclusively apply light to the n → π* absorption band, and this provides for more efficient photo isomerization from *cis*-to-*trans* isomerization after reaching PSS.

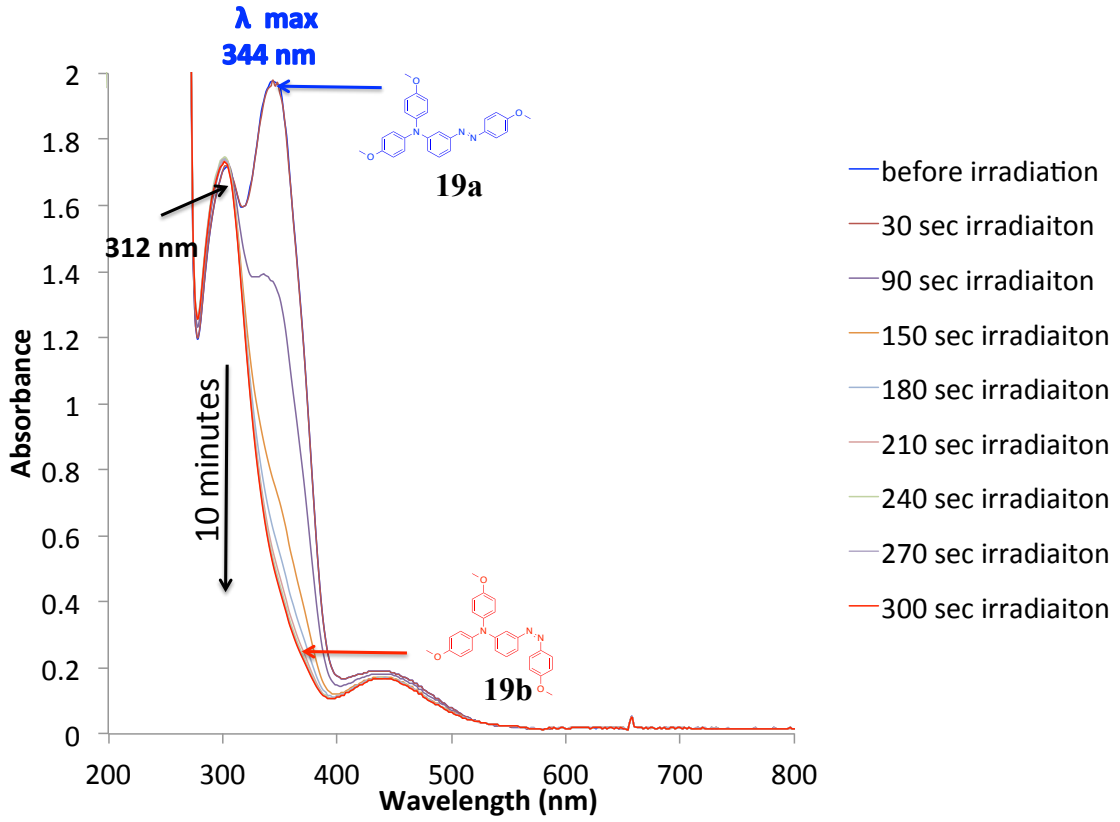

Figure 2.3.2. Optical spectrum of **19a** (6.55 x 10^{-4} M in C_6D_6) irradiated with 365 nm light at room temperature in a 0.1 cm quartz UV-Vis cell.

Figure 2.3.2 shows the photochemistry of **19a** to **19b** isomerization process. Upon irradiation of the π → π* absorption band using a 365 nm light source, **19a** isomerized to **19b** with an isosbestic point occurring at 312 nm. The time-dependence of PSS establishment for **19a** was determined by following the absorption maximum at 344 nm during irradiation. After approximately 3 minutes of irradiating, no changes in absorbance were observed. Figure 2.3.3 demonstrates the plateau in absorbance that indicates a PSS was reached.

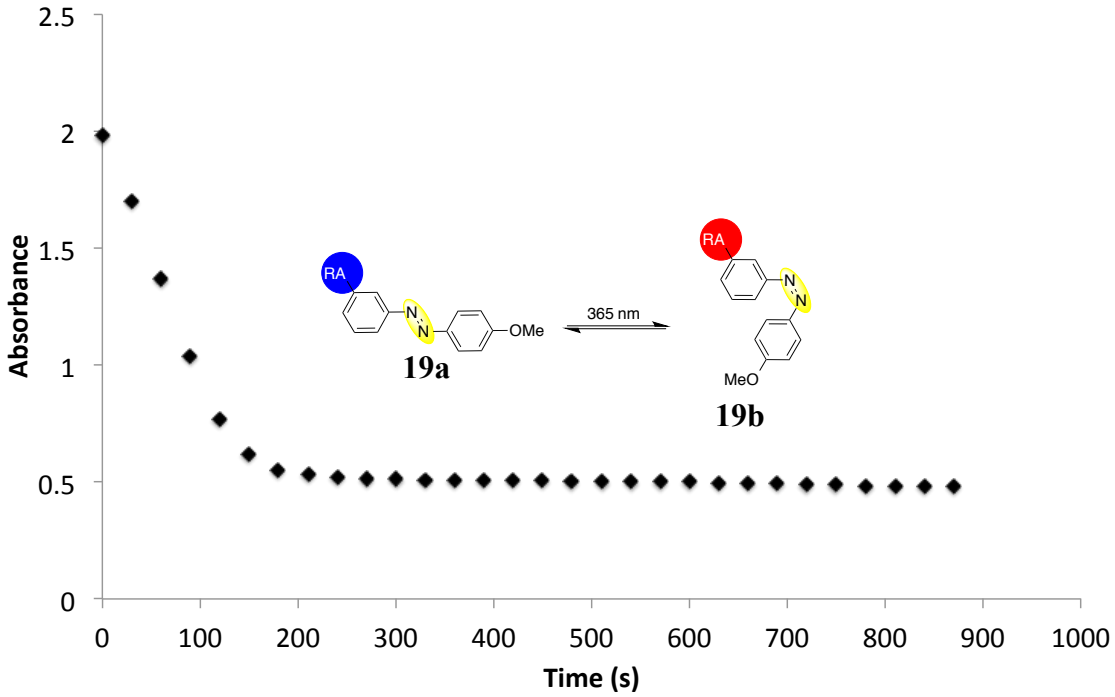

Figure 2.3.3. Absorption intensity was monitored at 344 nm and shows the establishment of a PSS for **19a** (6.55 x 10^{-4} M in deaerated C_6D_6) using 0.1 cm quartz UV-Vis cell at room temperature.

The isomeric ratio of **19b**:**19a** at PSS was determined via ^{1}H NMR spectroscopy in C_6D_6 at room temperature. Figure 2.3.4 shows the full spectrum of **19a** before irradiation. After irradiating with a 365 nm light, a PSS with an 80:20 ratio of **19b**:**19a** was confirmed. Figure 2.3.5 shows the full spectrum of **19** at PSS.

Expanded views of the aromatic sections in the ^{1}H NMR spectra of **19a** before irradiation and at PSS are shown and compared in Figure 2.3.6a and Figure 2.3.6b, respectively. As a result of different spatial orientations in the two isomers, **19b** and **19a** have different signals in the aromatic sections of the ^{1}H NMR spectra. The isomeric ratio of **19b:19a** at PSS was determined by using the integrations of the methoxy signals in the alkyl section of the ^{1}H NMR spectrum, as shown in Figure 2.3.7. The signals in the alkyl section verified that some amounts of **19a** persist at PSS.

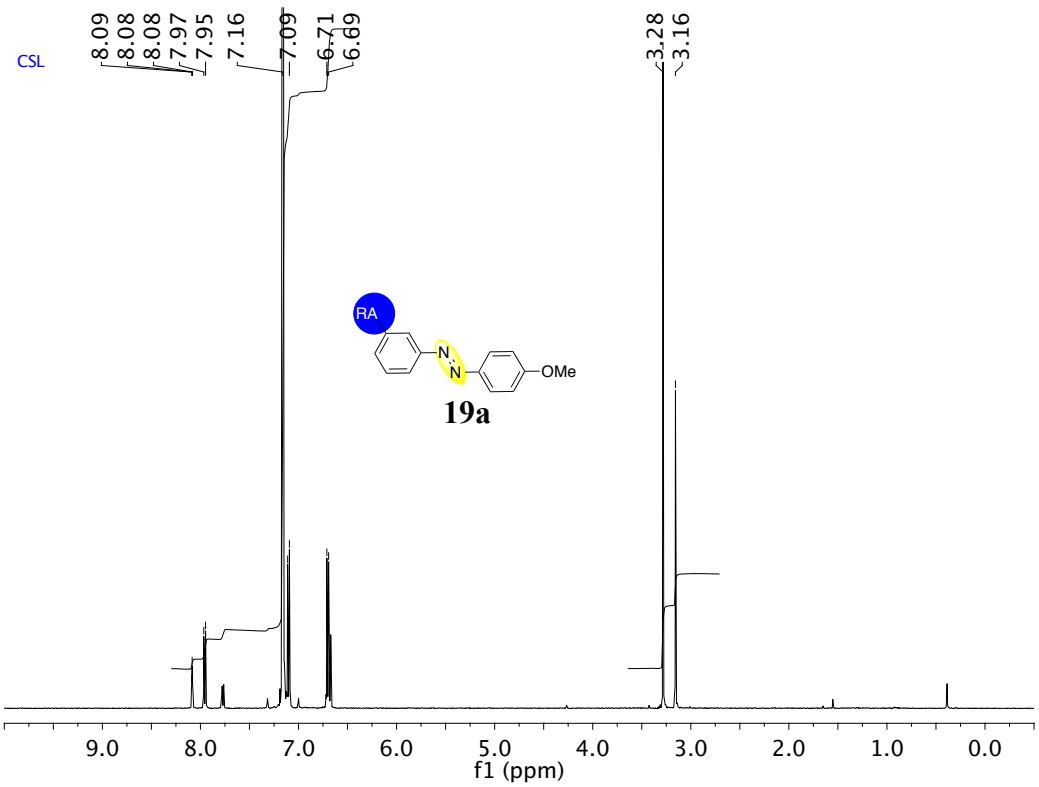

Figure 2.3.4. Full ^{1}H NMR spectrum of **19a** (1.67×10^{-2} M in C_6D_6) before irradiation.

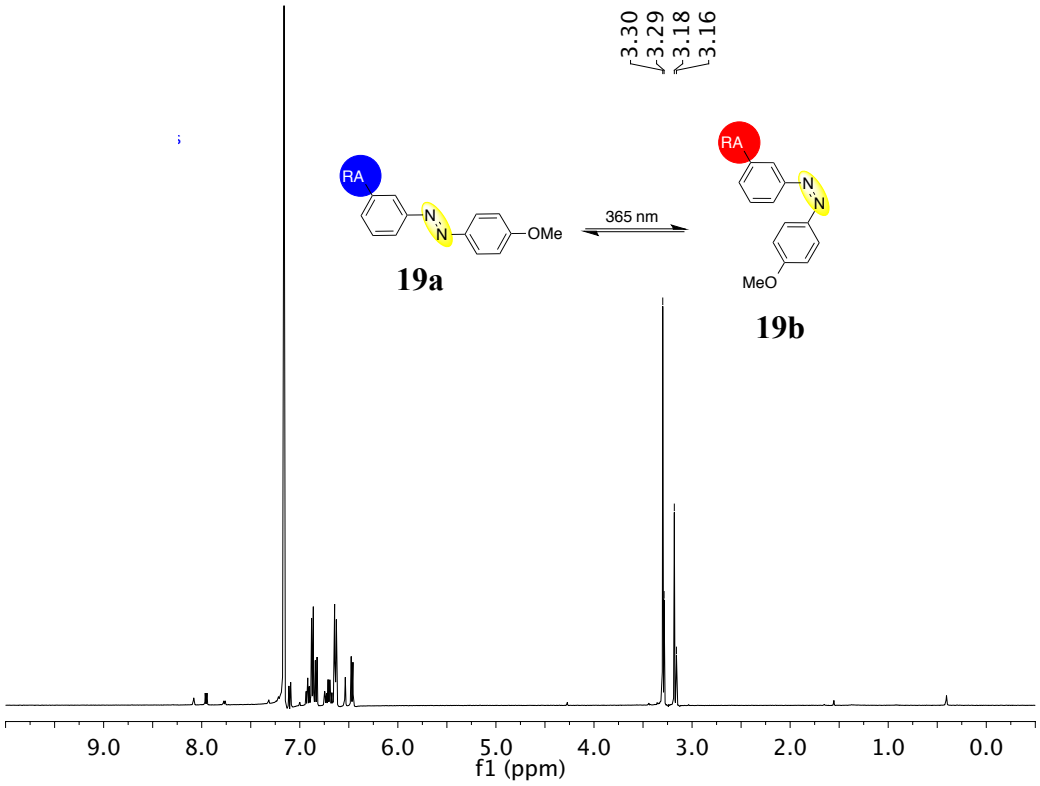

Figure 2.3.5. Full ^{1}H NMR of **19** (1.67 x 10^{-2} M) *m*AA-Ph-N=N-An in C_6D_6 irradiated with 365 nm light. A PSS with an 80:20 ratio of **19b**:**19a** at room temperature.

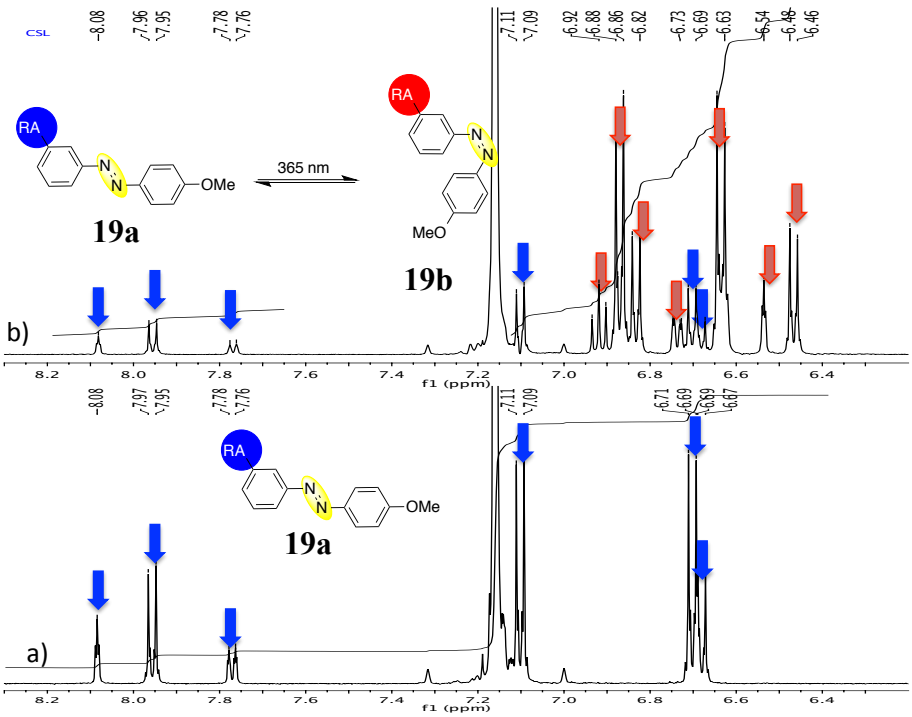

Figure 2.3.6. Expanded view of the aromatic section in the ^{1}H NMR spectrum of **19a** (1.67 x 10^{-2} M in C_6D_6) **a**) Spectrum before irradiation **b**) PSS after irradiation with 365 nm light. PSS is established at a 20:80 **19a**:**19b** ratio at room temperature. Blue arrows indicate **19a** and red arrows indicate **19b**.

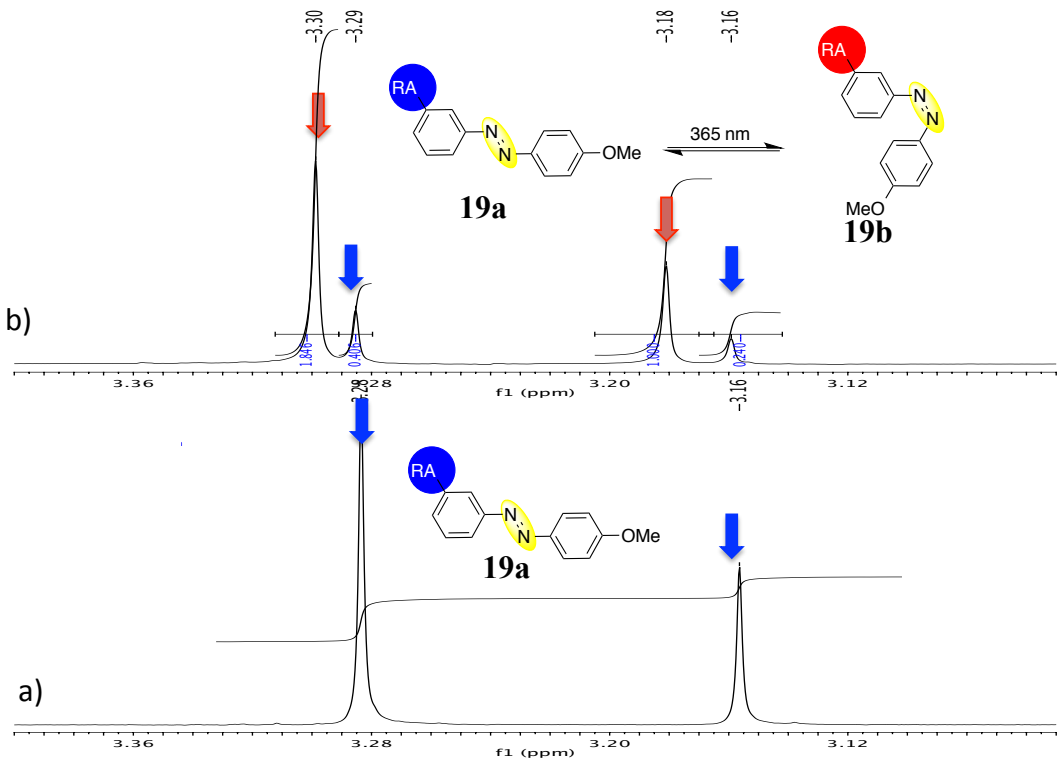

Figure 2.3.7. Expanded view of the alkyl section of the ^{1}H NMR spectrum of **19** (1.67 x 10^{-2} M in C_6D_6) **a**) Before irradiation **b**) PSS after irradiation with 365 nm light. A PSS is established at a 20:80 **19a**:**19b** ratio at room temperature. Blue arrows indicate **19a** and red arrows indicate **19b**.

2.3.2 Thermal *cis*-to-*trans* isomerization of 19a

After obtaining the isomeric ratio of **19b**:**19a** at PSS**,** the thermal isomerization process of **19b** to **19a** at room temperature was examined to understand the thermodynamic effect of the RA moiety on the thermal reversibility.

As performed for **4b** and **5b**, ultraviolet-visible spectroscopy was utilized to monitor the thermal isomerization of **19b** to **19a**. The experiment was conducted in the dark and was monitored for 250 hours. After reaching a PSS, spectra were taken every 60 minutes in the dark until there were no changes in the maximum absorbance. Figure 2.3.8 shows the thermal isomerization process from **19b** to **19a**.

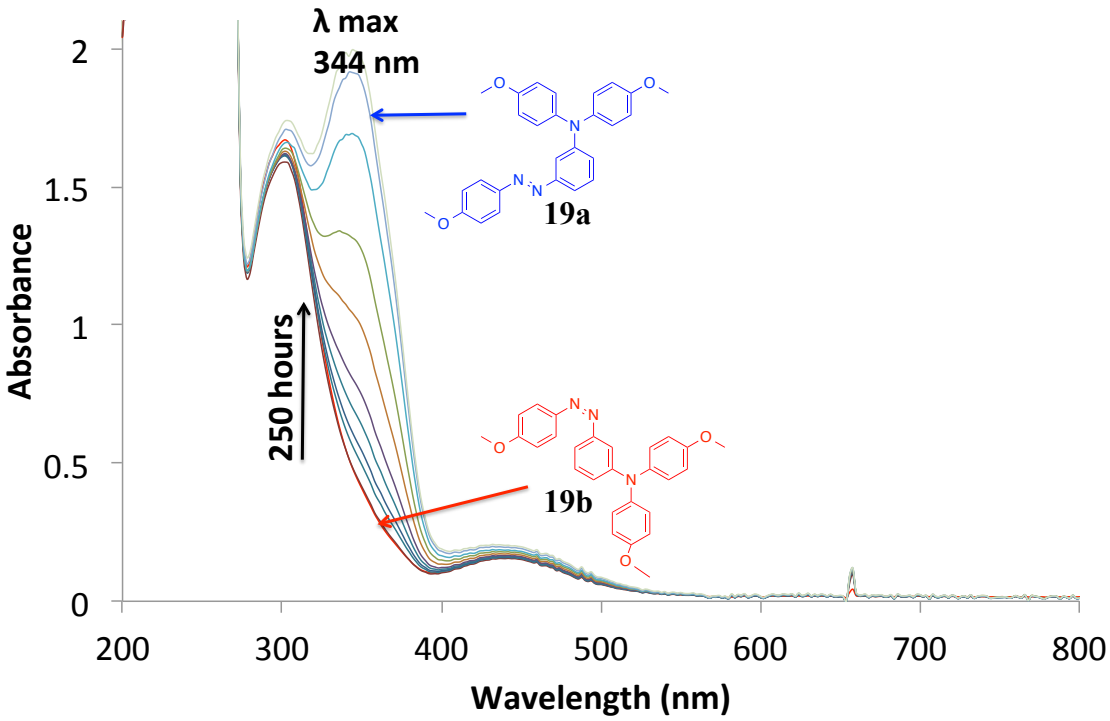

Figure 2.3.8. Optical spectrum of the thermal isomerization of **19b** to **19a** (6.55 x 10^{-4} M in C_6D_6) recorded every 60 minutes in the dark at room temperature in a 0.1 cm quartz cell after irradiating with 365 nm light to a PSS (80:20 **19b**:**19a** ratio).

The absorbance maximum was also utilized to monitor the thermal recovery of **19a** from **19b** in the dark until no **19b** was present. The absorbance maximum at 344 nm was plotted after irradiating with the 365 nm bulbs as shown in Figure 2.3.9.

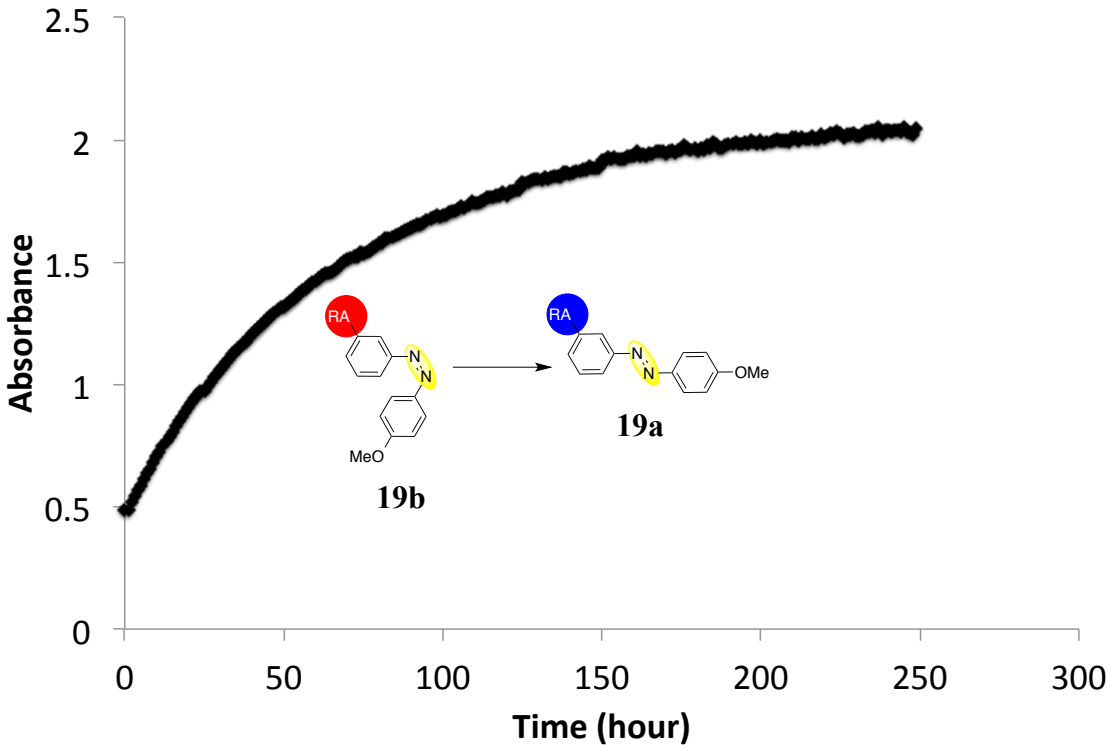

Figure 2.3.9. Optical spectrum of the thermal isomerization of **19b** (6.55 x 10^{-4} M in deaerated C_6D_6) recorded every 60 minutes in the dark at room temperature in a 0.1 cm quartz cell after irradiating with 365 nm light to PSS (80:20 **19b**:**19a** ratio). Showing the max absorbance at 344 nm.

The thermal isomerization of **19b** was compared to the thermal isomerization of **4b, 5b** and **1b**. Experimental measurements indicated that **4b** and **5b** are less stable at room temperature than **19b**. It was measured that **19b** thermally isomerized to **19a** at a rate of 4.1 x 10^{-6} +/- 9.5 x 10^{-9} s^{-1} with a half-life of approximately 47 hours, as illustrated in Figure 2.3.10. Relocating the RA moiety to the 3-position to the -N=N- group increased the thermal stability of **19b** relative to **4b** and **5b** at room temperature. Table 2.3.1 illustrates the thermal isomerization comparisons between **19b**, **4b** and **5b**.

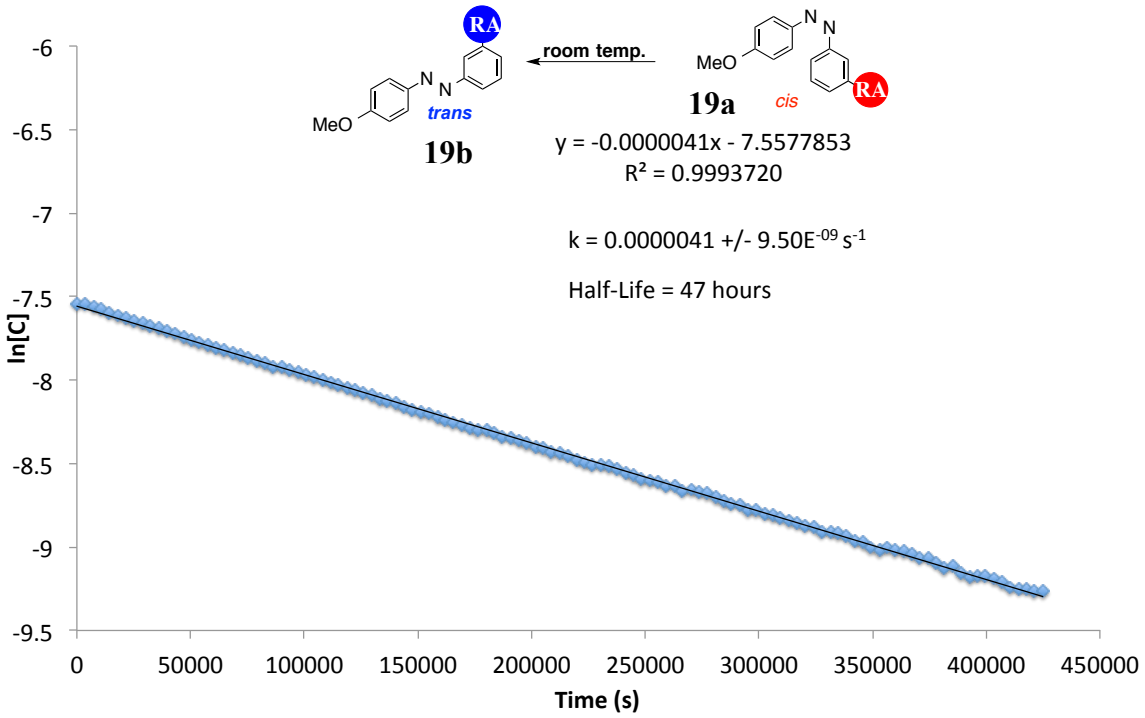

Figure 2.3.10. ln[C] vs. Time plot to determine the rate at which **19b** thermally converts to **19a** over 250 hours.

To further investigate the effect of the RA group in the 3- position, it was necessary to experimentally measure the $\Delta G^{\neq}$ for the thermal isomerization process of **19b** to **19a**. Figure 2.3.11 displays the effect of the RA group on the $\Delta G^{\neq}$ of **19b** at room temperature. The barrier height for **19b** to **19a** was experimentally measured to be approximately 24.8 kcal mol^{-1}, which is lower than the experimentally measured $\Delta G^{\neq}$ for **1b** to **1a**, which is known to be approximately 25.8 kcal mol^{-1}.[66,67]

[66] Blevins A. A.; Blanchard G. J. Effect of Positional Substitution on The Optical Response of Symmetrical Disubstituted Azobenzene Derivatives *J. Phys. Chem. B.* , **2004**, *108*, 4962-4968.
[67] Crecca R. C.; Roitberg A.E. Theoretical Study of the Isomerization Mechanism of Azobenzene and Disubstituted Azobenzene Derivatives. *J. Phys. Chem. A.,* **2006**, *110*, 8188-8203.

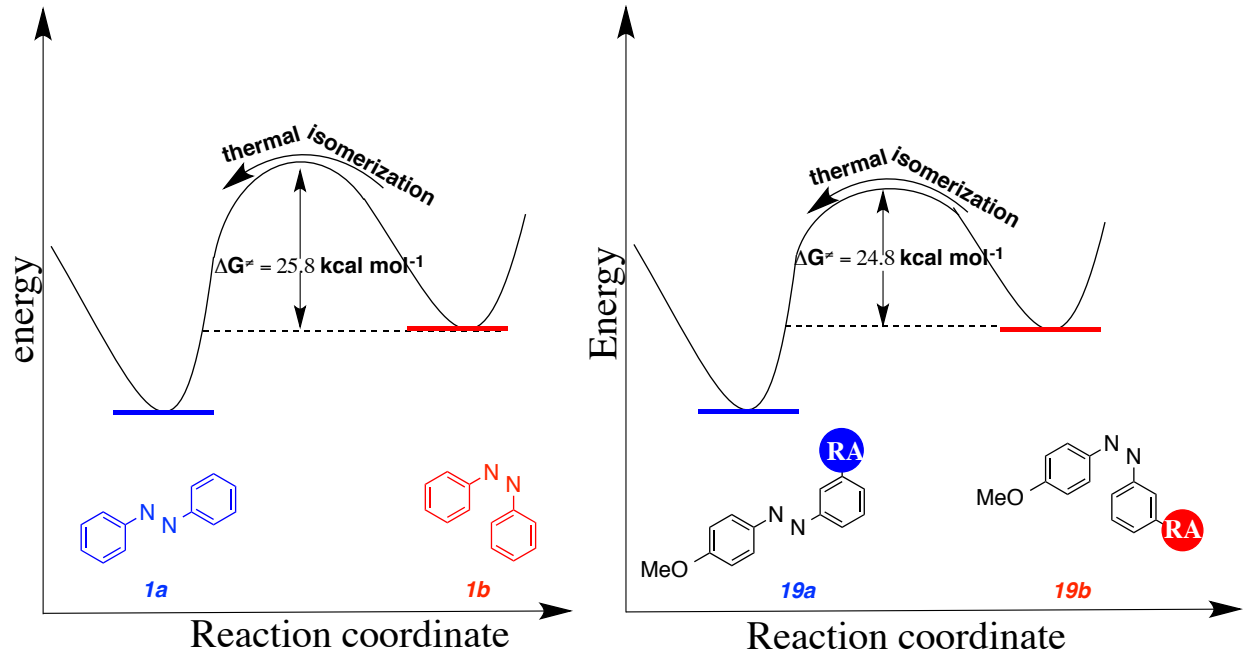

Figure 2.3.11. Potential energy diagram of azobenzene (left) and **19a** (right). It illustrates the effects of the RA on the $\Delta G^{\neq}$ of **19b → 19a**.

The crystal structure of **19a** shown in Figure 2.3.12 reveals that the three-bladed propeller shaped seen in triphenylamine is loss and the phenyl rings of the RA moiety are tremendously twisted with dihedral angles ∠C26C21N1C14 (113.32°) and ∠C15C14N1C21 (97.32°) while the AB core is completely planar compared **4a** and **5a**. The phenyl ring located between the -N=N- group and the RA group in **19a** has dihedral angles ∠C2C1N1C14 (1.29°) and ∠C6C1N1C21 (10.80°) and is less twisted than the analogous phenyl rings in **4a** and **5a**. The additional twisting observed in the phenyl rings of the RA group of **19a** is necessary because the lone pair of electrons on the nitrogen atom of the RA moiety is now primarily conjugated to the two-anisyl groups but not to the -N=N- group. As a result, there is no donor-acceptor interaction between the -N=N- group and the lone pair on the central nitrogen of the RA group in **19a**.

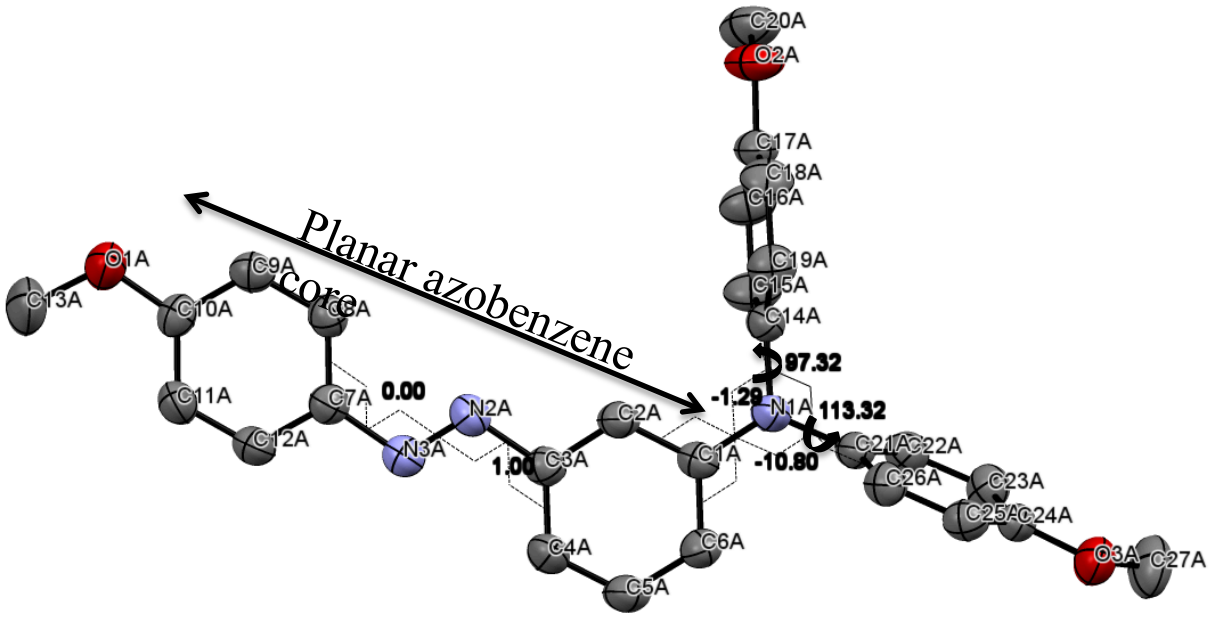

Figure 2.3.12. Crystal structure of **19a** illustrating additional twisting observed in the RA group at the *meta*- position and the loss of the triphenylamine geometry.

The decrease of the thermal isomerization rate from **19b** to **19a** and the increase in the barrier height compared to **4b** and **5b** can be explained by several factors. First, the relocation of the RA moiety from 4- position to 3- position decreases the stabilization of **19a** relative **19b**, as **19a** does not possess the conjugation that extends from the RA group to the -N=N- group as seen in **4a** and **5a**. The lone pair electrons on the nitrogen of the RA group is only in conjugation with the electron poor phenyl ring as illustrated in Figure 2.3.13a. Therefore, the stabilizing donor-acceptor interaction between the nitrogen atom of the RA group and to the -N=N- group that exists in **4a** and **5a** does not occur in **19a**. The second factor is the decreased steric interactions in the *cis* isomer that results in moving the RA group away from the azobenzene ring containing the $-OCH_3$ group as shown in Figure 2.2.13b. Table 2.3.1 shows the comparison between **4a** and **5a** in more details.

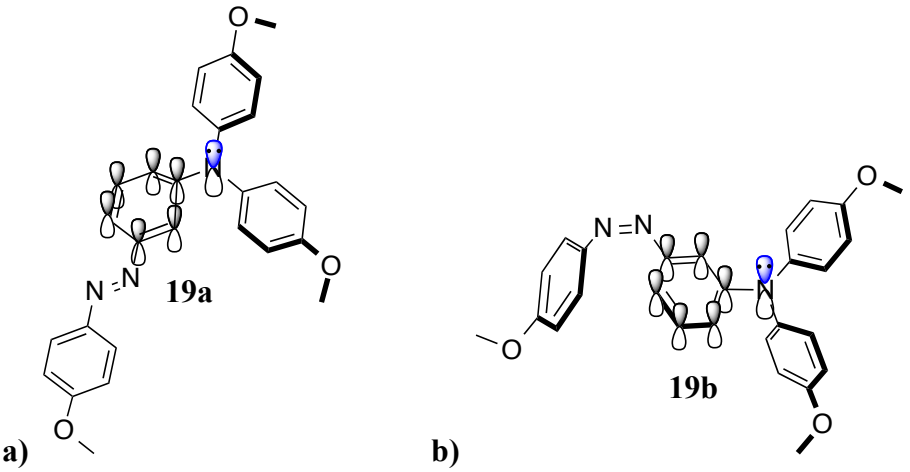

a) b)

Figure 2.3.13. a) **19a** does not contain an extended conjugated pi system between the RA group and the azobenzene core. The lone pair on the center nitrogen of the RA group is in conjugation with the two-anisyl groups. b) In **19b**, the steric interaction is decreased by moving the RA group away from the benzene ring containing the -OMe group.

The molecular orbital of the *trans* isomer were computed using density-functional theory with the B3LYP/6-31G** basis set to locate the energy level of the HOMO for **19a**. Figure 2.3.14 illustrates that the HOMO is predominantly located around at the RA moiety and at the phenyl ring between the -N=N- group and the RA group. It also indicates that no electron density was observed on the -N=N- group or on the phenyl ring deprived of the RA group because there is no resonance between the RA group and the -N=N- group. As a consequence, the donor-acceptor interaction seen in **4a** and **5a** is not observed in **19a**.

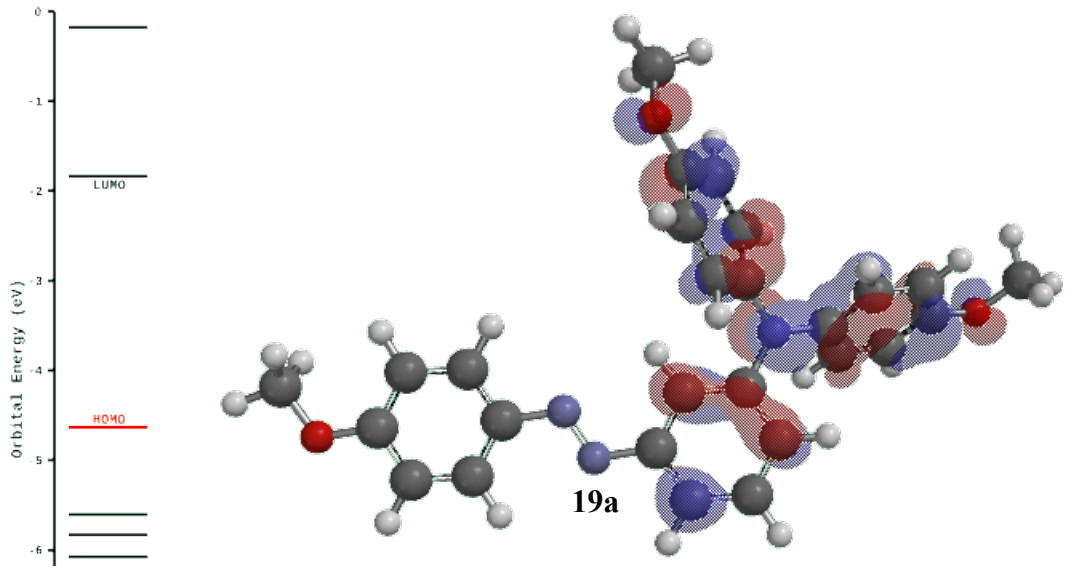

Figure 2.3.14. The molecular orbital of the *trans* isomer were computed using density-functional theory with the B3LYP/6-31G** basis set to locate the energy level of the HOMO for **19a**. The HOMO is predominantly located at and around the central nitrogen atom of the RA group. No electron density is observed near the -N=N- group. The blue and red lobes indicate where the electron densities are located.

2.3.3 Electron transfer catalysis of *cis-to- trans-* isomerization

In order to determine if relocating the RA group to the 3- position of the -N=N- group will interfere with the electrical stimulation of *cis*-to-*trans* isomerization of **19b**, it was necessary to attempt to oxidize **19b** in an effort to replicate the catalytic electron transfer cycle of the *para*-arylaminoazobenzenes. The cyclic voltammogram of **19a,** shown in Figure 2.3.15, provides the E° of **19a** as 0.85 V vs. SCE, which is lower than the E° of **6** (1.25 V vs. SCE). The lower oxidation potential of **19a** compared to that of **4a** and **5a** can be explained by the loss of conjugation between the electron withdrawing, -N=N- group, and the electron rich, RA group. As a result, the RA group of **19a** is easier to oxidize because it does not share its electron density with the -N=N- group.

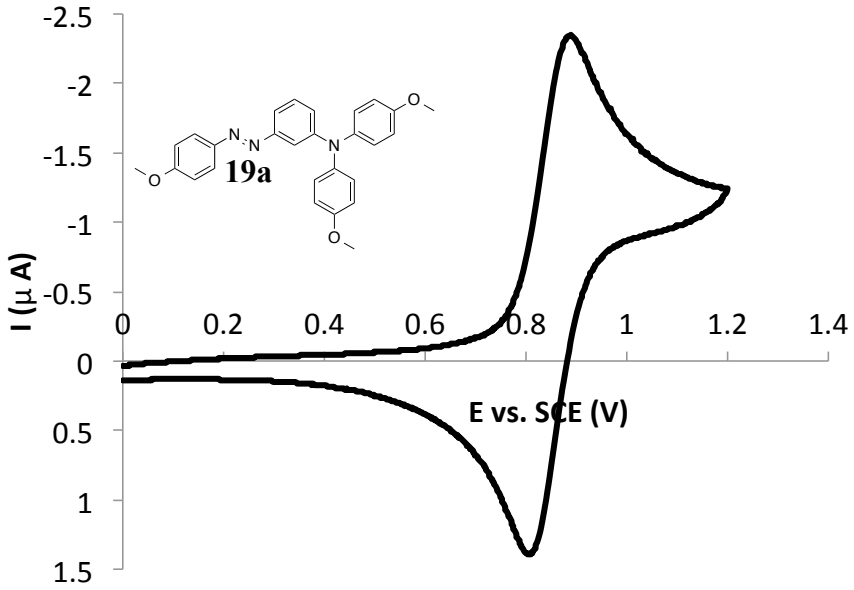

Figure 2.3.15. Cyclic voltammogram of **19a** (1.0 mM in dichloromethane with 0.1 M $TBABF_4$) at 20 mV/s scan rate with an $E^{\circ} = 0.85$ V (vs. SCE).

Before attempting to oxidize **19b**, the molecular orbital of the *cis* isomer were computed using density-functional theory with the B3LYP/6-31G** basis set to locate the energy level of the HOMO and to confirm that the RA group would be the moiety interacting with the oxidant. B3LYP/6-31G** molecular orbital calculations will also clarify if the pi orbitals of the RA group will overlap with the -N=N- group in the *cis* form. Figure 2.3.16 illustrates the location of the molecular orbitals of the HOMO in **19b**. It shows that the HOMO is predominantly located around and at the central nitrogen atom of the RA moiety. Remarkably, a small amount of electron density is noticed on the -N=N- group in **19b**, which was not observed in **19a**. This small amount of electron density on the -N=N- group is due to the orientation of the *cis* isomer. It helps create some overlap between the pi orbitals of the -N=N- group and the lone pair of the nitrogen item of the RA group. This results signified that there is a minor donor-acceptor interaction between the -N=N- group and the RA moiety in the *cis* conformation. This spatial arrangement also signifies that the removal of an electron from **19b** should perturb the -N=N-

group. As a result, removal of an electron from the RA moiety of **19b** would cause the -N=N- bond to break and convert into -N-N- triggering isomerization back to **19a**. Density-functional theory with the B3LYP/6-31G** basis set indicates that the RA group would be the redox-active moiety in **19b**.

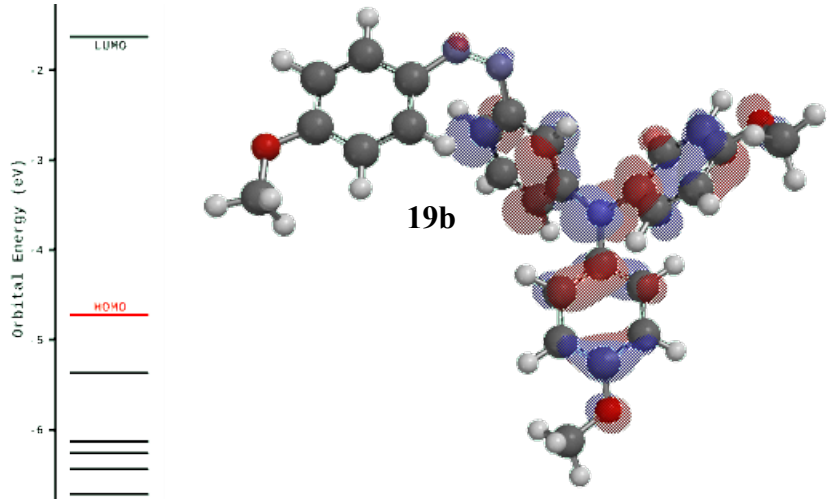

Figure 2.3.16. B3LYP/6-31G** molecular orbital calculations of **19b**. The HOMO is predominantly located at and around the central nitrogen atom of the RA group. A small amount of electron density is noticed on the –N=N- group in **19b**. The blue and red lobes indicate where the electron densities are located.

To test our hypothesis, 1% mole of **6** was injected into a solution of **19b** in deaerated benzene at PSS. Based on our results, 1% mole of **6** was sufficient to oxidized **19b** and initiates the electrical catalysis cycle shown in Scheme 2.3.2. Upon injection and mixing, **19b** isomerized back to **19a** in less than 2 seconds, as judged by optical spectra analysis illustrated in Figure 2.3.17.

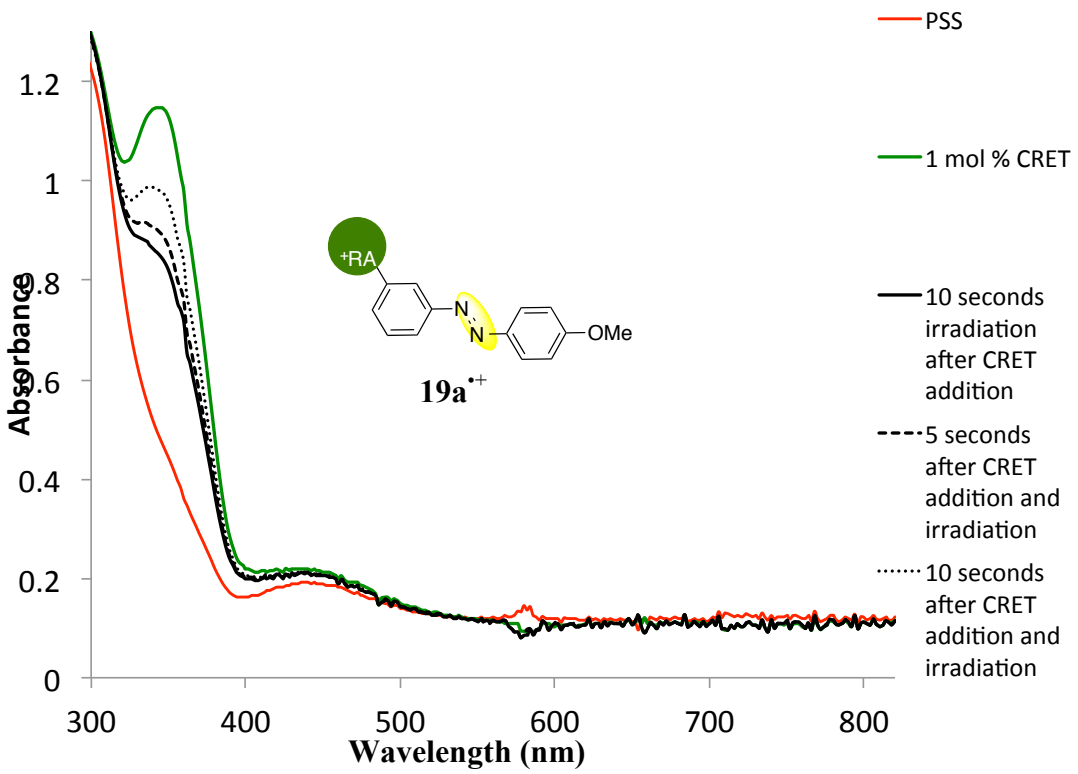

Figure 2.3.17. Optical spectrum of **19a** (6.19 x 10^{-4} M in C_6D_6) irradiated with 365 nm light and CRET injection (1% mole in DCM) at PSS at room temperature in 0.1 cm quartz UV-Vis cell.

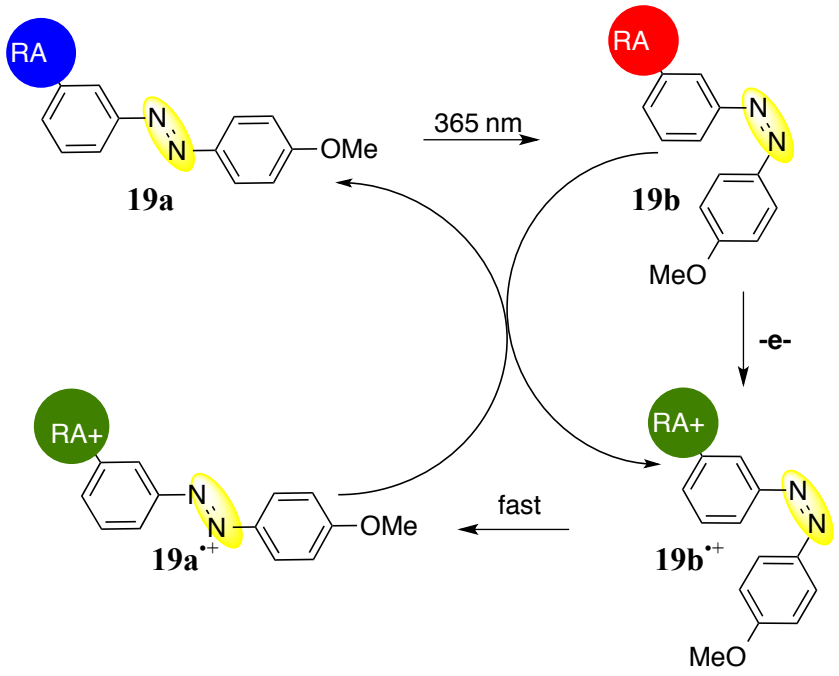

Scheme 2.3.2. Postulated photo-electro catalysis mechanism of **19a.**

To test the reliability of our photo-electro catalysis cycle, *m*AA$^{\bullet+}$-Ph-N=N-An sample was irradiated multiple times after the addition of **6**. As illustrated in Figure 2.3.17, **19b** was regenerated with slow increase in **19a** after irradiated for 10 seconds. This result suggests that *trans*-*m*AA$^{\bullet+}$-Ph-N=N-An is degrading faster that its radical cation as a result of no pi orbitals overlapping in **19a** between the RA group and the -N=N- group. In summary, moving the RA group from 4- position to 3- position relative to the -N=N- group destabilized the *trans*-*m*AA$^{\bullet+}$-Ph-N=N-An, **19b**, and decreased its half-life compared to the highly conjugated **4a** and **5a**.

For the *para*- RA-appended azobenzenes, the electro-catalytic conversion of *cis* isomer to *trans* isomer occurs so rapidly that irradiating to increase the proportion of *cis* isomer proves futile (or "does not appreciably affect the proportion of *cis*- isomer") because the photoisomerization process is completely counteracted by the more rapid electro-catalytic isomerization from *cis*-to-*trans*. However, if the *trans* radical cation degrades quickly, this will decrease the total concentration of oxidative species in solution, and, as a result, the electro-

catalytic cycle will no longer be able to completely counteract photoisomerization of *trans*-to-*cis*. Thus, if irradiation after the addition of oxidant leads to an increase in the proportion of *cis* isomer, this indicates that the *trans* radical cation degrades rapidly. In solutions of **4** or **5** to which oxidant had already been introduced, the proportion of *cis* isomer did not appreciably increase upon irradiation. Thus, the radical cations of both **4a** and **5a** do not degrade rapidly. However, after adding **6** to a solution of **19b**, the solution was irradiated for ten seconds, and the amount of *cis* isomer noticeably increased. This increase in the proportion of **19b** indicates that the radical cation of **19a** degrades rapidly.

2.3.4 Conclusions

The ultimate goal of this section was to elucidate the effects of relocating the RA moiety from the 4- position to the 3- position in reference to the -N=N- group. We investigated how the location of the RA group affects the rate of thermal *cis*-to-*trans* isomerization. We also investigated if the relocation of the RA group to the 3- position will interfere with the redox-induced *cis*-to-*trans* isomerization.

Based on our results, we established that moving the RA moiety from the 4- position to the 3- position decreased the rate of thermal *cis*-to-*trans* isomerization, when compared to **4a** and **5a**. Table 2.3.1 illustrates the comparison of thermal *cis*-to-*trans* isomerization rate between the *para*- substituted arylaminoazobenzenes, **4a** and **5a**, and the *meta*- substituted arylaminoazobenzene, **19a.** Relocating the RA group to the 3- position caused **19a** to behave more like unsubstituted-AB than **4a** or **5a**. Relocation of the RA moiety also resulted in an absorption spectrum that more closely resembled that of un-substituted AB than that of **4a** or **5a**.

Table 2.3.1. Comparison of the physical properties of *p*AA-Ph-N=N-Ph **4a**, *p*AA-Ph-N=N-An **5a** and *m*AA-Ph-N=N-An **19a**.

Compounds	*p*AA-Ph-N_2-Ph **4a**	*p*AA-Ph-N_2-An **5a**	*m*AA-Ph-N_2-An **19a**
PSS (*trans* : *cis*)[(a)]	29 : 71	32 : 68	20 : 80
Half-life[(b)]	2 hours 30 minutes	45 minutes	47 hours
Thermal *cis*-to-*trans* isomerization rate[(b)]	8.4×10^{-5} $\pm 8.6 \times 10^{-7} s^{-1}$	2.6×10^{-4} $\pm 2.8 \times 10^{-6}$ s^{-1}	4.1×10^{-6} $\pm 9.5 \times 10^{-9}$ s^{-1}
$\Delta G^{\neq}$	23.0 kcal mol^{-1}	22.4 kcal mol^{-1}	24.8 kcal mol-1
E°[(c)]	0.94 V (vs. SCE)	0.85 V (vs. SCE)	0.85 V (vs. SCE)
***cis*- HOMO energy[(d)]**	- 4.8 eV	- 4.7 eV	- 4.7 eV
Photo-electro catalysis [(e)]	Yes	Yes	Yes but short lived radical cationic species

[(a)]Deaerated C_6D_6 at room temperature after irradiating with a 430 nm LED. ^1H NMR spectra were recorded on Bruker AM-500 instrument.
[(b)] Deaerated C_6D_6 at room temperature in a 0.1 cm quartz cell in the dark.
[(c)] 1.0 mM in DCM with 0.1 M $TBABF_4$ at 20 mV/s scan rate.
[(d)] MacSPARTAN ´10 Quantum Mechanics Program: (x86/Darwin) build 1.1.0v4.
[(e)] 0.0021 mmol dissolved in 0.25 mL Tol_3TBABF_4 gel. The gel solution was applied to ITO glass anode. Cycling conditions were: 30 seconds irradiation with 430 nm LED and 0.0 V, then 1.5 V for 30 s with no irradiation (Cyclic Voltammetry Scan Rate: 2 V/s). Spectrophotometer Reading- 30 s intervals.

We also established that moving the RA moiety from the 4- position to the 3- position does not interfere with the redox-induced *cis*-to-*trans* isomerization. However, the *meta*-substituted radical cation has a shorter half-life than the *para*- substituted radical cation. As illustrated in Figure 2.3.17, **19b** is regenerated after populating **19a** via the photo-electro catalysis cycle.

Experimental details for X-ray structures:

Table 2.3.2 . Experimental Details for the Crystal Structure of *m*AA-Ph-N=N-Ph **18a** and *m*AA-Ph-N=N-An **19a**.

Structure		***m*AA-Ph-N=N-An**	***m*AA-Ph-N=N-Ph**
Reference code		scb266	scb273
Empirical Formula		$C_{27}H_{25}N_3O_3$	$C_{26}H_{23}N_3O_2$
Formula Weight		439.51	409.47
Crystal Dimensions (mm)		0.06 x 0.04 x 0.01	0.34 x 0.12 x 0.11
Crystal System, Space Group		Triclinic, P-1	Triclinic, P-1
Lattice Parameters:	a	9.648(5)	9.2384(4)
	b	15.123(7)	9.7733(4)
	c	16.095(8)	12.5100(6)
	α	97.776(6)	84.944(3)
	β	96.549(7)	80.298(2)
	γ	94.044(7)	75.010(2)
Volume ($Å^3$), Z		2303.0(19), 4	1074.30(8), 2
D_{calc} (g/cm^3)		1.241	1.266
F_{000}, μ(MoKα) (mm^{-1})		880, 0.112	432, 0.081
Diffractometer		Siemens SMART	Siemens SMART
Wavelength (Å), Temperature		0.71073, -100 °C	0.71073, -100 °C
θ range for data collection		1.29 to 26.32 °C	1.65 to 31.76
Limiting indices		-12<=h<=11	-13<=h<=13
		-18<=k<=18	-14<=k<=14
		-19<=l<=19	-18<=l<=18
Reflections Measured-Total		44346	21301
	Unique	9299 (R_{int} 0.0978)	7236 (R_{int} 0.0344)
Corrections:	Decay	No	No
	Absorption	No	No
	Secondary Extinction	coeff: 0.0011(9)	coeff: 0.0001(19)
Structure Solution		Direct	Direct
Data/restraints/parameters		9299/0/601	7236/0/281
GOF on F^2		0.937	1.031
Final R indices [I>2σ(I)] (R_1, wR_2)		0.0546, 0.1013	0.0512, 0.1323
R indices (all data) (R_1, wR_2)		0.1699, 0.1365	0.0801, 0.1523
Largest diff. peak and hole ($e^-Å^{-3}$)		0.155, -0.183	0.308 and -0.212

2.4 Synthesis experimental details

Materials and general instrumentation. Starting materials and solvents were purchased from Aldrich Chemical Co., Alfa Aesar, Oakwood Chemical, Ark Pharm Inc., Chem-Impex International, Inc., TCI America and used without further purification. N_2 gas was purchased from Airgas. All Pd-catalyzed reactions were performed under N_2 atmosphere. $Pd(dba)_2$, $Pd_2(dba)_3$, $P(tBu)_3$ and NaOtBu were all weighed out in a dry box. Activity III alumina were prepared by the addition of 6% H_2O to basic alumina (Aldrich, activated Brockmann I, ~150 mesh).

Apparatus- FT-IR spectra were recorded on a Bruker Alpha FTIR instrument (Bruker Optics Inc., Billerica, MA). All samples were placed over the detector and crushed using the anvil on a Bruker Alpha FTIR instrument (Bruker Optics Inc., Billerica, MA) featuring an attenuated total reflection (ATR) sampler equipped with a diamond crystal. Spectra were obtained in the range of 600–4000 cm^{-1}.

UV-Vis Optical spectra were recorded on a HP8452A Diode Array Spectrophotometer. Electrochemistry was performed on a PAR 273 electrochemical potentiostat (EG&G Instruments). Spectro electrochemistry data were recorded using both the spectrophotometer and potentiostat in tandem. The working electrode and counter electrode was ITO. The system was referenced to the platinum counter electrode.

Solution Cyclic Voltammetry was performed on a PAR 273 electrochemical potentiostat (EG&G Instruments). Methylene chloride, a CV solvent (Fisher) was pre-dried by stirring over H_2SO_4, washed & neutralized, and finally distilled from CaH_2 under N_2 atmosphere according to standard literature procedures.[69]

^{1}H and ^{13}C NMR spectra were recorded on Bruker AM-360 or AM-500 instruments with chemical shifts reported relative to the deuterated solvent or TMS.

Crystal diffraction data was gathered on a Siemens CCD SMART diffractometer and calculated using the Siemens Corporation SHELXTL crystallographic software package.[68] The Column Chromatography was performed on a Teledyne ISCO CombiFlash® Rf 200i.

All CHN analyses were performed by Atlantic Microlab Inc., Norcross, GA.

Light source for irradiation- Light-emitting diode sources were purchased from Zhongshan LED Technology Co., Ltd. The 430 nm and 450 nm light source was composed of 7x1 W Diamond Grow LED with an input Voltage of AC 90-264 Volts. The 7x1 W LEDs were housed in a 3.70 inches x 3.86 inches Fins Slotted Aluminum casing. The 365 nm light source was purchase from Salon Edge (model number: MAN-UV2009). It was composed of 4x9 W Pixnor U-shaped 365 nm Lamp bulb Tube for Nail Dryer UV Lamp.

Tetrabutylammonium tetrafluoroborate ($TBABF_4$)- A supporting electrolyte, was purchased from *TCI America* and was purified according to standard literature procedures, [69] or recrystallized from 50 % ethanol three times, then dried in a vacuum oven (100 °C, 0.1 Torr) for 48 hours.

Preparation of Tol_3TBABF_4 gel[70]- In a 50 mL oven dried glass jar equipped with a stir bar, 5.33 g of $TBABF_4$ was dissolved in 15 mL of toluene by gently heating. The stirring was stopped after 5 min or when $TBABF_4$ dissolved to allow the colorless solution phases to settle. The bottom phase was Tol_3TBABF_4 gel (10 mL, 1.62 M) and the top phase was toluene (5 mL)

[68] SHELXTL/PC Version 6.14 Structure Analysis Package, Bruker AXS, 2000- 2003.
[69] Perrin, D. D. and Armarego, W. L. F., *Purification of Laboratory Chemicals*, Pergamon Press: Oxford, 1988
[70] Picket, C. J. A simple Hydrocarbon Electrolyte: Completing the Electron-transfer Series $[Fe_4S_4(SPh)_4]^{1-/2-/3-/4-}$, *J. Chem. Soc.* **1985**, 323-326.

as determined by ^{1}H NMR spectroscopy. The jar was then capped and stored in cabinet at room temperature under ambient conditions.

ITO glass cleaning procedure- ITO coated glass was purchased from Delta Technologies (part no. CB-50IN-1111). The slide was rinsed and soaked in ACS grade acetone for 5.0 min. It was then sonicated for 10 min in diluted aqueous soap solution. After sonication, the slide was rinsed thoroughly with distilled water, acetone, and methylene chloride, respectively. The surface was then dried using stream of dry N_2 gas. The ITO side of the slide was determined using multi-meter resistance measurement.

Preparation of plastic spacer- Polyethylene Plastic Sheeting (Husky Brand) was used as spacer in PECD. The thickness of the spacer was 88.9 μm. Before applying to clean ITO glass substrate, a square (area: ~0.8 cm^2) was cut out of the plastic sheet.

Preparation of photo electrochromic device (PECD)-trans-pAA-Ph-NN-Ph- (0.85 mg, 0.0021 mmol) was dissolved in 0.25 mL Tol_3TBABF_4 gel. The gel solution was applied to ITO glass anode (equipped with spacer); the ITO glass cathode was then added to complete sandwich-type device. The ITO sandwich was held together with two closed jaw compressor clamps for the duration of the experiment. For picture of PECD, see Figure 2.2.32. Cycling conditions were: 30 sec irradiation with 430 nm LED and 0.0 V, then 1.5 V for 30 s with no irradiation (Cyclic Voltammetry Scan Rate: 2 V/s). Spectrophotometer Reading- 30 s intervals.

Synthesis:

Preparation of Dianisylamine 3

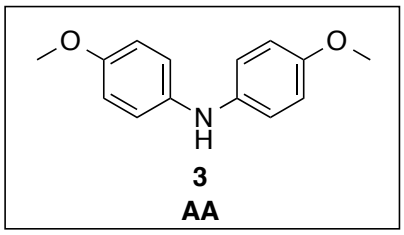

3
AA

p-anisidine (3.75 g, 30.4 mmol) and *p*-bromoanisole (5.64 g, 30.1 mmol) were added into a 100 mL flamed-dried rb flask. The mixture was transported

into a N_2 purged dry box. Toluene (anhyd. 50 mL) was added to the flamed-dried rb flask and stirred. $Pd(dba)_2$ (0.173 g, 0.302 mmol), $P(tBu)_3$ (0.067 g, 0.332 mmol) and toluene (anhyd. 2 mL) were added into an oven-dried vial and stirred for 10 min. The mixture in the vial was emptied into the flame-dried rb mixture and stirred for 5 minutes. NaOtBu (4.45g, 46.3 mmol) was then added with an addition of toluene (anhyd 10 mL). The mixture was capped with a rubber septum, removed from the dry box and stirred under N_2 for 10 h at 90 °C. The reaction mixture was monitored via TLC (ethyl acetate:hexanes 1:2) until both starting materials were no longer present and the product became visible. After the disappearance of the starting materials, the mixture was filtered through 20 g of basic alumina III by vacuum filtration and washed with 200 mL of ethyl acetate. The product was concentrated in vacuo to yield **3** (6.90 g, 30.1 mmol) as a light pink solid without any further purification. Ohta *et al.* previously prepared amine **3** with 67% yield by a Buchwald-Hartwig amination with BINAP as ligand.[71]

Yield: 99.9% MW = 229.28 mp = 98-100 °C (lit. 101-103 °C)[72]

^{1}H NMR (360 MHz, $CDCl_3$, 25 °C):

δ (ppm) 6.93 (d, J = 8.90 Hz, 4H), 6.81 (d, J = 8.86 Hz, 4H), 5.26 (s, 1H), 3.76 (s, 6H).

^{13}C NMR (125 MHz, CDCl3, 25 °C):

δ (ppm) 154.54; 138.23; 119.82; 114.99; 55.89

Preparation of *p*-Br-nitrosobenzene 8

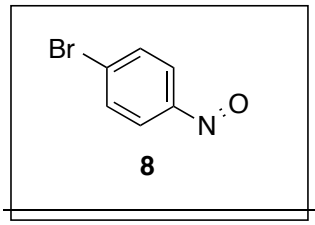

8

[71] Ohta, K.; Chiba, Y.; Kaise, A.; Endo, Y. Structure-activity relationship study of diphenylamine-based estrogen receptor antagonists. *Bioorg. Med. Chem.* **2015***, 23*, 861-867.

[72] Chudomel, J. M.; Yang, B.; Barnes, Michael D.; Achermann, M.; Mague, J. T.; Lahti, P. M. Highly Twisted Triarylamines for Photoinduced Intramolecular Charge Transfer. *Journal of Physical Chemistry A,* **2011**, *115(30),* 8361-8368.

Commercially available *p*-bromoaniline (2.01 g, 11.7 mmol) was placed in a 250 mL rb flask with DCM (20 mL) and stirred at room temperature until dissolved. To this solution, Oxone®

$2KHSO_5 \cdot KHSO_4 \cdot K_2SO_4$ (14.4 g, 23.4 mmol) dissolved in DI H_2O (60 mL) was added drop wise into the mixture of *p*-bromoaniline and DCM. The mixture turned green after the addition of the Oxone® solution. The solution was stirred vigorously for 6 h at room temperature. The organic layer was extracted with DCM (3 x 30 mL) and dried with Na_2SO_4. Gravity filtration was used to separate the drying agent from the green organic solution. The resulting green solution was concentrated in vacuo yielding **8 (**2.01 g, 10.8 mmol) as a tan solid (green solution) without any further purification. Priewisch *et al.* previously prepared nitroso **8** with a 70% yield. The purification method used was sublimation. [73]

Yield: 92% MW = 186.01 mp = 95-99 °C (lit. 95 °C)[74]

^{1}H NMR (360 MHz, $CDCl_3$, 25 °C):

δ (ppm) 7.76 (s, 4H).

^{13}C NMR (125 MHz, CDCl3, 25 °C):

δ (ppm) 164.06; 132.91; 131.86; 122.30

Preparation of *p-Br-Ph-N=N-Ph* 10

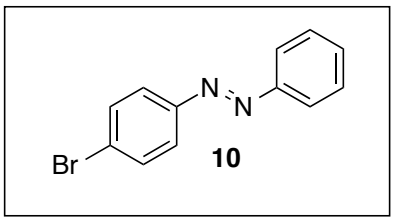

10

p-bromonitrosobenzene **8** (1.00 g, 5.37 mmol) and aniline (0.500 g, 5.37 mmol) were placed in a 25 mL rb flask with glacial acetic acid (10 mL) and stirred vigorously at room temperature. The solution turned red after 1 min. It was stirred for 24 h and the precipitate

[73] Priewisch, B.; Ruck-Braun, K.; Efficient Preparation of Nitrosoarenes for the Synthesis of Azobenzenes. *J. Org. Chem.*, **2011**, *70*, 2350-2352.
[74] Defoin, A., Simple Preparation of Nitroso Benzenes and Nitro Benzenes by Oxidation of Anilines with H2O2 Catalysed with Molybdenum Salts. *Synthesis,* **2004**, *5*, 706-710.

formed was filtered by vacuum filtration to give an orange solid. The orange solid was washed three times with 30 mL saturated aqueous $NaHCO_3$-solution. The solid was recrystallized in a hot EtOH yielding **10 (**.80 g, 3.1 mmol) as orange crystals. Kaiser *et al*. previously prepared **8** with 71% yield.[75]

Yield: 57% MW = 261.12 mp = 83 – 85 °C (lit. 88-89 °C)[76]

^{1}H NMR (500 MHz, $CDCl_3$, 25 °C):

δ (ppm) 7.51 (m, 3H), 7.63 (d, J = 8.75 Hz, 2H), 7.77 (d, J = 8.75 Hz, 2H), 7.90 (d, J = 6.75 Hz, 2H).

^{13}C NMR (125 MHz, $CDCl_3$, 25 °C):

δ (ppm) 152.76; 151.63; 132.56; 131.53; 129.37; 125.58; 124.59; 123.17

Preparation of *p*AA-Ph-N=N-Ph 4a

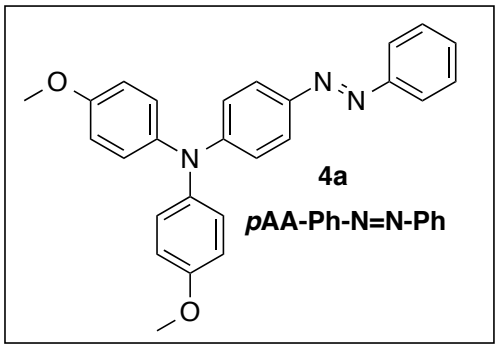

4a

***p*AA-Ph-N=N-Ph**

The synthesis of **4a** was prepared analogously to **3** from **10** (0.151 g, 0.577 mmol) and **3** (0.132 g, 0.577 mmol). $Pd(dba)_2$ (0.0033 g, 0.0057 mmol), $P(tBu)_3$ (0.0012 g, 0.0057 mmol) and NaOtBu (0.089 g, 0.924 mmol). Removal of the solvent gave a red solid, which was purified via column chromatography (benzene/hexanes) to afford **4a** (0.215 g, 0.525 mmol).

Yield: 91% MW = 409.49 mp = 157 – 159 °C

^{1}H NMR (500 MHz, $CDCl_3$, 25 °C):

[75] M., Kaiser; S.P., Leitner; C., Hirtenlehner; M., List; A., Gerisch; U., Monkowius; Azobenzene-functionalized N-heterocyclic carbenes as photochromic ligands in silver(I) and gold(I) complexes. *Dalton Trans.,* **2013**, *42*, 14749-14756 .

[76] Fraleoni-Morgera, A; Giorgini, L.; Zanirato, P. [Arylazobenzene–BF_3] dyes: Electronic absorption and NMR spectroscopic evidence for a novel class of dyes stable in aprotic solvents. *Dyes and Pigmnets.* **2008**, *76*, 394-399.

δ (ppm) 7.82 (d, J = 7.35 Hz, 2H), 7.75 (d, J = 8.63 Hz, 2H), 7.46 (t, J, 2H), 7.38 (t, J = 7.51 Hz, 1H), 7.11 (d, J = 8.63 Hz, 4H), 6.93 (d, J = 8.63 Hz, 2H), 6.86 (d, J = 8.63 Hz, 4H), 3.80 (s, 6H).

^{13}C NMR (125 MHz, $CDCl_3$, 25 °C):

δ (ppm) 156.96; 153.30; 151.69; 146.26; 140.05; 130.05; 129.18; 127.71, 124.55; 122.59; 118.84; 115.13; 55.71.

CHN ($C_{26}H_{23}N_3O_2$):

Calcd: C, 76.26; H, 5.66; N, 10.26.

Found: C, 75.98; H, 5.81; N, 10.11.

m/z

Calcd: 409.1790

Found: 409.1798

UV/Vis (benzene, λ_{max}/nm, (ε/L · mol^{-1} · cm^{-1})):

438 (27023)

IR (cm^{-1}):

2833, 1593, 1500, 1476, 1340, 1297, 1243, 1135, 1033, 826, 690.

Preparation of *p*-Br-Ph-N=N-An 13

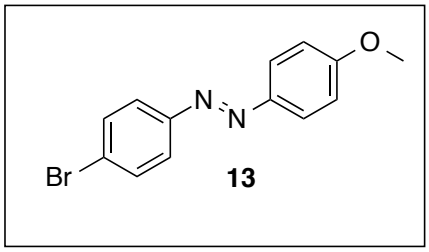

13

The synthesis of **13** was prepared analogously to **10** from **8** (0.580 g, 3.12 mmol), *p*-anisidine (0.384 g, 3.12 mmol) and glacial acetic acid (10 mL). The crude was recrystallized in hot EtOH yielding **13** (0.630 g, 2.16 mmol) as orange crystals.

Yield: 69% MW = 291.15 mp = 146- 150 °C

^{1}H NMR (360 MHz, $CDCl_3$, 25 °C):

δ (ppm) 7.90 (d, J = 8.30 Hz, 2H), 7.72 (d, J = 8.43 Hz, 2H), 7.61 (d, J = 8.43 Hz, 2H), 7.00 (d, J = 8.43 Hz, 2H), 3.88 (s, 3H).

^{13}C-NMR (125 MHz, $CDCl_3$, 25 °C):

δ (ppm) 162.59; 151.77; 147.14; 132.46; 125.13; 124.77; 124.31; 114.53; 55.83

Preparation of *p*AA-Ph-N=N-An <u>5a</u>

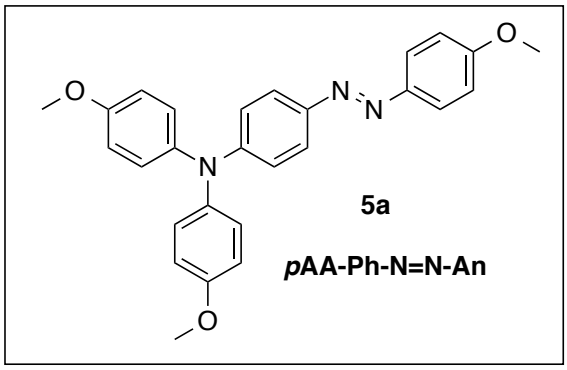

The synthesis of **5a** was prepared analogously to **3** from **13** (0.701 g, 2.41 mmol), **3** (0.550 g, 2.41 mmol), $Pd(dba)_2$ (0.042 g, .072 mmol), $P(tBu)_3$ (.015 g, .072 mmol), and NaOtBu (.231 g, 2.40 mmol). The product was concentrated in vacuo to afford a red solid**,** which was recrystallized from isopropanol to yield **5a** (0.94 g, 2.14 mmol) as an orange solid.

Yield: 89% MW = 439.52 mp = 100 - 104 °C

^{1}H NMR (500 MHz, $CDCl_3$, 25 °C):

δ (ppm) 7.83 (d, J = 9.01 Hz, 2H), 7.71 (d, J = 9.01 Hz, 2H), 7.10 (d, J = 9.01 Hz, 4H), 6.97 (d, J = 9.01 Hz, 2H), 6.94 (d, J = 9.01 Hz, 2H), 6.85 (d, J = 9.01 Hz, 4H), 3.86 (s, 3H), 3.80 (s, 6H).

^{13}C-NMR (125 MHz, $CDCl_3$, 25 °C):

δ (ppm) 161.47; 156.80; 147.62; 146.43; 140.27; 127.55; 124.33; 124.10, 119.19; 115.09; 114.36; 55.74; 55.71.

CHN ($C_{27}H_{25}N_3O_3$)

Calcd: C, 73.79; H, 5.73; N, 9.56;

Found: C, 73.56; H, 5.83; N, 9.47.

m/z

Calcd: 439.1896

Found: 439.1892

UV/Vis (benzene, λ_{max}/nm, (ε/L · mol^{-1} · cm^{-1})):

436 (24270)

IR (cm^{-1}):

2833, 1593, 1500, 1476, 1315, 1237, 1142, 1129, 1029, 828.

Preparation of *m*-Bromo-nitrosobenzene 15

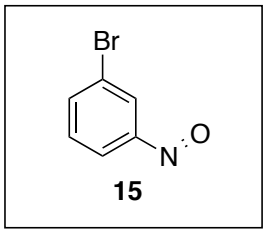

15

The synthesis of **15** was prepared analogously to **8** from *m*-bromoaniline (2.00 g, 11.6 mmol), and Oxone® $2KHSO_5 \cdot KHSO_4 \cdot K_2SO_4$ (14.3 g, 23.3 mmol per persulfate). The product was concentrated in vacuo yielding **15** (2.13 g (11.5 mmol) as a tan brown solid (green solution). Tibiletti et al. previously synthesized **15** with a 97% yield.[77]

Yield: 98% MW = 186.01 mp 78 – 80 °C (lit. 77 °C)77

^{1}H NMR (360 MHz, $CDCl_3$, 25 °C):

δ (ppm) 8.10 (d, J = 8.00 Hz, 1H), 7.82 (dt, J = 8.00 Hz, J = 1. Hz, 1H), 7.75 (t, J = 1.8 Hz, 1H), 7.55 (t, J = 7.55 Hz, 1H).

Preparation of *m*Br-Ph-N=N-Ph 16

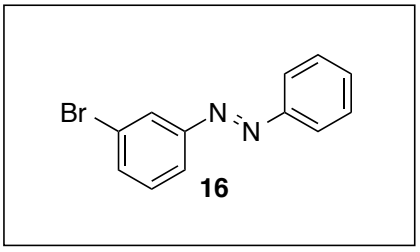

16

The synthesis of **16** was prepared analogously to **10** from **15** (1.01 g, 5.44 mmol), aniline (0.506 g, 0.544 mmol),

[77] Tibiletti, F.; Simonetti, K.; Palmisano, G.; Parravicini, M.; Imbesi, F.; Tollari, S.; and Penoni, A. One-pot Synthesis of Meridianins and Meridianin Analogues via Indolization of Nitrosoarenes. *Tetrahedron*, **2010**, *66*, 1280-1288.

and 8 mL of glacial acetic acid. After 24 hours, the solution turned red with no precipitate formed. The mixture was neutralized with saturated aqueous $NaHCO_3$-solution. The organic layer was extracted three times with 30 mL DCM and dried over Na_2SO_4. It was concentrated in vacuo to give a red solid which was purified (CC : ethyl acetate/hexanes) to yield **16** (0..82 g, 3.14 mmol) as an orange solid. Cao, Y. et al. previously synthesized **16** by a deoxygenative coupling of nitroarenes route with a 67% conversion.[78]

Yield: 58% MW = 261.12 mp = 65 – 70 °C (lit. 67- 69 °C)[79]

^{1}H NMR (360 MHz, $CDCl_3$, 25 °C):

δ (ppm) 8.03-8.05 (t, J= 2.10Hz, 1H), 7.92-7.85 (m, 3H), 7.60-7.47 (m, 4H), 7.41-7.37 (t, J = 8.28 Hz, 1H)

^{13}C-NMR (125 MHz, $CDCl_3$, 25 °C):

δ (ppm) 153.6; 152.4; 133.6; 131.5; 130.4; 129.2; 124.7; 123.1; 122.9

Preparation of *m*Br-Ph-N=N-An 17

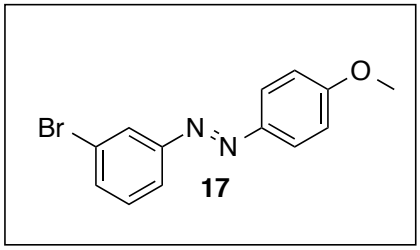

17

The synthesis of **17** was prepared analogously to **10** from **15** (0.101 g, 0.542 mmol), *p*-anisidine (0.067 g, 0.542 mmol), and 5 mL of glacial acetic acid. After 24 hours, the solution turned red with no precipitate formed. The mixture was neutralized with saturated aqueous $NaHCO_3$-solution. The organic layer was extracted three times with 30 mL DCM and dried over Na_2SO_4. It was concentrated in vacuo to give a red solid which was purified (CC : ethyl acetate /hexanes) to yield **17** (0.155 g, 0.531 mmol) as an orange solid.

[78] Li, H-Q.; Liu, X.; Zhang, Q.; Li, S-S.; Liu, Y-M.; He, H-Y.;Cao, Y., Deoxygenative coupling of nitroarenes for the synthesis of aromatic azo compounds with CO using supported gold catalysts. *Chem. Commun.,* **2015**, *51*, 11217-11220.

[79] Jaffe, H. H.; Gardner, R. W.; Tautomeric equilibria. IV. The basicities of monosubstituted azobenzenes. An acidity scale in 20% ethanolic aqueous sulfuric acid. *Journal of the American Society*, **1958**, *80*, 319-323.

Yield: 98% MW = 291.15 mp = 48 – 51 °C

^{1}H NMR (360 MHz, $CDCl_3$, 25 °C):

δ (ppm) 8.00 (s, 1H), 7.91 (d, J = 8.72 Hz, 2H), 7.81 (d, J = 8.07 Hz, 1H), 7.53 (d, J = 7.43 Hz, 1H), 7.36 (t, J = 7.43 Hz, 1H), 7.00 (d, J = 8.72 Hz, 2H) 3.88 (s, 3H).

^{13}C-NMR (125 MHz, $CDCl_3$, 25 °C):

δ (ppm) 162.76; 153.98; 147.03; 133.14; 130.58; 125.27; 124.63; 123.30; 122.85; 114.54; 55.84.

Preparation of *m*AA-Ph-N=N-Ph <u>18a</u>

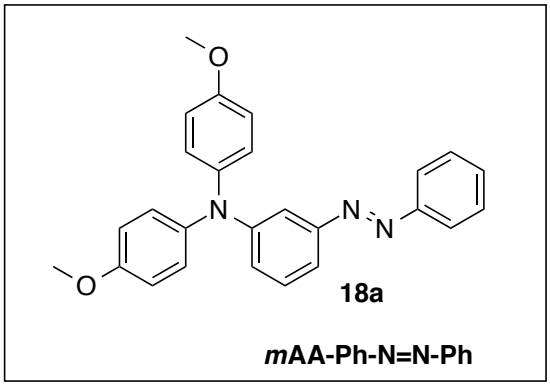

The synthesis of **18a** was prepared analogously to **4a** from **16** (0.159 g, 0.610 mmol), **3** (0.140 g, 0.610 mmol), $Pd(ba)_2$ (0.007 g, 0.012 mmol), $P(tBu)_3$ (0.003 g, 0.012 mmol), NaOtBu (0.094 g, 0.976 mmol), and toluene (anhy. 5 mL) for 24 hours at 90 °C. The product was concentrated in vacuo to afford a red orange solid which was purified (CC : ethyl acetate/hexanes) to yield **18a** **(**0.159 g, 1.55 mmol) as an orange solid.

Yield: 64% MW = 409.48 mp = 113 - 116 °C

^{1}H NMR (360 MHz, $CDCl_3$, 25 °C):

δ (ppm) 7.84-7.80 (m, 2H), 7.50-7.40 (m, 4H), 7.36 (d, J = 7.32 Hz, 1H), 7.26 (t, J = 8.05 Hz, 1H), 7.09 (d, J = 9.07 Hz, 4H), 7.01 (d, J = 8.14 Hz, 1H), 6.83 (d, J = 9.07 Hz, 4H), 3.79 (s, 6H).

^{13}C-NMR (125 MHz, $CDCl_3$, 25 °C):

δ (ppm) 156.31; 153.94; 152.92; 149.96; 140.96; 131.04; 129.61; 129.22; 126.96; 123.02; 122.97; 115.56; 115.06; 114.27; 55.72.

CHN ($C_{26}H_{23}N_3O_2$)

Calcd: C, 76.26; H, 5.66; N, 10.26

Found: C, 76.48; H, 5.86; N, 10.11

m/z

Calcd: 409.1790

Found: 409.1796

Preparation of *m*AA-Ph-N=N-An 19a

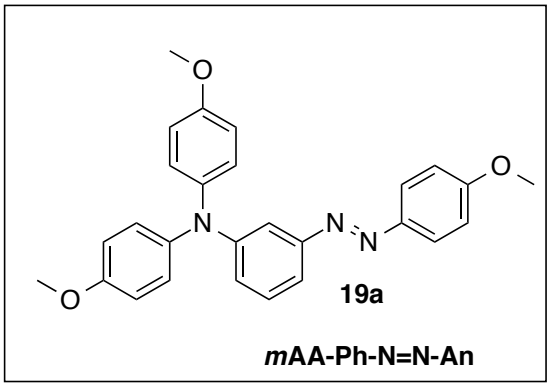

The synthesis of **19a** was prepared analogously to **4a** from **17** (0.228 g, 0.783 mmol), **3** (0.197 g, 0.861 mmol), $Pd(ba)_2$ (0.009 g, 0.016 mmol), $P(tBu)_3$ (0.004 g, 0.017 mmol), and NaOtBu (0.124 g, 1.29 mmol) for 24 hours at 90 °C. The product was concentrated in vacuo to afford a red orange solid which was purified (CC : ethyl acetate/hexanes) to yield **19a** (0.288 g, 0.655 mmol) as an orange solid.

Yield: 84% MW = 439.52 mp = 132 - 135 °C

^{1}H NMR (360 MHz, $CDCl_3$, 25 °C):

δ (ppm) 7.84 (d, J = 9.07 Hz, 2H), 7.45 (t, J = 1.9 Hz, 1H), 7.33 (d, J = 7.32 Hz, 1H), 7.23 (t, J = 8.05 Hz, 1H), 7.09 (d, J = 9.07 Hz, 4H), 6.99 (d, J =2.40 Hz, 1H), 6.96 (d, J = 8.63 Hz, 2H), 6.83 (d, J = 9.07 Hz, 4H), 3.86 (s, 3H), 3.79 (s, 6H).

^{13}C-NMR (125 MHz, $CDCl_3$, 25 °C):

δ (ppm) 161.99; 153.84; 147.05; 140.85; 126.67; 124.72; 122.38; 115.26; 114.81; 114.15; 113.94; 55.56; 55.50.

CHN ($C_{27}H_{25}N_3O_3$)

Calcd: C, 73.79; H, 5.73; N, 9.56.

Found: C, 73.43; H, 5.84; N, 9.40.

m/z

Calcd: 439.1896

Found: 439.1895

UV/Vis (benzene, λ_{max}/nm, (ε/L · mol^{-1} · cm^{-1})):

344 (30764)

IR (cm^{-1}):

2833.4, 1598.6, 1594.4, 1503.8, 1438.6, 1284.3, 1241.8, 1178.1, 1144.1, 1104.4, 1026.6.

CHAPTER 3

BIS(AMINO)AZOBENZENES AS PHOTO-ELECTRO SWITCHES

3.1 Introduction

As stated in chapter 2, incorporating an electron rich redox-active (RA) arylamino moiety in the 4- position to the -N=N- group of AB resulted in a redshift of the $\pi \rightarrow \pi^*$ absorption band, resulting in an overlap of the $\pi \rightarrow \pi^*$ and the $n \rightarrow \pi^*$ absorption bands. Furthermore, incorporating a RA moiety at the 4- position to the -N=N- group of AB causes an increase in the rate of the thermal isomerization from *cis*-to-*trans* compared to AB. These new *para*- arylamino redox-appended azo switches are capable of efficient "photo-closing" to the *cis* isomer and rapidly isomerized to their *trans* isomer (within picoseconds) upon one electron removal.

Furthermore, we have shown that relocating the RA group to the 3- position to the -N=N- group causes the *meta*- arylamino azobenzenes to exhibit absorption spectra similar to unsubstituted-AB and behave analogously. These new *meta*- arylamino redox-appended azo switches are also capable of efficient "photo-closing" to the *cis* isomer and rapidly isomerized to their *trans* isomer upon one electron removal.

To better understand such systems, it is essential to understand the effects of introducing an additional RA moiety at the 4′- position of **4a** and **19a**. Figure 3.1.1 shows the model of the two Bis(arylamino) azobenzenes. The *trans* isomer (blue) isomerizes to the *cis* isomer (red) by photo-absorption, and the *cis* isomer (red) then rapidly isomerizes to the *trans* isomer (blue) upon one electron removal.

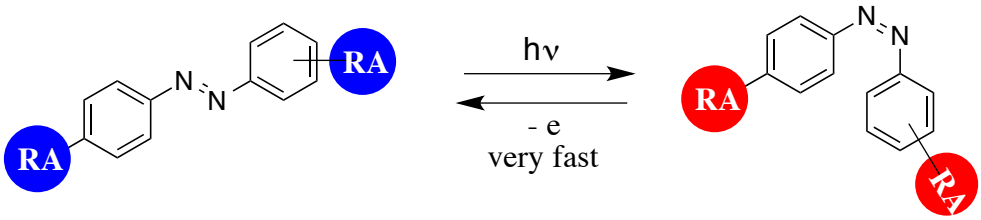

Figure 3.1.1 Model of the bis(amino)azobenzene photo-electro switch. The *trans* isomer (blue) isomerizes to the *cis* isomer (red) by photo-absorption, and the *cis* isomer (red) then rapidly isomerizes to the *trans* isomer (blue) upon oxidation.

We hypothesized that having two RA groups at the 4- and 4′- positions to the -N=N- group will cause the bis(*para*-arylamino) azobenzenes, **27a**, to behave similarly to **4a**. The addition of the additional RA at the 4′- position should result in an acceleration of the thermal *cis*-to-*trans* isomerization and decrease the $\Delta G^{\neq}$ for the thermal isomerization for **27a**. We also hypothesized that placing an additional RA group at the 4′- position to the -N=N- group of **19a** will cause the Bis(*para-meta*- arylamino) azobenzenes, **28a**, to behave more similarly to **4a** than unsubstituted-AB. The additional RA group should lead to an increase in the rate of the thermal *cis*-to-*trans* isomerization and a decrease in the $\Delta G^{\neq}$ for the thermal isomerization. In this section, we will investigate the effects of the additional RA group on the thermal *cis*-to-*trans* isomerization rate. We will also investigate the effect of the additional RA group on the redox-induced *cis*-to-*trans* isomerization.

3.2 Bis(arylamino)azobenzenes: *p*AA-Ph-N=N-Ph-*p*AA 27a and *p*AA-Ph-N=N-Ph- *m*AA 28a

As in chapter 2, arylamine **3** was utilized as our redox auxiliary (RA) moiety because of its excellent redox properties; it is chemically stable in both neutral and radical cation forms. The basic premise of our work is that the radical cation, $AA^{\bullet+}$-azo-AA, will be much more reactive toward *cis*-to-*trans* isomerization than its neutral *cis* form. Thus, removal of one

electron from *cis*-AA-azo-AA to make *cis*-AA$^{\bullet+}$-azo-AA induces rapid *cis*-to-*trans* isomerization of the azo moiety. Scheme 3.2.1 and Scheme 3.2.2 depict their synthetic routes, respectively.

Synthesis:

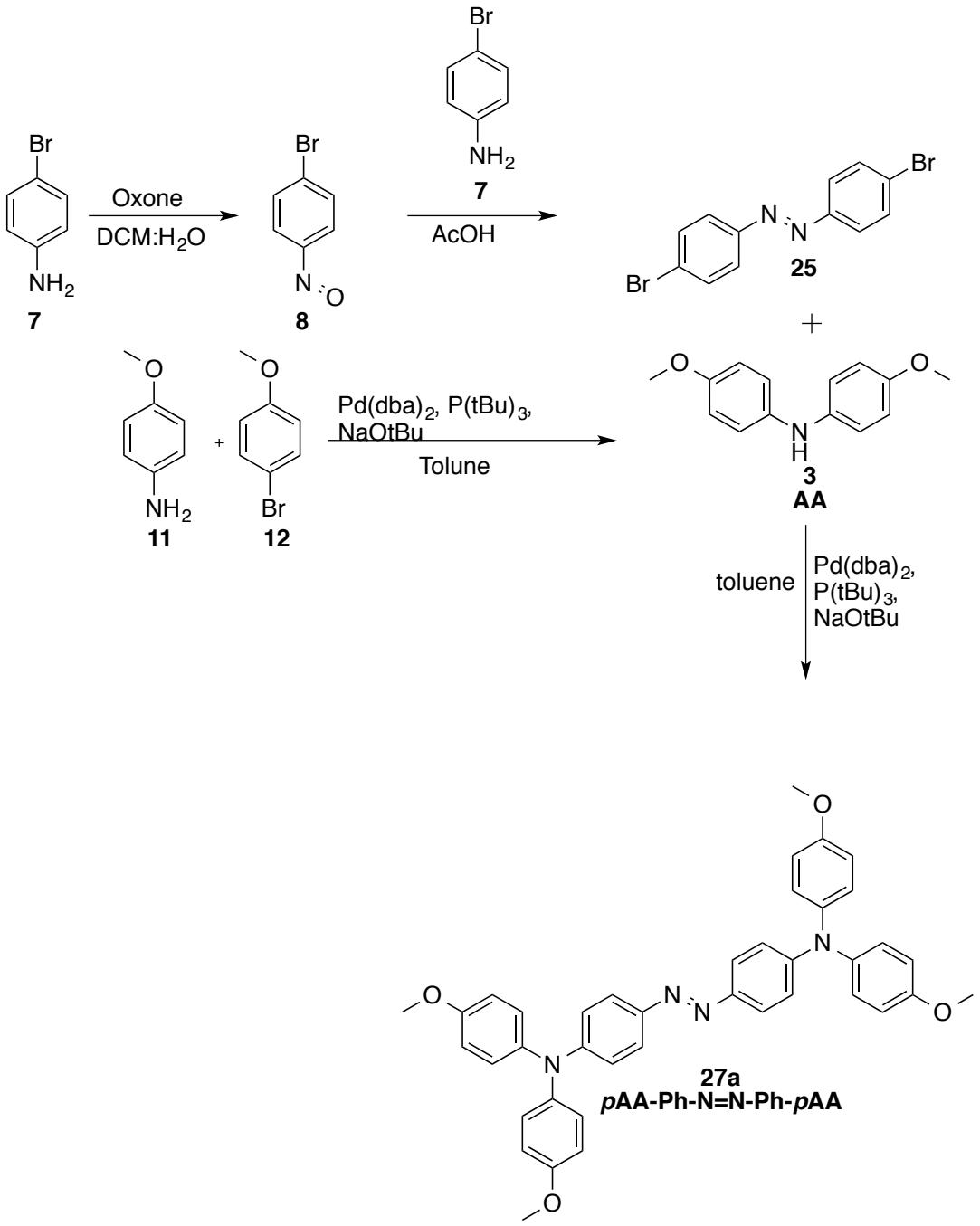

Scheme 3.2.1 Synthetic route to obtain *p*AA-Ph-N=N-Ph-*p*AA **27a**.

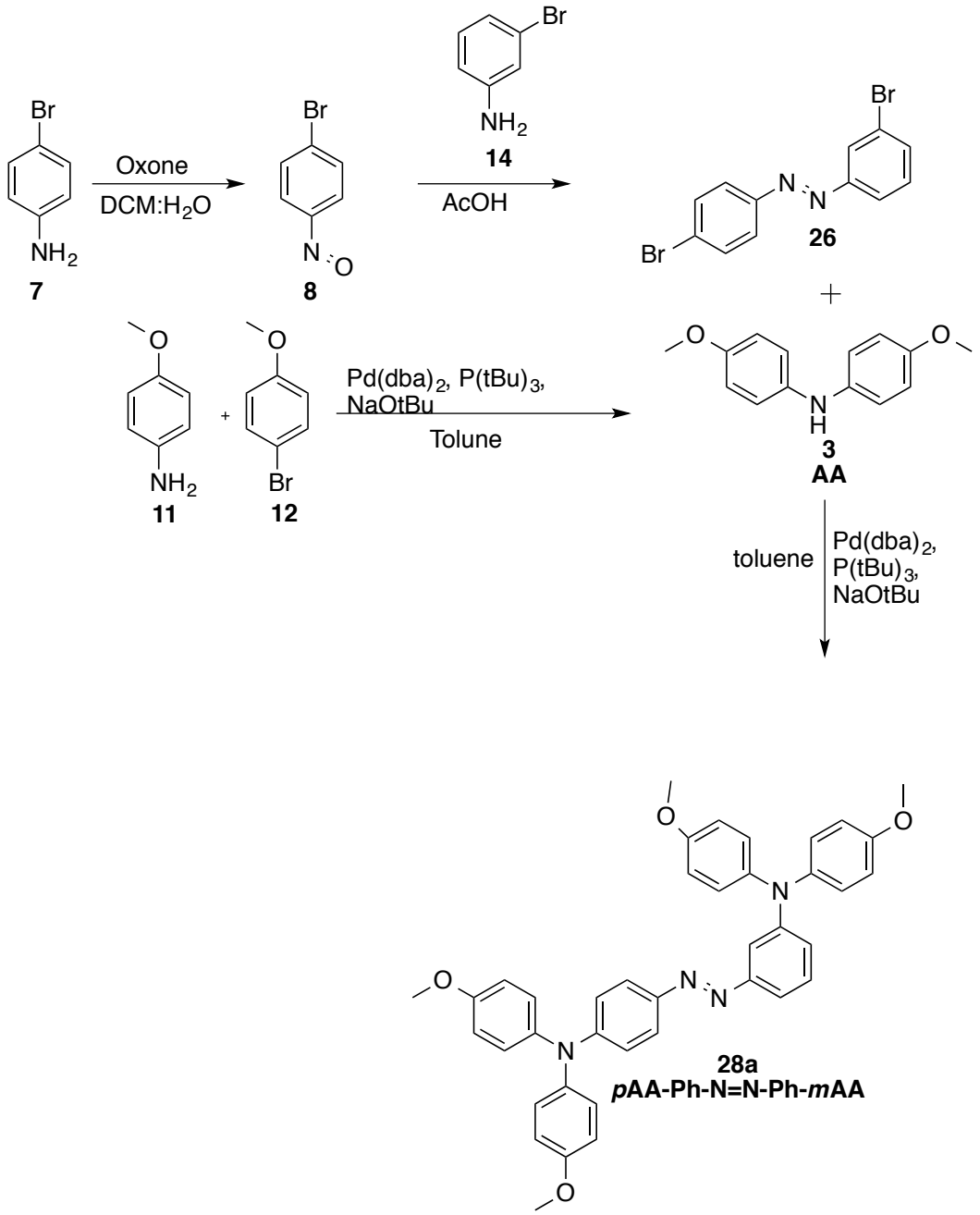

Scheme 3.2.2. Synthetic route to obtain *p*AA-Ph-N=N-Ph-*m*AA **28a**.

3.2.1 Photochemistry and optical absorption of 27a and 28a

The incorporation of an additional RA group at the 4´- position of **4a** and **19a** resulted in a bathochromic shift of the $\pi \rightarrow \pi^*$ absorption band in the absorption spectrum. Consequently, the maximum absorbances are shifted to longer wavelengths in comparison to **4a** and **19a**. Figure 3.2.1 and Figure 3.2.2 depict the optical spectra of **27a** and **28a**, respectively. As in the *para*- arylamino azobenzenes, the $\pi \rightarrow \pi^*$ and the $n \rightarrow \pi^*$ absorption bands are overlapping. As a result, the $\pi \rightarrow \pi^*$ absorption bands of both **27a** and **28a** are positioned in the visible region of the spectrum where visible light can easily be applied to isomerize both compounds, **27a** and **28a**, to their respective *cis* isomers, **27b** and **28b**. However, in these two systems, return to the *trans* isomer via "photo-opening" is not possible due to the overlap of the two transitions. The isomerization of **27b** and **28b** to their corresponding *trans* isomers can only occur by allowing the *cis* isomers to thermally isomerized to their respective *trans* isomers, which poses a problem when using AB derivatives as molecular switches because it cannot be turn on and off on demand as stated previously.

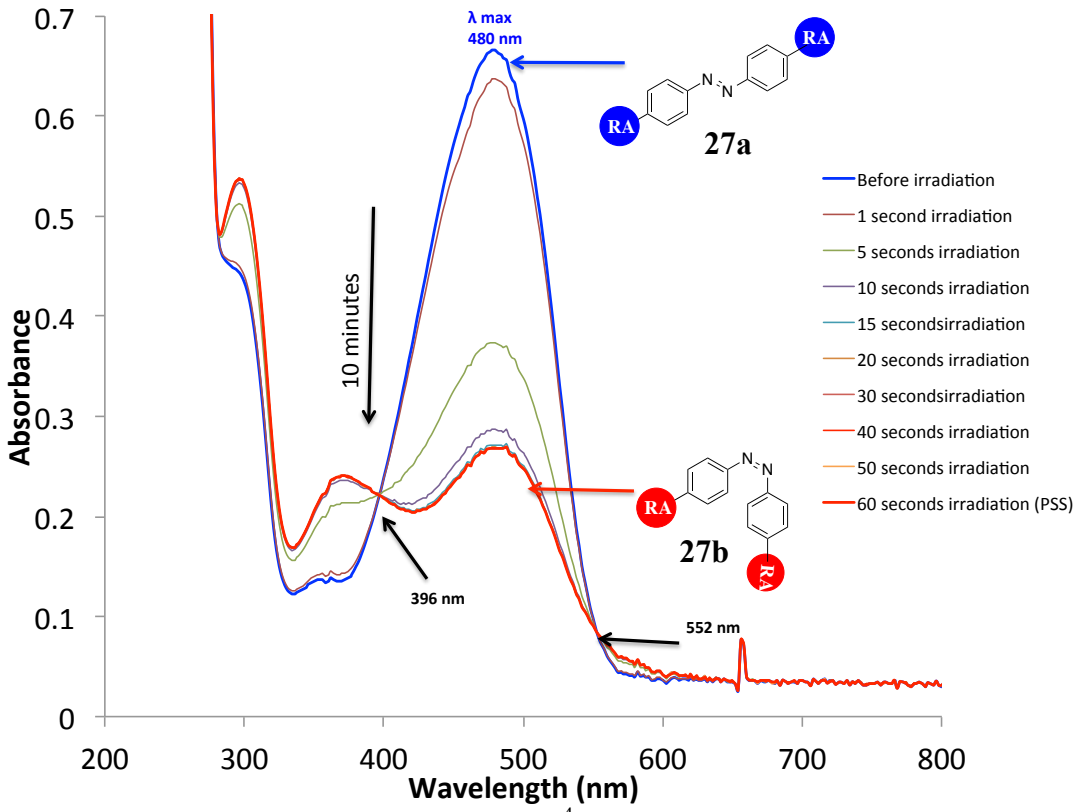

Figure 3.2.1. Optical spectrum of **27a** (4.89 x 10^{-4} M in C_6D_6) irradiated with a 450 nm LED at room temperature in 0.1 cm quartz UV-Vis cell.

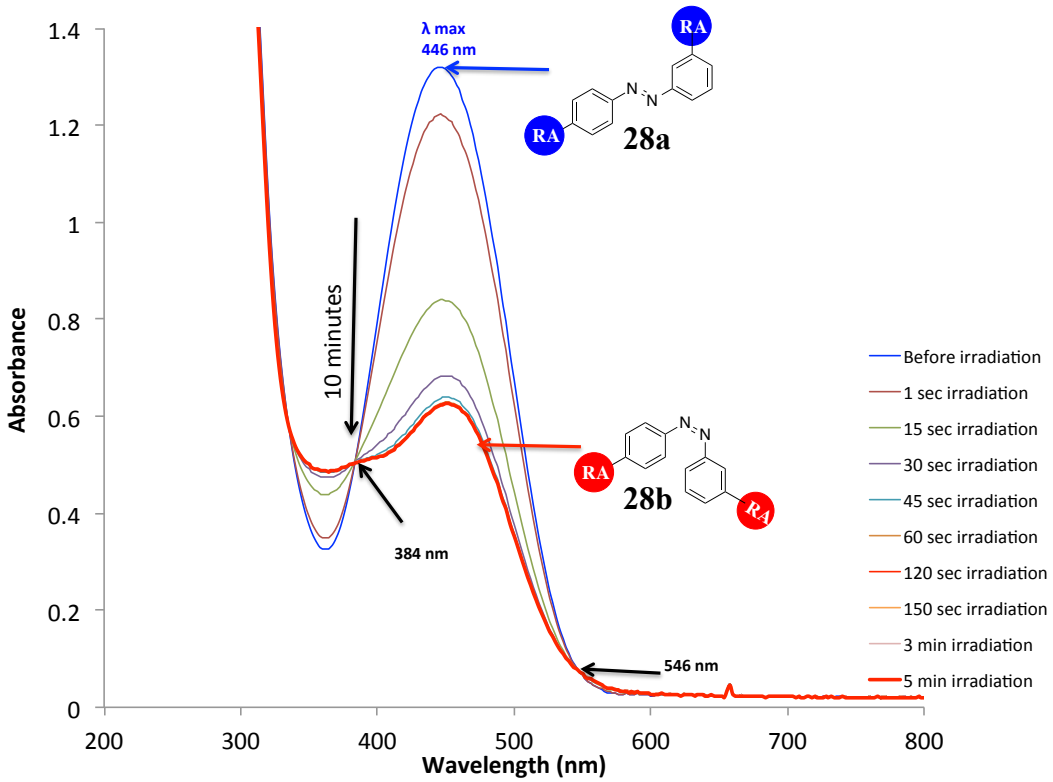

Figure 3.2.2. Optical spectrum of **28a** (6.01 x 10^{-4} M in C_6D_6) irradiated with a 450 nm LED at room temperature in 0.1 cm quartz UV-Vis cell.

Figure 3.2.1 and Figure 3.2.2 show the photochemistry of **27a** to **27b** and **28a** to **28b** isomerization process, respectively. Ultraviolet-visible spectroscopy is used to determine the time at which the PSS is reached. In both bis(arylamino) azobenzenes, **27a** and **28a**, the *trans*-to-*cis* isomerization occurs upon excitation of the π → π* absorption band at 400-515 nm (2.41 eV), while the *cis*-to-*trans* isomerization cannot occur via excitation of the n → π* absorption band because of its overlap with the π → π* absorption band. *Cis*-to-*trans* isomerization can only occur thermally.

The optical spectra in Figure 3.2.1 and Figure 3.2.2 show a strong π → π* absorption maximum at 480 nm for **27a** and 446 nm for **28a**. The n → π* absorption bands cannot be

resolved until the lowering of the absorbance attributed to the π → π* transition band. However, after irradiating the π → π* absorption band with a 450 nm LED light source and reaching the PSS, the n → π* absorption bands become visible for both Bis(arylamino) azobenzenes with two isosbestic points at 396 nm and 552 nm for **27a** and two isosbestic points at 384 nm and 546 nm for **28a**.

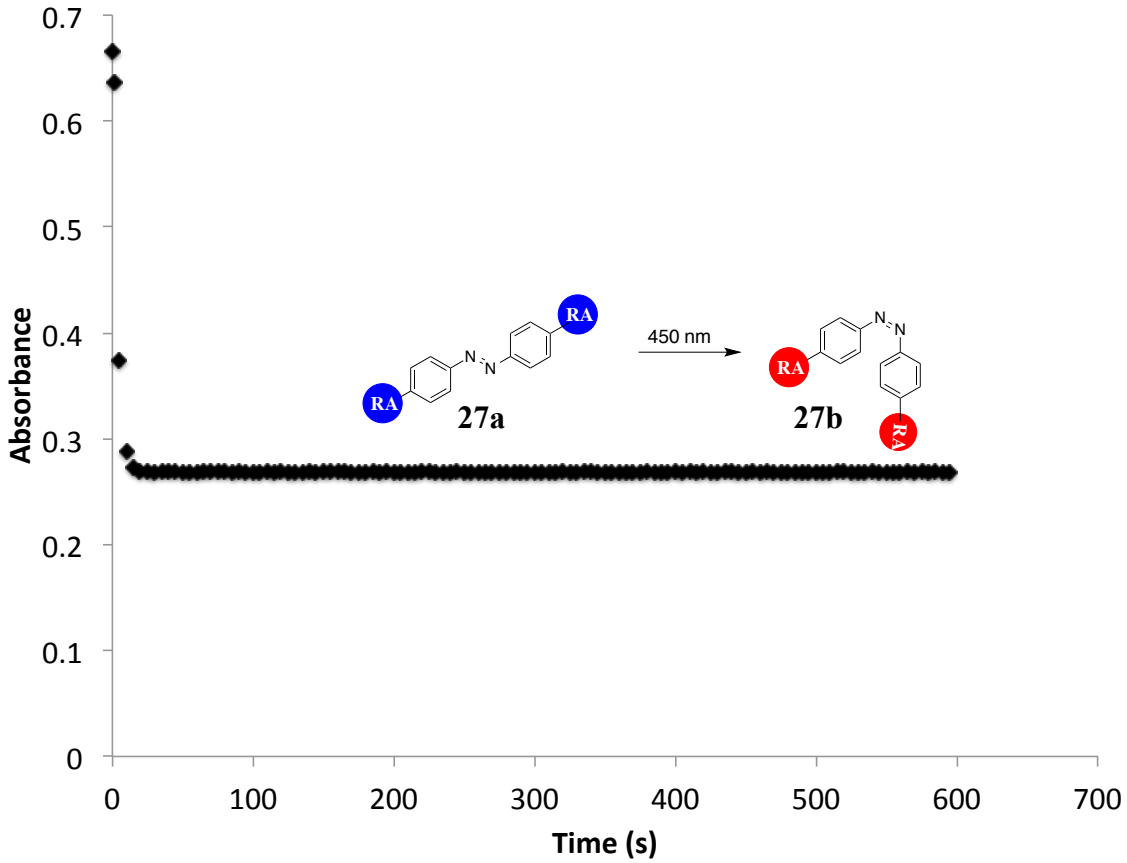

Figure 3.2.3. Absorption intensity was monitored at 480 nm and shows the establishment of a PSS for **27a** (4.89 x 10^{-4} M in deaerated C_6D_6) using 0.1 cm quartz UV-Vis cell at room temperature.

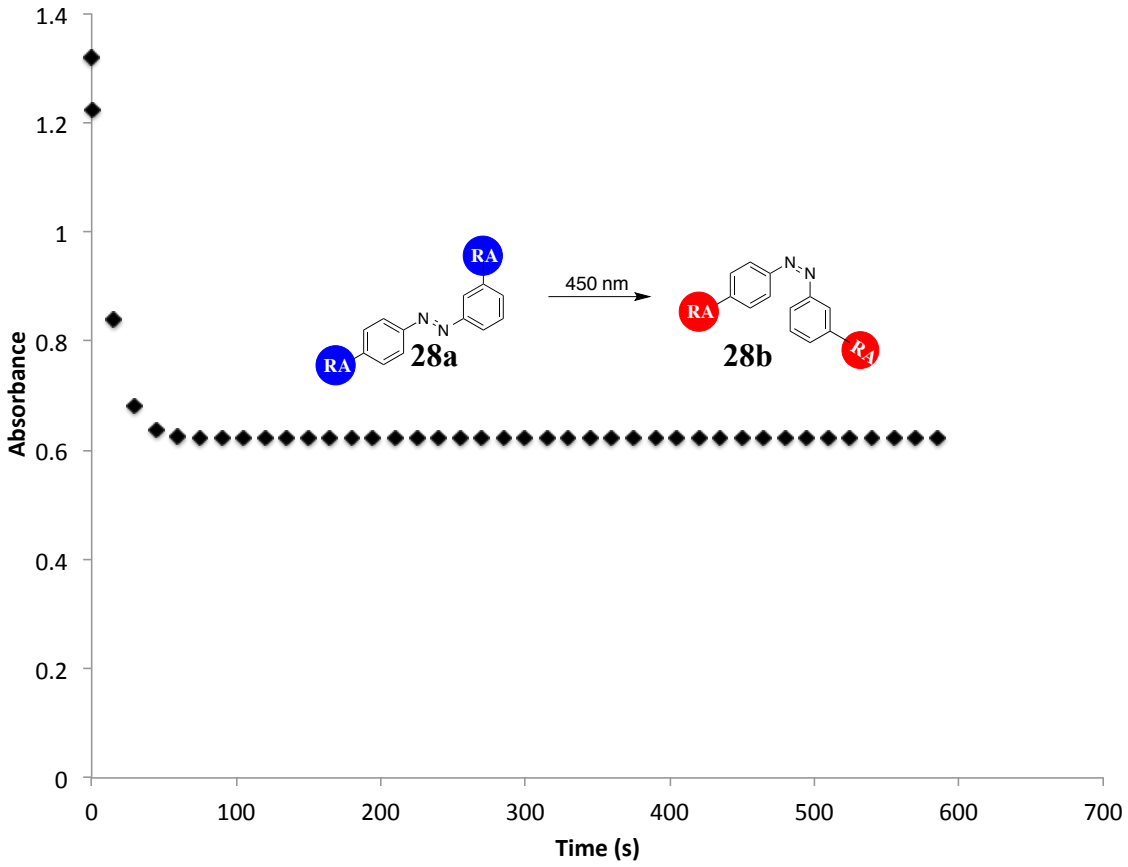

Figure 3.2.4. Absorption intensity was monitored at 446 nm and shows the establishment of a PSS for **28a** (6.01 x 10^{-4} M in deaerated C_6D_6) using 0.1 cm quartz UV-Vis cell at room temperature.

The time to reach the PSS was determined by following the absorption maximum at 480 nm and 446 nm for **27a** and **28a** during irradiation, respectively as illustrated in Figure 3.2.3 and Figure 3.2.4. After about 1 minute of irradiation, no changes in absorbance were observed. Figures 3.2.3 and 3.2.4 show that the PSS was established for both systems as shown by the plateau of the absorbance.

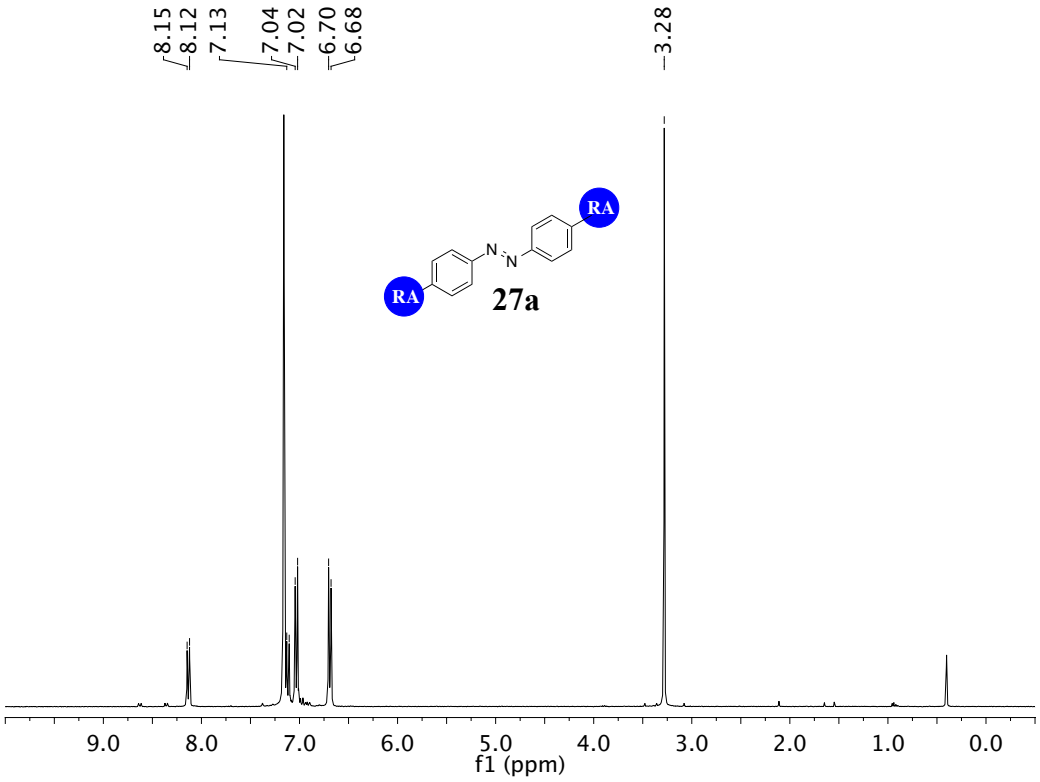

Figure 3.2.5. Full ^{1}H NMR spectrum of completely **27a** (1.17×10^{-2} M in C_6D_6) before irradiation.

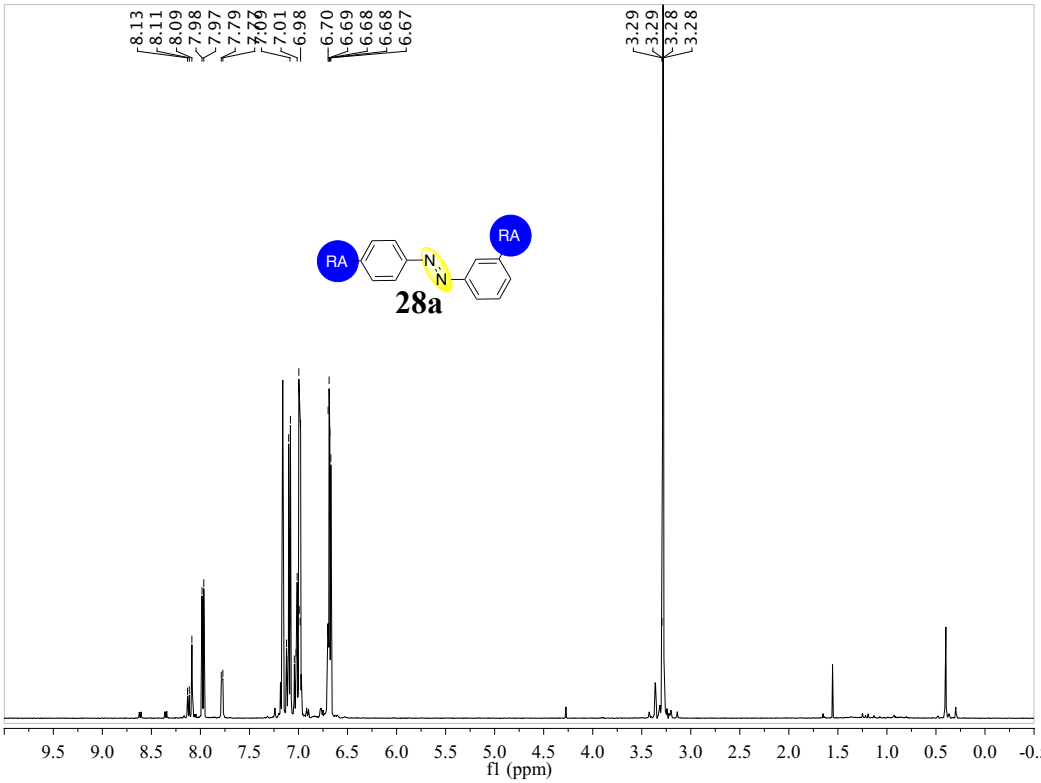

Figure 3.2.6. Full ^{1}H NMR spectrum of completely **28a** (9.63 x 10^{-3} M in C_6D_6) before irradiation.

The isomeric ratio of **27b**:**27a** and **28b**:**28a** at PSS were determined via ^{1}H NMR spectroscopy in C_6D_6 at room temperature. Figure 3.2.5 and Figure 3.2.6 show the full spectra for **27a** and **28a** in C_6D_6 before irradiation, respectively.

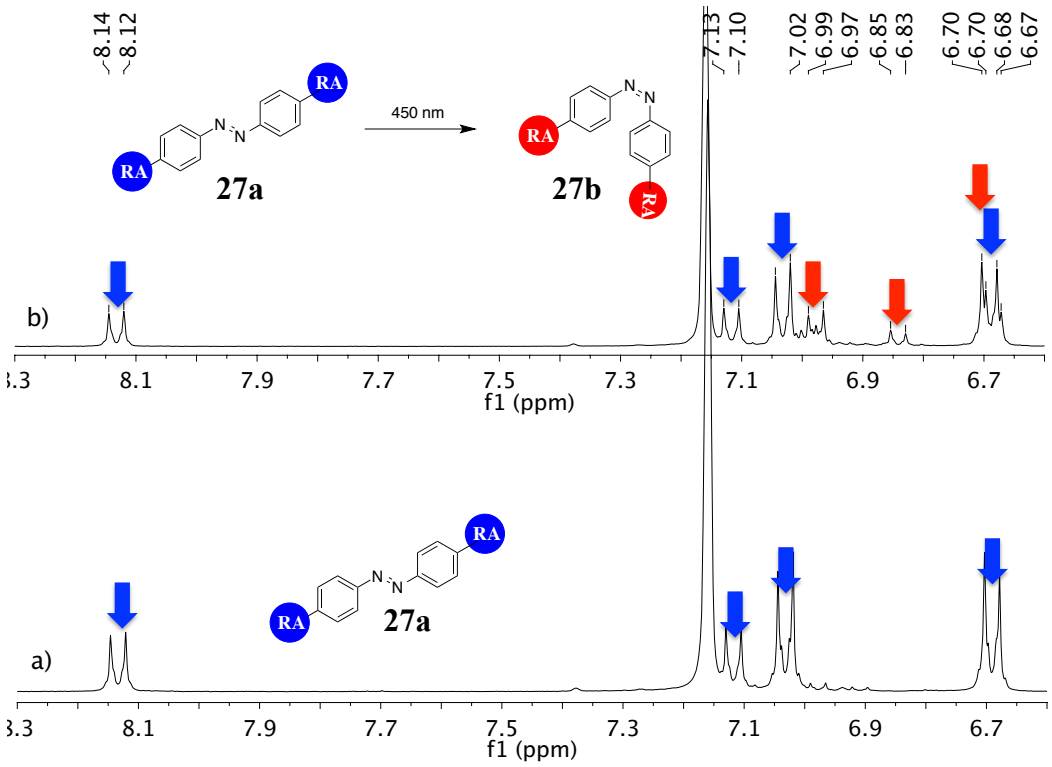

Figure 3.2.7. Expanded view of the aromatic section in the ^{1}H NMR spectrum of **27a** (1.17×10^{-2} M in C_6D_6) **a**) Spectrum before irradiation **b**) PSS spectrum after irradiation with a 450 nm LED light. The PSS is established at a 69:31 **27a**:**27b** ratio at room temperature. Blue arrows indicate **27a** and red arrows indicate **27b**.

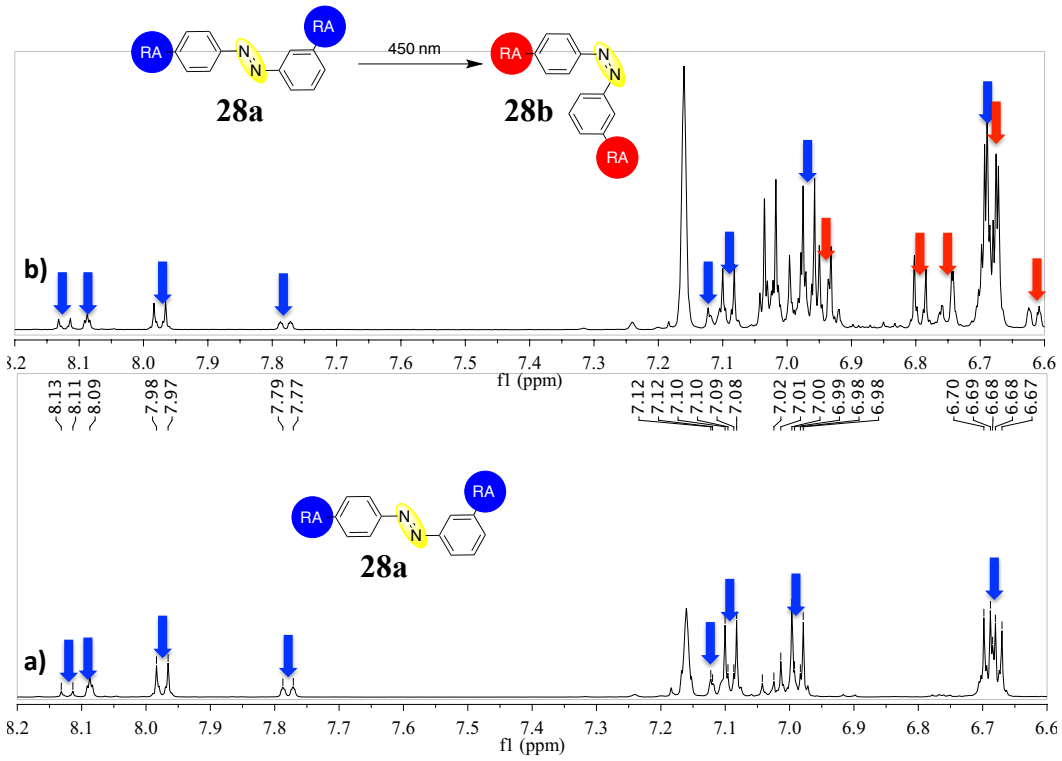

Figure 3.2.8. Expanded view of the aromatic section in the ^{1}H NMR spectrum of **28a** (9.63×10^{-3} M in C_6D_6). **a**) Spectrum before irradiation. **b**) PSS spectrum after irradiation with 450 nm LED light. PSS is established at a 49:51 **28a**:**28b** ratio at room temperature. Blue arrows indicate **28a** and red arrows indicate **28b**.

Expanded views of the aromatic sections in the ^{1}H NMR spectra of **27a** and **28a** before irradiation and at the PSS are shown in Figure 3.2.7 and Figure 3.2.8, respectively. The spectra of the aromatic sections confirm there are mixtures of *ci*- and *trans* isomers at the PSS.

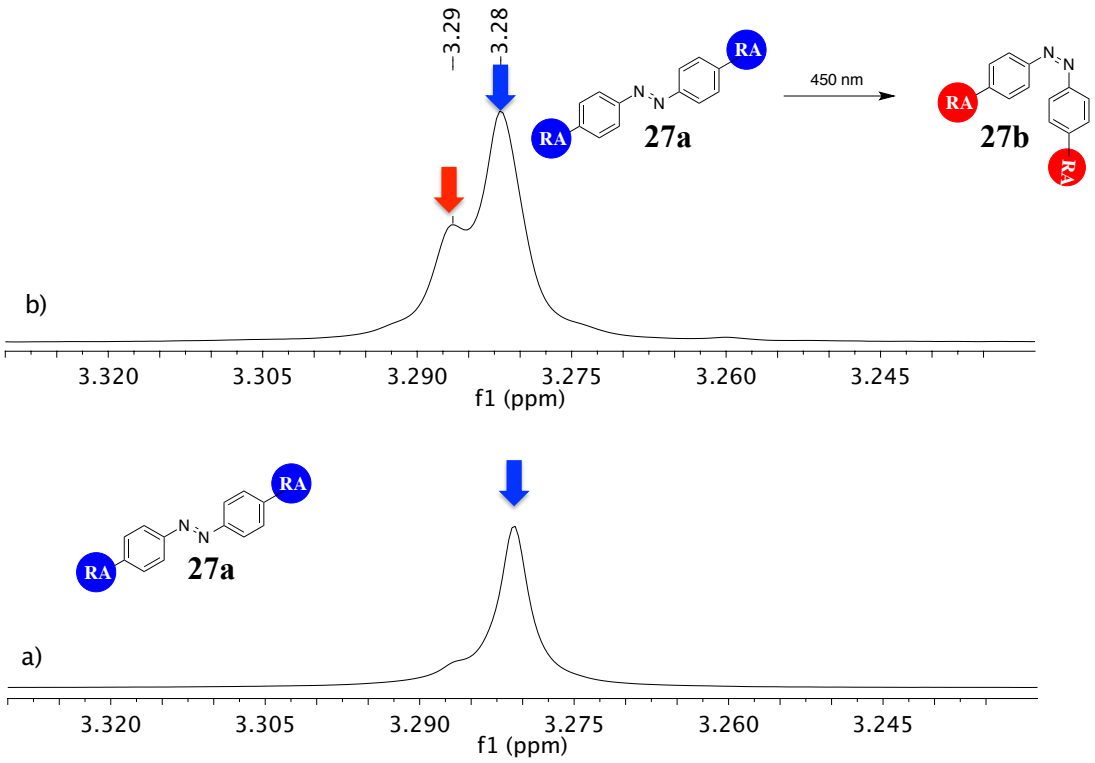

Figure 3.2.9. Expanded view of the alkyl section in the ^{1}H NMR spectrum of **27a** (1.17 x 10^{-2} M in C_6D_6) **a**) Spectrum before irradiation **b**) PSS spectrum after irradiation with 450 nm LED light. A PSS is established at a 69:31 **27a**:**27b** ratio at room temperature. Blue arrows indicate **27a** and red arrows indicate **27b**.

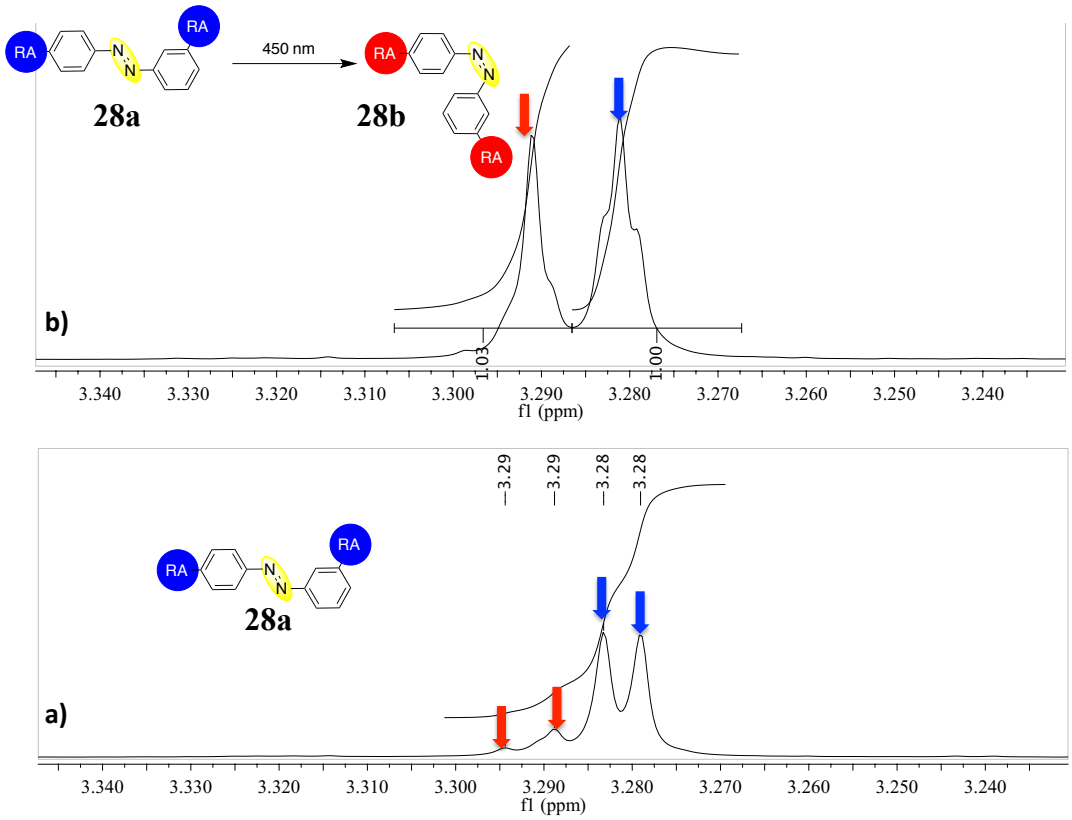

Figure 3.2.10. Expanded view of the alkyl section in the ^{1}H NMR spectrum of **28a** (9.63 x 10^{-3} M in C_6D_6). **a**) Spectrum before irradiation. **b**) PSS spectrum after irradiation with 430 nm LED light. A PSS is established at a 49:51 **28a**:**28b** ratio at room temperature. Blue arrows indicate **28a** and red arrows indicate **28b**.

Similarly, the alkyl section in the ^{1}H NMR spectra of **27b** and **28b** should be distinct from the alkyl sections of their corresponding *trans* isomers, as illustrated in Figure 3.2.9 and Figure 3.2.10, respectively. Integration of the methoxy peaks in the alkoxy section of the ^{1}H NMR spectra in Figures 3.2.9 and 3.2.10 were used to evaluate the isomeric ratios of **27a**:**27b** (69:31) and **28a**:**28b** (49:51) in the mixtures at the PSS.

3.2.2 Thermal *cis*-to-*trans* isomerization of 27a and 28a

After obtaining the isomeric ratios of **27a**:**27b** and **28a**:**28b** at the PSS**,** the stability of **27b** and **28b** were examined at room temperature to understand the thermodynamic effect of the additional RA moiety on the rate of the *cis*-to-*trans* thermal isomerization.

The thermal reversibility of **27b** to **27a** and **28b** to **28a** was monitored over a period of 24 hours via UV-Vis spectroscopy. After establishing the PSS for **27a** and **28a**, spectra were taken at room temperature in the dark until there were no changes in the maximum absorbances.

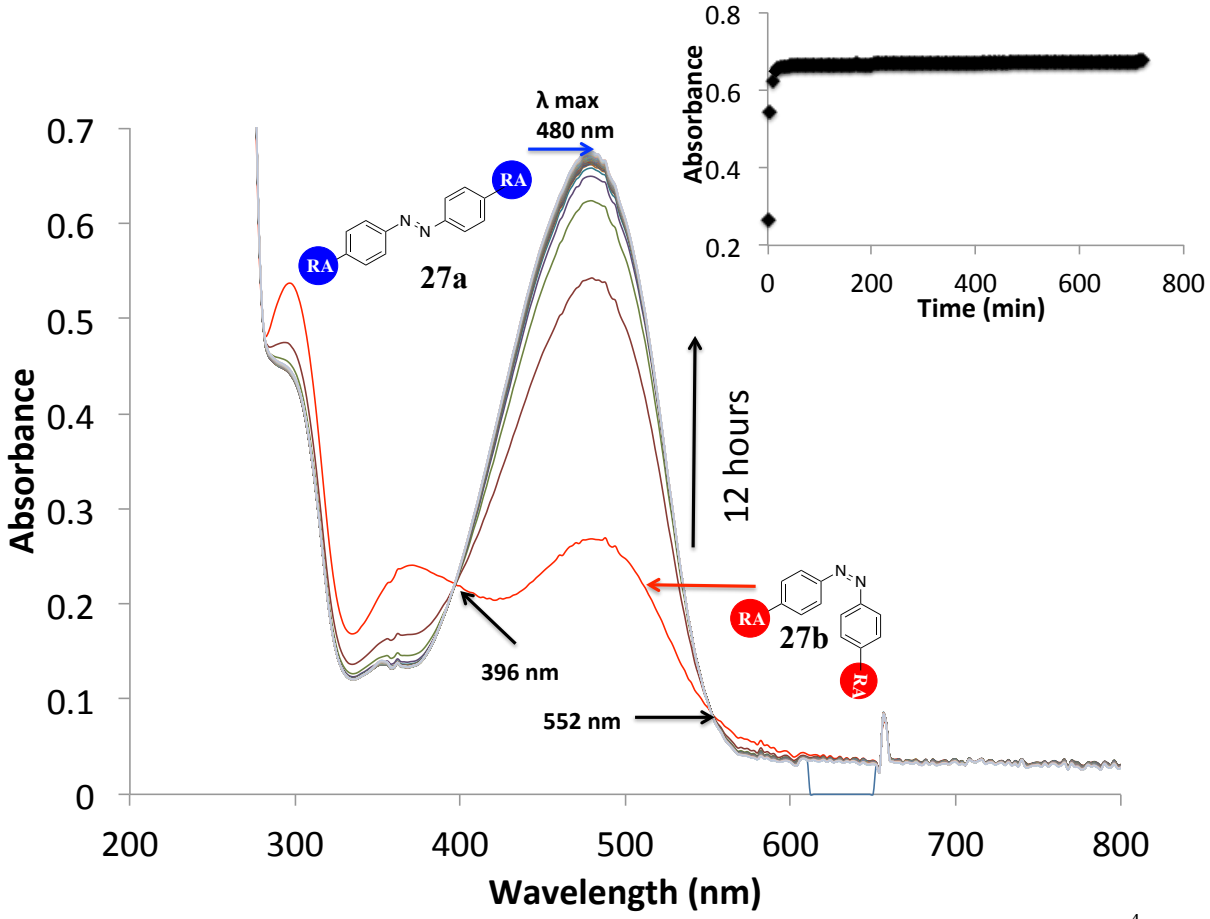

Figure 3.2.11. Optical spectrum of the thermal isomerization of **27b** to **27a** (4.89×10^{-4} M in C_6D_6) recorded every 5 minutes in the dark at room temperature in a 0.1 cm quartz cell after irradiating with a 450 nm LED to PSS.

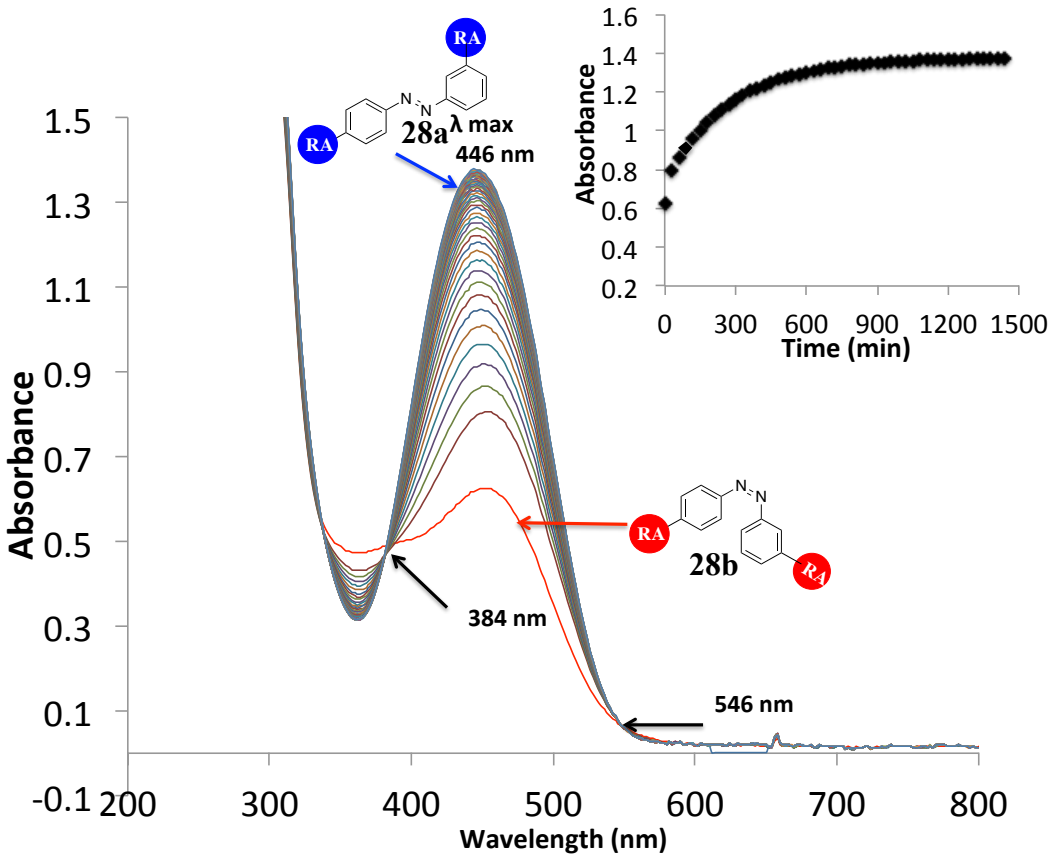

Figure 3.2.12. Optical spectrum of the thermal isomerization of **28b** to **28a** (6.01 x 10^{-4} M in C_6D_6) recorded every 30 minutes in the dark at room temperature in a 0.1 cm quartz cell after irradiating with a 450 nm LED to a PSS.

Figure 3.2.11 and Figure 3.2.12 show the decaying of the *cis* isomers and the recovery of the *trans* isomers over time in the dark until there were no changes in the spectra. The rates of the thermal isomerization of **27b** and **28b** were compared to that of **4b** and **19b**, respectively. The thermal half-life of **4b** in solution at room temperature was experimentally measured to be approximately 2 hours 30 minutes with a thermal isomerization rate of 8.4 x 10^{-5} ± 8.6 x 10^{-7} s^{-1}. Whereas, **27b** thermally isomerized to **27a** at a rate of 2.4 x 10^{-3} ± 2.9 x 10^{-4} s^{-1} with a half-life of approximately 4 minutes 49 seconds, as illustrated in Figure 3.2.13. As expected, the thermal isomerization rate of **27b** to **27a** is faster than that of **4b** to **4a**. This increase in rate can be explained by the presence of the additional RA group at the 4′-position. The addition of a

secondary RA group increases the steric interactions in the *cis* form and destabilizes **27b** relative to **4b**.

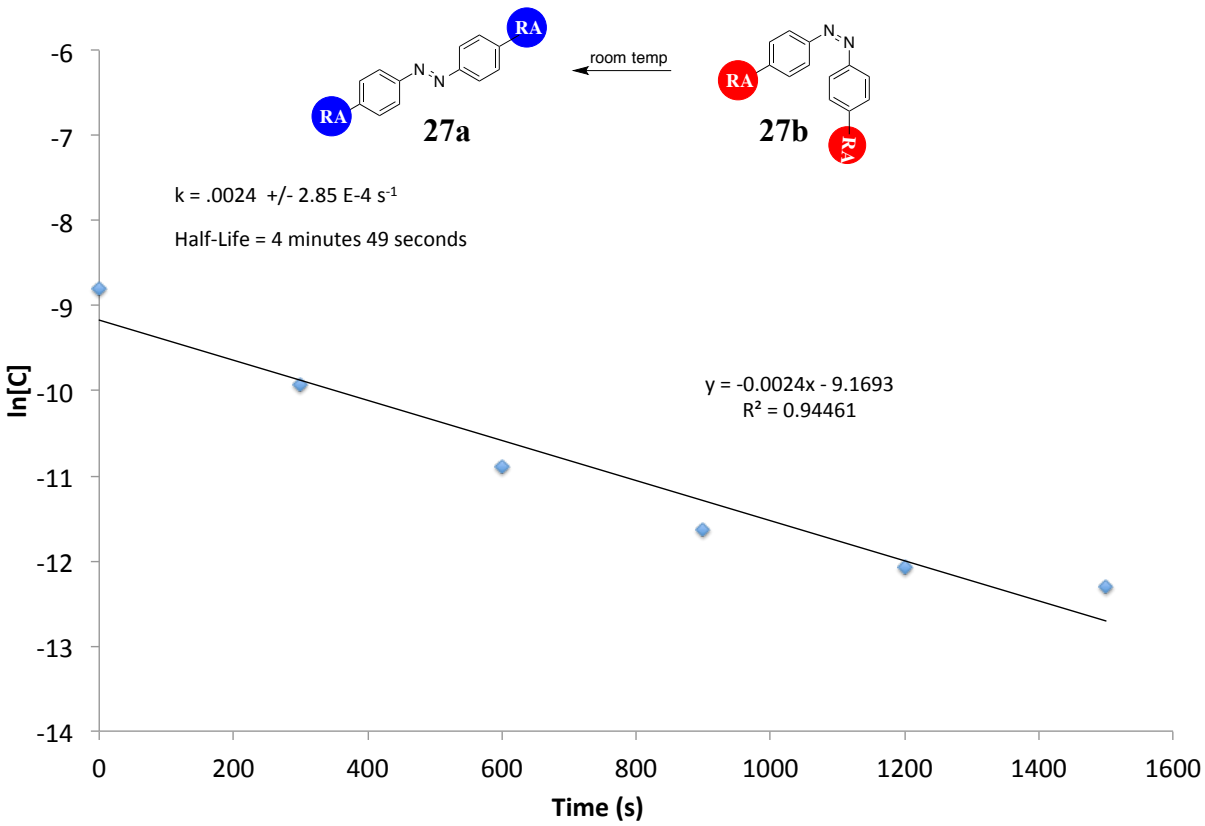

Figure 3.2.13. Determination of the thermal isomerization rate of **27b** to **27a** over 12 hours using a plot of ln[C] vs. Time where C is the ratio of *cis*-to-*trans*.

The thermal half-life of **19b** in solution at room temperature was experimentally measured to be approximately 47 hours with a thermal isomerization rate of $4.1 \times 10^{-6} \pm 9.5 \times 10^{-9}\ s^{-1}$. Whereas, **28b** thermally isomerized to **28a** at a rate of $6.0 \times 10^{-5} \pm 3.9 \times 10^{-7} s^{-1}$ with a half-life of approximately 3 hours and 13 minutes as illustrated in Figure 3.2.14. As expected, the rate of the thermal isomerization of **28b** to **28a** is faster than that of **19b** to **19a**. This increase in rate can be explained by the presence of the additional RA group at the 4′- position. The addition of a secondary RA group introduced a donor-acceptor interaction in **28a** that is not

present in **19a**, and disrupting this donor-acceptor interaction in **28a** by isomerizing to **28b** destabilizes **28b** in comparison to **19b**. As a result, introducing an additional electron rich RA moiety at the 4´- position of **19b** increased its thermal isomerization rate and caused it to behave similarly to **4b**.

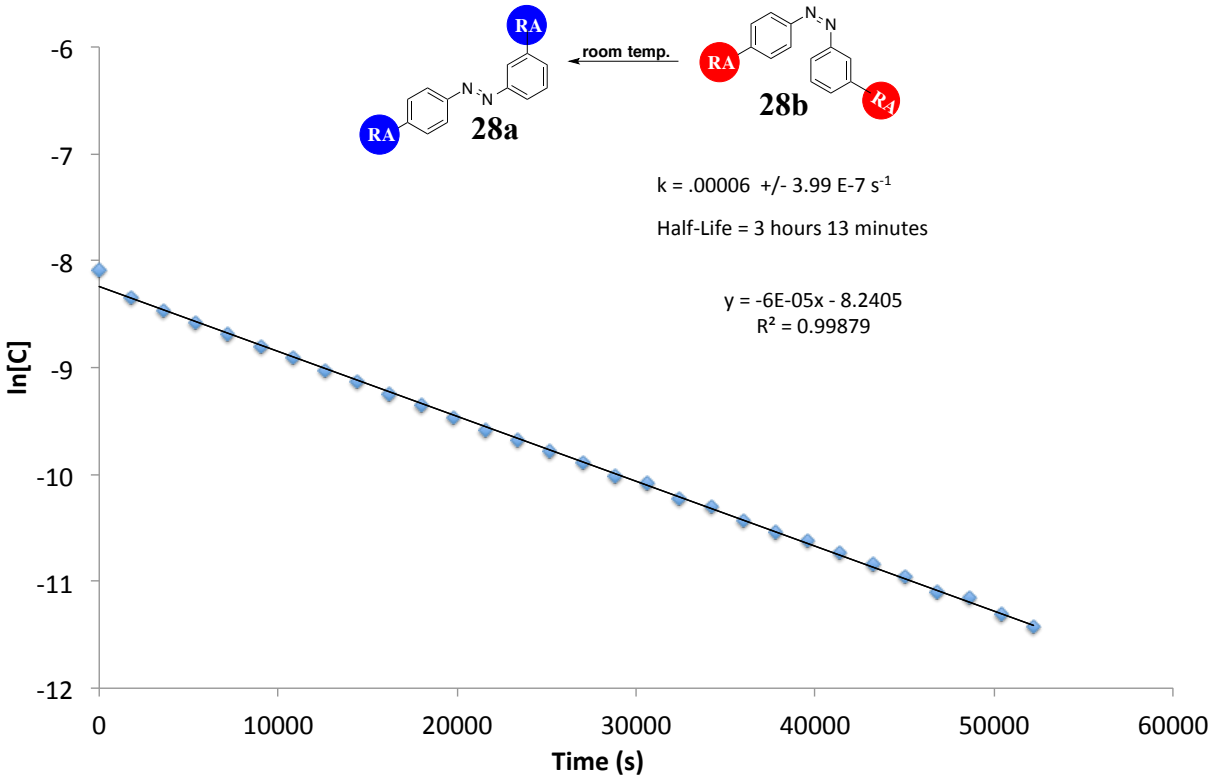

Figure 3.2.14. Determination of the thermal isomerization rate of **28b** to **28a** over 27 hours using a plot of ln[C] vs. Time where C is the ratio of *cis*-to-*trans*.

To comprehend the thermodynamic effect of the additional RA group on **27b** and **28b,** it was necessary to experimentally measure the $\Delta G^{\neq}$ for their *cis*-to-*trans* thermal isomerization relations to their rates**.** The $\Delta G^{\neq}$ for **27b** to **27a** was experimentally measured to be approximately 21.0 kcal mol^{-1}, which is lower than the $\Delta G^{\neq}$ for **4b** to **4a**, which was measured to be approximately 23.0 kcal mol^{-1}. Figure 3.2.15 displays a potential diagram that portrays the effect of the RA group on the $\Delta G^{\neq}$ of **27b** at room temperature in comparison with **4b**.

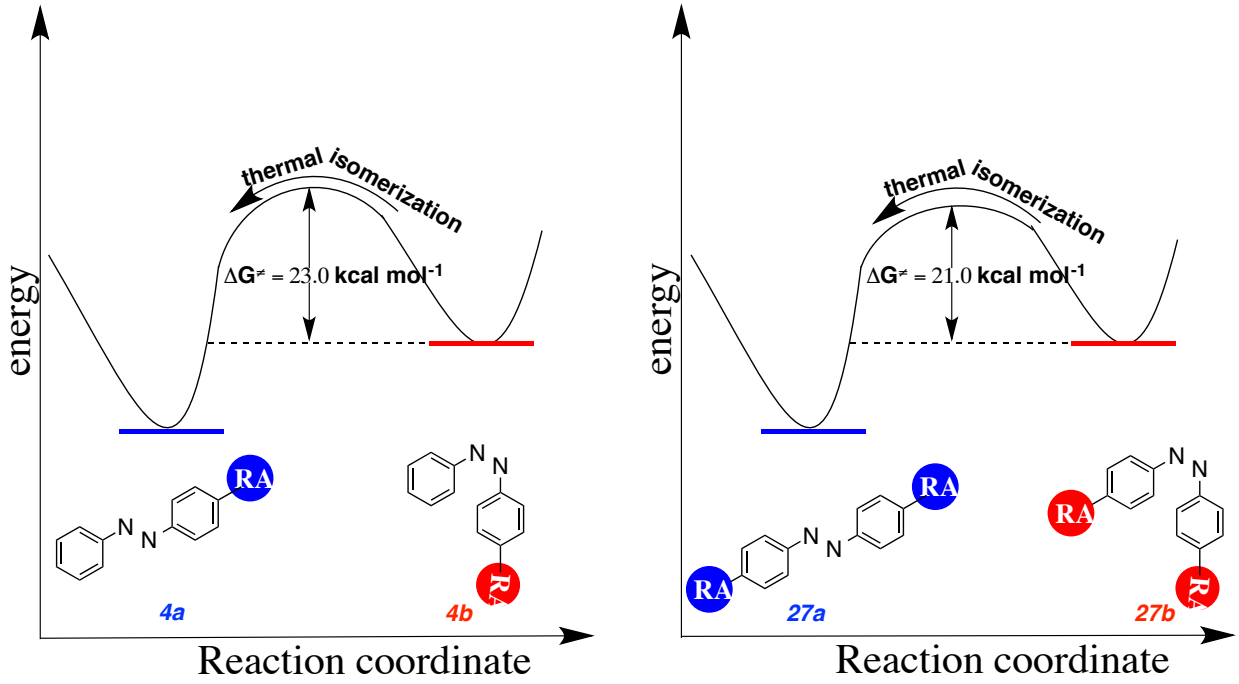

Figure 3.2.15. A potential energy diagram of **4a** (left) and **27a** (right) that illustrates the effects of **3** on the thermal isomerization $\Delta G^{\neq}$ for isomerization from **27b** to **27a.**

The $\Delta G^{\neq}$ for the *cis*-to-*trans* thermal isomerization from **28b** to **28a** was experimentally measured to be approximately 23.2 kcal mol^{-1}, which is lower than the $\Delta G^{\neq}$ for **19b** to **19a** that was measured to be approximately 24.8 kcal mol^{-1}. Figure 3.2.16 displays a potential diagram that portrays the effect of the additional RA group on the thermal isomerization $\Delta G^{\neq}$ of **28b** at room temperature in comparison with **19b**.

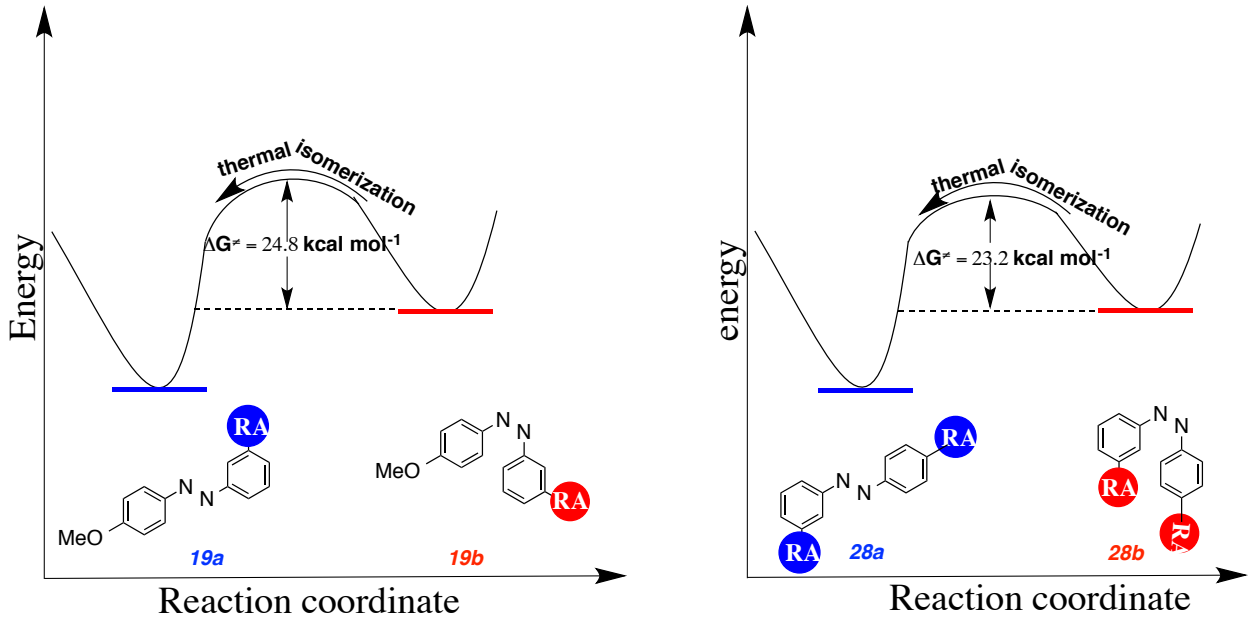

Figure 3.2.16. A potential energy diagram of **19a** (left) and **28a** (right) that illustrates the effects of **3** on the thermal isomerization $\Delta G^{\neq}$ for isomerization from **28b** to **28a.**

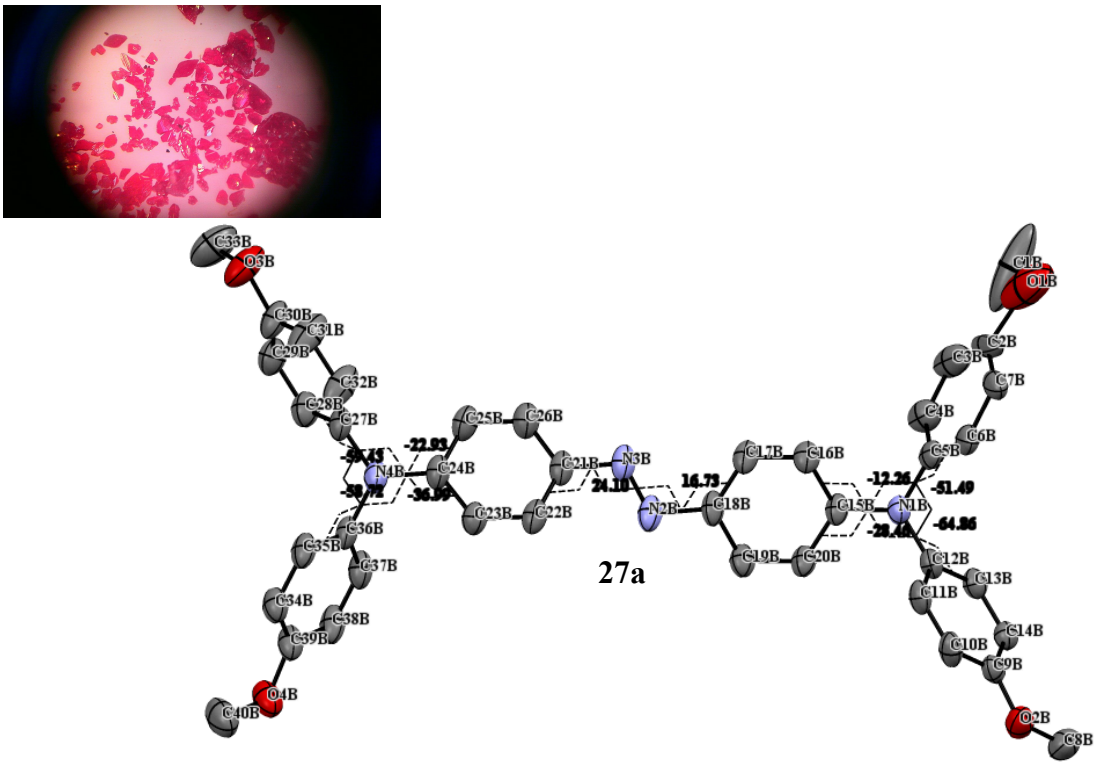

Figure 3.2.17. Ellipsoid diagram of the crystal structure of **27a**. It shows twisting in both RA groups. The pi orbitals of the AB's phenyl groups are twisted out of conjugation with the lone pair of the nitrogen atoms on the RA groups and the pi orbitals of the -N=N- group.

The crystal structure of **27a** is shown in Figure 3.2.17. It illustrates that the additional RA group at the 4′- position causes the phenyl groups of the RA groups to adopt a geometry similar to triphenylamine. The three-bladed propeller-shaped is maintained on both sides of **27a**. The phenyl groups of the two RA moieties are twisted with dihedral angles ∠C6C5N1C12 (51.49°), ∠C13C12N1C5 (64.86°) at the 4- position and ∠C35C36N4C27 (58.72°), ∠C28C27N4C36 (59.43°) at the 4′- position. As a result, the two phenyl groups of the AB core are more twisted in **27a** than in **4a** with dihedral angles ∠C16C15N1C5 (12.26°), ∠C20C15N1C12 (28.46°) at the 4- position and dihedral angles ∠C25C24N4C27 (22.93°), ∠C23C24N4C36 (36.99°) at the 4′- position. The AB core is twisted and no longer possesses its planar geometry with dihedral angles ∠C17C18N2N3 (16.73°) and ∠C22C21N3N2 (24°10) as illustrated in Figure 3.2.17 and Figure 3.2.18.

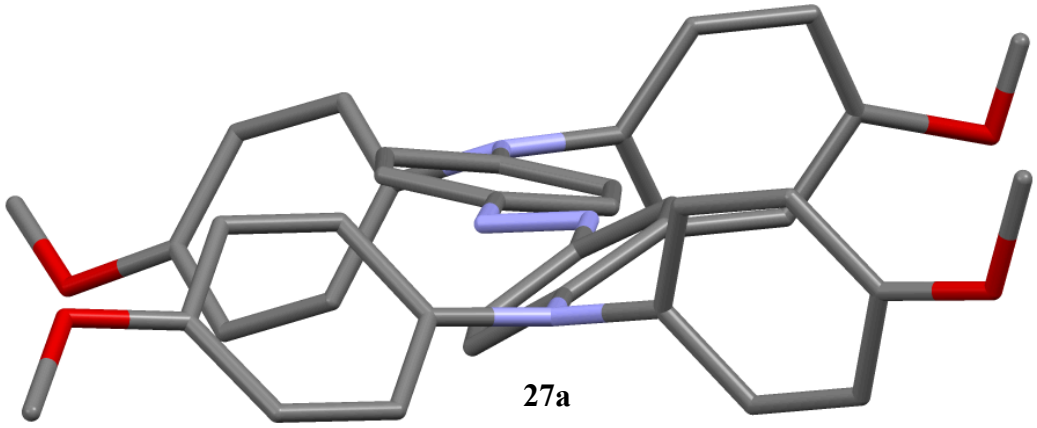

Figure 3.2.18. Cap and stick diagram of the crystal structure of **27a**. It illustrates that the AB core is no longer planar because the phenyl groups adapted geometry similar to triphenylamine. The pi orbitals of the AB phenyl groups are twisted out of conjugation with the lone pair of the nitrogen atoms on the RA groups and the pi orbitals of the -N=N- group.

As a result of the increased twisting of the phenyl groups in the AB core, the pi orbitals of the AB's phenyl groups are twisted out of conjugation with the lone pair of the nitrogen atoms on the RA groups and the pi orbitals of the -N=N- group as show in Figure 3.2.18.

Although the phenyl rings of the AB core are twisted out of conjugation in **27a**, there is still a donor-acceptor interaction between each RA group and the -N=N- group through the extended pi system and conjugation as illustrated in Figure 3.2.19a. However, due to a change in 3-D conformation resulting from isomerization of **27a** to **27b**, the extended pi system is disrupted, thus the conjugation that had extended from the -N=N- group to the lone pairs of the nitrogen of the two RA groups in **27a** is broken upon isomerization to **27b**. Furthermore, steric interactions between the two RA groups in the *cis* conformation also destabilize **27b**, thus

increasing its energy in comparison to **4b**. These effects in turn increase the energy of **27b** and decreased its stability compared to the **4b**, as demonstrated in Figure 3.2.19b.

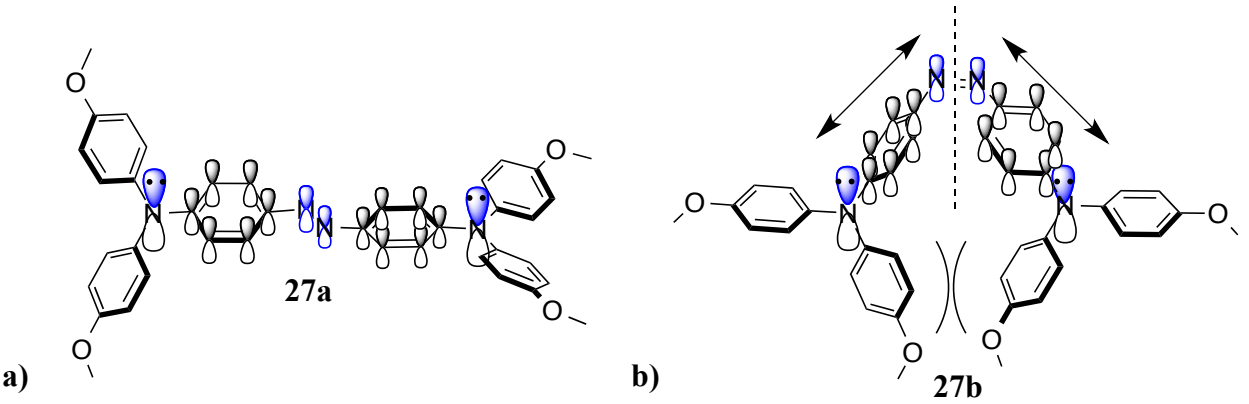

Figure 3.2.19. a) Donor-acceptor interaction between both RA groups and the -N=N- group through the extended pi system. **b**) The extended pi system is broken between the -N=N- group and the lone pairs of the nitrogens of RA groups, steric interactions between the two RA groups in the *cis*- conformation also destabilize **27b**, thus increasing its energy in comparison to **4b**.

In comparison, **27b** has more factors contributing to its destabilization than **4b**. As mentioned in chapter 2, three major factors contribute to the destabilization of **4b**. The first factor is the steric interaction of the two benzene rings in the *cis* conformation. The second factor is the close proximity of the two lone pairs on the -N=N- group that result in repulsion in the *cis* form. The third factor is the loss of the extended pi system throughout the molecule that results in the loss of the donor-acceptor interaction between the -N=N- group and the lone pair of the nitrogen atom of RA group. However, four factors are contributing to the destabilization of **27b**. The first factor is the steric interaction of the two benzene rings in the *cis* conformation just as in **4b**. The second factor is the close proximity of the two lone pairs on the -N=N- group resulting in repulsion in the *cis* form just as in **4b**. The third factor is the loss of the extended pi system throughout the molecule resulting in the loss of the donor-acceptor-donor interaction between the -N=N- group and the lone pairs of the nitrogen atom of the RA group, also as in **4b.**

The fourth factor is the increase of steric interactions between the two RA groups in the *cis* conformation as shown in Figure 3.2.19b. This fourth additional factor resulted in a supplementary destabilization of **27b** and raised its energy relative to that of **4b**. As a result, the $\Delta G^{\neq}$ of the thermal isomerization for **27b** to **27a** is lower than that of **4b** to **4a**, and this decreased in $\Delta G^{\neq}$ leads to a decreased half-life from 2.5 hours for **4b** to 4 minutes and 49 seconds for **27b**.

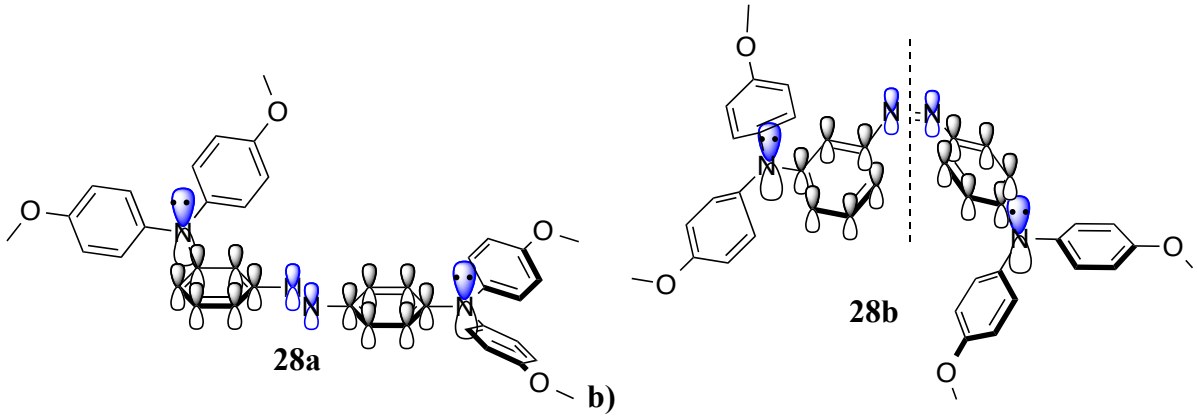

Figure 3.2.20. a) The planarity of the AB core helps stabilize **28a** by forming an extended pi system between the electron-withdrawing group, -N=N-, and the electron rich group, the lone pair of the nitrogen of RA moiety in the 4'- position **b**) The extended pi system is broken between the -N=N- group and the lone pair of the nitrogen of RA moiety, thus increasing the energy of **28b**.

It was not possible to obtain a crystal structure for **28a**. However, an educated guess of the geometry of **28a** can be assumed based on the crystal structure of **4a**, **19a**, and **27a**. Figure 3.2.20 shows the assumed geometry of **28a** and **28b**. The planarity of the AB core is essential because it helps stabilize **28a** by creating an extended pi system between the electron withdrawing moiety, -N=N-, and the lone pair of the nitrogen atom of the RA group at the 4´-position, as illustrated in Figure 3.2.20a. This spatial arrangement of **28a** allows for a donor-acceptor interaction through the extended pi system. However, due to a change in 3-D conformation resulting from isomerization from **28a** to **28b**, the planarity of the extended pi system is disrupted, thus the conjugation that had extended from the -N=N- group to the lone

pair of the nitrogen of RA group in **28a** is broken upon isomerization to **28b**. This effect in turn increased the energy of **28b** and decreased its stability compared to that of **28a**, as demonstrated in Figure 3.2.20b.

In comparison to **19b**, **28b** has more factors contributing to its destabilization. The first factor is the steric interaction of the two benzene rings in the *cis* conformation, just as in **19b**. The second factor is the close proximity of the two lone pairs on the azo nitrogen atoms resulting in repulsion in the *cis* form, just as in **19b**. The third factor is the loss of the extended pi system throughout the molecule resulting in the loss of the donor-acceptor interaction between the -N=N- group and the lone pair of the nitrogen atom of the RA group at the 4′-position. This third additional factor results in a supplementary destabilization of **28b** by raising its energy relative to that of **19b**. As a result, the $\Delta G^{\neq}$ for the thermal isomerization for **28b** to **28a** is lower than that of **19b** to **19a**, and this decreased $\Delta G^{\neq}$ leads to a decreased half-life from 47 hours for **4b** to approximately 3 hours and 13 minutes for **28b**.

3.2.3 Electron transfer catalysis of *cis-to-trans* isomerization

In order to test whether the isomerization time of *cis* → *trans* for **27a** and **28a** could be exponentially decreased via the catalytic electron transfer cycle, it was necessary to select an oxidant with an oxidation potential greater than the oxidation potential of **27a** and **28a**. Figure 3.2.21 and Figure 3.2.22 show the cyclic voltammograms of **27a** and **28a**. The cyclic voltammograms provide the reversible oxidation potentials of **27a** as E° = (1) 0.94 V (vs. SCE), (2) 0.78 V (vs. SCE) and **28a** as E° = (1) 1.01 V (vs. SCE), (2) 0.82 V (vs. SCE), respectively.

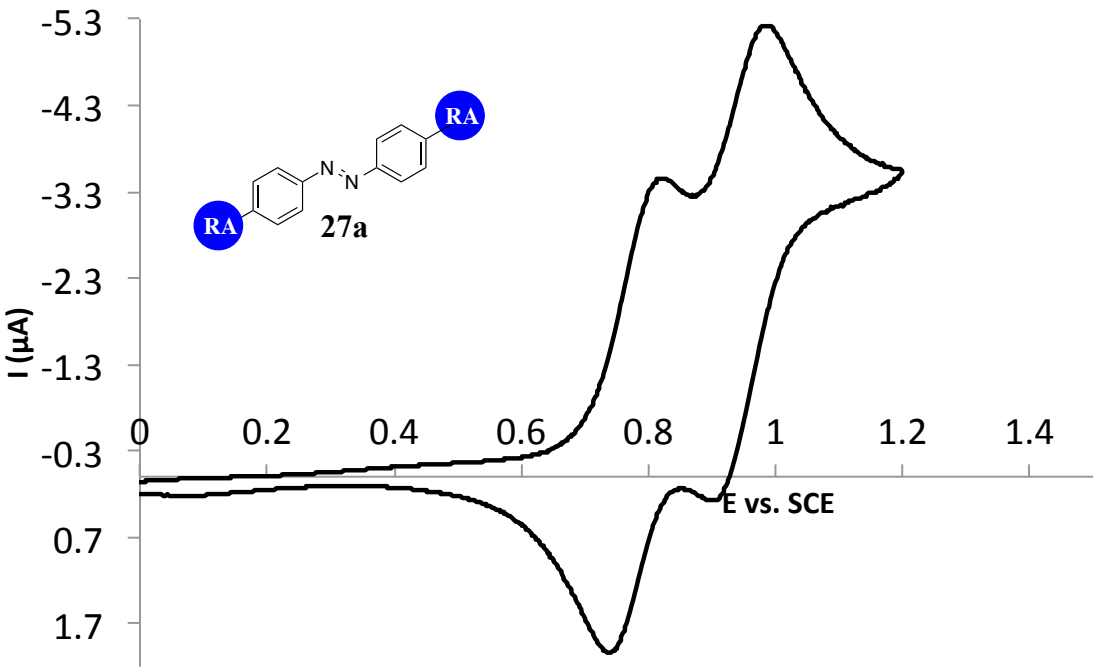

Figure 3.2.21. Cyclic voltammogram of **27a** (1.0 mM in dichloromethane with 0.1 M $TBABF_4$) at 20 mV/s scan rate with two E° = (1) 0.94 V (vs. SCE). (2) 0.78 V (vs. SCE).

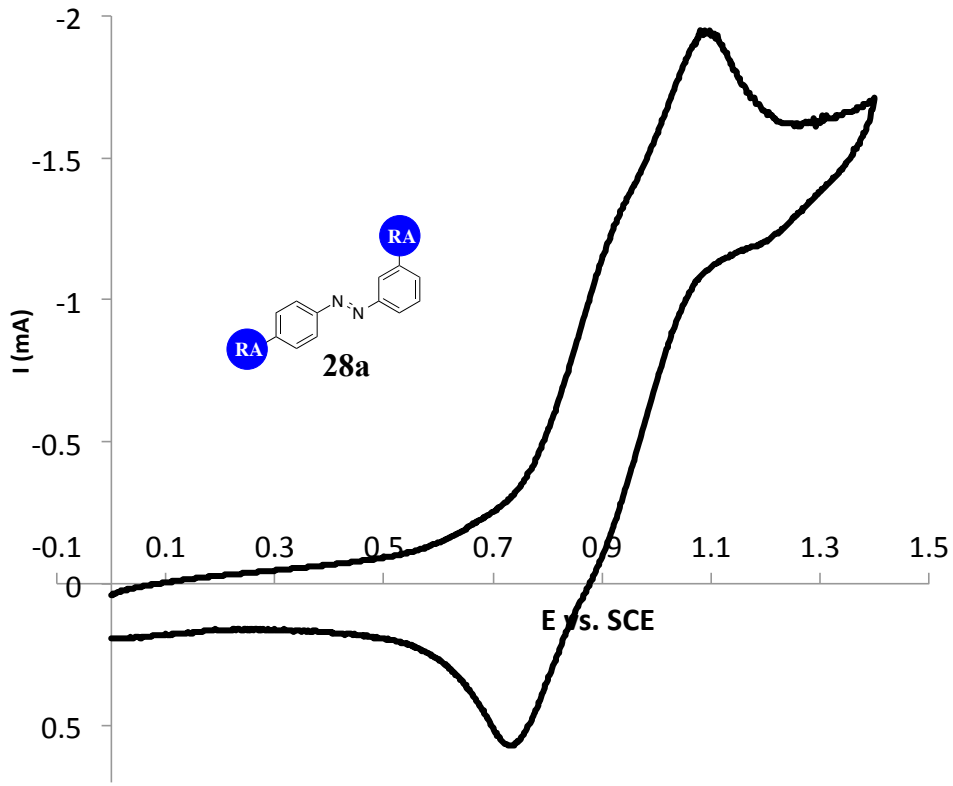

Figure 3.2.22. Cyclic voltammogram of **28a** (1.0 mM in dichloromethane with 0.1 M $TBABF_4$) at 20 mV/s scan rate with an E° = (1) 1.01 V (vs. SCE), (2) 0.82 V (vs. SCE).

Figure 3.2.23 illustrates the cyclic voltammetry of the chosen oxidant, **6**. The oxidant, **6**, was also the chosen oxidant because of its stability at room temperature and its potent oxidation potential of 1.25 V (vs. SCE) that is higher than the oxidation potentials of **27a** and **28a**.

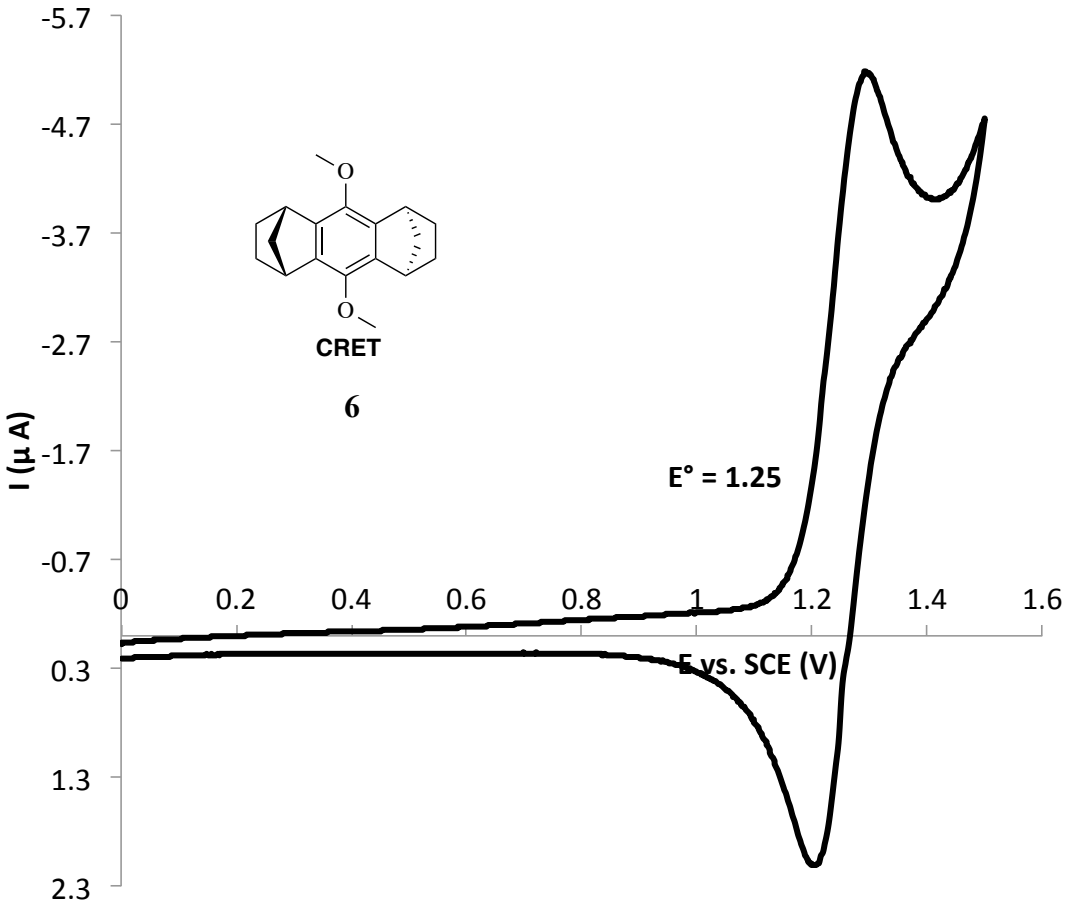

Figure 3.2.23. Cyclic voltammogram of **6** (1.0 mM in dichloromethane with 0.1 M $TBABF_4$) at 20 mV/s scan rate with an $E^{\circ} = 1.25$ V (vs. SCE).

Before attempting to oxidize **27b** and **28b**, the molecular orbital of the *cis* isomers were computed using density-functional theory with the B3LYP/6-31G** basis set to locate the energy level of the HOMO and to confirm that the RA group would be the moiety interacting with the oxidant. Figure 3.2.24 illustrates the molecular orbitals in the HOMO of **27b**. It shows that the HOMO is predominantly located around and at the central nitrogen atom of the RA moiety. It also illustrates that the phenyl rings attached to both RA groups possess a large amount of electron density. It also indicates that both electron-dense phenyl rings are planar to the -N=N- group pi orbitals and there are orbital overlap between the two phenyl rings and both

RA groups. This spatial arrangement of **27b** indicates that the lone pair of the central nitrogen atoms of the RA groups are in conjugation with the electron acceptor, -N=N- group pi orbitals, thus forming an acceptor-donor-acceptor interaction in the *cis* form. This spatial arrangement also signifies that the removal of an electron from **27b** should disturb the -N=N-. As a result, it would cause the -N=N- bond to break and convert into -N-N- then isomerize back to **27a**. Based on the results of B3LYP 6-31G** molecular orbital calculations of **27b**, it was safe to continue testing our electron transfer catalysis of *cis*-to-*trans* isomerization on **27b**.

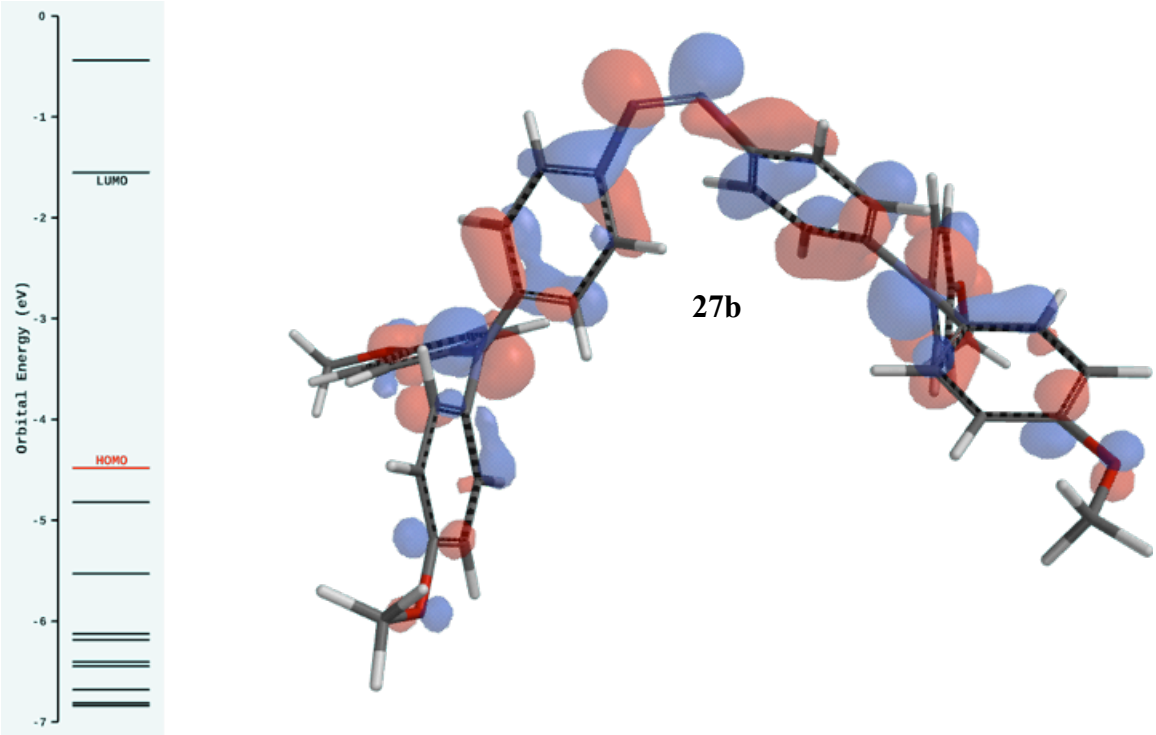

Figure 3.2.24. The molecular orbital of **27b** were computed using density-functional theory with the B3LYP/6-31G** basis set to locate the energy level of the HOMO. The HOMO is predominantly located at and around the central nitrogen atom of the RA group. The blue and red lobes indicate the orbital phases of the HOMO.

The molecular orbital of the **28b** were computed using density-functional theory with the B3LYP/6-31G** basis set to locate the energy level of the HOMO and to confirm that the RA group would be the moiety interacting with the oxidant. Figure 3.2.25 illustrates the HOMO is

predominantly located around and at the central nitrogen atom of the RA moiety. It also illustrates that the phenyl ring attached to the RA group possesses a large amount of the electron density and both phenyl rings are planar and in conjugation with the -N=N- group pi orbitals. Because of the planarity of the phenyl rings attached to the RA group, we can conclude that the spatial arrangement of **28b** positions the lone pair of the central nitrogen atom of the RA group in the 4- position with the -N=N- group pi orbitals, thus forming a donor-acceptor interaction. Based on the results of B3LYP 6-31G** molecular orbital calculations of **28b**, it was safe to continue testing our electron transfer catalysis of *cis*-to-*trans* isomerization on **28b**.

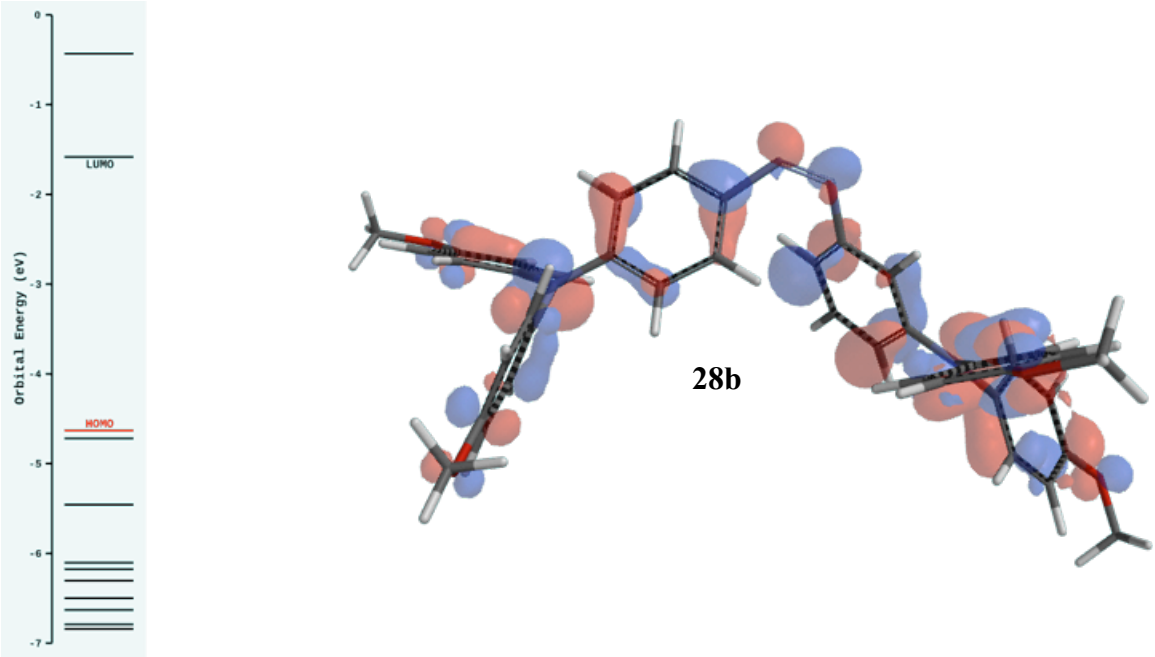

Figure 3.2.25. B3LYP/6-31G** molecular orbital calculations of **28b**. The HOMO is predominantly located at and around the central nitrogen atom of the RA group. The blue and red lobes indicate the orbital phases of the HOMO.

To test our hypothesis, 1% mole of **6** was injected into a solution of **27b** and a solution of **28b** in deaerated benzene at the PSS, respectively. Upon injection and mixing, both isomers, **27b** and **28b** isomerized back to their corresponding *trans* isomers in less than 2 seconds as judged by optical spectra analysis illustrated in Figure 3.2.26 and Figure 3.2.27, respectively.

Based on these results, it was concluded that a catalytic amount (1% mole) of **6** was sufficient to oxidize **27b** to **27b**$^{\square+}$ and **28b** to **28b**$^{\square+}$, thus initiating and forming the electrical catalysis cycle shown in Scheme 3.2.3.

To test the dependability of our photo-electro catalysis cycle, the new oxidized sample of **27a** and **28a** were irradiated for a total of 15 minutes in order to re-form their respective *cis* isomers. After this prolonged irradiation the *cis* isomers were not observed as displayed in Figures 3.2.26 and 3.2.27.

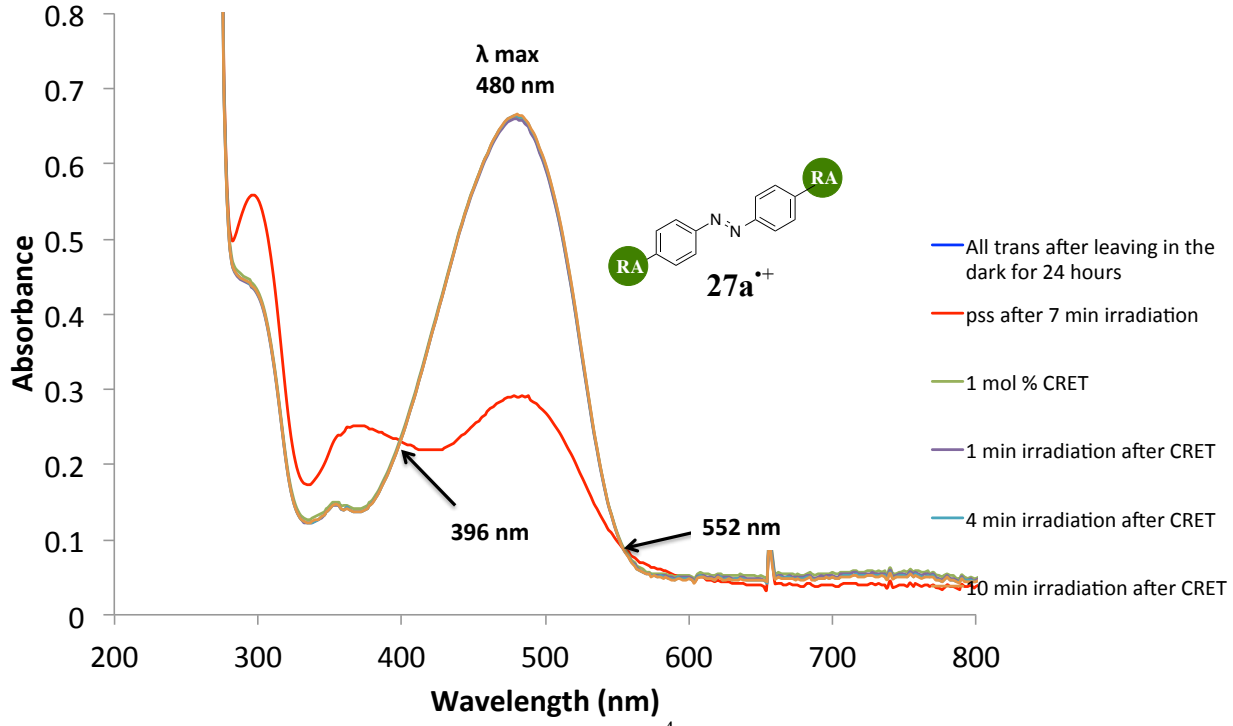

Figure 3.2.26. Optical spectrum of **27a** (4.89 x 10^{-4} M in C_6D_6) irradiated with a 450 nm LED and CRET injection (1% mole in DCM) at room temperature in 0.1 cm quartz UV-Vis cell.

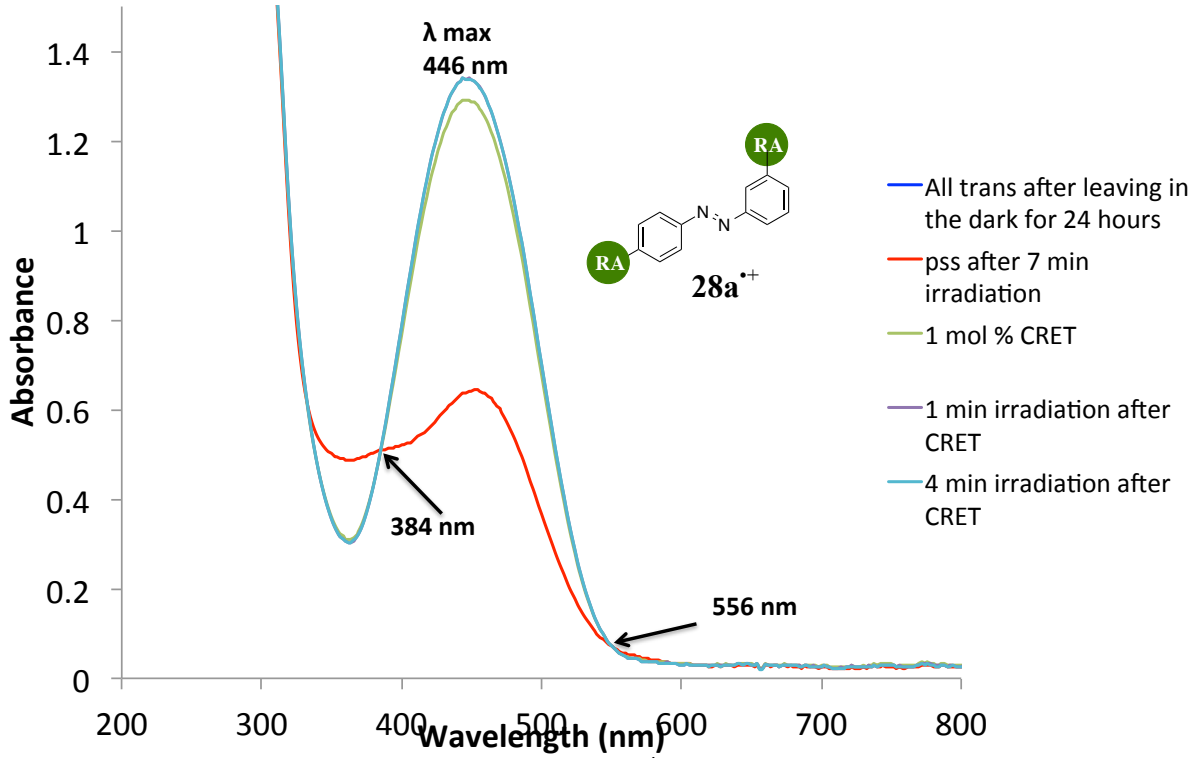

Figure 3.2.27. Optical spectrum of **27a** (6.01 x 10^{-4} M in C_6D_6) irradiated with a 450 nm LED and CRET injection (1% mole in DCM) at room temperature in 0.1 cm quartz UV-Vis cell.

Because the *trans*-AA$^{\bullet+}$-azo-AA is exceptionally chemically stable, it is able to exchange an electron with other neutral *cis* isomers thereby generating a catalytic cycle for azo-unfolding as shown in Scheme 3.2.3. Grounded on this result, we postulated a new photo-electro isomerization catalysis mechanism that accounts for the fast relaxation from *cis*-to-*trans*. The photo-electro catalysis mechanism cycle in Scheme 3.2.3 demonstrates that a 450 nm LED can be used to isomerize **27a** and **28a** to their corresponding *cis* isomers. Subsequent addition of a catalytic amount of oxidant will regenerate the *trans* isomers, thus exponentially increasing the rate at which the *cis* isomer relaxes back to the *trans* isomer.

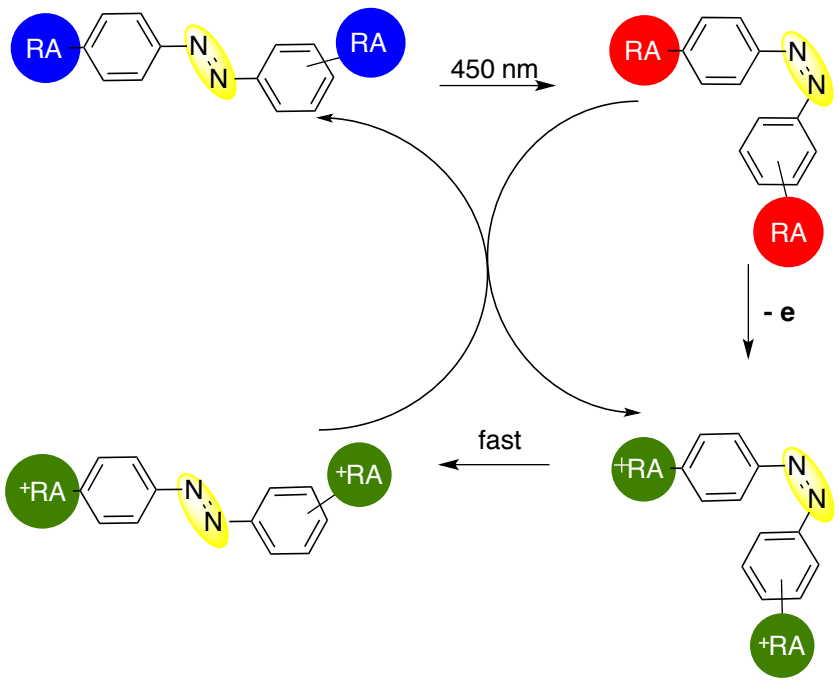

Scheme 3.2.3. Postulated photo-electro catalysis mechanism of **27a** and **28a.**

3.2.4 Conclusions

We have synthesized two new Bis(arylamino) azobenzene photo-electro switches, **27a** and **28a**. We have demonstrated that adding an additional electron rich RA moiety at the 4′-position to the -N=N- group of **4a** and **19a** results in a redshift of the π → π* absorption band for both **27a** and **28a**. As a result, both the π → π* and the n → π* absorption bands overlapped as shown in Scheme 3.2.1 and Scheme 3.2.2. Consequently, **27a** and **28a** can easily be isomerized to their respective *cis* isomers by light irradiation but can only be thermally isomerized back to the *trans* isomers.

We have shown that placing an additional RA group at the 4′- positions of the -N=N- group of **19a** causes the Bis(arylamino) azobenzene, **28a**, to behave similarly to **4a**. We have also shown that the addition of the additional RA group at the 4′- position resulted in an acceleration of the thermal *cis*-to-*trans* isomerization rate and a decrease in the $\Delta G^{\neq}$ for the thermal isomerization for both **27a** and **28a**. We have also demonstrated that the addition of the

RA moiety to the AB core creates a new route to chemically control the isomerization from the *cis* to the *trans* isomer by assisting as a trigger in the oxidizing state. This oxidation can either be chemically induced or electrically induced by the removal of an electron from the RA moiety.

Table 3.2.1. Comparisons of the physical properties between *p*AA-Ph-N=N-Ph **4a**, *p*AA-Ph-N=N-Ph-*p*AA **27a**, *m*AA-Ph-N=N-An **19a** and *p*AA-Ph-N=N-Ph-*m*AA **28a**.

Compounds	*p*AA-Ph-N_2-Ph **4a**	*p*AA-Ph-N_2-Ph-*p*AA **27a**	*m*AA-Ph-N_2-An **19a**	*m*AA-Ph-N_2-Ph-*p*AA **28a**
PSS (*trans* : *cis*)[(a)]	29 : 71	69 : 31	20 : 80	49 : 51
Half-life	2 hours 30 minutes	4 minutes 49 seconds	47 hours	3 hours and 13 minutes
Thermal *cis*-to-*trans* isomerization rate[(b)]	8.4×10^{-5} $\pm 8.6 \times 10^{-7} s^{-1}$	2.4×10^{-3} $\pm 2.9 \times 10^{-4}$ s^{-1}	4.1×10^{-6} $\pm 9.5 \times 10^{-9} s^{-1}$	6.0×10^{-5} $\pm 3.9 \times 10^{-7} s^{-1}$
$\Delta G^{\neq}$	23.0 kcal mol^{-1}	21.0 kcal mol^{-1}	24.8 kcal mol^{-1}	23.2 kcal mol^{-1}
E°[(c)]	0.94 V (vs. SCE)	(1) 0.78 V (vs. SCE) (2) 0.94 V (vs. SCE)	0.85 V (vs. SCE)	(1) 0.82 V (vs. SCE) (2) 1.01 V (vs. SCE)
***cis*- HOMO energy[(d)]**	- 4.8 eV	-4.5 eV	- 4.7 eV	-4.6 eV
Photo-electro catalysis[(e)]	Yes	Yes	Yes, but short lived radical cationic species	Yes

[(a)]Deaerated C_6D_6 at room temperature after irradiating with a 430 nm LED. ^{1}H NMR spectra were recorded on Bruker AM-500 instrument.
[(b)] Deaerated C_6D_6 at room temperature in a 0.1 cm quartz cell in the dark.
[(c)] 1.0 mM in DCM with 0.1 M $TBABF_4$ at 20 mV/s scan rate.
[(d)] MacSPARTAN ´10 Quantum Mechanics Program: (x86/Darwin) build 1.1.0v4.
[(e)] 0.0021 mmol dissolved in 0.25 mL Tol_3TBABF_4 gel. The gel solution was applied to ITO glass anode. Cycling conditions were: 30 seconds irradiation with 430 nm LED and 0.0 V, then 1.5 V for 30 s with no irradiation (Cyclic Voltammetry Scan Rate: 2 V/s). Spectrophotometer Reading- 30 s intervals.

Table 3.2.2 Experimental Details for the Crystal Structures of *p*AA-Ph-N=N-Ph-pAA **27a**.

Structure	***p*AA-Ph-N=N-Ph-*p*AA**
Reference code	scb270
Empirical Formula	$C_{40}H_{36}N_4O_4$
Formula Weight	636.73
Crystal Dimensions (mm)	
Crystal System, Space Group	Monoclinic, P2 (1)/C
Lattice Parameters: a	20.537(4)
b	9.8261(18)
c	34.073(6)
α	90
β	104.074(3)
γ	90
Volume ($Å^3$), Z	6670(2), 8
D_{calc} (g/cm^3)	1.268
F_{000}, μ(MoKα) (mm^{-1})	2688, 0.083
Diffractometer	Siemens SMART
Wavelength (Å), Temperature	0.71073, -100 °C
θ range for data collection	1.02 to 26.41 °C
Limiting indices	-25<=h<=25
	-12<=k<=12
	-42<=l<=42
Reflections Measured-Total	167427
Unique	13662 (R_{int} 0.1164)
Corrections: Decay	No
Absorption	No
Secondary Extinction	coeff: 0.0007(3)
Structure Solution	Direct
Data/restraints/parameters	13662/0/866
GOF on F^2	1.244
Final R indices [I>2σ(I)] (R_1, wR_2)	0.0813, 0.1933
R indices (all data) (R_1, wR_2)	0.1573, 0.2303
Largest diff. peak and hole ($e^-Å^{-3}$)	0.904, -0.698

3.3 Synthesis experimental details

Preparation of *pBr-Ph-N=N-pBr 25*

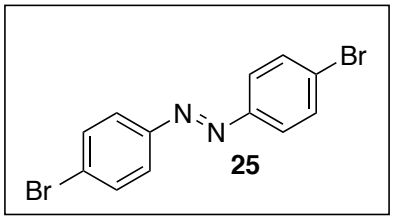

The synthesis of **25** was prepared analogously to **10** from *p*-bromonitroso **8** (1.01 g, 5.44 mmol), *p*-bromoaniline (0.936 g, 5.44 mmol), and glacial acetic acid (10 mL). After 24 hours, the solution turned red-orange and the precipitate formed was filtered to give an orange solid. The solid was recrystallized in hot EtOH yielding **25** (1.63 g, 4.80 mmol) as orange crystals.

Yield: 88% MW = 340.01 mp = 204 – 206 °C (lit. 203-204 C)

^{1}H NMR (500 MHz, $CDCl_3$, 25 °C):

δ (ppm) 7.77 (d, J = 8.75 Hz, 4H), 7.63 (d, J = 8.75 Hz, 4H)

^{13}C NMR (125 MHz, $CDCl_3$, 25 °C):

δ (ppm) 151.44; 132.65; 126.00; 124.65.

Preparation of *pBr-Ph-N=N-mBr 26*

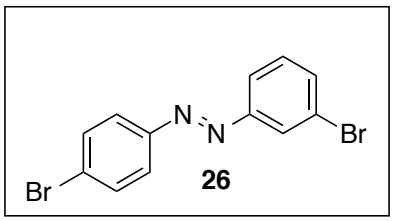

The synthesis of **26** was prepared analogously to **10** from *p*-bromonitroso **8** (0.548 g, 2.95 mmol), m-bromoaniline (0.507 g, 2.95 mmol), and glacial acetic (6 mL). After 24 hours, the solution turned red-orange and the precipitate formed was filtered to give an orange solid. The solid was recrystallized in hot EtOH yielding **26** (0.760 g, 2.24 mmol) as orange crystals.

Yield: 76% MW = 340.01 mp = 112 – 116 °C

^{1}H NMR (360 MHz, $CDCl_3$, 25 °C):

δ (ppm) 8.03 (t, J = 1.80 Hz. 1H), 7.86 (d, J = 8.19 Hz, 1H), 7.78 (d, J = 8.55 Hz, 2H), 7.64 (d, J = 8.55 Hz, 2H), 7.59 (d, J = 8.07 Hz, 1H), 7.39 (t, J = 7.59 Hz, 1H).

^{13}C NMR (125 MHz, $CDCl_3$, 25 °C):

δ (ppm) 153.59; 151.29; 134.13; 132.67; 130.72; 126.27; 124.94; 124.74; 123.42; 123.26.

Preparation of *p*AA-Ph-N=N-Ph-*p*AA 27a

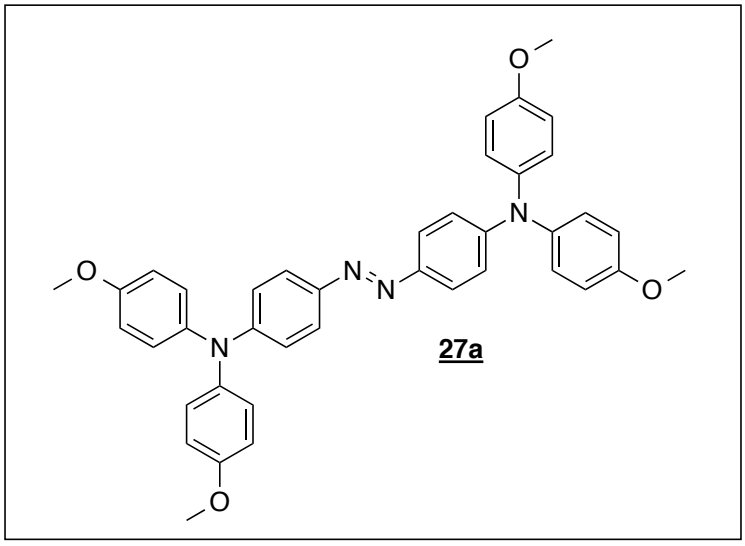

27a

The synthesis of **27a** was prepared analogously to **3** from **25** (0.205 g, 0.603 mmol), **3** (0.280 g, 1.21 mmol), $Pd(dba)_2$ (0.007 g, 0.012 mmol), $P(tBu)_3$ (0.0026 g, 0.0126 mmol), NaOtBu (0.233 g, 2.42 mmol), and anhyd toluene (15 mL). The product was concentrated in vacuo to yield a red solid which was purified via column chromatography (CC : benzene/hexanes) to afford **27a** (0.343 g, 0.540 mmol) as a red solid.

Yield: 90% MW = 636.74 mp = 197 – 200 °C

^{1}H NMR (500 MHz, $CDCl_3$, 25 °C):

δ (ppm) 7.66 (d, J = 8.97 Hz, 4H), 7.09 (d, J = 8.97 Hz, 8H), 6.93 (d, J = 8.97 Hz, 4H), 6.84 (d, J = 8.97 Hz, 8H), 3.79 (s, 12H).

^{13}C NMR (125 MHz, $CDCl_3$, 25 °C):

δ (ppm) 156.69; 150.75; 146.82; 140.41, 127.45; 123.88; 119.45; 115.05; 55.72.

CHN ($C_{26}H_{23}N_3O_2$)

Calcd: C, 75.45; H, 5.70; N, 8.80

Found: C, 75.34; H, 5.76; N, 8.71

m/z

Calcd: 636.2737

Found: 636.2753

UV/Vis (benzene, λ_{max}/nm, (ε/L · mol^{-1} · cm^{-1})):

480 (13814)

IR (cm^{-1}):

2832, 1585.9, 1493.8, 1474.1, 1321.1, 1281.5, 1236.1, 1145.5, 1103.1, 1030.8, 828.3, 725, 638.6, 574.9.

Preparation of *p*AA-Ph-N=N-Ph-*m*AA 28a

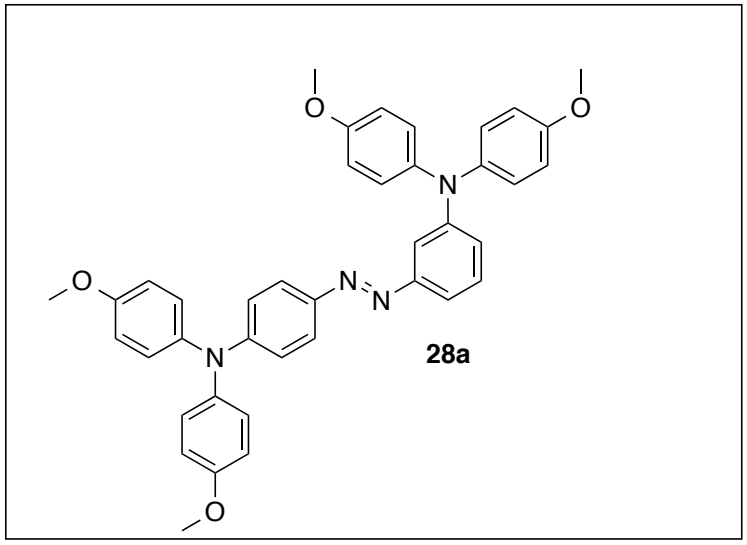

28a

The synthesis of **28a** was prepared analogously to **3** from **26** (0.204 g, 0.600 mmol), **3** (0.275 g, 1.20 mmol), $Pd(dba)_2$ (0.007 g, 0.012 mmol), $P(tBu)_3$ (0.0025 g, 0.012 mmol), NaOtBu (0.231 g, 2.40 mmol), and anhyd toluene (15 mL). The product was concentrated in vacuo yielding a red solid, which was purified via column chromatography (CC: benzene/hexanes) to afford **28a** (0.340 g, 0.534 mmol) as a red solid.

Yield: 89% MW = 636.74 mp = 71 – 75 °C with decomposition

^{1}H NMR (500 MHz, $CDCl_3$, 25 °C):

δ (ppm) 7.65 (d, J = 8.85 Hz, 2H), 7.40 (t, J = 2.11 Hz, 1H), 7.30 (t, J = 1.70 Hz, 1H), 7.28 (t, J = 1.51 Hz, 1H), 7.21 (d, J = 8.06 Hz, 1H), 7.08 (d, J = 9.03 Hz, 4H), 7.07 (d, J = 9.03 Hz, 4H), 6.89 (d, J = 9.13 Hz, 2H), 6.84 (d, J = 10.65 Hz, 4H), 6.81 (d, J = 10.67 Hz, 4H) 3.79 (s, 6H), 3.78 (s, 6H).

^{13}C-NMR (125 MHz, $CDCl_3$, 25 °C):

δ (ppm) 156.92; 156.15; 154.42; 151.56; 149.82; 146.32; 141.17; 140.43; 140.11; 129.51; 127.65; 127.45; 126.81; 124.48; 122.32; 118.90; 115.53; 115.12; 115.07; 115.00; 114.08; 55.72

CHN ($C_{26}H_{23}N_3O_2$)

Calcd: C, 75.45; H, 5.70; N, 8.80;

Found: C, 74.67; H, 5.69; N, 8.51

m/z

Calcd: 636.2737

Found: 636.2751

UV/Vis (benzene, λ_{max}/nm, (ε/L · mol^{-1} · cm^{-1})):

446 (22895)

IR (cm^{-1}):

2833.4, 1590.2, 1500.9, 1474.1, 1323.9, 1280.1, 1237.6, 1179.5, 1145.5, 1032.3, 825.5, 688.2, 637.2, 574.9.

CHAPTER 4

BIS(AZOBENZENE) DERIVATIVE AS PHOTO-ELECTRO SWITCH

4.1 Introduction

To better understand the electronics effect of the RA group throughout the molecule, we have designed and synthesized a bis(azobenzene) derivative. We have combined into the same molecular entity an An_2N-azobenzene, which has the RA build-in, and azoanisole that lacks the RA as shown in Figure 4.1.1 An ethylene glycol linker is used as a spacer to electronically decoupled the two azo compounds. The two sides of the bis(azobenzene) molecule should be able to be manipulated separately by photoisomerization from the *trans* to the *cis* isomer. The redox active side should behave similarly to **4a** and photoisomerize from *trans* to *cis* isomer by photo irradiation with a visible light source. The redox inactive should behave as an unsubstituted-azobenzene and photoisomerize from *trans* to *cis* isomer by photo irradiation with an ultraviolet light source. The isomeric structures of the bis(azobenzene) derivative are shown in Figure 4.1.1

In this section, we will investigate the electronic effects of the RA group on the azobenzene core. We hypothesized that it should be achievable to photoisomerized each side of the bis(azobenzene) derivatives seperately. However, the oxidative-opening from *cis* to *trans* on exposure to an oxidant or a voltage should only occur on the redox active side of the molecule and as a result, the thermal rate of the *cis*-to-*trans* isomerization of the redox active side should decrease exponentially. The synthetic route to obtain **33a** is shown in Scheme 4.1.1.

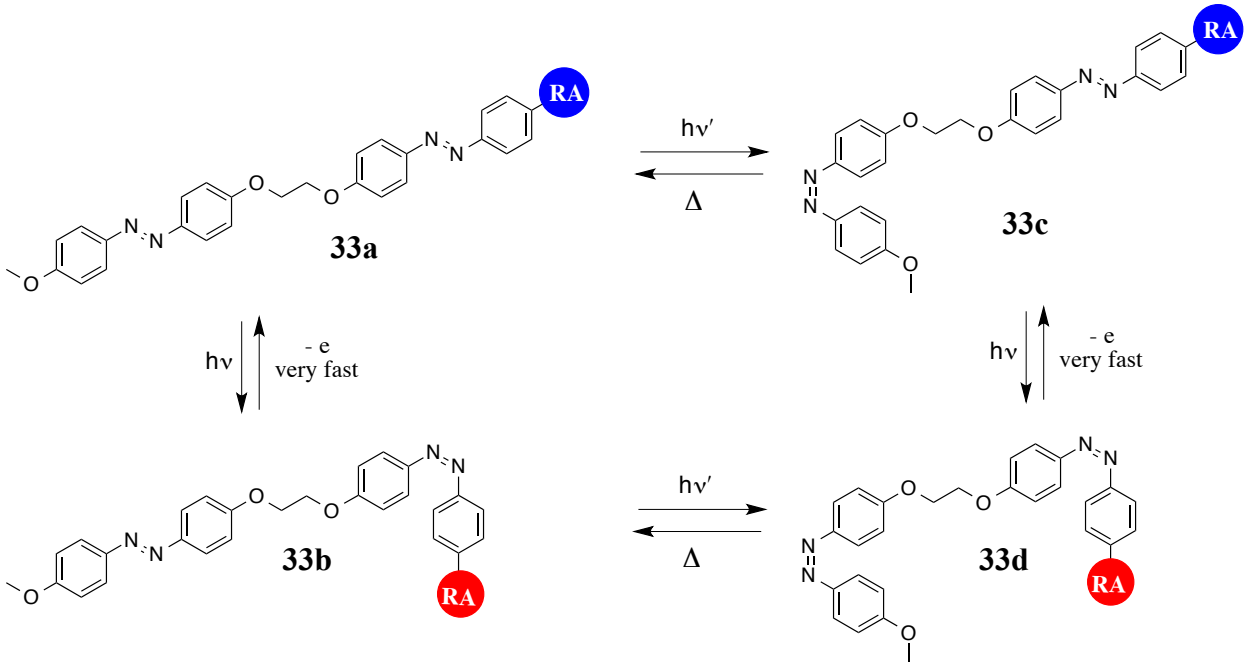

Figure 4.1.1 Model of the bis(azo) photo-electro switch. The *trans* isomer (blue) isomerizes to the *cis* isomer (red) by utilizing light, and the *cis* isomer (red) then rapidly isomerizes to the *trans* isomer (blue) upon removal of an electron.

Synthesis:

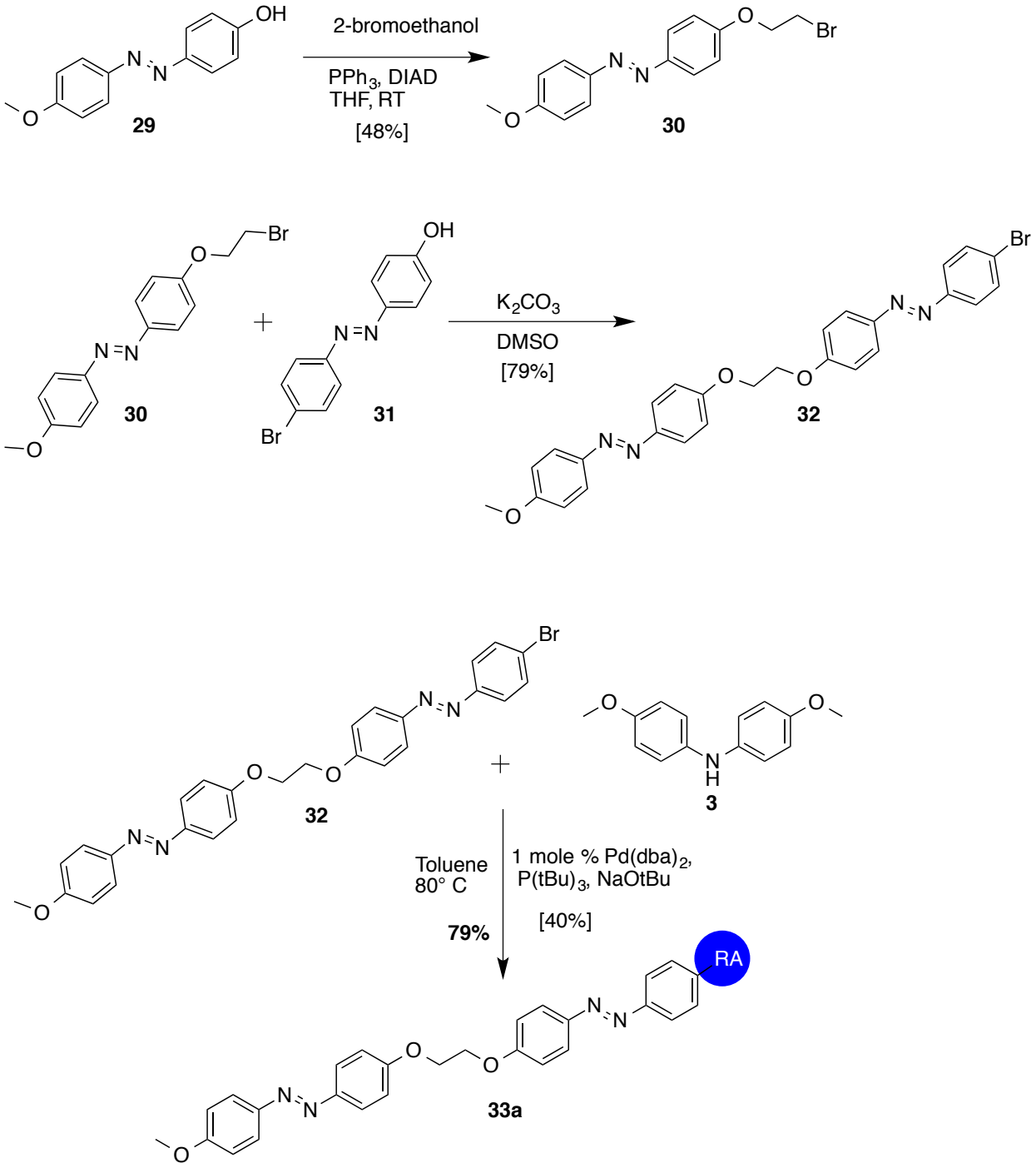

Scheme 4.1.1 Synthetic route to obtain **33a**.

4.1.1 Photochemistry and Optical Absorption of 33a

We hypothesized that including a spacer, an ethylene glycol spacer, to electronically decouple the two azo compounds will result in spectral features similar to azoanisole and **4a**. Figure 4.1.2 shows and overlay of the optical spectra of **4a**, azoanisole, and **33a**.

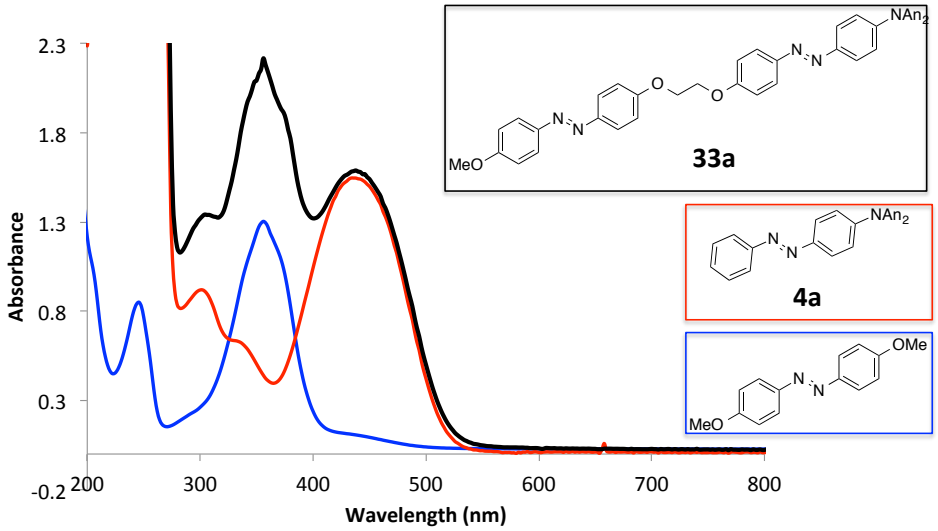

Figure 4.1.2. Optical spectrum of **33a** (6.18 x 10^{-4} M in C_6D_6) (black), **4a** (6.37 x 10^{-4} M in C_6D_6) (red), azoaznisole (6.09 x 10^{-4} M in acetonitrile) (blue) at room temperature in a 0.1 cm quartz UV-Vis cell.

Two π → π* absorption bands are observed for **33a**. Figure 4.1.3 illustrates the optical spectrum of **33a**, which features two strong π → π* absorption bands having an absorption maximum at 358 nm and 442 nm. The π → π* absorption band at 358 nm belongs to azoanisole (the redox inactive side), and the π → π* absorption band at 442 nm corresponds to **4a** (the redox active side).

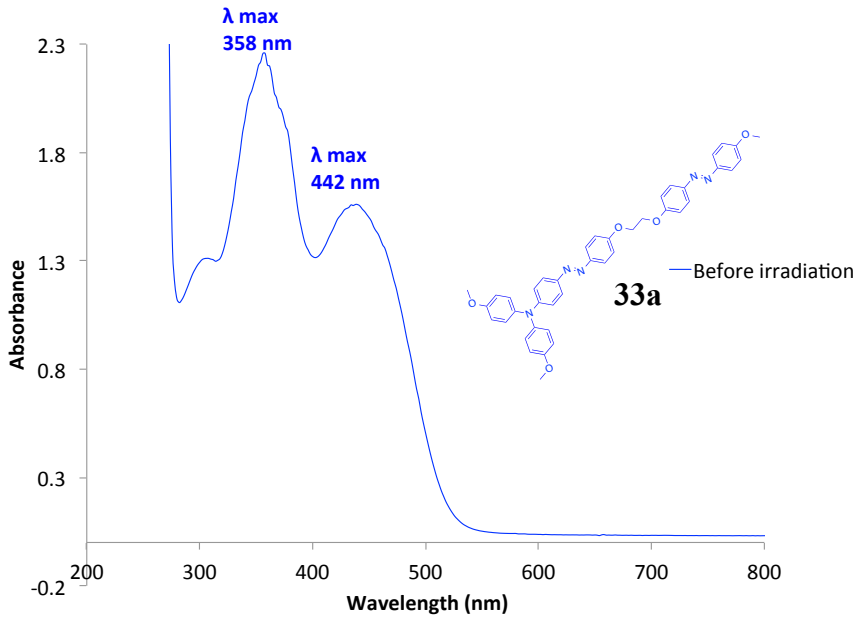

Figure 4.1.3. Optical spectrum of **33a** (6.18 x 10^{-4} M in C_6D_6) at room temperature in an 0.1 cm quartz UV-Vis cell.

Figure 4.1.4 shows the photoisomerization process of **33a** to **33b**. Upon irradiation of the $\pi \rightarrow \pi^*$ absorption band using a 450 nm light source, **33a** isomerized to **33b** with two isosbestic points occurring at 316 nm and 516 nm. The time-dependence of PSS establishment for **33b** was determined by following the absorption maximum at 442 nm during the photo irradiation process. After approximately 3 minutes of irradiating, no changes in absorbance were observed based on the plateau in absorbance that indicates a PSS was reached.

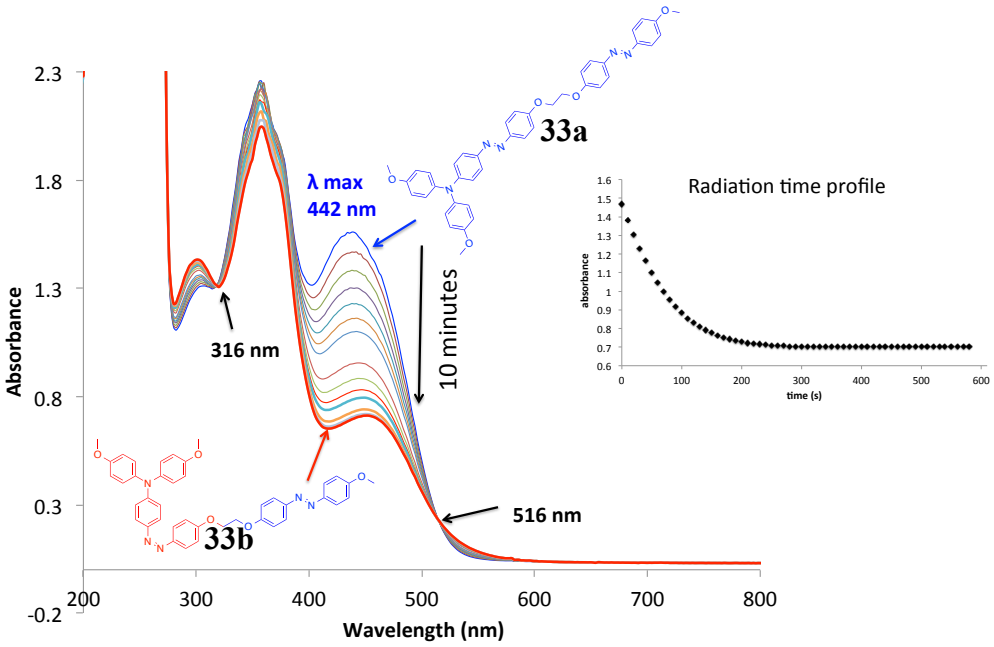

Figure 4.1.4. Optical spectrum of **33a** (6.18 x 10^{-4} M in C_6D_6) irradiated with a 450 nm LED at room temperature in 0.1 cm quartz UV-Vis cell.

The PSS of the redox inactive side was also obtain by irradiating with a 365 nm light source. Figure 4.1.5 shows the photoisomerization of **33a** to **33c.** Upon irradiation of the π → π* absorption band using a 365 nm light source, **33a** photoisomerized to **33c** with two isosbestic points occurring at 320 nm and 510 nm. The time-dependence of PSS establishment for **33c** was determined by following the absorption maximum at 358 nm during the irradiation process. After approximately 3 minutes of irradiating, no changes in absorbance were observed based on the plateau in absorbance that indicates a PSS was reached.

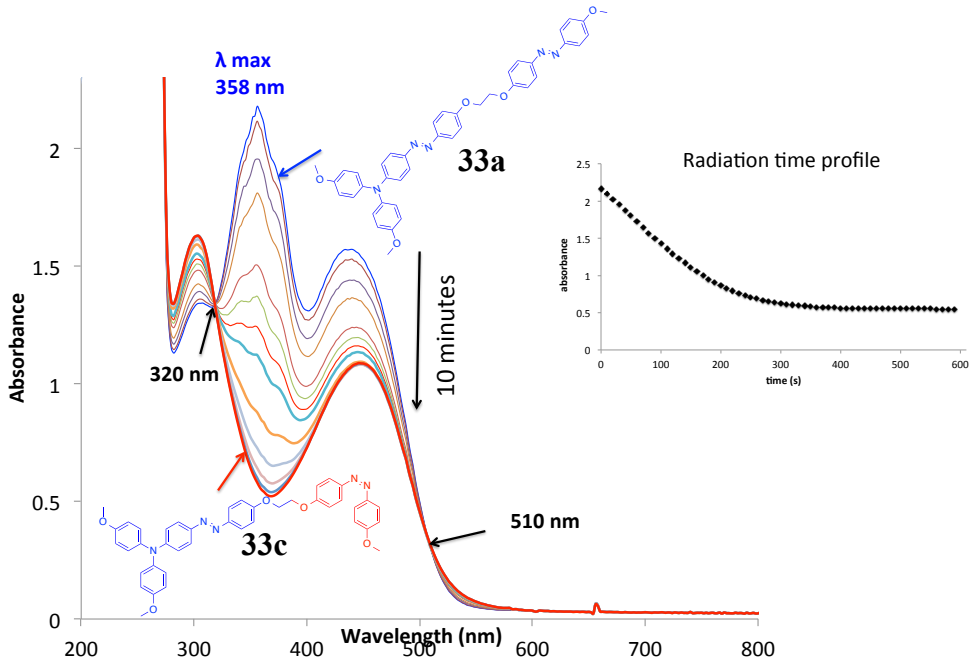

Figure 4.1.5. Optical spectrum of **33a** (6.18 x 10^{-4} M in C_6D_6) irradiated with a 365 nm light at room temperature in 0.1 cm quartz UV-Vis cell.

4.1.2 Thermal *cis*-to-*trans* isomerization of 33a

After reaching a PSS**,** the thermal isomerization process of **33b** to **33a** and **33c** to **33a** at room temperature was examined to understand the thermodynamic effect of the RA moiety on the thermal reversibility of both sides of **33a**.

As performed for the other arylamino azobenzenes, ultraviolet-visible spectroscopy was also utilized to monitor the thermal isomerization processes. The experiment was conducted in the dark and was monitored for 12 hours for the redox active side of the molecule and 48 hours for the redox inactive side. After reaching a PSS, spectra were taken in the dark for both sides until there were no changes in the maximum absorbances. Figure 4.1.6 and Figure 4.1.7 show the thermal isomerization process from **33b** to **33a** and for **33c** to **33a**, respectively.

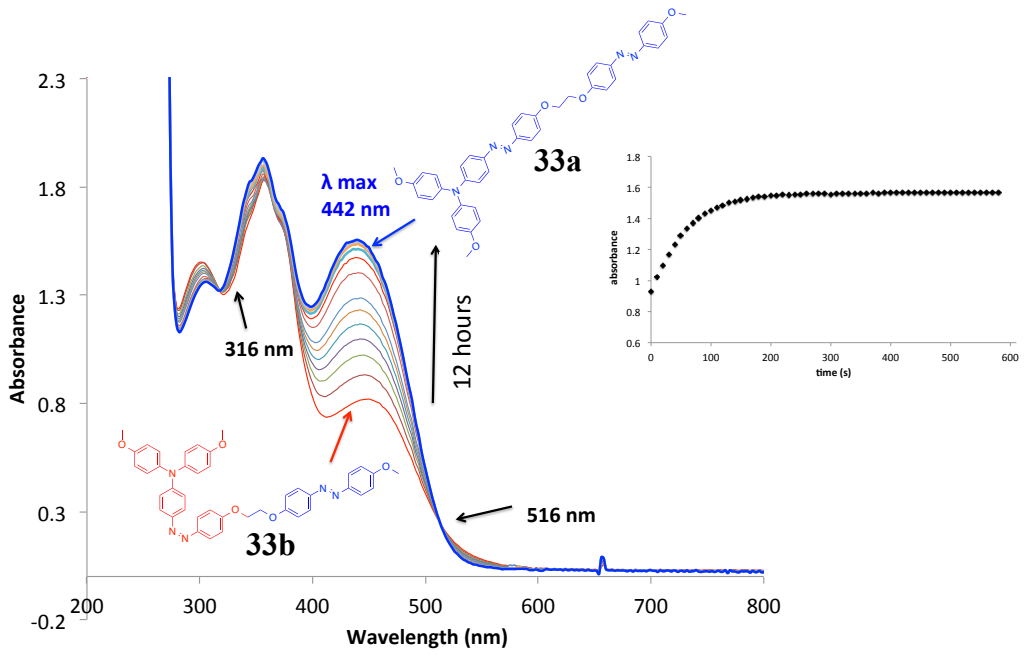

Figure 4.1.6. Optical spectrum of the thermal isomerization of **33b** to **33a** (6.18 x 10^{-4} M in C_6D_6) recorded in the dark at room temperature in a 0.1 cm quartz cell after irradiating with 450 nm light to a PSS.

The absorbance maximum at 442 nm was utilized to monitor the thermal recovery of **33a** from **33b** in the dark until no **33b** was present. After irradiating with the 450 nm light source, the absorbance maximum at 442 nm was plotted to prove that all **33b** was converted back to **33a** as shown in Figure 4.1.6. Similarly, the absorbance maximum at 358 nm was utilized to monitor the thermal recovery of **33a** from **33c** in the dark until no **33c** was present.

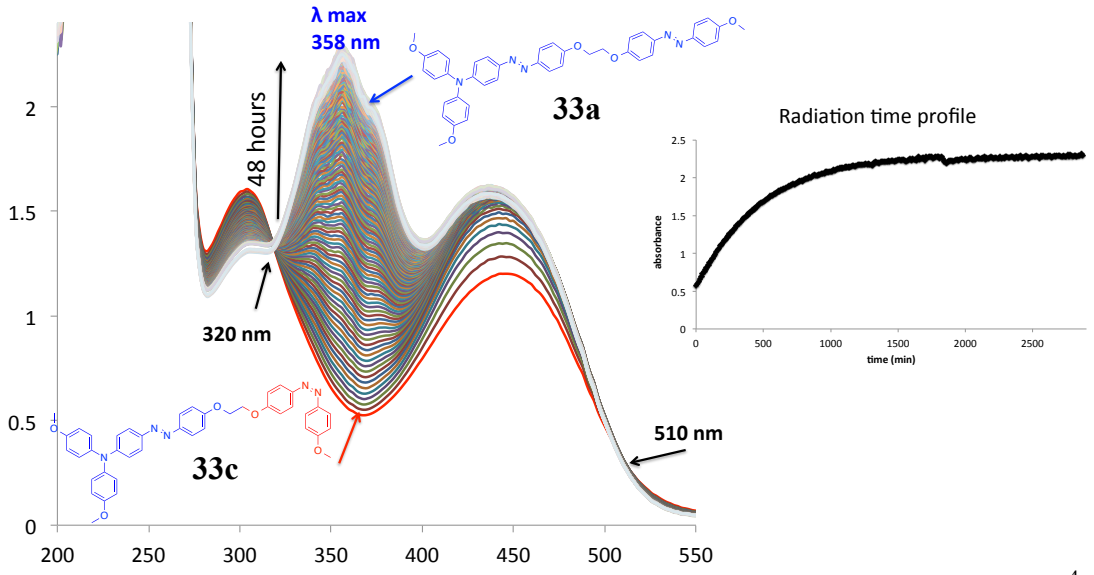

Figure 4.1.7. Optical spectrum of the thermal isomerization of **33c** to **33a** (6.18 x 10^{-4} M in C_6D_6) recorded in the dark at room temperature in a 0.1 cm quartz cell after irradiating with 365 nm light to a PSS.

4.1.3 Electron transfer catalysis of *cis-to-trans*- isomerization

In order to determine if the addition of ethylene glycol linker will interfere with the electrical stimulation of *cis* to *trans* isomerization of **33d**, it was necessary to attempt to oxidize **33d** in effort to replicate the catalytic electron transfer cycle of the previous arylamino azobenzenes. Before attempting to oxidize **33d**, the molecular orbitals were computed using density-functional theory with the B3LYP/6-31G** basis set to locate the energy level of the HOMO and to confirm that the RA group would be the moiety interacting with the oxidant. B3LYP/6-31G** molecular orbital calculations will also clarify if the pi orbitals of the RA group will overlap with the -N=N- group pi orbitals in the *cis* form. Figure 4.1.8 illustrates the location of the molecular orbitals of the HOMO in **33d**. It shows that the HOMO is predominantly located around and at the central nitrogen atom of the RA moiety. It also shows a large amount of electron density on redox active side of the molecule. This large amount of electron density observed on the redox active side helps create some overlap between the pi orbitals of the -N=N-

group and the lone pair of the nitrogen item of the RA group. However, no electron density is observed on the redox inactive side of the molecule. This result signifies that there is a donor-acceptor interaction between the -N=N- group and the RA moiety in the **33d**. This spatial arrangement also signifies that the removal of an electron from **33d** should perturb the -N=N- group. As a result, removal of an electron from the RA moiety of **33d** would cause the -N=N- bond to break and convert into -N-N- triggering isomerization back to **33a**

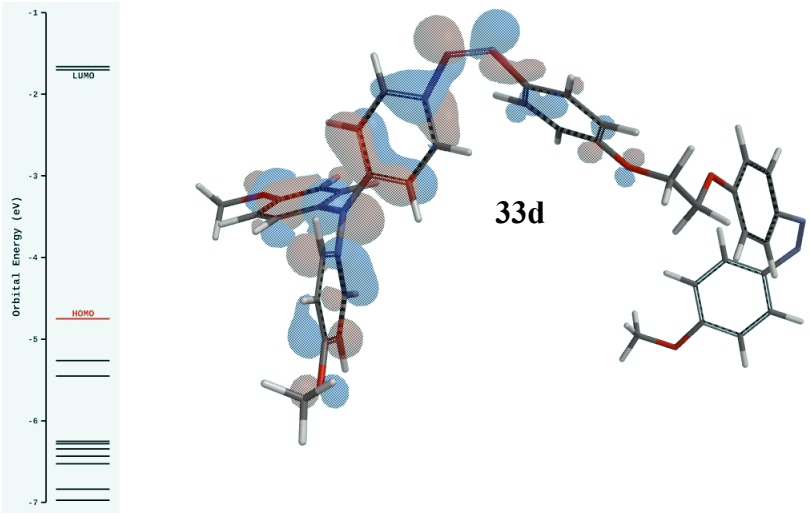

Figure 4.1.8. B3LYP/6-31G** molecular orbital calculations of **33d**. The HOMO is predominantly located at and around the central nitrogen atom of the RA group. The blue and red lobes indicate where the electron densities are located.

To test our hypothesis, 1% mole of **6** was injected into a solution of **33d** in deoxygenated benzene at PSS. Based on our results, 1% mole of **6** was sufficient to oxidized **33d** and initiates the electrical catalysis cycle shown in Scheme 4.1.2. Upon injection and mixing, **33d** isomerized back to **33c** in less than 2 seconds, as judged by optical spectra analysis illustrated in Figure 4.1.9.

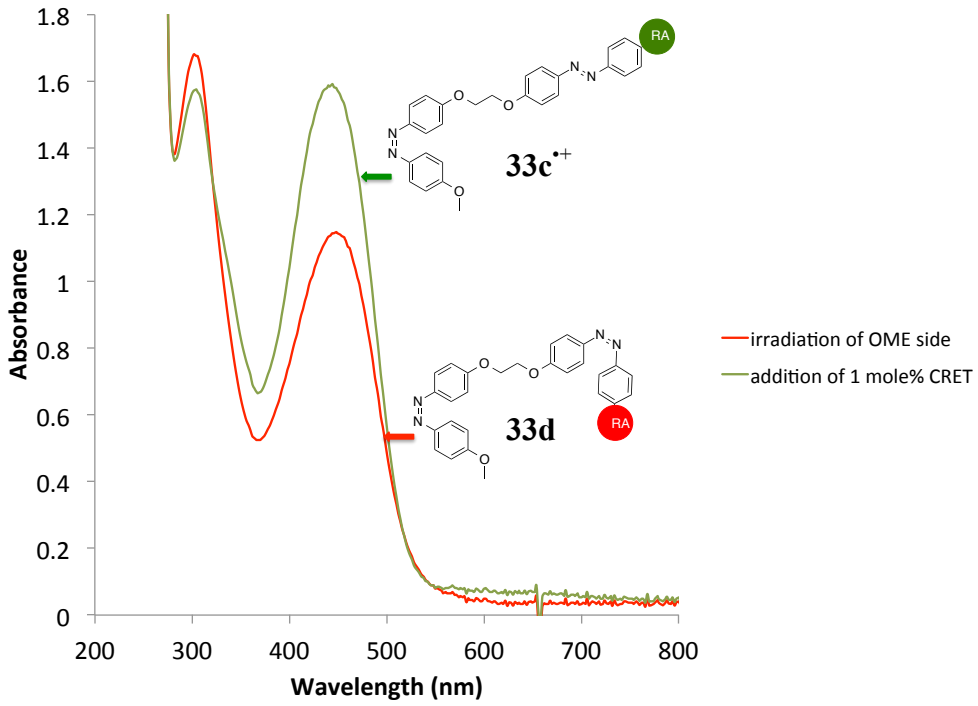

Figure 4.1.9. Optical spectrum of **33a** (6.18 x 10^{-4} M in C_6D_6) irradiated with 365 nm and 450 nm light source and CRET injection (1% mole in DCM) at PSS at room temperature in 0.1 cm quartz UV-Vis cell.

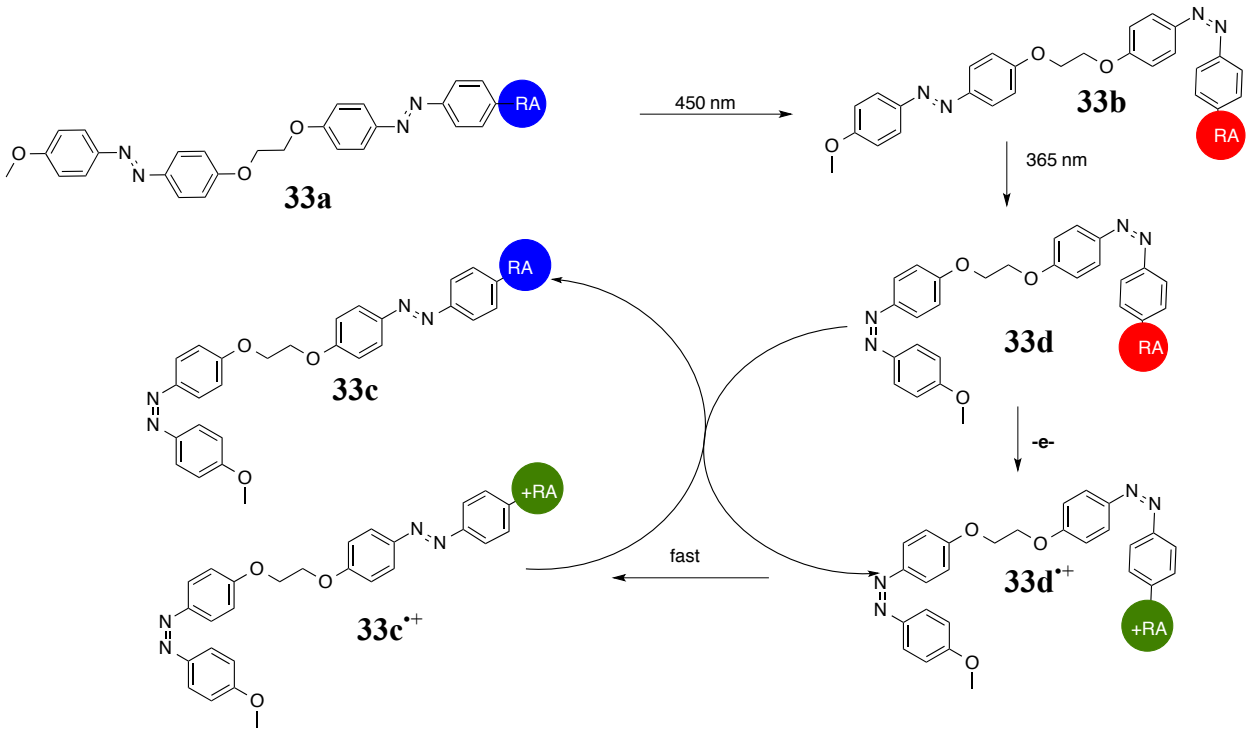

Scheme 4.1.2. Postulated photo-electro catalysis mechanism of **33a.**

To test the reliability of our photo-electro catalysis cycle, bis-azo$^{\bullet+}$ sample was irradiated multiple times after the addition of **6**. After this prolonged irradiation, **33d** was not observed as displayed in Figure 4.1.10. However, as a result of the n → π* of azoanisole and the π → π * of **4a** overlapping, irradiating the oxidized sample regenerated *trans*- azonisole without degrading the electro catalysis cycle on the RA side of the bis azo (Figure 4.1.10).

This result suggests that *trans bis-azo* $^{\bullet+}$ is exceptionally chemically stable, it is able to exchange an electron with other neutral *cis* isomers, **33d**, thereby generating a catalytic cycle for bis-azo unfolding as shown in Scheme 4.1.2. Grounded on this result, we postulated a new photo-electro isomerization catalysis mechanism that accounts for the fast relaxation of *cis*-to-*trans*. The photo-electro catalysis mechanism cycle in Scheme 4.1.2 demonstrates that a 450 nm LED light source can be used to photoisomerize the RA active side of the bis-azo from **33a** to **33b**, similarly a 365 nm light source can be used to photoisomerize the RA inactive side of the bis-azo from **33c** to **33d**. Subsequent addition of a catalytic amount of oxidant will regenerate the *trans* isomers of the RA active side, thus exponentially increasing the rate at which the *cis* isomer relaxes back to the *trans* isomer.

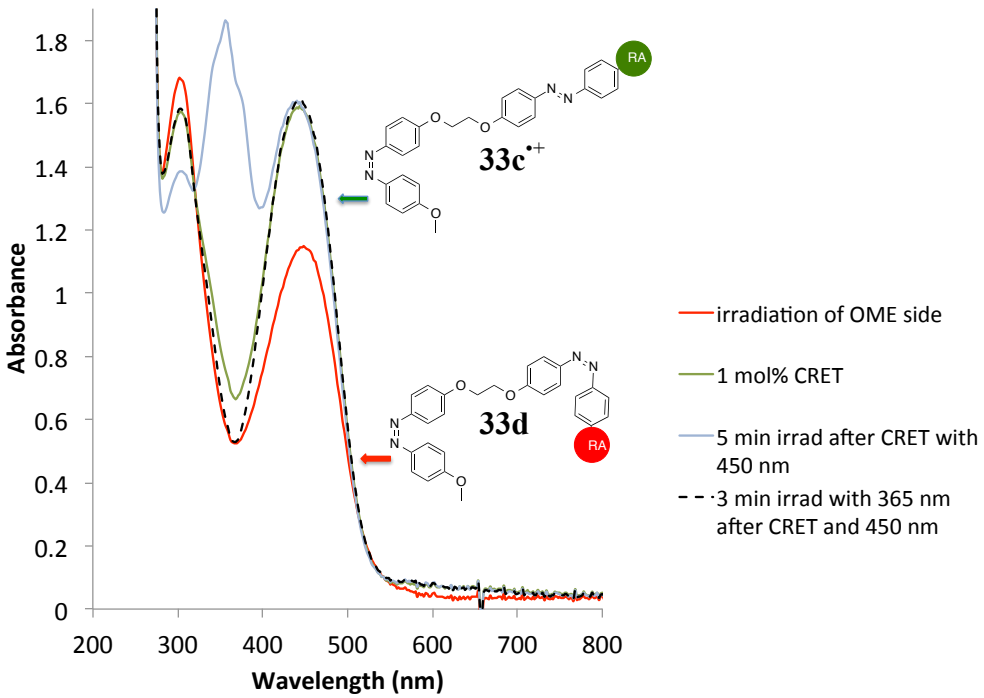

Figure 4.1.10. Optical spectrum of **33a** (6.18 x 10^{-4} M in C_6D_6) irradiated with 365 nm and 450 nm light source and CRET injection (1% mole in DCM) at PSS with prolonged irradiation at room temperature in 0.1 cm quartz UV-Vis cell.

4.1.4 Conclusions

The ultimate goal of this section was to better understand the electronics effect of the RA group throughout the azobenzene core. We have combined into the same molecular entity an An_2N-azobenzene, which has the RA group build-in, and azoanisole that lacks the RA group. A spacer, an ethylene glycol linker, was used to electronically decouple the two azo compounds. We also investigated the oxidative-opening from *cis* to *trans* on exposure to an oxidant or a voltage. This oxidative-opening only occurs on the redox active side of the molecule and as a result, the thermal rate of the *cis*-to-*trans* isomerization of the redox active side decreased. Further research on the bis-azobenzene derivative is still requires to determine the isomeric ratios at PSS, we also need to evaluate the oxidation potential of the **33a**. The stability of the *cis* isomer at room temperature also needs to be evaluate in order to calculate the rate constant.

4.2 Synthesis experimental details

Synthesis of 4-methoxy-4´-hydroxyazobenzene 29

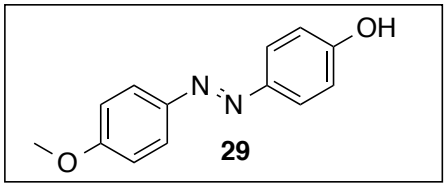

29

p-anisidine (3.48g, 28.3 mmol) was dissolved in a mixture of 1 M HCl (75 mL) and acetone (25 mL) at 0-5 °C. After *p*-anisidine was dissolved, a mixture of $NaNO_2$ in H_2O (25 mL) was added dropwise for 20 min into the *p*-anisidine mixture. After forming the diazonium salt, a mixture of phenol (4.00 g, 42.5 mmol), NaOH (1.80 g, 45.00 mmol) and Na_2CO_3 (7.20g, 68.0 mmol) in H_2O (25 mL) was added dropwise into the diazonium mixture for 20 min. The solution turned orange and was stirred for 3 h at room temp. The orange precipitate formed was filtered and collected. The product was recrystallized in 1:1 MeOH/water to yield **[29]** (6.09g, 22.0mmol) as orange crystals. Yeong-Soon previously prepared **29** with an 80% yield.[80]

Yield: 94% MW= 277.12g/mol mp 143-147 °C (lit. 144- 146 °C)[80]

^{1}H-NMR (360 MHz, $CDCl_3$, 25 °C):

δ (ppm) 7.86 (d, J= 8.93 Hz, 2H), 7.81 (d, J = 8.98 Hz, 2H), 6.98 (d, J = 8.99 Hz, 2H), 6.90 (d, J = 8.99 Hz, 2H), 5.33 (s, 1H), 3.87 (s, 3H).

^{13}C-NMR (500 MHz, CDCl3, 25 °C):

δ (ppm) 161.87; 157.90; 147.53; 147.27; 124.80; 124.60; 115.97; 114.43; 55.79

Synthesis of p-MeO-Ph-N=N-Ph-p-O-$(CH_2)_2$-Br 30

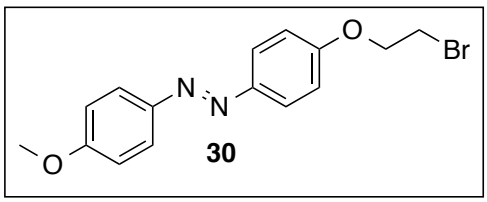

30

A 100 mL rb flask was flamed dried and transported into the N_2 filled dry box where **29** (2.00 g, 8.76 mmol), DIPAD (2.07 mL, 10.5 mmol), PPh_3 (2.76 g, 10.5 mmol), and THF (anhy.17 mL) was added. The reaction vessel was capped with a rubber

[80] Yeong-Soon, G.; Sung-Ho, J.; Jong-Wook, P.; Sung-Hoon, K.; Won, S. L.; Kwon, T. L. electro-Optical and Electrochemical Properties of an Ionic Polyacetylene Derivtive with Azobenzene Anisole Moieties. *Journal of Industrial and Engineering Chemistry,* **2012**, 55-60.

septum and transported outside of the dry box. The reaction was stirred for 2 h at room temp under N_2 atmosphere. Then 2-bromoethanol (1.20 g, 9.64 mmol) was added dropwise to the mixture and the resulting solution was then stirred for 72 hours at room temp under N_2 atmosphere. The product was concentrated in vacuo yielding a yellow solid. The crude was purified via column chromatography (CC: ethyl acetate/hexanes 1:1) to afford the product **30** as a yellow solid (1.44g, 4.29mmol). Garcia-Amoros previously prepared **30** with a 76% yield. [81]

Yield: 48% MW= 335.20g/mol mp 125-127 °C (lit. 98-100 °C)[82]

^{1}H-NMR (360 MHz, CDCl3, 25 °C):

δ (ppm) 7.86 (d, J= 8.80 Hz, 4H), 6.99 (d, J = 8.35 Hz, 4H), 4.35 (t, J = 6.35 Hz, 2H), 3.87 (s, 3H), 3.66 (t, J = 6.04 Hz, 2H).

^{13}C-NMR (500 MHz, CDCl3, 25 °C):

δ (ppm) 161.71; 159.96; 147.56; 147.07; 124.42; 124.39; 114.92; 114.19; 68.05; 55.56; 28.77.

Synthesis of 4-methoxy-4´-bromoazobenzene 31

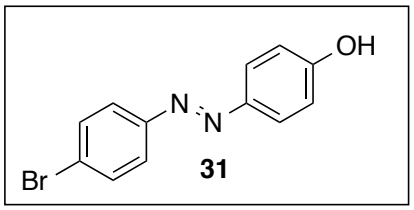

31

The synthesis of **31** was prepared analogously to **29** from p-bromoaniline (4.86 g, 28.3 mmol), 1 M HCl (75 mL), acetone (25 mL), $NaNO_2$ (3.00 g, 43.5 mmol), phenol (4.00 g, 42.5 mmol), NaOH (1.80g, 45 mmol), Na2CO3 (7.20 g, (68.0 mmol). The precipitate formed was collected and used without any further purification (7.11 g, 25.65 mmol).

Yield: 91% MW= 277.12g/mol mp 155-160 °C (lit. 155 °C)[83]

[81] Garcia-Amoros, J.; Reig, M.; Cuadrado, A.; Ortega, M.; Nonell, S.; Velasco, D. A Photoswitchable Bis-Azo Derivative with High Temporal Resolution. *Chem. Comm.,* **2014**, 11462-11464.
[82] He, C.; Zhang, C.; Zhang, O. Synthesis and thermal behaviours of side-chain liquid-crystalline poly[N-(4-methoxyazobenzene-4′-oxyalkyl)ethyleneimine]. *Liquid Crystals,* **2009**, *4*, 379-387.

^{1}H-NMR (360 MHz, CDCl3, 25 °C):

δ (ppm) 7.85 (d, J= 8.97 Hz, 2H), 7.74 (d, J = 8.80 Hz, 2H), 7.61 (d, J = 8.85 Hz, 2H), 6.92 (d, J = 8.97 Hz, 2H), 5.12 (s, 1H).

^{13}C-NMR (500 MHz, CDCl3, 25 °C):

δ (ppm) 158.80; 151.46; 146.97; 132.25; 125.13; 124.60; 124.08; 115.91

Synthesis of bis(azo) 4-methoxy-4´-hydroxyazobenzene-$(CH_2)_2$4-methoxy-4´-bromoazobenzene 32.

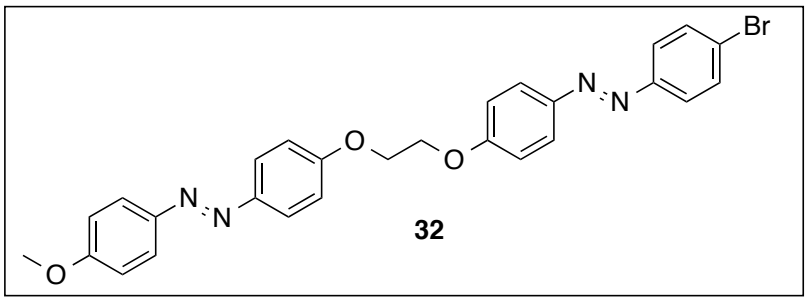

32

To a 25 mL rb flask, **30** (0.200g, 0.586 mmol), **31** (0.173 g, 0.626 mmol), and DMSO (5 mL) was added and stirred for 15 minutes at 65 °C. Then K_2CO_3 (0.091 g, 0.6563 mmol) was added to the mixture and stirred for 36 h at 65 °C. The resulting precipitate formed was filtered and rinsed with DMSO and water to afford **32** the product as a yellow solid (0.252 g, 0.474 mmol).

Yield: 79% MW=531.41g/mol mp 243-245 °C

[83] Zhang, C-Z.; Wang, C-Y.; Im, C.; Lu, G-Y.; Wang, C-S. Significant Effect of Bromo Substituents on Nonlinear Optical Properties of Polymer and Chromophores. *J. Phys. Chem. B.*, **2010**, *114*, 42-48.

Preparation of bis(azobenzene) 33a

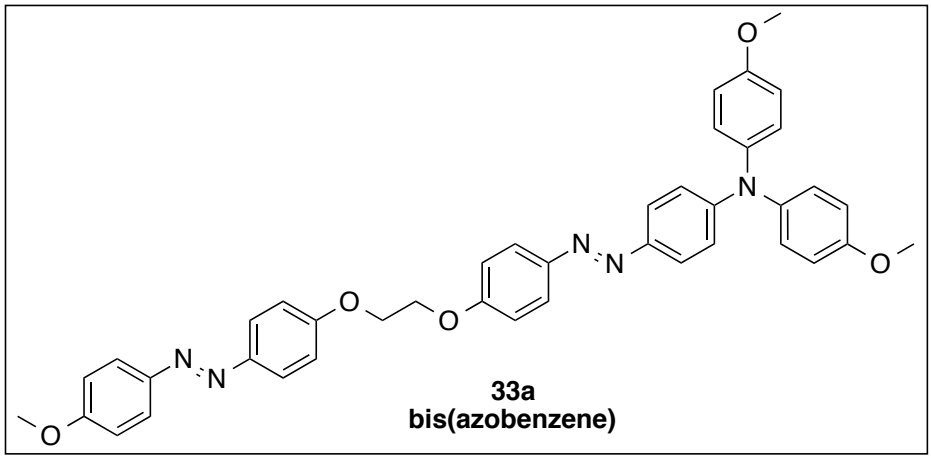

33a
bis(azobenzene)

The synthesis of **33a** was prepared analogously to **3** from **32** (0.100 g, 0.188 mmol) and **3** (0.044 g, 0.192 mmol). $Pd(dba)_2$ (0.001 g, 0.0019 mmol), $P(tBu)_3$ (0.00045 g, 0.0022 mmol) and NaOtBu (0.027 g, 0.282 mmol). Removal of the solvent gave **33a** (0.059 g, 0.087 mmol) as an orange solid.

Yield: 46% MW = 679.76

^{1}H NMR (360 MHz, $CDCl_3$, 25 °C):

δ (ppm) 7.72 (m, 6H), 7.72 (d, J = 8.44 Hz, 2H), 7.11 (d, J = 9.28 Hz, 4H), 7.08 – 6.91 (m, 8H), 6.86 (d, J = 9.28 Hz, 4H), 4.40 (s, 4H), 3.87 (s, 3H), 3.80 (s, 6H).

CHAPTER 5

TRIS(AZOBENZENE) DERIVATIVE

5.1 Introduction

This chapter will focus, solely, on the preliminary data of the tris(azobenzene) derivative. Further research on the tris(azobenzene) derivative is still required as future work. The synthetic route to obtain the tris(azobenzene) derivative, **37**, and the experimental details for the crystal structures will be presented.

5.2 Synthesis experimental details

Preparation of *p*nitro-nitrosobenzene 34

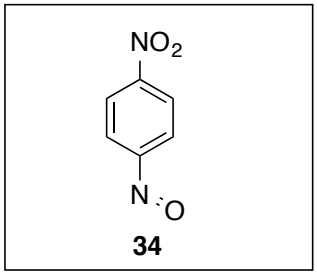

34

The synthesis of **34** was prepared analogously to **8** from *p*-nitroaniline (2.02 g, 14.6 mmol), and Oxone® $2KHSO_5 \cdot KHSO_4 \cdot K_2SO_4$ (17.9 g, 29.2 mmol). The product was concentrated in vacuo yielding **34** (2.18 g (14.3 mmol) as a yellow solid (green solution).

Yield: 98% MW = 152.11

^{1}H NMR (500 MHz, $CDCl_3$, 25 °C):

δ (ppm) 8.49 (d, J = 8.92 Hz, 2H), 8.03 (d, J = 9.21 Hz, 2H)

Preparation of *p*NO_2-Ph-N=N-An 35

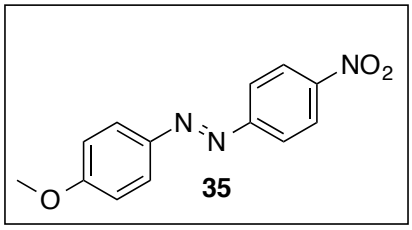

The synthesis of **35** was prepared analogously to **10** from *p*-nitro-nitrosobenzene **34** (2.19 g, 14.4 mmol), p-anisidine (1.77g, 14.4 mmol), glacial acetic (18 mL) and ethanol (42 mL). After 24 hours, the solution turned red-orange and the precipitate formed was filtered to give an orange solid. The solid was recrystallized in hot EtOH yielding **35** (2.89 g, 11.23 mmol) as orange crystals.

Yield: 78% MW = 257.25

^{1}H NMR (360 MHz, $CDCl_3$, 25 °C):

δ (ppm) 8.35 (d, J = 9.09 Hz. 2H), 7.96 (d, J = 9.09 Hz, 2H), 7.95 (d, J = 9.09 Hz, 2H), 7.03 (d, J = 9.09 Hz, 2H), 3.90 (s, 3H).

Preparation of *p*NH_2-Ph-N=N-An 36

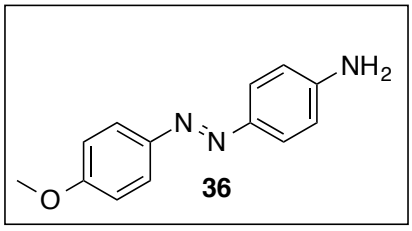

A solution of NaS_2□$9H_2O$ (1.42 g, 5.91 mmol) in H_2O (20 mL) was added dropwise into a solution of **35** (.760 g, 2.95 mmol) in ethanol (60 mL) at room temperature. After the addition, the mixture was refluxed for 24 h and the solution turned red. The ethanol was evaporated in vacuo to yield the product (.642 g, 2.82 mmol) as an orange solid without any further purification.

Yield: 96% MW = 227.26

^{1}H NMR (360 MHz, $CDCl_3$, 25 °C):

δ (ppm) 7.82 (d, J = 9.31 Hz. 2H), 7.75 (d, J = 8.66 Hz, 2H), 6.97(d, J = 9.02 Hz, 2H), 6.72 (d, J = 9.31 Hz, 2H), 3.97 (br,s, 2H), 3.86 (s, 3H)

Preparation of Tris(azo) 37

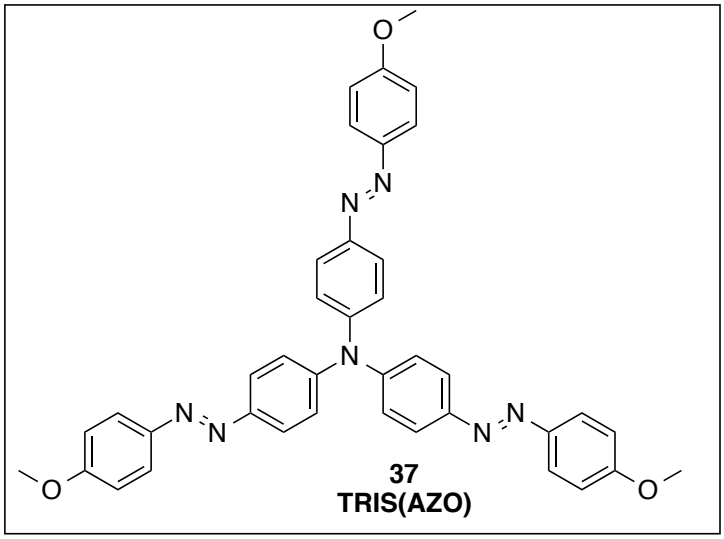

The synthesis of **37** was prepared analogously to **3** from **13** (0.448 g, 1.54 mmol) and **36** (0.175 g, 0.770 mmol). $Pd(dba)_2$ (0.009 g, 0.015 mmol), $P(tBu)_3$ (0.003 g, 0.017 mmol) and NaOtBu (0.222 g, 2.31 mmol). Removal of the solvent gave a red solid, which was purified via column chromatography (benzene/hexanes) to afford **37** (0.493 g, 0.761 mmol).

Yield: 98.8% MW = 647.72 mp = 181 – 185 °C

^{1}H NMR (500 MHz, $CDCl_3$, 25 °C):

δ (ppm) 7.88 (d, J = 1.71 Hz, 6H), 7.86 (d, J = 1.71 Hz, 6H), 7.31 (d, J = 8.84 Hz, 6H), 7.13 (d, J = 8.84 Hz, 6H), 3.86 (s, 9H).

Table 5.1. Experimental Details for the Crystal Structures of tris(azobenzene) **37**.

Structure	**tris(azobenzene)**
Reference code	scb268b
Empirical Formula	$C_{39}H_{33}N_7O_3$
Formula Weight	647.72
Crystal Dimensions (mm)	0.01 x 0.15 x 0.21
Crystal System, Space Group	Monoclinic, P2 (1)/C
Lattice Parameters: a	10.3748(18)
b	11.2019(19)
c	28.907(5)
α	90
β	96.833(2)
γ	90
Volume ($Å^3$), Z	3335.7(10), 4
D_{calc} (g/cm^3)	1.290
F_{000}, μ(MoKα) (mm^{-1})	1360, 0.084
Diffractometer	Siemens SMART
Wavelength (Å), Temperature	0.71073, -100 °C
θ range for data collection	1.42 to 26.32 °C
Limiting indices	-12<=h<=12
	-13<=k<=13
	-35<=l<=36
Reflections Measured-Total	82674
Unique	6756 (R_{int} 0.0684)
Corrections: Decay	No
Absorption	No
Secondary Extinction	coeff: 0.0002(4)
Structure Solution	Direct
Data/restraints/parameters	6756/0/443
GOF on F^2	1.007
Final R indices [I>2σ(I)] (R_1, wR_2)	0.0485, 0.1102
R indices (all data) (R_1, wR_2)	0.0868, 0.1303
Largest diff. peak and hole ($e^-Å^{-3}$)	0.187, -0.188

REFERENCES

1. Zollinger, H. Azo and Diazo Chemistry: Aliphatic and Aromatic Compounds, Interscience Publishers, New York and London, 1961; Zollinger, H. Colour Chemistry: Synthesis, Properties and Applications of Organic Dyes. 3rd Ed. Wiley-VCH, Weinheim 1987.

2. Bock, H.; Rudolph, G.; Baltin, E.; Kroner, J. Farbe und Konstitution bel Azoverbindungen. *Angew. Chem.,* **1965,** *77*, 469-516; Color and Constitution of Azo Compounds *Angew. Chem. Intl. Ed. Engl.*, **1965,** *4*, 457-541.

3. Bruce, M.I. Cyclometalation Reactions. *Angew.Chem*. *Int.Ed. Engl.,* **1977**, *16*, 73-86.

4. Mitscherlich, E. Ueber das Stickstoffbenzid. *Ann. Pharm.*, **1834**, *12*, 311-314.

5. Merino, E.; Ribagorda, M. Control over Molecular Motion Using the *Cis-Trans* Photoisomerization of the Azo Group. *Beilstein J. Org. Chem.*, **2012**, *8*, 1071-1090.

6. Hartley, G. S. The *Cis*-form of Azobenzene. *Nature,* **1937**, 140, 281-282.

7. Griffiths, J. Photochemistry of Azobenzene and Its Derivatives. *Chemical Society Reviews,* **1972**, *1*, 481-493.

8. Dhammika Bandara, H. M.; Burdette, S.C. Photoisomerization in Different Classes of Azobenzene. *Chem. Soc. Rev.,* **2012**, *41*, 1809-1825.

9. Ramakrishnan, V.; Yamamoto, D.; Sasamoto, S.; Shimada, T.; Nabetani, Y.; Tachibana, H.; Inoue, H. Remarkable Enhancement of the Photoreactivity of a Polyfluoroalkyl Azobenzene Derivative in an Organic-Inorganic Nano-layered Microenvironment. *Phys. Chem. Chem. Phys.* **2014**, *16*, 23663-23670.

10. Hamm, P.; Ohline, S.M.; Zinth, W. Vibrational Cooling After Ultrafast Photoisomerization of Azobenzene Measured by Femtosecond Infrared Spectroscopy. *J. Chem. Phys.,* **1997,** *106*, 519-529**.**

11. Lednev, I.K.; Ye, T.Q.; Matousek, P.; Towrie, M.; Foggi, P.; Newahl, F.V.R.; Umapathy, S.; Hester, R.E.; Moore, J.N. Femtosecond Time-Resolved UV-visible Absorption Spectroscopy of *Trans*-azobenzene: Dependence on Excitation Wavelength. *Chem. Phys. Lett.,* **1998**, *290*, 68-74.

12. Forber, C.L.; Kelusky, E. C.; Bunce, N. J.; Zerner, M. C. Electronic spectra of cis- and trans-azobenzenes: consequences of ortho substitution. *J. Am. Chem. Soc.*, **1985**, *107*, 5884-5890.

13. Cusati, T.; Graniccu, G.; Persico, M.; Spighi, G. Oscillator Strength and Polarization of the Forbidden n→pi* Band of *Trans*- azobenzene: A Computational Study. *J. Chem. Phys.* **2008**, *128, 19*, 194312/194311-194312/194319.

14. Rau, H. in Photoreactive Organic Thin Films, Academic Press, San Diego, 2002, S. 3-47.

15. Zhang, Q.M.; Li, X.; Islam, M.R.; Wei, M.; Serpe, M.J. Light Switchable Optical Materials from Azobenzene Crosslinked Poly(*N*-isopropylacrylamide)-based Microgels. *J. Mater. Chem. C.,* **2014**, *2*, 6961-6965.

16. Mahimwalla Z.; Yager K.; Mamiya J.-i.; Shishido A.; Priimagi A.; Barrett C. Azobenzene Photomechanics: Prospects and Potential Applications. *Polymer Bulletin*, **2012**, *69*, 967-1006.

17. Rau, H. Azo compounds. *In Photochromism: Molecules and Systems*; Durr, H., Bouas-Laurent, H., Eds.; Elsevier: *Amsterdam*, 1990, p. 165.

18. Bortolus, P.; Monti, S. Cis-Trans Phtoisomerization of Azobenzene- Solvent and Triplet Donor Effects. *J. Phys. Chem.*, **1979**, *83*, 648-652.

19. Schulze, F. W.; Petrick, H. J.; Cammenga, H. K.; Klinge, H. Hermodynamic Properties of the Structural Analogues Benzo[c]-cinnoline, Trans-Azobenzene and Cis-Azobenzene. *Z. Phys. Chem. Neue. Fol.,* **1977**, *1*, 107.

20. Knoll, H., Handbook of Organic Photochemistry and Photobiology, 2nd Ed. CRC Press, Boca Raton, FL, 2004, page 89/81–89/16.

21. Rau, H.; Lueddecke, E. On the Rotation-Inversion Controversy on Photoisomerization of Azobenzenes. Experimental Proof of Inversion. *J. Am. Chem. Soc.,* **1982**, *104*, 1616–1620.

22. Durr, H.; Bouas-Laurent, H. *Photochromism: Molecules and Systems.* 1st Ed., Elsevier: *Amsterdam*, 2003, p.68.

23. Waldeck, D. H. Photoisomerization Dynamics of Stilbenes. *Chem. Rev.,* **1991**, *91*, 415-436.

24. Meier, H. The Photochemistry of Stilbenoid Compounds and Their Role in Materials Technology. *Angew. Chem. Int. Edn.,* **1992**, *31*, 1399-1420.

25. Tamai, N.; Miyasaka, H. Ultrafast Dynamics of Photochromic Systems. *Chem. Rev.,* **2000**, *100*, 1875–1890.

26. Fangha¨nel, D.; Timpe, G.; Orthman, V. In *Organic Photochromes*; El'tsov, A. V., Ed.; Consultants Bureau: New York, 1990; p 105.
27. Blevins, A. A.; Blanchard, G. J. Effect of Positional Substitution on The Optical Response of Symmetrical Disubstituted Azobenzene Derivatives. *J. Phys. Chem. B*., **2004**, *108*, 4962-4968.

28. Cembran, A.; Bernadi, F.; Garavelli, M.; Gagliari, L.; Orlandi, G. On the Mechanism of the cis−trans Isomerization in the Lowest Electronic States of Azobenzene: S_0, S_1, and T_1. *J. Am. Chem. Soc.*, **2004**, *126*, 3234-3243.

29. Cattaneo, P.; Persico, M. An ab initio study of the photochemistry of azobenzene. *Phys. Chem. Chem. Phys.*, **1999**, *1*, 4739-4743.

30. Tamaoki, N.; Ogata, K.; Koseki, K.; Yamaoka, T. (4,4′) Azobenzene. Synthesis, structure, and Cis-Trans Isomerization. *Tetrahedron,* **1990**, *46*, 5931-5942.

31. Garcia-Amoros, J.; Velasco, D. Recent Advances towards Azobenzene-based light-Driven Real-Time Information-Transmitting materials. *Beilstein J. Org. Chem*., **2012**, *8*, 1003-1007.

32. Gegiou, D.; Muszkat, K. A.; Fischer, E. Temperature Dependence of Photoisomerization. V. Effect of Substituents on the Photoisomerization of Stilbenes and Azobenzenes. *J. Am. Chem. Soc.,* **1968**, *90*, 3907–3918.

33. Tamai, N.; Miyasaka, H. Ultrafast Dynamics of Photochromic Systems. *Chem. Rev.*, **2000**, *100*, 1875-1890.

34. Brode, W. R.; Gould, J. H.; Wyman, G. M. The Relation between the Absorption Spectra and the Chemical Constitution of Dyes. XXV. Phototropism and Cis-trans Isomerism in Aromatic Azo Compounds *J. Am. Chem. Soc.,* **1952**, *74*, 4641–4646.

35. Tang, Z.; Johal, M. S.; Scudder, P.; Caculitan, N.; Magyar, R. J.; Tretiak, S.; Wang, H.-L. Control Formation of Functional Nanoscaled using Langmuir-Blodgett Method: Interplay between p-p and Dipole-dipole Interactions. *Thin Solid Films,* **2007**, *516*, 58–66.

36. Lednev, I. K.; Ye, T.-Q.; Abbott, L. C.; Hester, R. E.; Moore, J. N. Photoisomerization of a Caped Azobenzene in Solution Probed by Ultrafast Time-Resolved Electronic Absorption Spectroscopy. *J. Phys. Chem. A,* **1998**, *102*, 9161–9166.

37. Zacharias, P. S.; Ameerunisha, S.; Korupoju, S. R. Photoinduced Fluorescence changes on E-Z Isomerization in Azobenzene Derivatives. *J. Chem. Soc., Perkin Trans. 2,* **1998**, 2055–2060.

38. Ohtani, O.; Furukawa, T.; Sasai, R.; Hayashi, E.; Shichi, T.; Yui, T.; Takagi, K. Effect of Fluorinated Ammonium Counterions upon the Reversibility in E-Z Photoisomerization of Azobenzene Ion Pair Films *J. Mater. Chem.,* **2004**, *14*, 196–200.

39. Wazzan, N. *Cis-Trans* Isomerisation of Azobenzenes Studied by NMR Spectroscopy with *In situ* Laser Irradiation and DFT Calculations. Ph.D. Thesis, The University of Edinburgh, Edinburgh, Scotland, 2009.

40. Cilento, G.; Miller, E. C.; Miller, J. A. On The Addition of Protons to Derivatives of 4-Aminoazobenzene *J. Am. Chem. Soc*., **1956**, *78*, 1718-1722.

41. YA, Q.; Dong, X.-Z.; Chen, W.-Q.; Duan, X.-M. The Synthesis of Aminoazobenzenes and The Effect of Intermolecular Hydrogen Bonding on Their Photoisomerization *Dyes Pigm*., **2008**, *79*, 159-165.

42. Zakerhamidi, M.S.; Ghanadzadeh, A.; Moghadam, M. Solvent Effects on the UV/Visble Absorption Spectra of Some Aminoazobenzene. *Chem. Sci. Trans*., **2012**, *1*, 1-8.

43. Reichardt, C. Solvent and Solvent Effects in Organic Chemistry, 3rd ed.; Wiley-VCH: Weinheim/Germany, 2002, p. 184.

44. Yager, K. G.; Barrett, C. J. Novel Photo-Switching Using Azobenzene Functional Materials. *Journal of Photochemistry and Photobiology A: Chemistry,* **2006,** *182*, 250-261.

45. Irie, M. Photochromism: Memories and Switches – Introduction. *Chem. Rev.,* **2000**, 100(5), 1683–1684.

46. Norikane, Y.; Tamaoki, N. Light-Driven Molecular Hinge: A New Molecular Machine Showing a Light-Intensity-Dependent Photoresponse that Utilizes the *Trans−Cis* Isomerization of Azobenzene *Org. Lett.* **2004**, *6*, 2595-2598.

47. Muraoka, T.; Kinbara, K.; Aida, T. Mechanical Twisting of a Guest by a Photoresponsive Host *Nature* **2006**, *440*, 512-515.

48. Feringa, B. L., *Molecular switches.* 2nd Ed.; Wiley-VCH: Weinheim, 2001; page 281.

49. Balzani V.; Credi, A.; Venturi, M. *Molecular Devices and Machines*; Wiley-VCH: Weinheim, 2008; page 308.

50. Hugel, T.; Holland, N. B.; Cattani, A.; Moroder, L.; Seitz, M.; Gaub, H. E. Single-Molecule Optomechanical Cycle *Science* **2002***, 296*, 1103-1106.

51. Jiang, C.-W.; Xie, R.-H.; Li, F.-L.; Allen, R. E. Comparative Studies of the *Trans−Cis* Photoisomerizations of Azobenzene and a Bridged Azobenzene *J. Phys. Chem. A* **2011**, *115* (3), 244–249.

52. Feringa, B. L., *Molecular switches.* 2nd Ed.; Wiley-VCH: Weinheim, 2001; page 67.

53. Zhang, L.; Wang, D.; Hu, P.; Zha, J-W.; You, F.; Li, S-T.; Dang, Z-M Highly improved Electro-Actuation of Dielectric Elastomers by Molecular Grafting of Azobenzenes to Silicon Rubber. *J. Mater. Chem. C.* **2015**, *3*, 4883-4889.

54. Takuzo, M.; Kazushi, K.; Yuka, K.; Takahiro, M. Light-Driven Open-Close Motion of Chiral Molecular Scissors *J. Am. Chem. Soc*. **2003**, *125*, 5612-5613.

55. Muraoka, T.; Kinbara, K.; Aida, T. Reversible Operation of Chiral Molecular Scissors by Redox and UV light *Chem. Commun.* **2007**, 1441-1443.

56. Zhang, Z.; Burns, D.C.; Kumita, J.R.; Smart, O.S.; Woolley, G.A. A Water-Soluble Azobenzene Cross-linker for Photocontrol of Peptide Conformation *Bioconjug Chem.* **2003**, *4*, 824-829.

57. **(a)**Woolley, G. A.; Jaikaran, A. S. I.; Berezovski, M.; Calarco, J. P.; Krylov, S. N.; Smart, O. S.; Kumita, J. R. Reversible Photocontrol of DNA Binding by a Designed GCN4-bZIP Protein. *Biochemistry,* **2006**, *45*, 6075–6084. **(b)** Renner, C.; Kusebauch, U.; Löweneck, M.; Milbradt, A. G.; Moroder, L. J. Azobenzene as Photoresponsive Conformational Switch in Cyclic Peptides. *Pept. Res*., **2005**, *65*, 4–14. **(c)** Pieroni, O.; Fissi, A.; Angelini, N.; Lenci, F. Photoresponsive Polypeptides. *Acc. Chem. Res.,* **2001**, *34*, 9–17. **(d)** Renner, C.; Moroder, L. Azobenzene as Conformational Switch in Model Peptides. *ChemBioChem,* **2006**, *7*, 868–878. **(e)** Aaemissegger, A.; Kräutler, V.; van Gunsteren, W. F.; Hilvert, D. A Photoinduced β-Hairpin. *J. Am. Chem. Soc*., **2005**, *127*, 2929–2936**. (f)** Beharry, A. A.; Woolley, G. A. Azobenzene Photoswitches for Biomolecules. *Chem. Soc. Rev.* **2011**, *40*, 4422–4437. **(g)** Sadovski, O.; Beharry, A. A.; Zhang, F.; Woolley, G. A. Spectral Tuning of Azobenzene Photoswitches for Biological Applications. *Angew. Chem., Int. Ed.,* **2009**, *48*, 1484–1486. **(h)** Beharry, A. A.; Sadovski, O.; Woolley, G. A. Azobenzene Photoswitching Without Ultraviolet Light *J. Am. Chem. Soc*., **2011**, *133*, 19684–19687.

58. Lien, L.; D. Jaikaran, C. J.; Zhang, Z.; Woolley, G. A. Photomodulated Blocking of Gramicidin Ion Channels, *J. Am. Chem. Soc.* **1996**, *118*, 12222–12223.

59. Mourot, A.; Kienzler, M. A.; Banghart, M. R.; Fehrentz, T.; Huber, F. M. E.; Stein, M.; Kramer, Trauner, R. H. D.Tuning Photochromic Ion Channel Blockers *ACS Chem. Neurosci*., **2011**, *2*, 536–543.

60. Hilf, R. J. C.; Bertozzi, C.; Zimmermann, I.; Reiter, A.; Trauner, D.; Dutzler, R. Structural Basis of Open Channel Block in a Prokaryotic Pentameric Ligand-gated Ion Channel. *Nat. Struct. Mol. Biol*., **2010**, *17*, 1330–1336.

61. Bredenbeck, J. ; Helbing, J. ; Kumita, J. R. ; Woolley, G. A. ; Hamm, P. α-Helix Formation in a Photoswitchable Peptide Tracked from Picoseconds to Microseconds by

Time-resolved IR Spectroscopy. *Proc. Natl. Acad. Sci. U. S. A*., **2005**, *102*, 2379–2384.

62. Guerrero, L.; Smart, O. S.; Woolley, G. A.; Allemann, R. K. Photocontrol of DNA Binding Specificity of a Miniature Engrailed Homeodomain. *J. Am. Chem. Soc.,* **2005**, *127*, 15624–15629.

63. Banghart, M.; Borges, K.; Isacoff, E.; Trauner, D.; Kramer, R. H. Light-Activated Ion Channels for Remote Control of Neuronal Firing. *Nat. Neurosci*., **2004**, *7*, 1381–1386.

64. Blevins, A. A.; Blanchard, G. J. Effect of Positional Substitution on The Optical Response of Symmetrical Disubstituted Azobenzene Derivatives" *J. Phys. Chem. B*. ,**2004**, *108*, 4962-4968.

65. Crecca, R. C.; Roitberg, A.E. Theoretical Study of the Isomerization Mechanism of Azobenzene and Disubstituted Azobenzene Derivatives. *J. Phys. Chem. A.,* **2006**, *110*, 8188-8203.

66. SHELXTL/PC Version 6.14 Structure Analysis Package, Bruker AXS, 2000- 2003.

67. Perrin, D. D. and Armarego, W. L. F., *Purification of Laboratory Chemicals*, Pergamon Press: Oxford, 1988.

68. Picket, C. J. A simple Hydrocarbon Electrolyte: Completing the Electron-transfer Series $[Fe_4S_4(SPh)_4]^{1-/2-/3-/4-}$" *J. Chem. Soc.* **1985**, 323-326.

69. Ohta, K.; Chiba, Y.; Kaise, A.; Endo, Y. Structure-activity relationship study of diphenylamine-based estrogen receptor antagonists. *Bioorg. Med. Chem.* **2015***, 23*, 861-867.

70. Chudomel, J. M.; Yang, B.; Barnes, Michael D.; Achermann, M.; Mague, J. T.; Lahti, P. M. Highly Twisted Triarylamines for Photoinduced Intramolecular Charge Transfer. *Journal of Physical Chemistry A,* **2011**, *115(30),* 8361-8368.

71. Priewisch, B.; Ruck-Braun, K.; Efficient Preparation of Nitrosoarenes for the Synthesis of Azobenzenes. *J. Org. Chem.*, **2011**, *70*, 2350-2352.

72. Defoin, A., Simple Preparation of Nitroso Benzenes and Nitro Benzenes by Oxidation of Anilines with H2O2 Catalysed with Molybdenum Salts. *Synthesis,* **2004**, *5*, 706-710.

73. M., Kaiser; S.P., Leitner; C., Hirtenlehner; M., List; A., Gerisch; U., Monkowius; Azobenzene-functionalized N-heterocyclic carbenes as photochromic ligands in silver(I) and gold(I) complexes. *Dalton Trans.,* **2013**, *42*, 14749-14756.

74. Fraleoni-Morgera, A; Giorgini, L.; Zanirato, P. [Arylazobenzene–BF_3] dyes: Electronic absorption and NMR spectroscopic evidence for a novel class of dyes stable in aprotic solvents. *Dyes and Pigmnets.* **2008**, *76*, 394-399.

75. Tibiletti, F.; Simonetti, K.; Palmisano, G.; Parravicini, M.; Imbesi, F.; Tollari, S.; and Penoni, A. One-pot Synthesis of Meridianins and Meridianin Analogues via Indolization of Nitrosoarenes. *Tetrahedron*, **2010**, *66*, 1280-1288.

76. [1] Li, H-Q.; Liu, X.; Zhang, Q.; Li, S-S.; Liu, Y-M.; He, H-Y.;Cao, Y., Deoxygenative coupling of nitroarenes for the synthesis of aromatic azo compounds with CO using supported gold catalysts. *Chem. Commun.,* **2015**, *51*, 11217-11220.

77. Jaffe, H. H.; Gardner, R. W.; Tautomeric equilibria. IV. The basicities of monosubstituted azobenzenes. An acidity scale in 20% ethanolic aqueous sulfuric acid. *Journal of the American Society*, **1958**, *80*, 319-323.

78. Yeong-Soon, G.; Sung-Ho, J.; Jong-Wook, P.; Sung-Hoon, K.; Won, S. L.; Kwon, T. L. electro-Optical and Electrochemical Properties of an Ionic Polyacetylene Derivtive with Azobenzene Anisole Moieties. *Journal of Industrial and Engineering Chemistry,* **2012**, 55-60.

79. Garcia-Amoros, J.; Reig, M.; Cuadrado, A.; Ortega, M.; Nonell, S.; Velasco, D. A Photoswitchable Bis-Azo Derivative with High Temporal Resolution. *Chem. Comm.,* **2014**, 11462-11464.

80. He, C.; Zhang, C.; Zhang, O. Synthesis and thermal behaviours of side-chain liquid-crystalline poly[N-(4-methoxyazobenzene-4′-oxyalkyl)ethyleneimine]. *Liquid Crystals,* **2009**, *4*, 379-387.

81. Zhang, C-Z.; Wang, C-Y.; Im, C.; Lu, G-Y.; Wang, C-S. Significant Effect of Bromo Substituents on Nonlinear Optical Properties of Polymer and Chromophores. *J. Phys. Chem. B.*, **2010**, *114*, 42-48.

APPENDIX A

NMR SPECTRA

List of NMR Spectra

Page

Figure A1.1. ^{1}H NMR spectrum (360 MHz) of **3** in $CDCl_3$ 161

Figure A1.2. ^{13}C NMR spectrum (125 MHz) of **3** in $CDCl_3$ 162

Figure A1.3. ^{1}H NMR spectrum (500 MHz) of **4a** in $CDCl_3$ 163

Figure A1.4. ^{13}C NMR spectrum (125 MHz) of **4a** in $CDCl_3$ 164

Figure A1.5. ^{1}H NMR spectrum (500 MHz) of **5a** in $CDCl_3$ 165

Figure A1.6. ^{13}C NMR spectrum (125 MHz) of **5a** in $CDCl_3$ 166

Figure A1.7. ^{1}H NMR spectrum (360 MHz) of **8** in $CDCl_3$ 167

Figure A1.8. ^{13}C NMR spectrum (125 MHz) of **8** in $CDCl_3$ 168

Figure A1.9. ^{1}H NMR spectrum (360 MHz) of **10** in $CDCl_3$ 169

Figure A1.10. ^{13}C NMR spectrum (125 MHz) of **10** in $CDCl_3$ 170

Figure A1.11. ^{1}H NMR spectrum (360 MHz) of **13** in $CDCl_3$ 171

Figure A1.12. ^{13}C NMR spectrum (125 MHz) of **13** in $CDCl_3$ 172

Figure A1.13. ^{1}H NMR spectrum (360 MHz) of **15** in $CDCl_3$ 173

Figure A1.14. ^{1}H NMR spectrum (360 MHz) of **16** in $CDCl_3$ 174

Figure A1.15. ^{13}C NMR spectrum (125 MHz) of **16** in $CDCl_3$ 175

Figure A1.16. ^{1}H NMR spectrum (360 MHz) of **17** in $CDCl_3$ 176

Figure A1.17. ^{13}C NMR spectrum (125 MHz) of **17** in $CDCl_3$ 177

Figure A1.18. ^{1}H NMR spectrum (360 MHz) of **18a** in $CDCl_3$ 178

Figure A1.19. ^{13}C NMR spectrum (125 MHz) of **18a** in $CDCl_3$ 179

Figure A1.20. ^{1}H NMR spectrum (360 MHz) of **19a** in $CDCl_3$ 180

Figure A1.21. ^{13}C NMR spectrum (125 MHz) of **19a** in $CDCl_3$ 181

Figure A1.22. ^{1}H NMR spectrum (360 MHz) of **20** in $CDCl_3$ 182

Figure A1.23. ^{13}C NMR spectrum (125 MHz) of **20** in $CDCl_3$ 183

Figure A1.24. ^{1}H NMR spectrum (360 MHz) of **21** in $CDCl_3$ 184

Figure A1.25. ^{13}C NMR spectrum (125 MHz) of **21** in $CDCl_3$ 185

Figure A1.26. ^{1}H NMR spectrum (360 MHz) of **22** in $CDCl_3$ 186

Figure A1.27. ^{13}C NMR spectrum (125 MHz) of **22** in $CDCl_3$ 187

Figure A1.28. ^{1}H NMR spectrum (360 MHz) of **23a** in $CDCl_3$ 188

Figure A1.29. ^{13}C NMR spectrum (125 MHz) of **23a** in $CDCl_3$ 189

Figure A1.30. ^{1}H NMR spectrum (360 MHz) of **25** in $CDCl_3$ 190

Figure A1.31. ^{13}C NMR spectrum (125 MHz) of **25** in $CDCl_3$ 191

Figure A1.32. ^{1}H NMR spectrum (500 MHz) of **26** in $CDCl_3$ 192

Figure A1.33. ^{13}C NMR spectrum (125 MHz) of **26** in CDCl3.....193

Figure A1.34. ^{1}H NMR spectrum (360 MHz) of **27a** in $CDCl_3$ 194

Figure A1.35. ^{13}C NMR spectrum (125 MHz) of **27a** in $CDCl_3$ 195

Figure A1.36. ^{1}H NMR spectrum (360 MHz) of **28a** in $CDCl_3$ 196

Figure A1.37. ^{13}C NMR spectrum (125 MHz) of **28a** in $CDCl_3$ 197

Figure A1.38. ^{1}H NMR spectrum (360 MHz) of **29** in $CDCl_3$ 198

Figure A1.39. ^{13}C NMR spectrum (125 MHz) of **29** in $CDCl_3$ 199

Figure A1.40. ^{1}H NMR spectrum (360 MHz) of **30** in $CDCl_3$ 200

Figure A1.41. ^{13}C NMR spectrum (125 MHz) of **30** in $CDCl_3$ 201

Figure A1.42. ^{1}H NMR spectrum (360 MHz) of **31** in $CDCl_3$ 202

Figure A1.43. ^{13}C NMR spectrum (125 MHz) of **31** in $CDCl_3$ 203

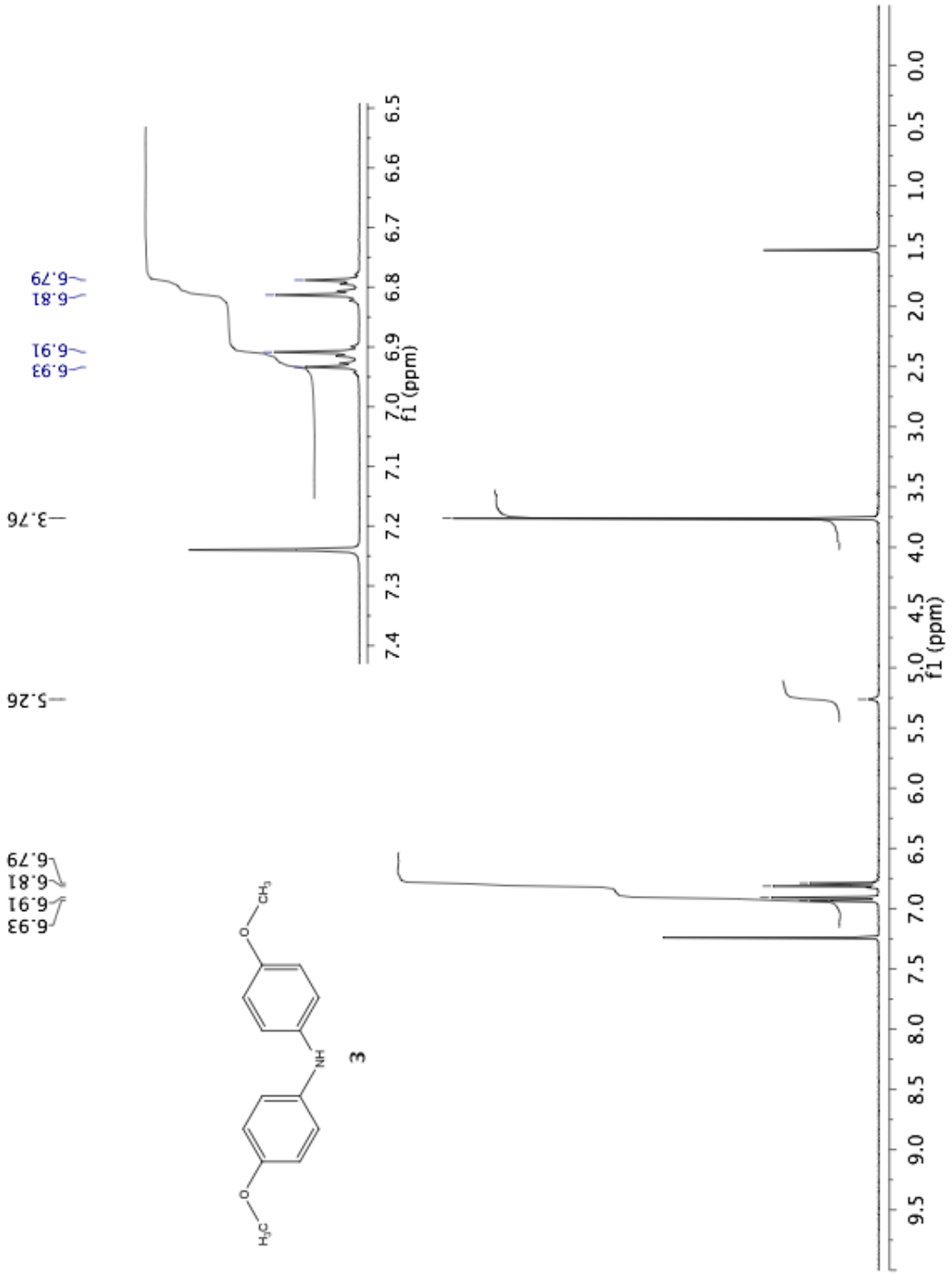

Figure A1.1. ^{1}H NMR spectrum (360 MHz) of **3** in $CDCl_3$.

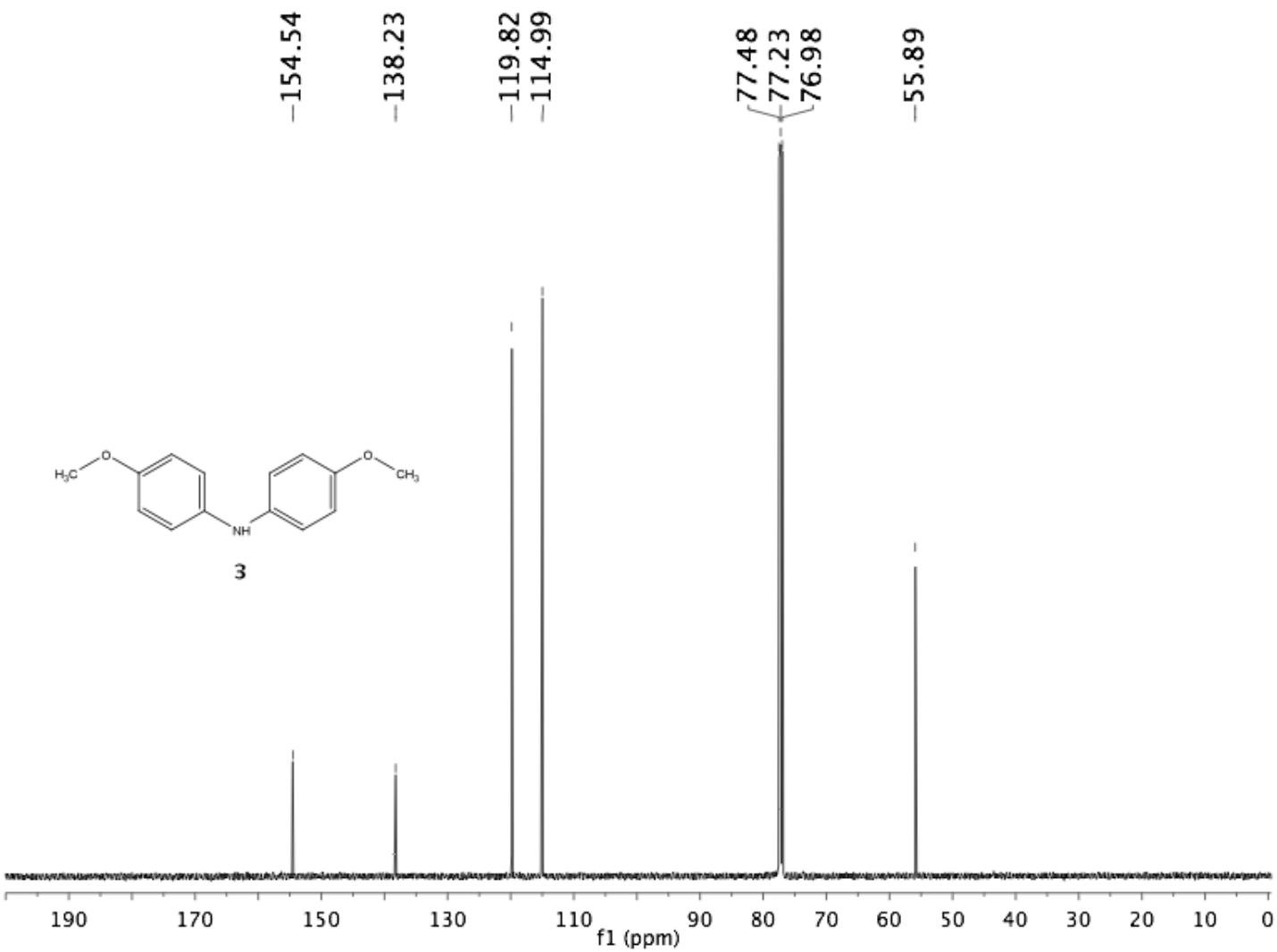

Figure A1.2. ^{13}C NMR spectrum (125 MHz) of **3** in $CDCl_3$

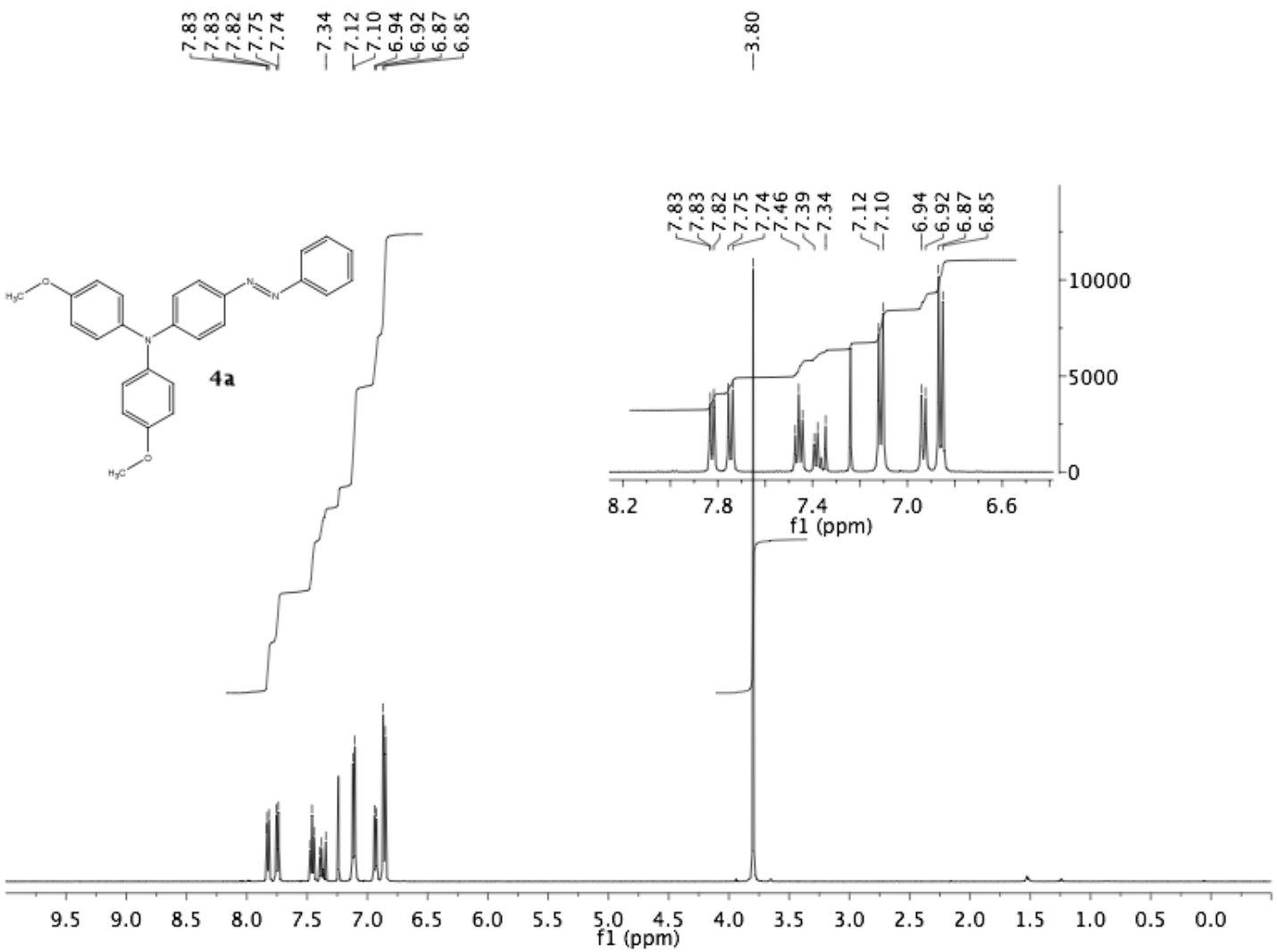

Figure A1.3. ^{1}H NMR spectrum (500 MHz) of **4a** in $CDCl_3$.

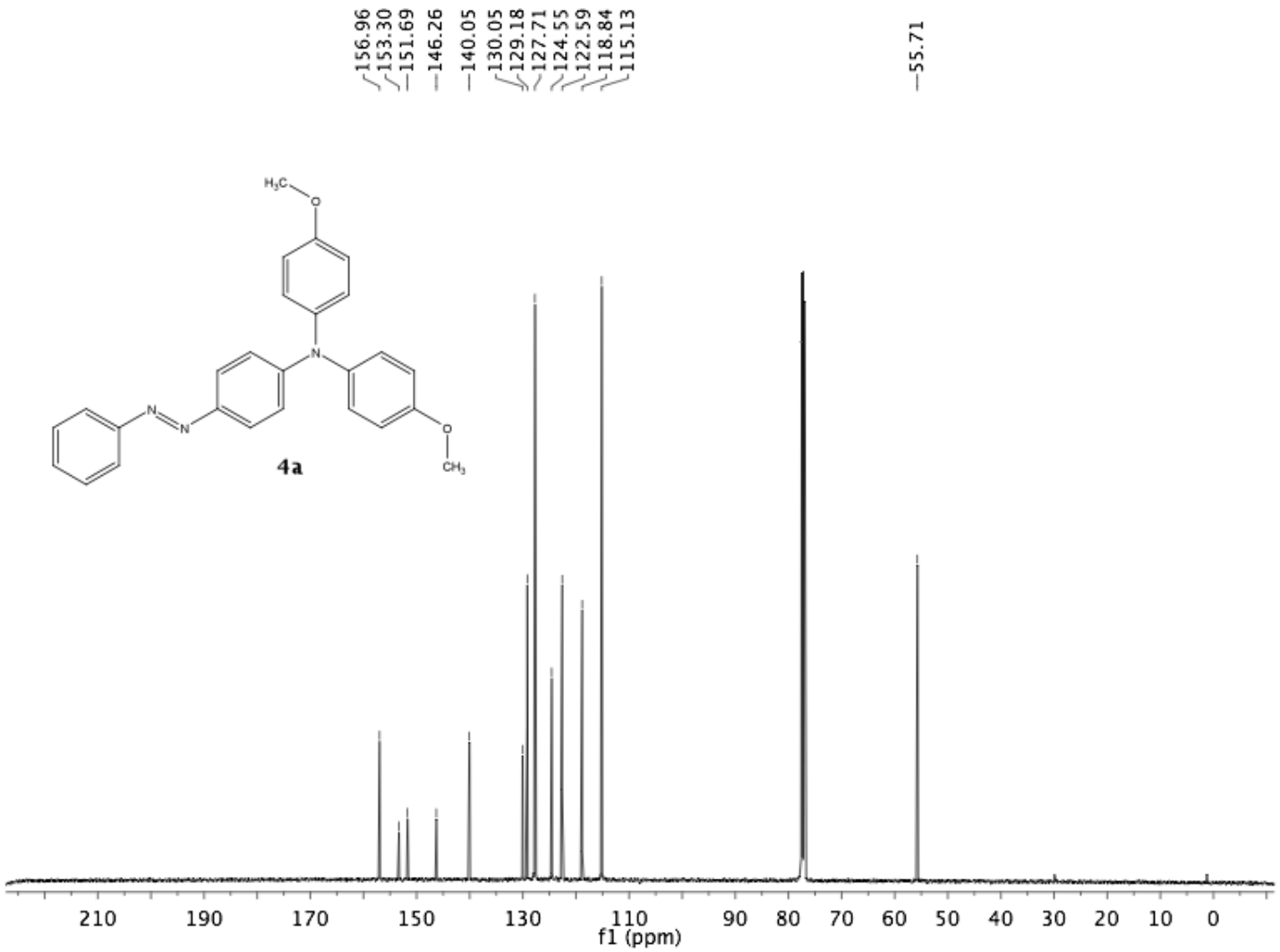

Figure A1.4. ^{13}C-NMR spectrum (125MHz) of **4a** in $CDCl_3$.

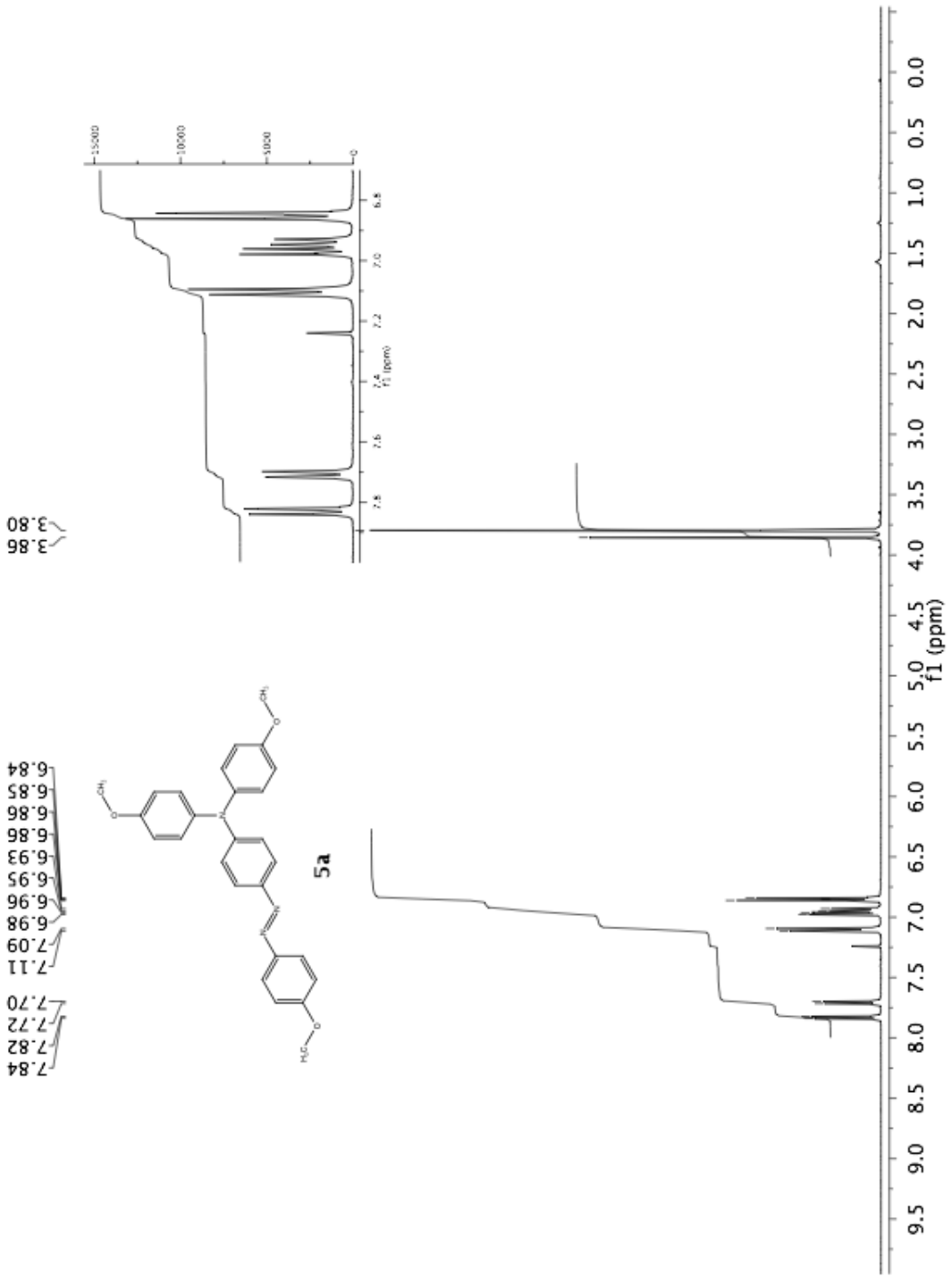

Figure A1.5. ^{1}H NMR spectrum (500 MHz) of **5a** in $CDCl_3$

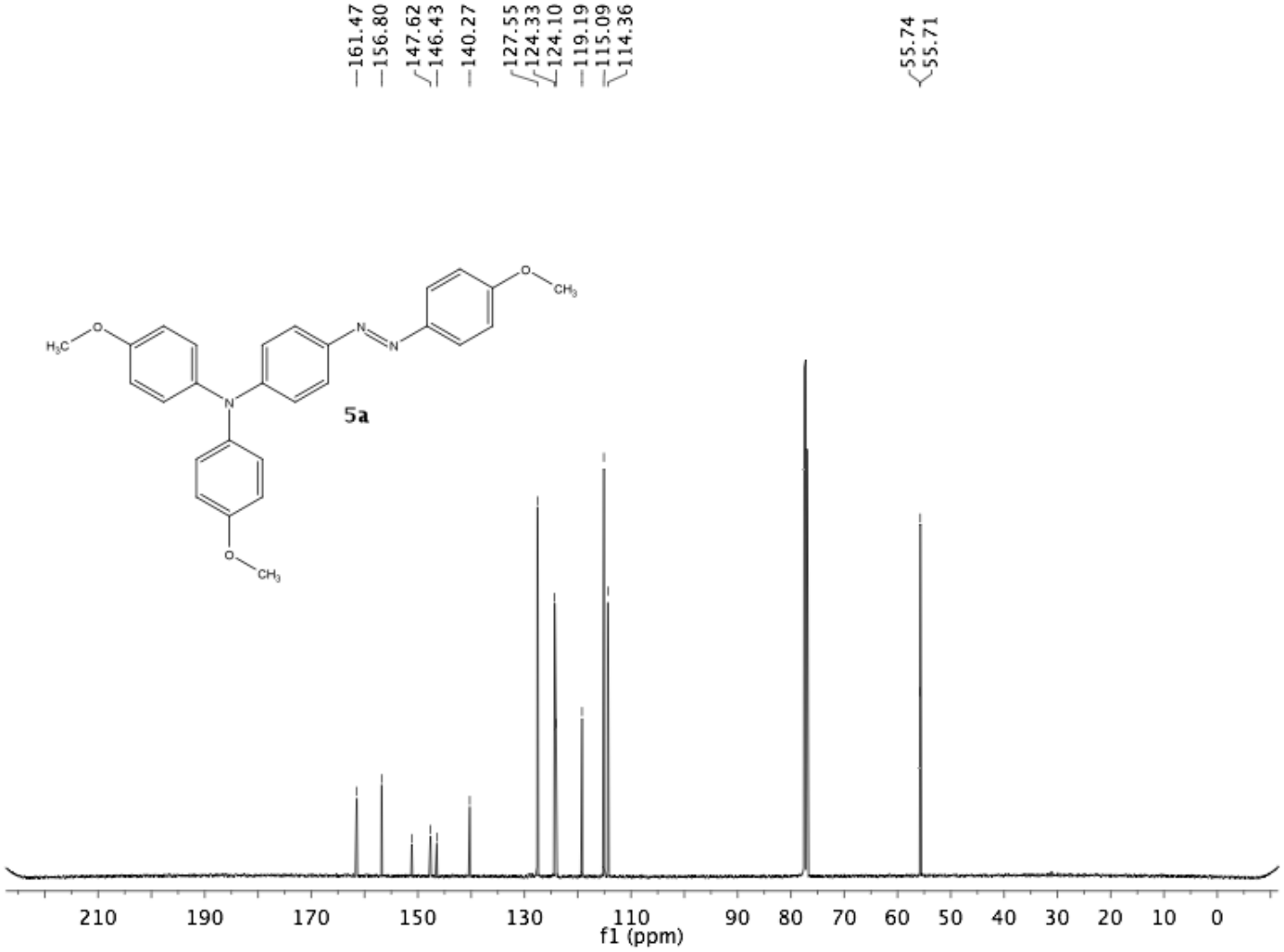

Figure A1.6. ^{13}C NMR spectrum (125 MHz) of **5a** in $CDCl_3$

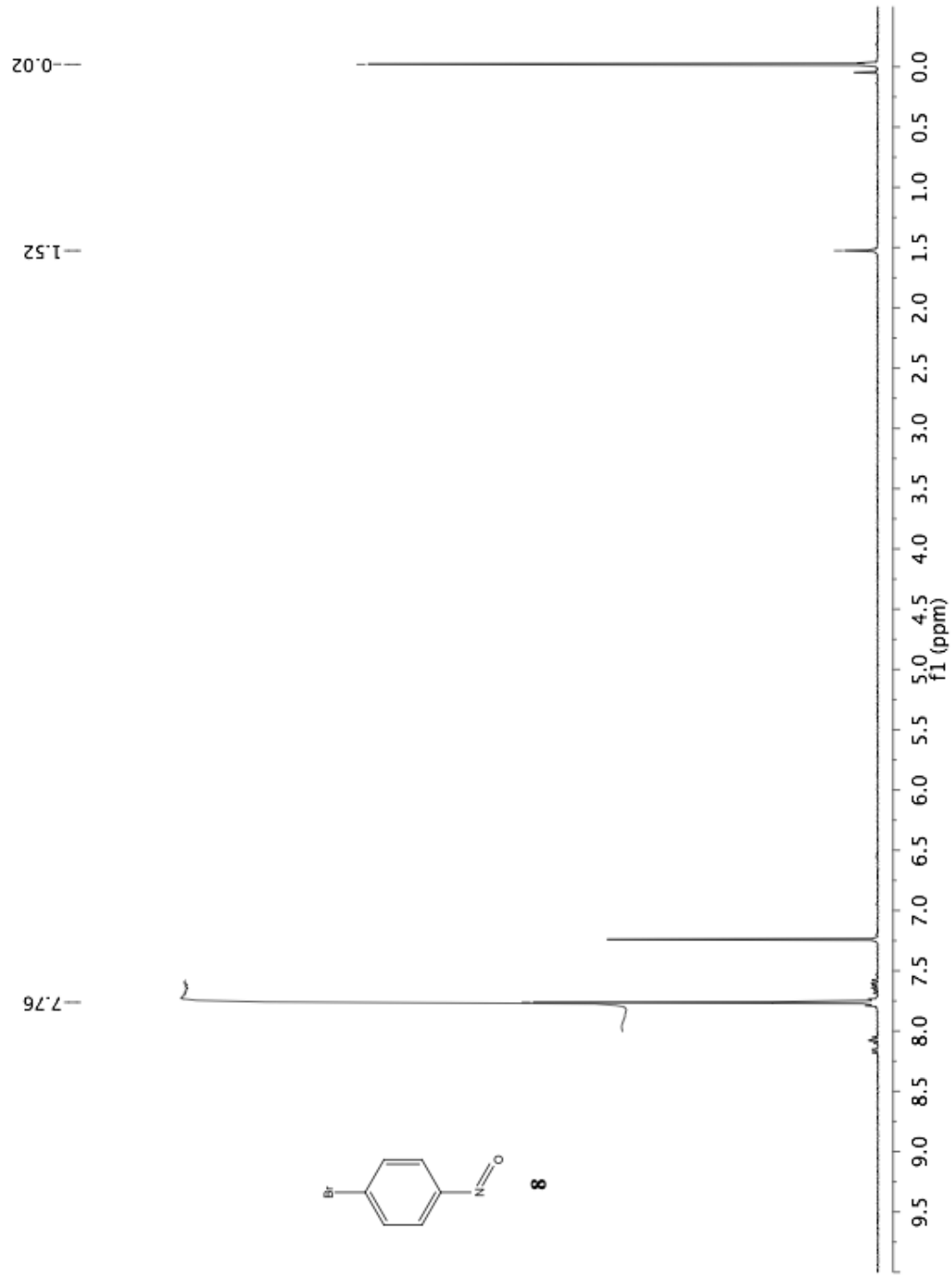

Figure A1.7. ^{1}H NMR spectrum (360 MHz) of **8** in $CDCl_3$

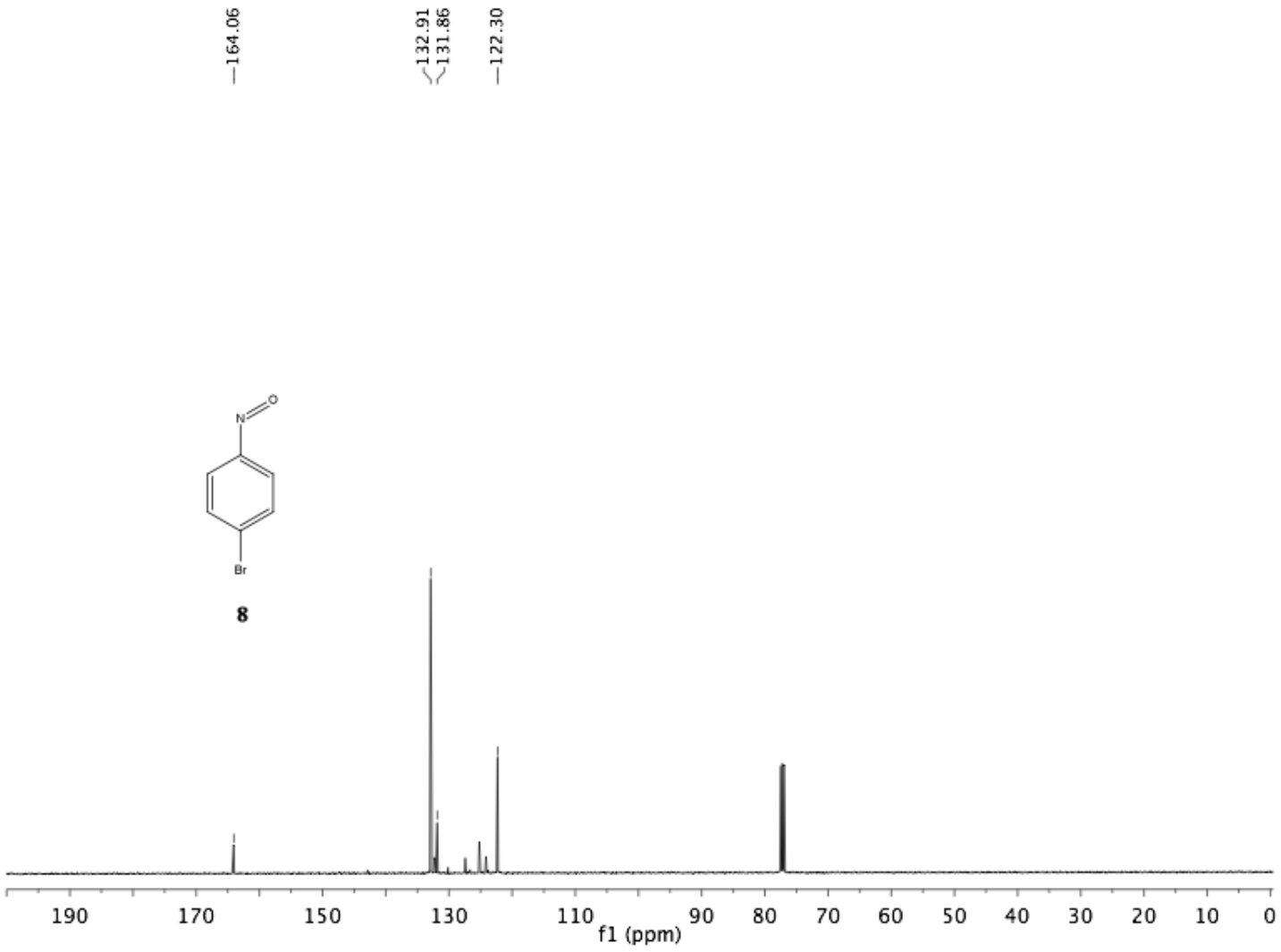

Figure A1.8. ^{13}C NMR spectrum (125MHz) of **8** in $CDCl_3$

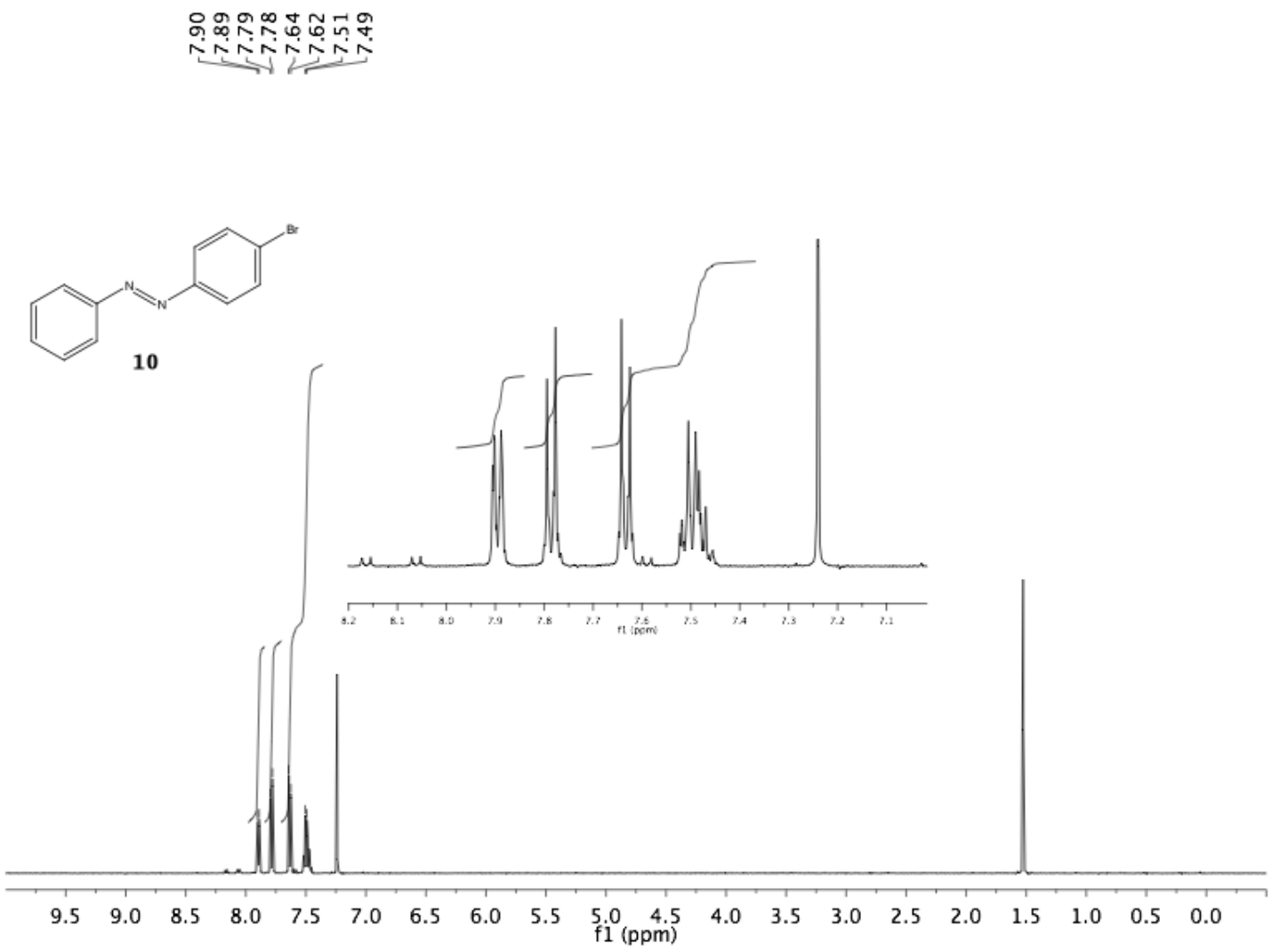

Figure A1.9. ^{1}H NMR spectrum (360 MHz) of **10** in $CDCl_3$

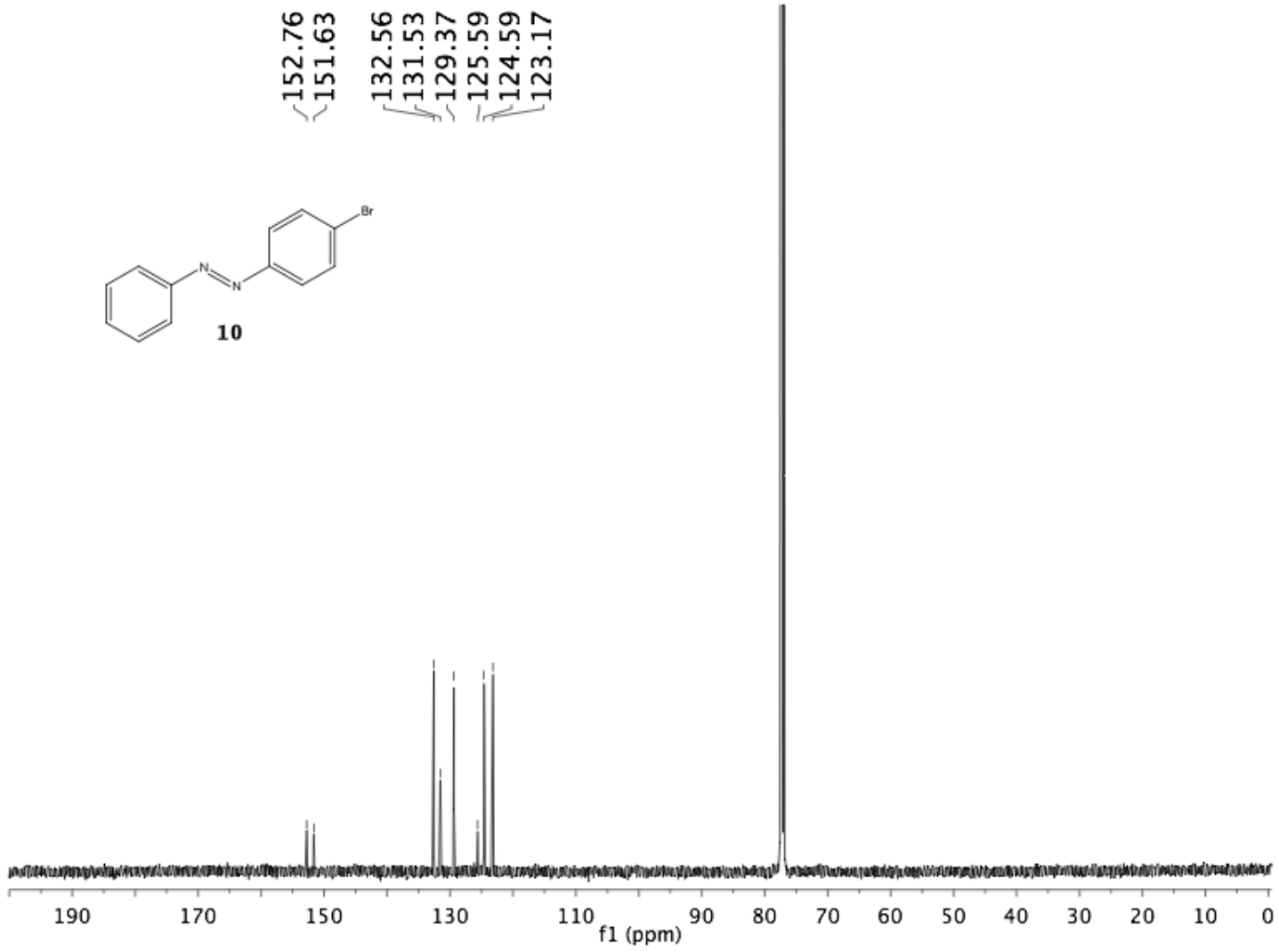

Figure A1.10. ^{13}C NMR spectrum (125MHz) of **10** in $CDCl_3$

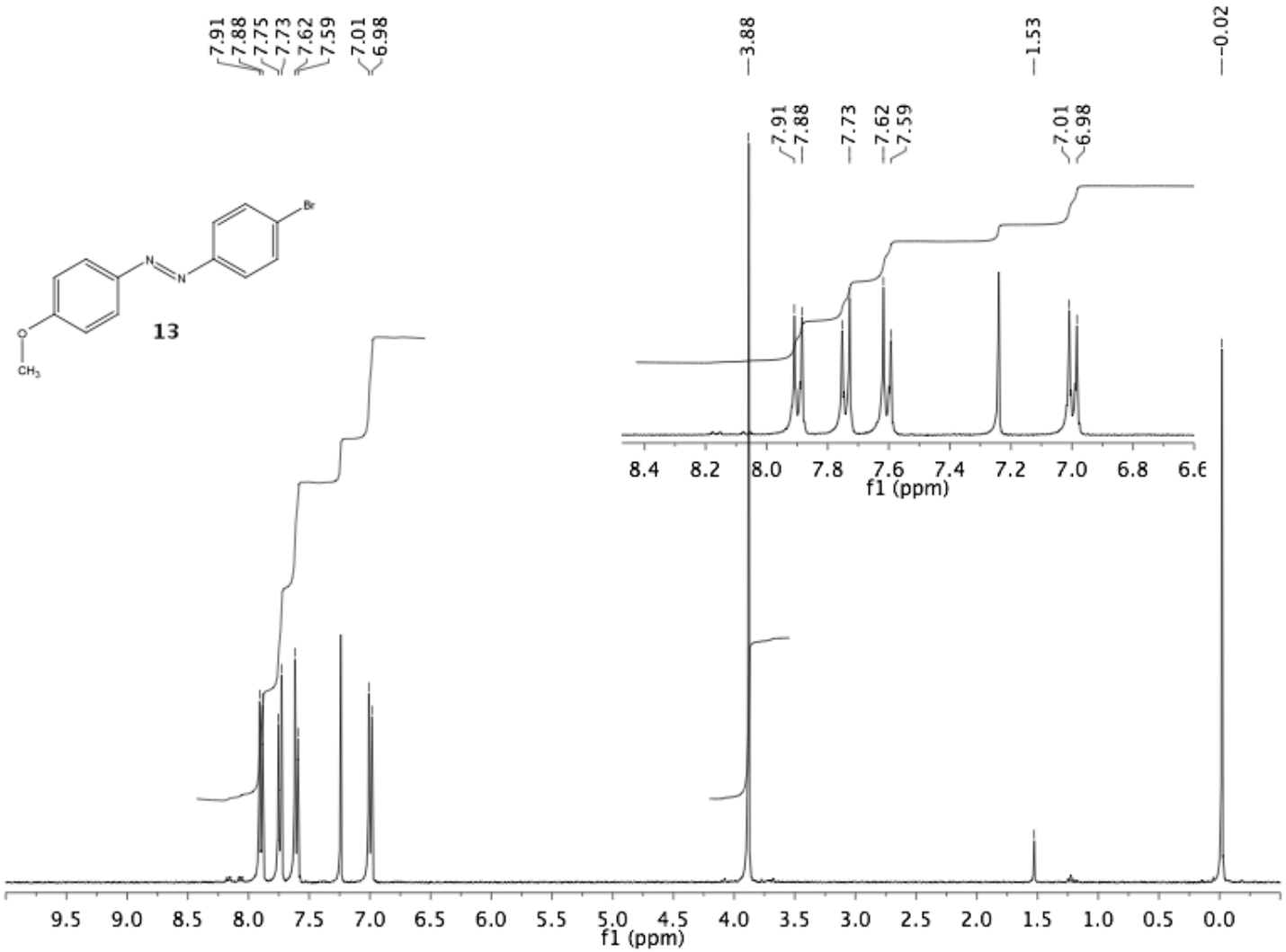

Figure A1.11. ^{1}H NMR spectrum (360 MHz) of **13** in $CDCl_3$

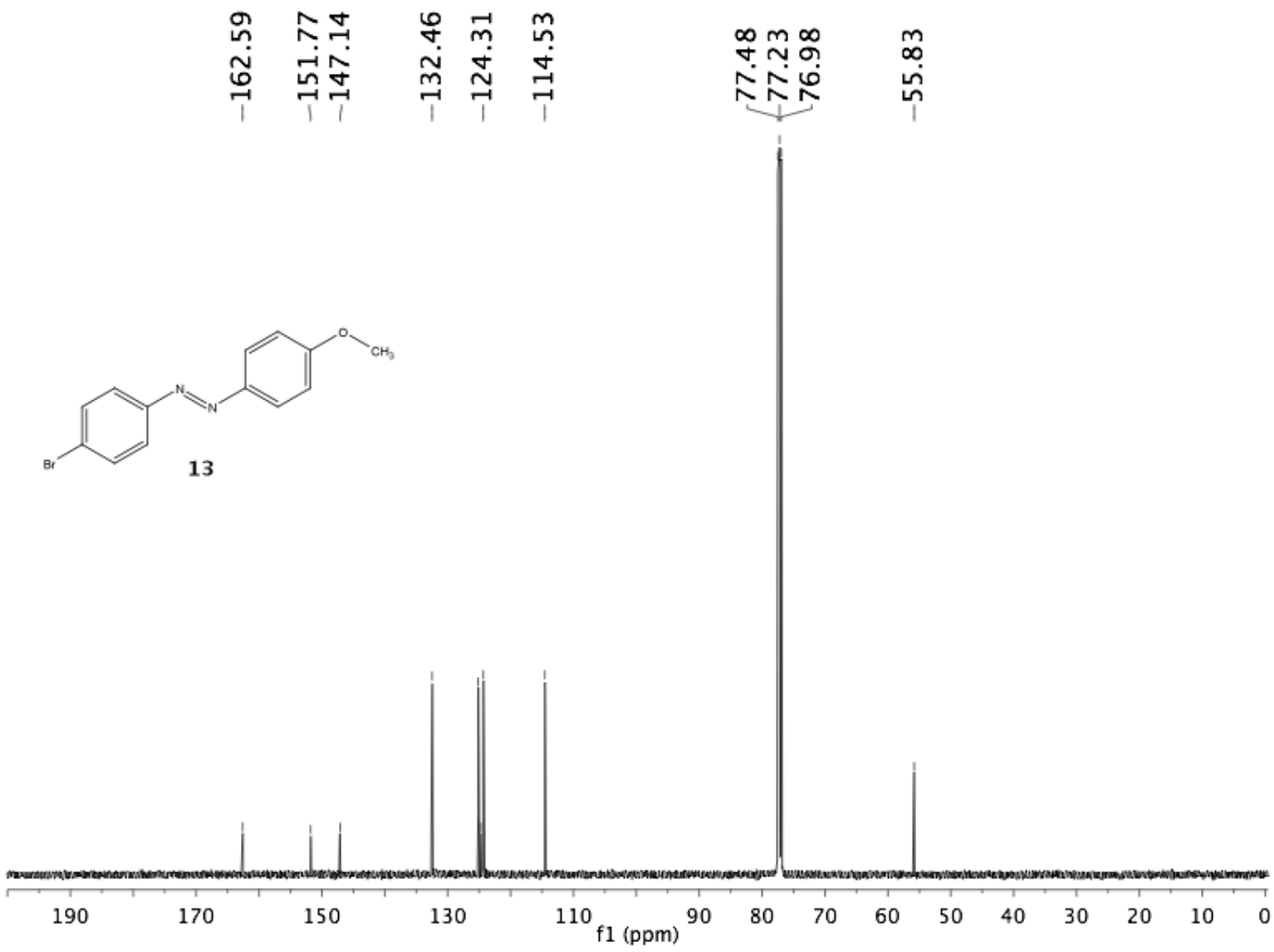

Figure A1.12. ^{13}C NMR spectrum (125MHz) of **13** in $CDCl_3$

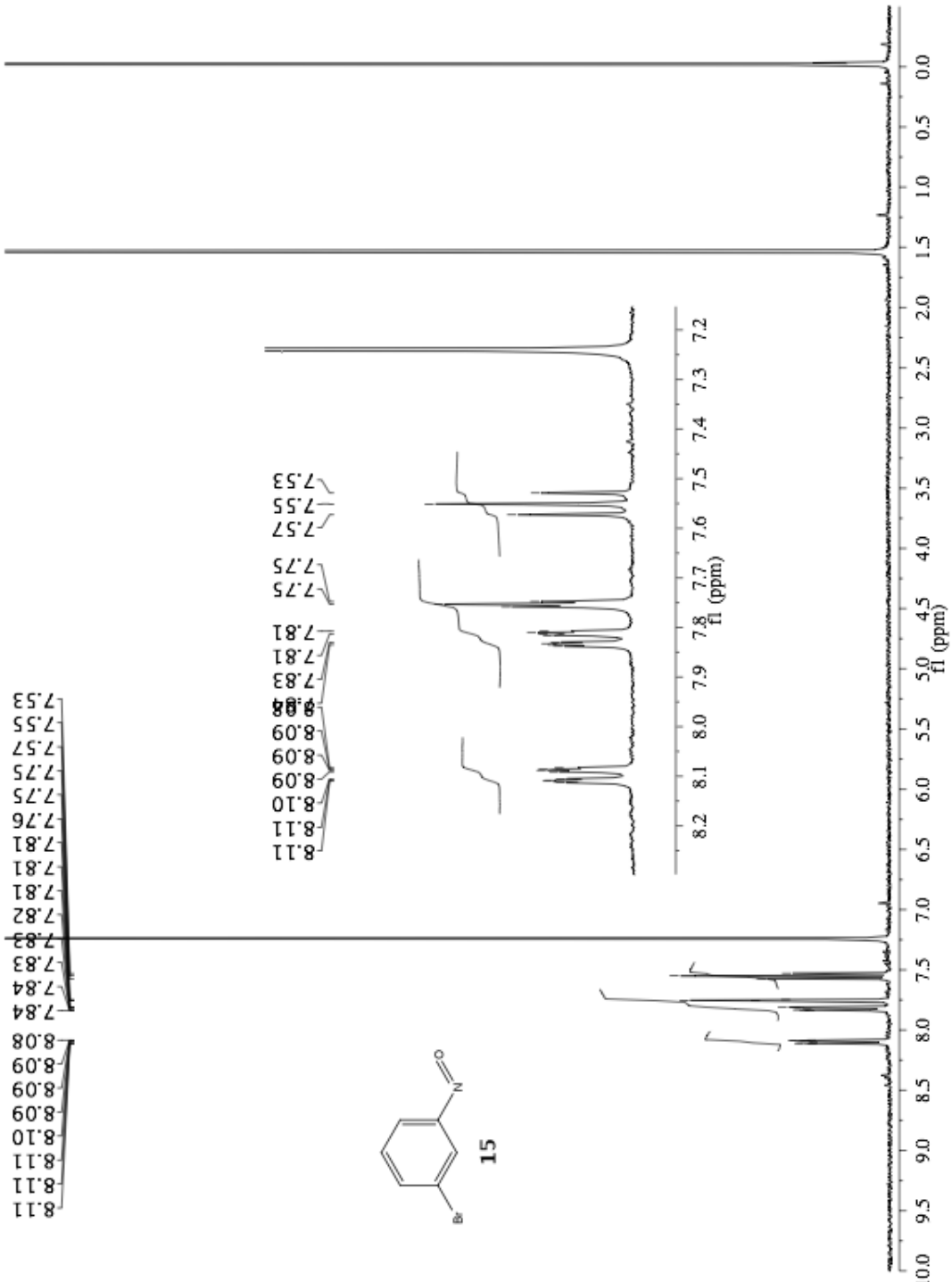

Figure A1.13. ^{1}H NMR spectrum (125 MHz) of **15** in $CDCl_3$

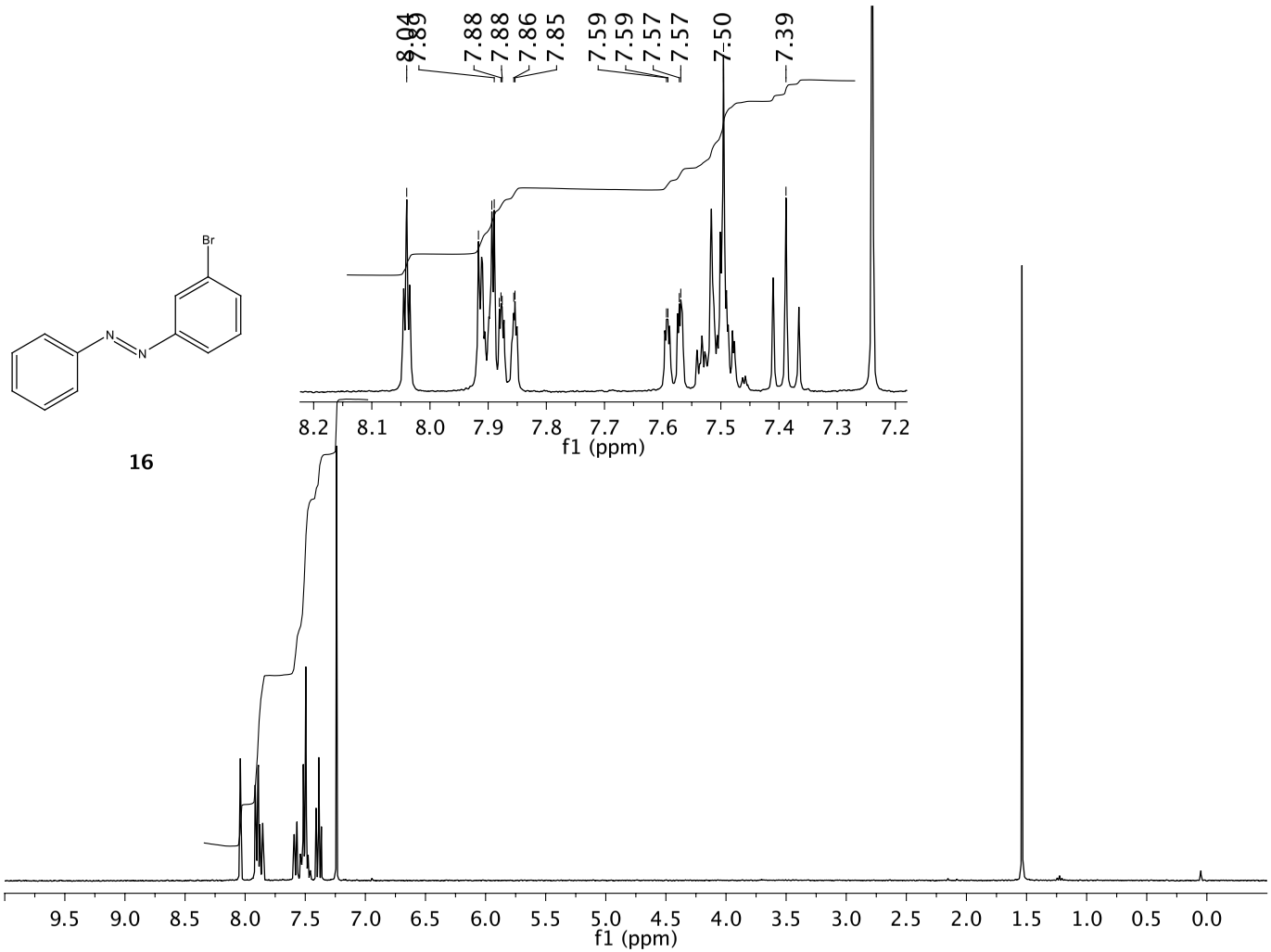

Figure A1.14. ^{1}H NMR spectrum (360 MHz) of **16** in $CDCl_3$

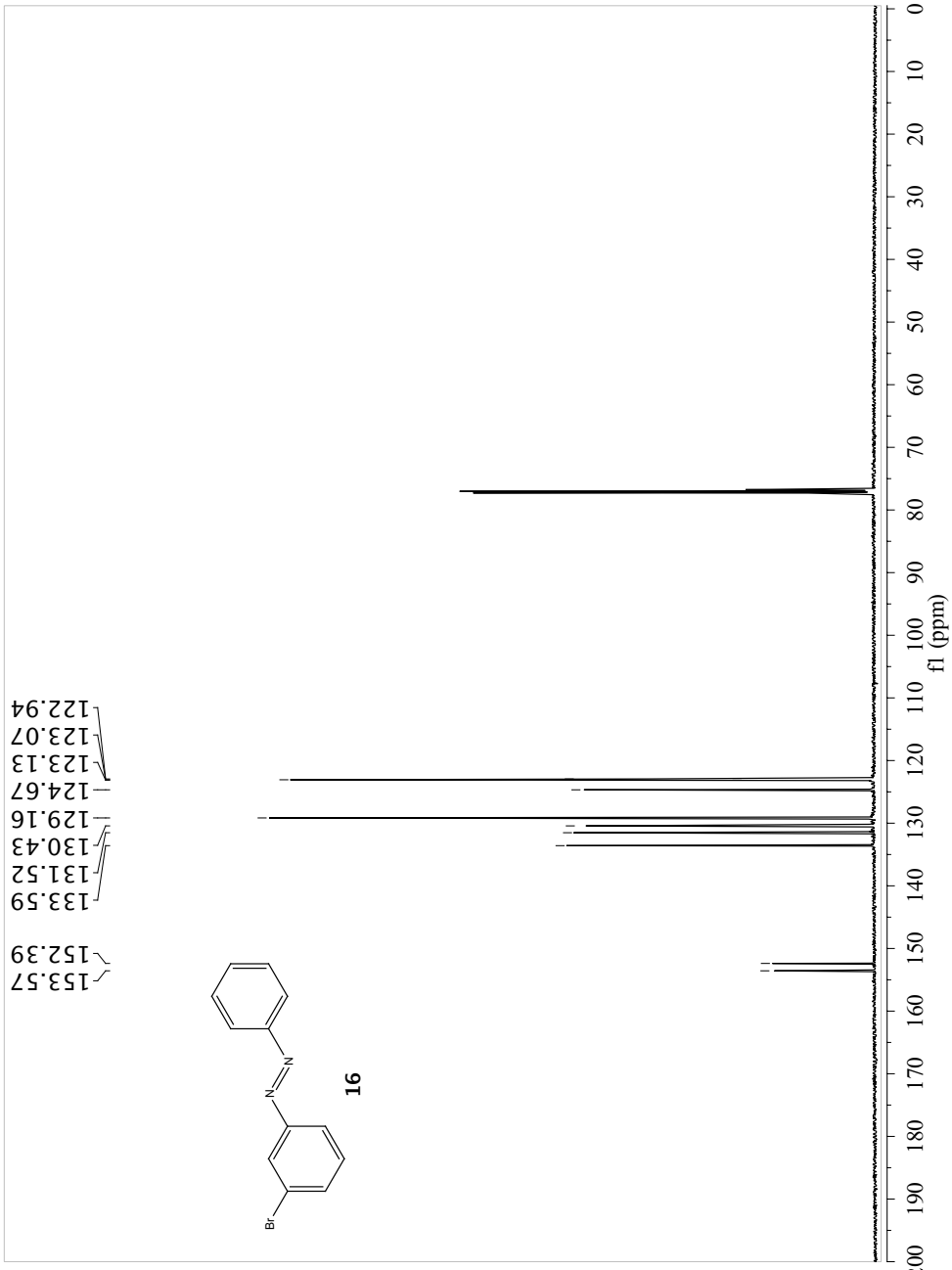

Figure A1.15. ^{13}C NMR spectrum (125 MHz) of **16** in $CDCl_3$

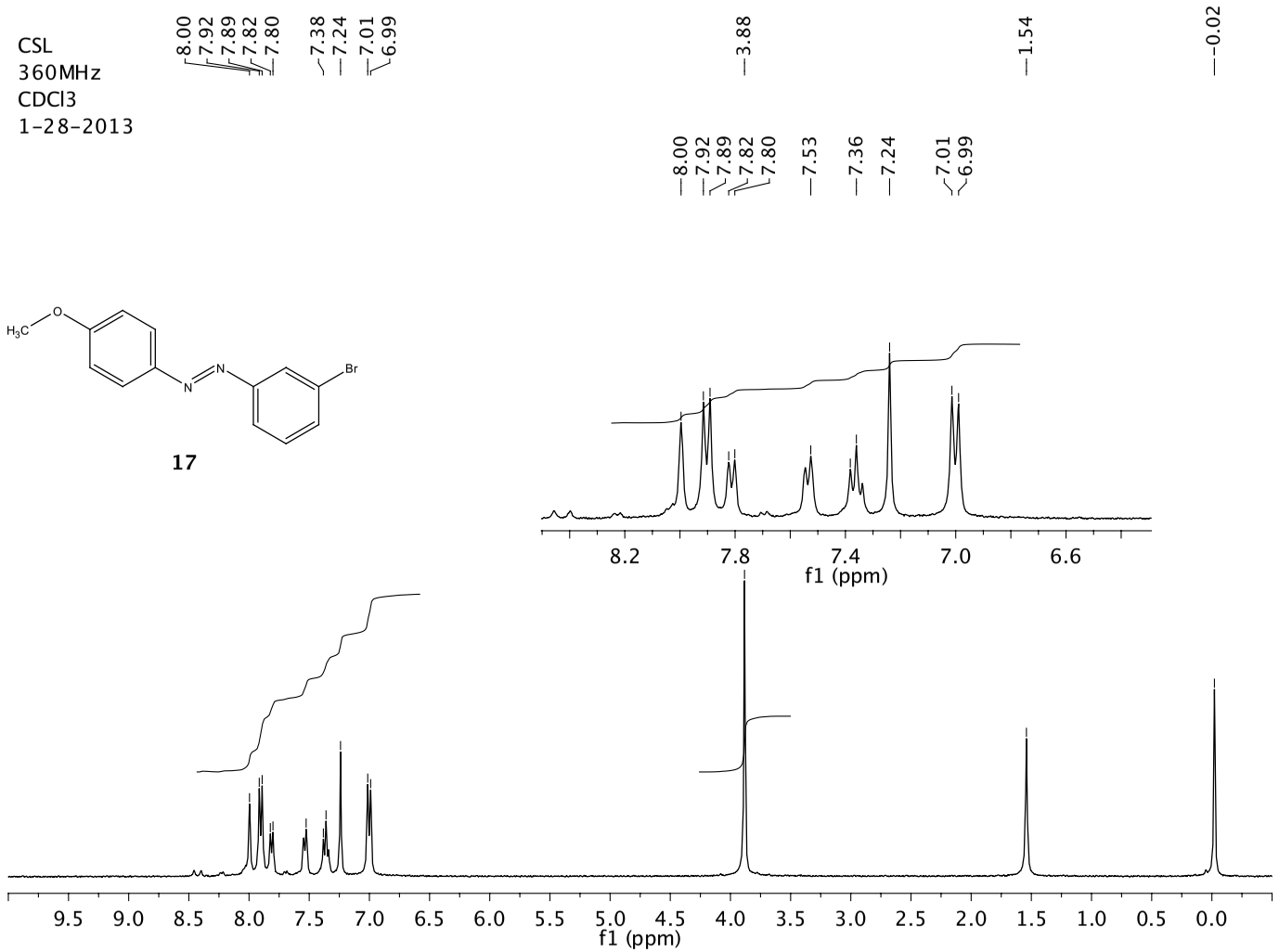

Figure A1.16. ^{1}H NMR spectrum (360 MHz) of **17** in $CDCl_3$

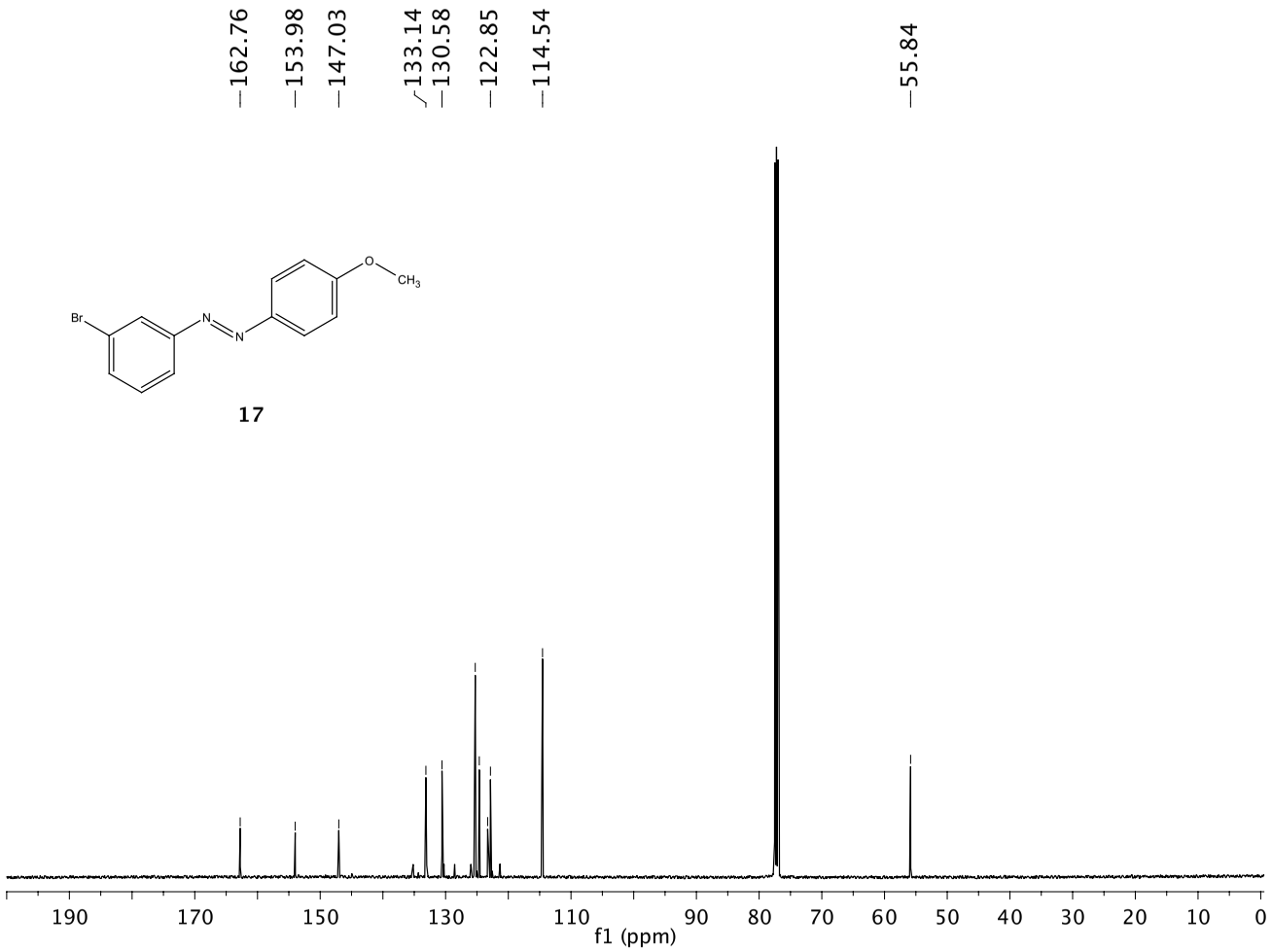

Figure A1.17. ^{13}C NMR spectrum (125 MHz) of **17** in $CDCl_3$

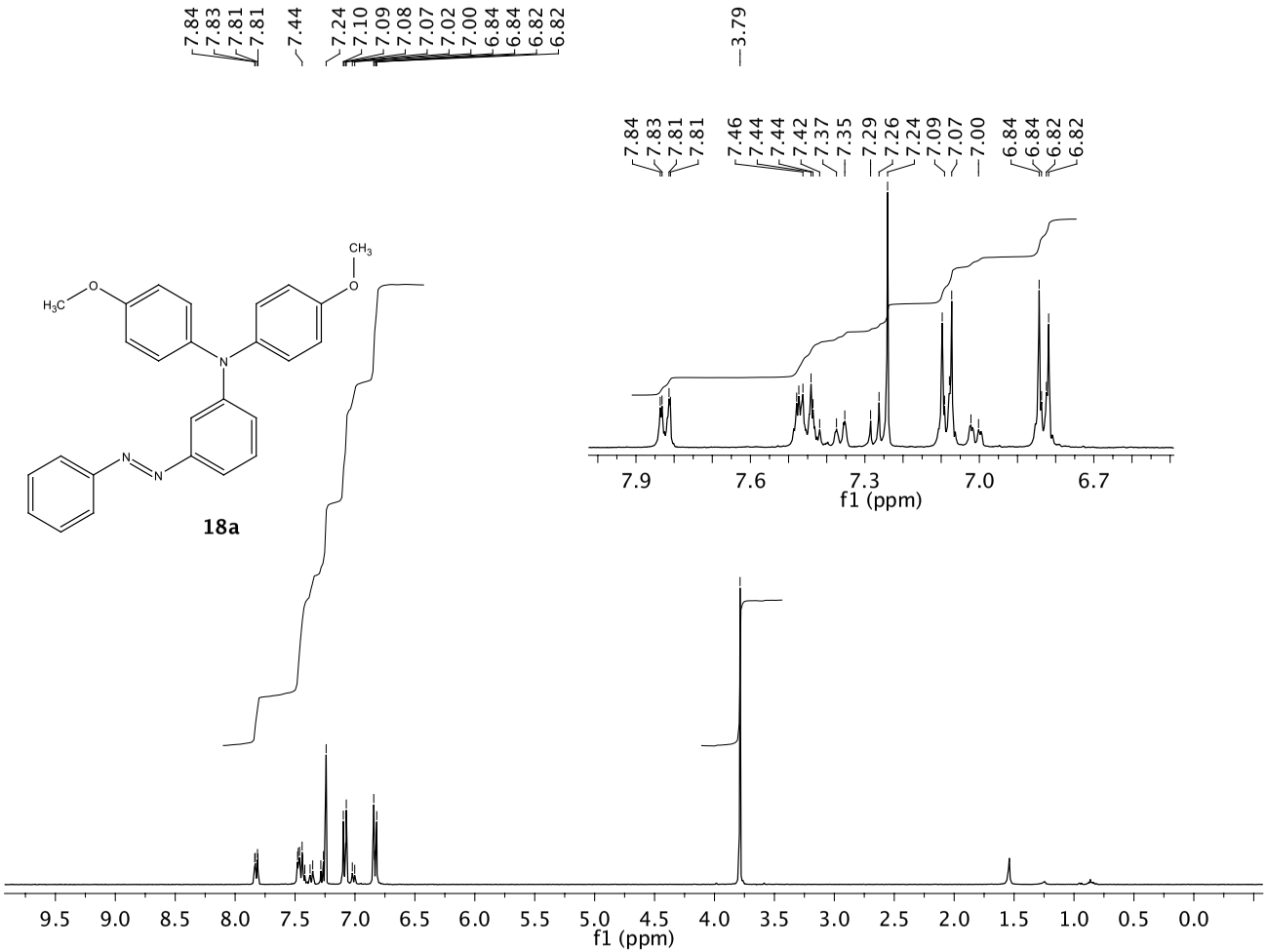

Figure A1.18. ^{1}H NMR spectrum (360 MHz) of **18a** in $CDCl_3$

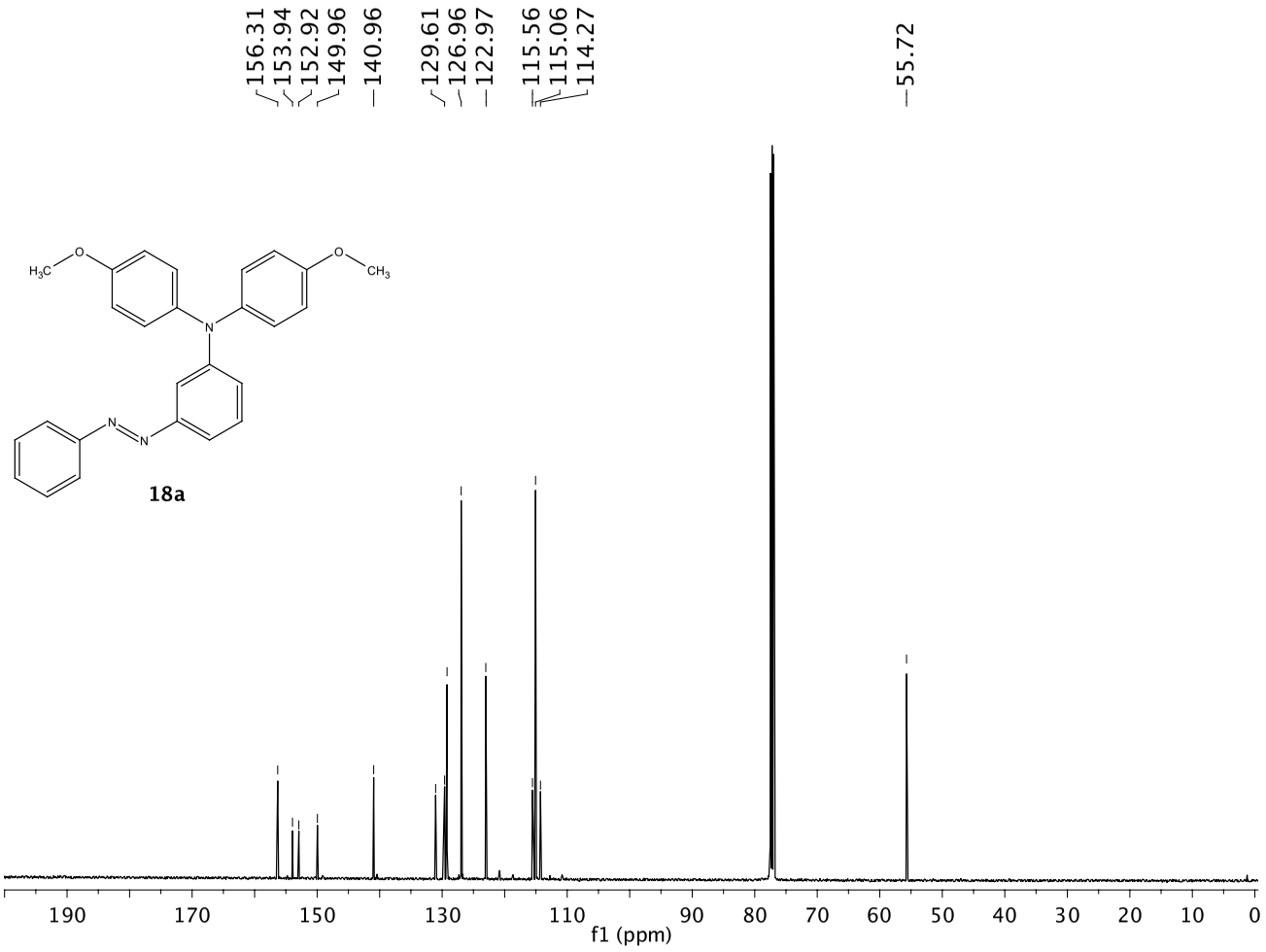

Figure A1.19. ^{13}C NMR spectrum (125 MHz) of **18a** in $CDCl_3$

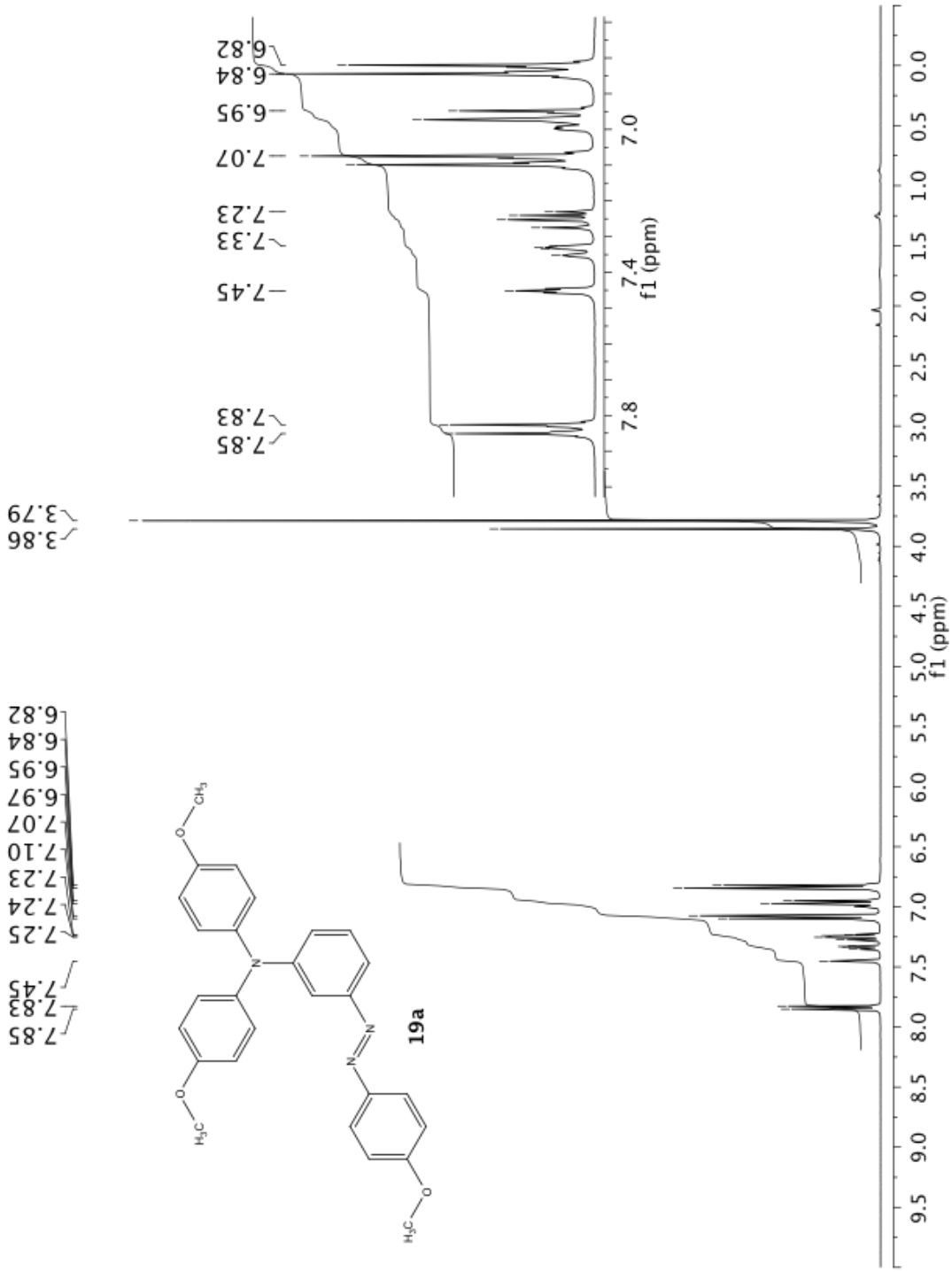

Figure A1.20. ^{1}H NMR spectrum (360 MHz) of **19a** in $CDCl_3$

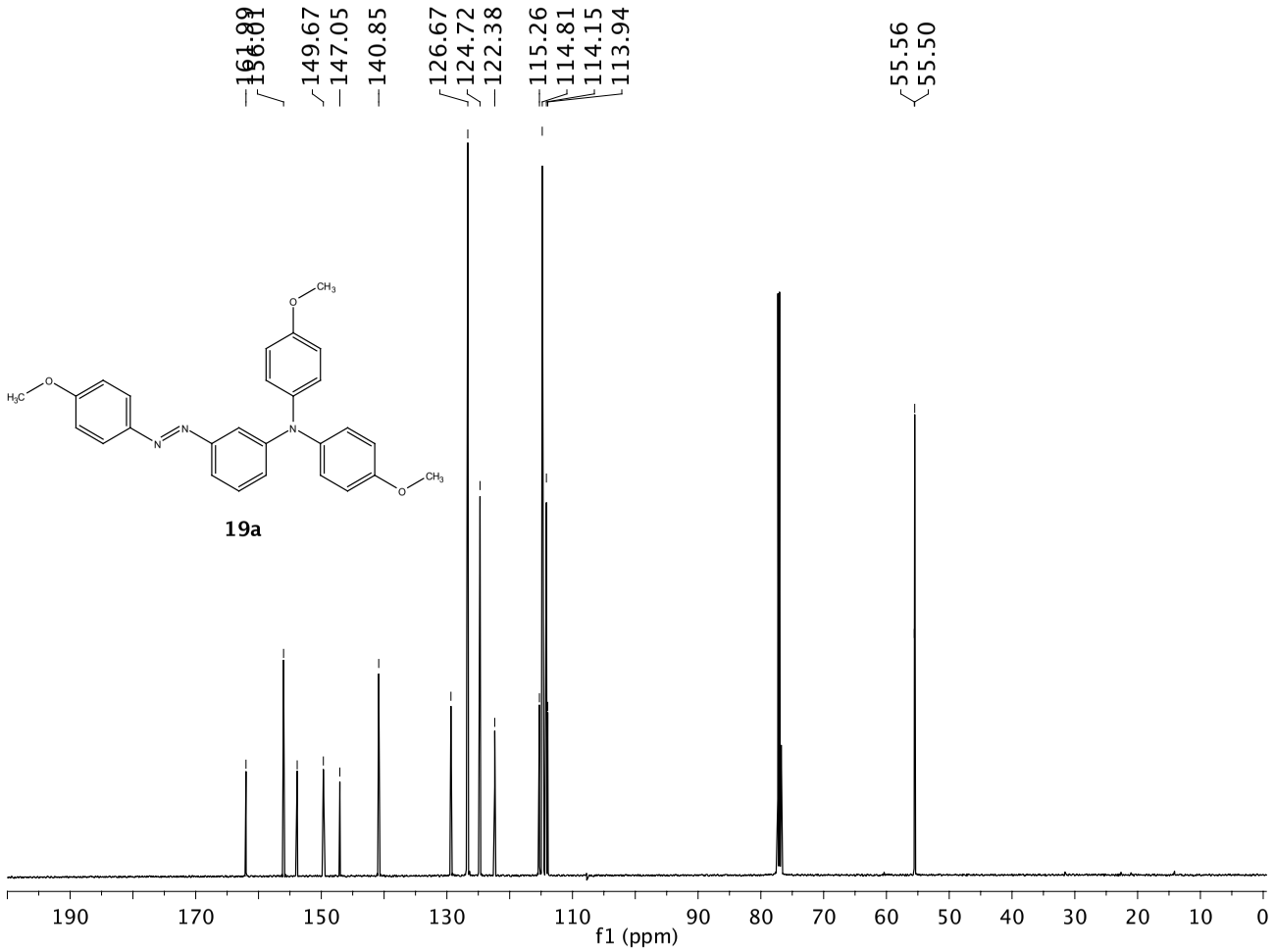

Figure A1.21. ^{13}C NMR spectrum (125 MHz) of **19a** in $CDCl_3$

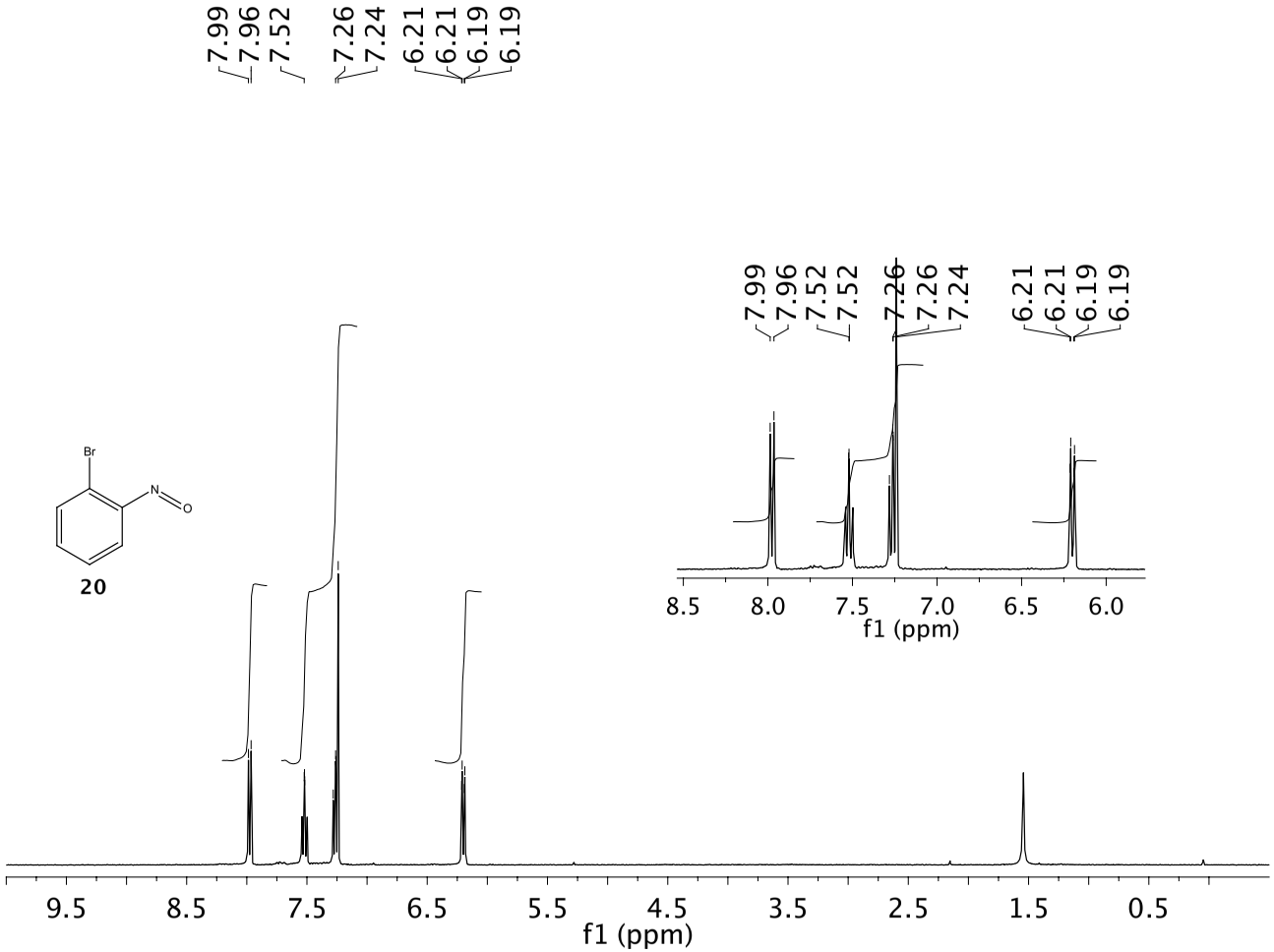

Figure A1.22. ^{1}H NMR spectrum (360 MHz) of **20** in $CDCl_3$

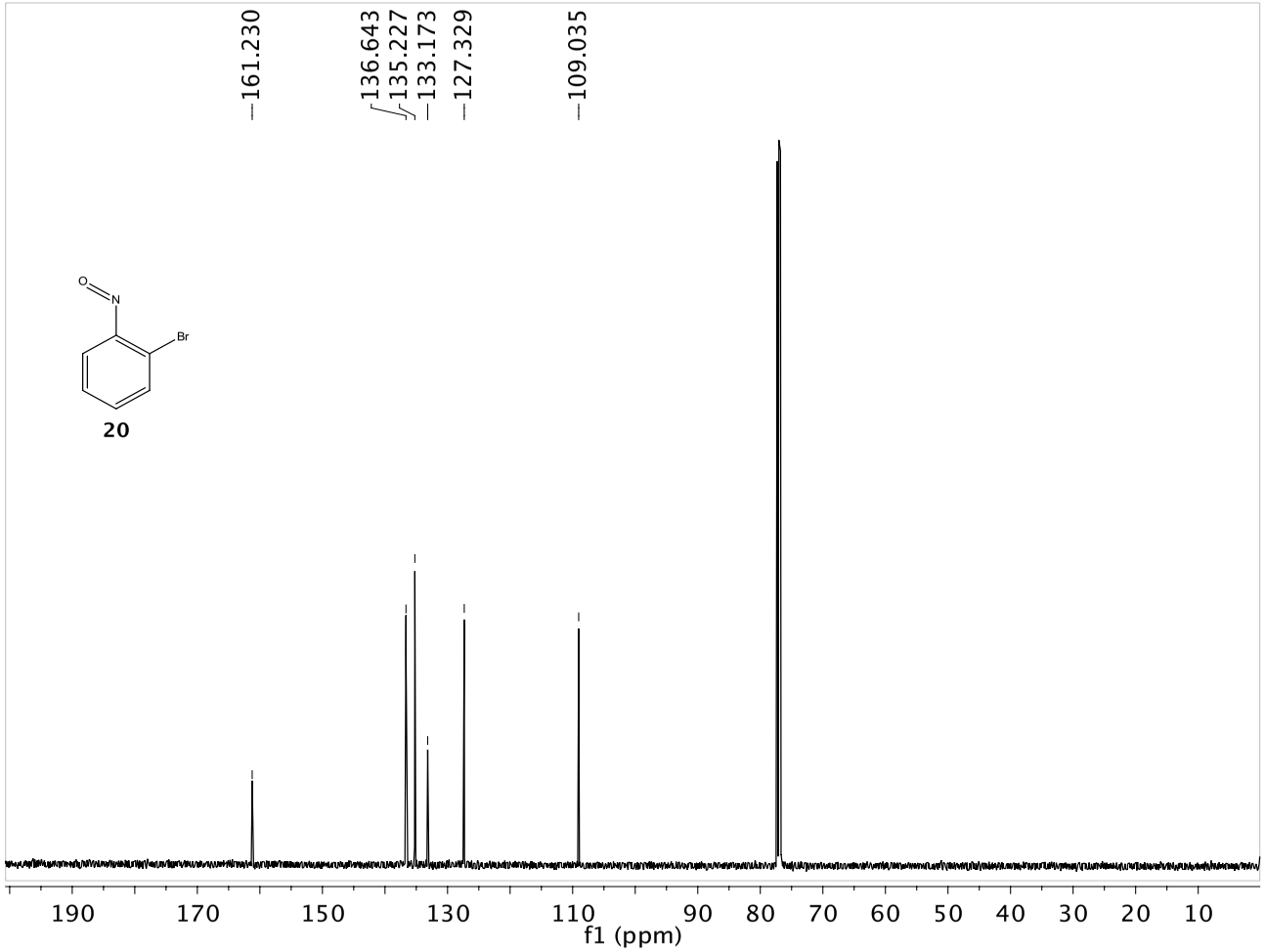

Figure A1.23. ^{13}C NMR spectrum (125 MHz) of **20** in $CDCl_3$

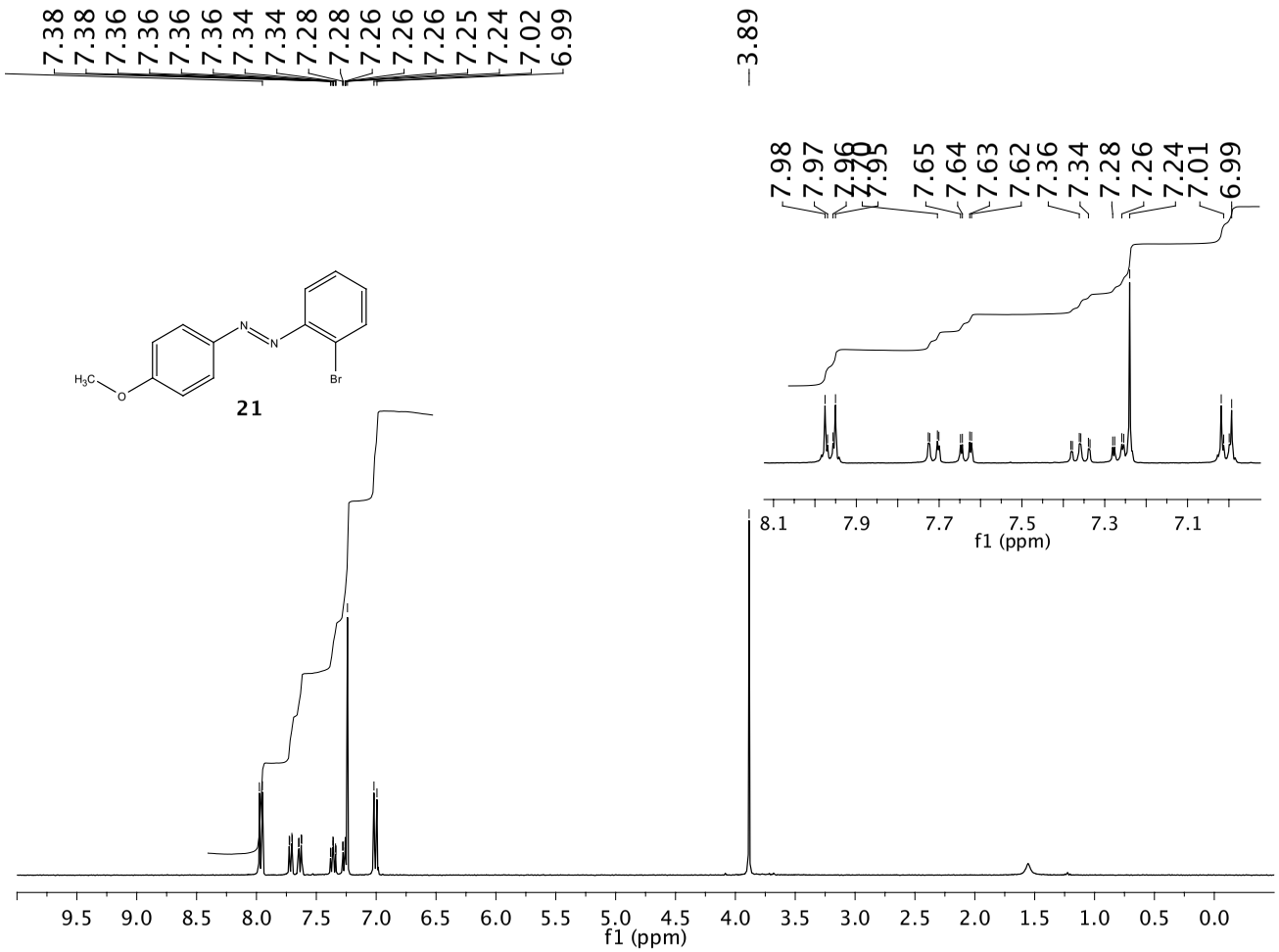

Figure A1.24. ^{1}H NMR spectrum (360 MHz) of **21** in $CDCl_3$

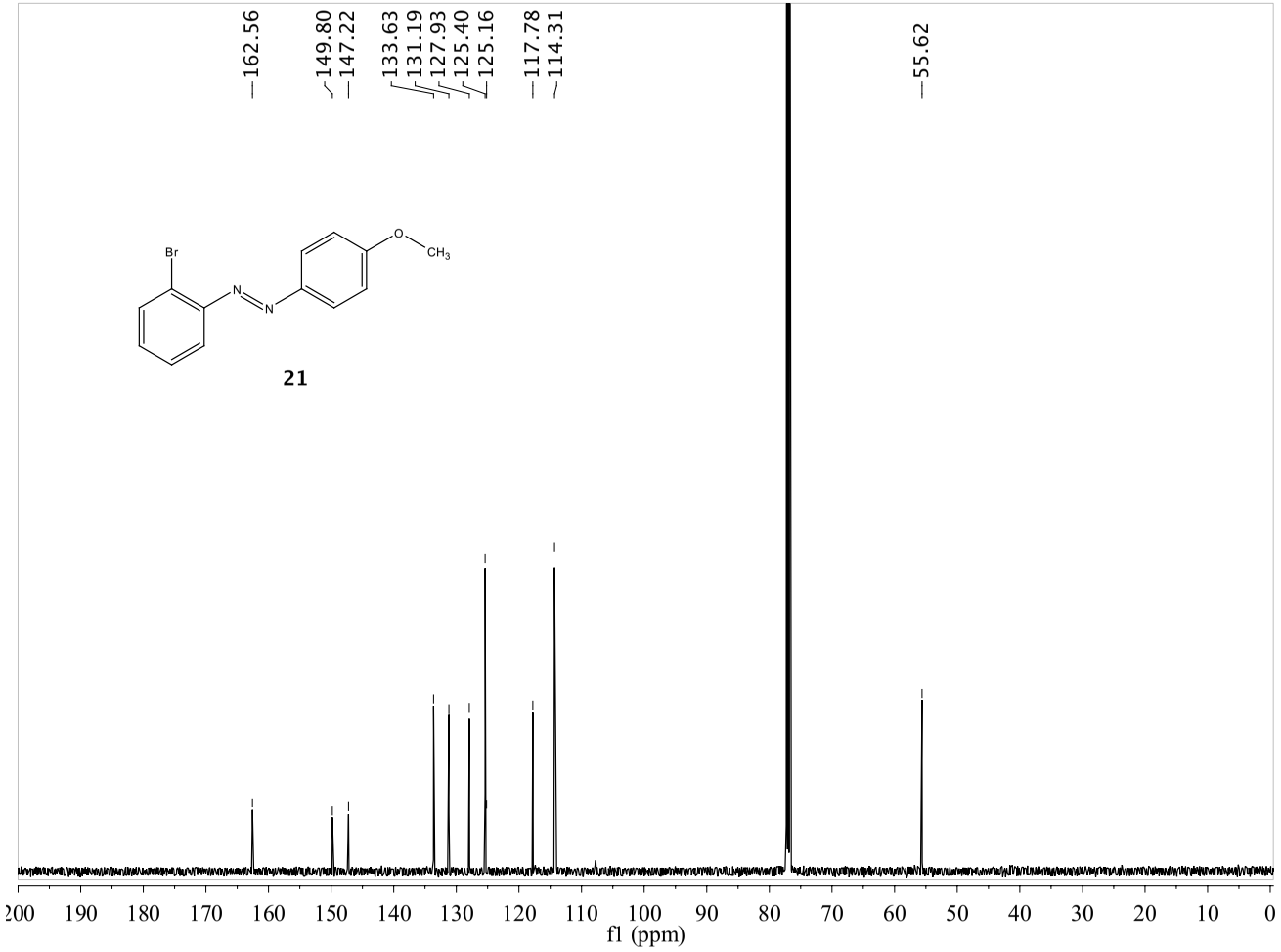

Figure A1.25. ^{13}C NMR spectrum (125 MHz) of **21** in $CDCl_3$

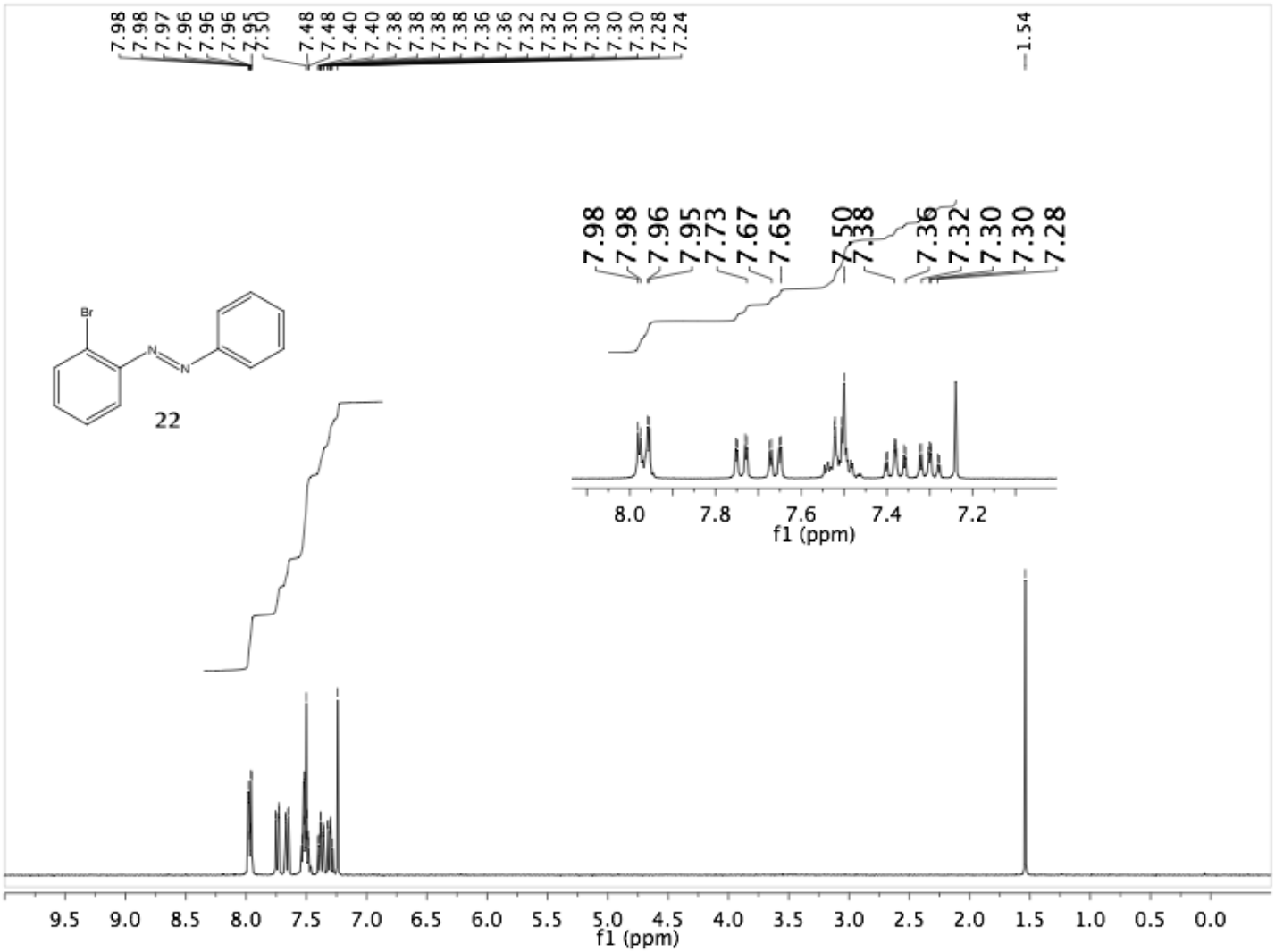

Figure A1.26. ^{1}H NMR spectrum (360 MHz) of **22** in $CDCl_3$

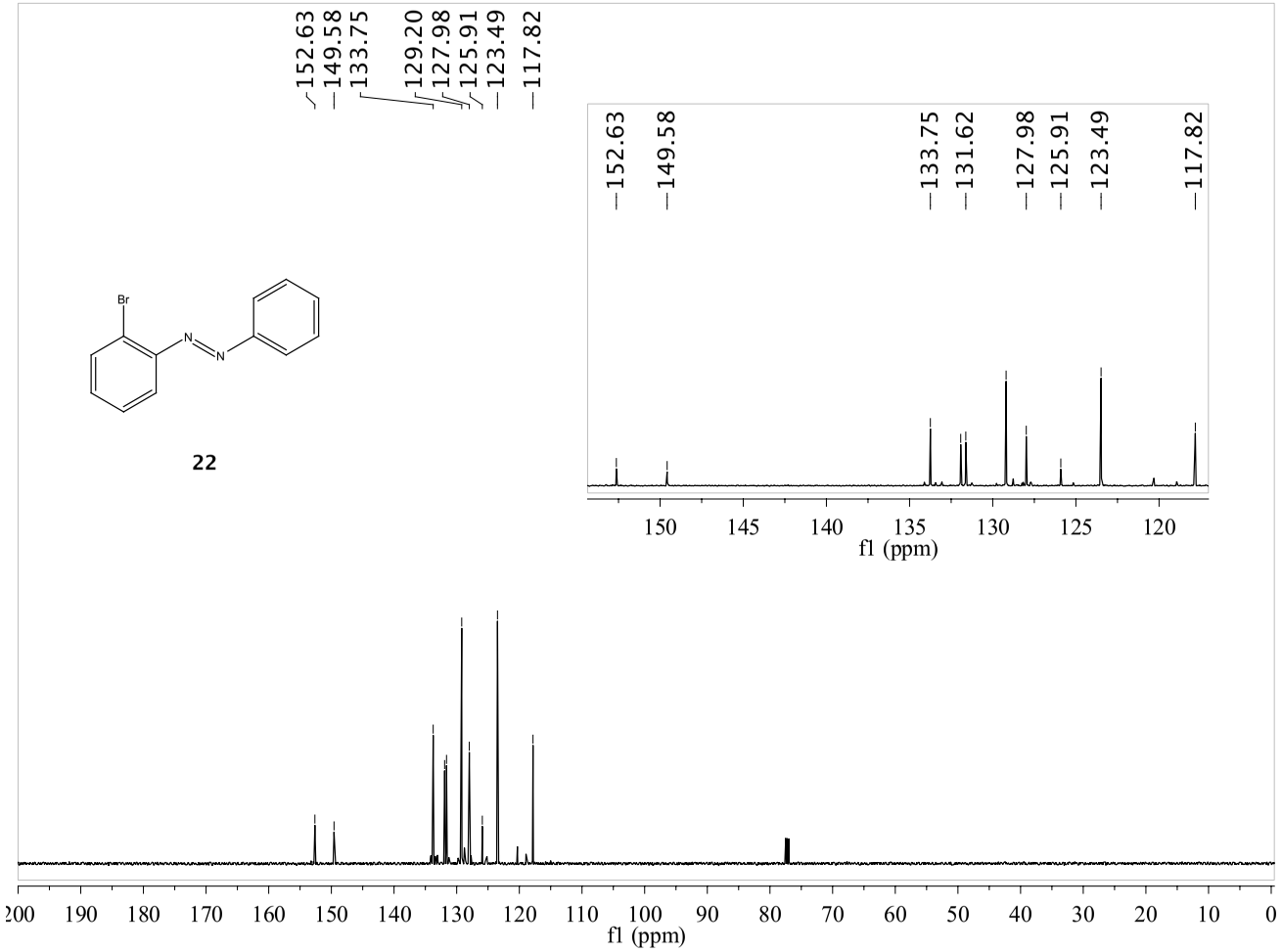

Figure A1.27. ^{13}C NMR spectrum (125 MHz) of **22** in $CDCl_3$

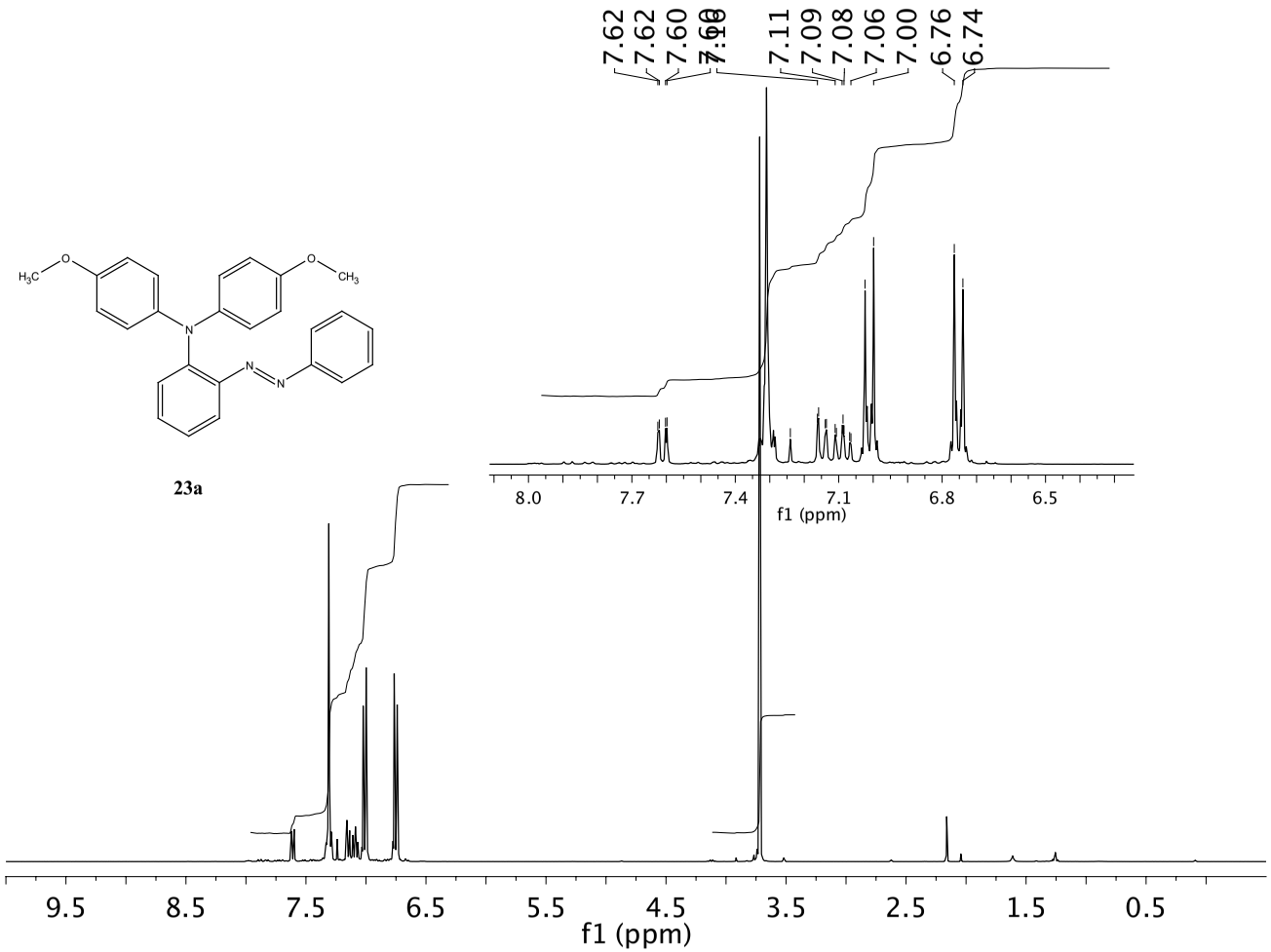

Figure A1.28. ^{1}H NMR spectrum (360 MHz) of **23a** in $CDCl_3$

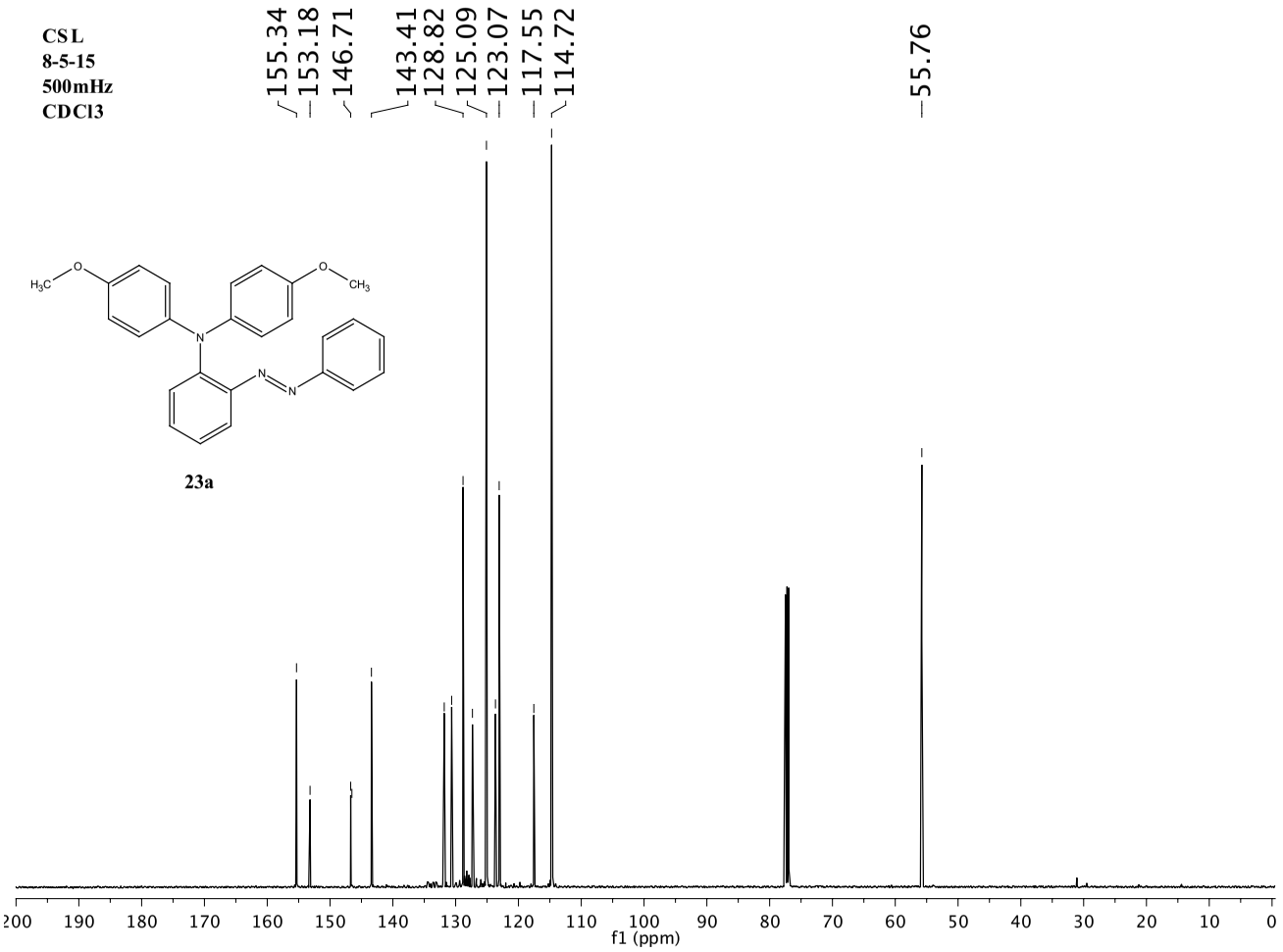

Figure A1.29. ^{13}C NMR spectrum (125 MHz) of **23a** in $CDCl_3$

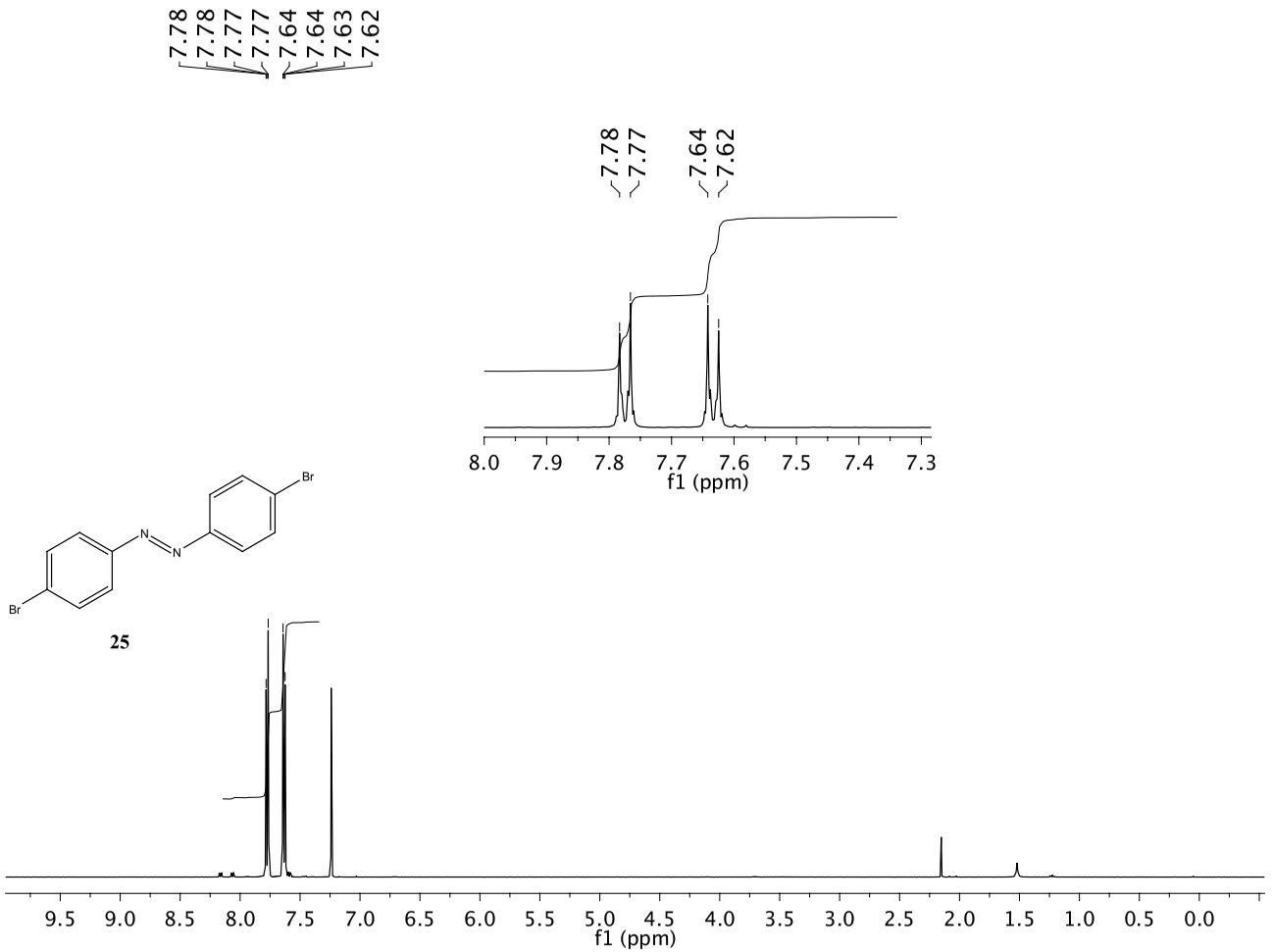

Figure A1.30. ^{1}H NMR spectrum (500 MHz) of **25** in $CDCl_3$

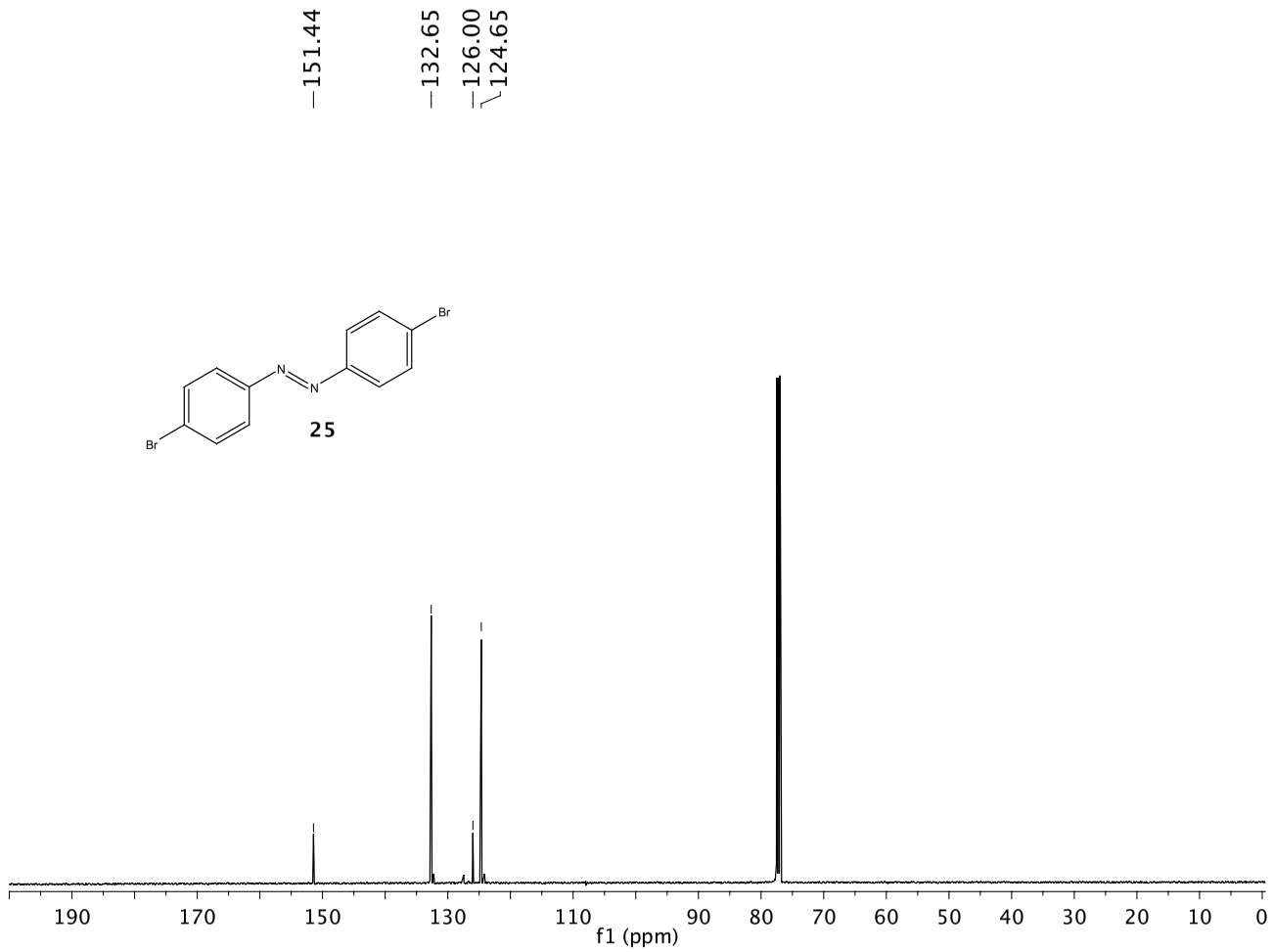

Figure A1.31. ^{13}C NMR spectrum (125 MHz) of **25** in $CDCl_3$

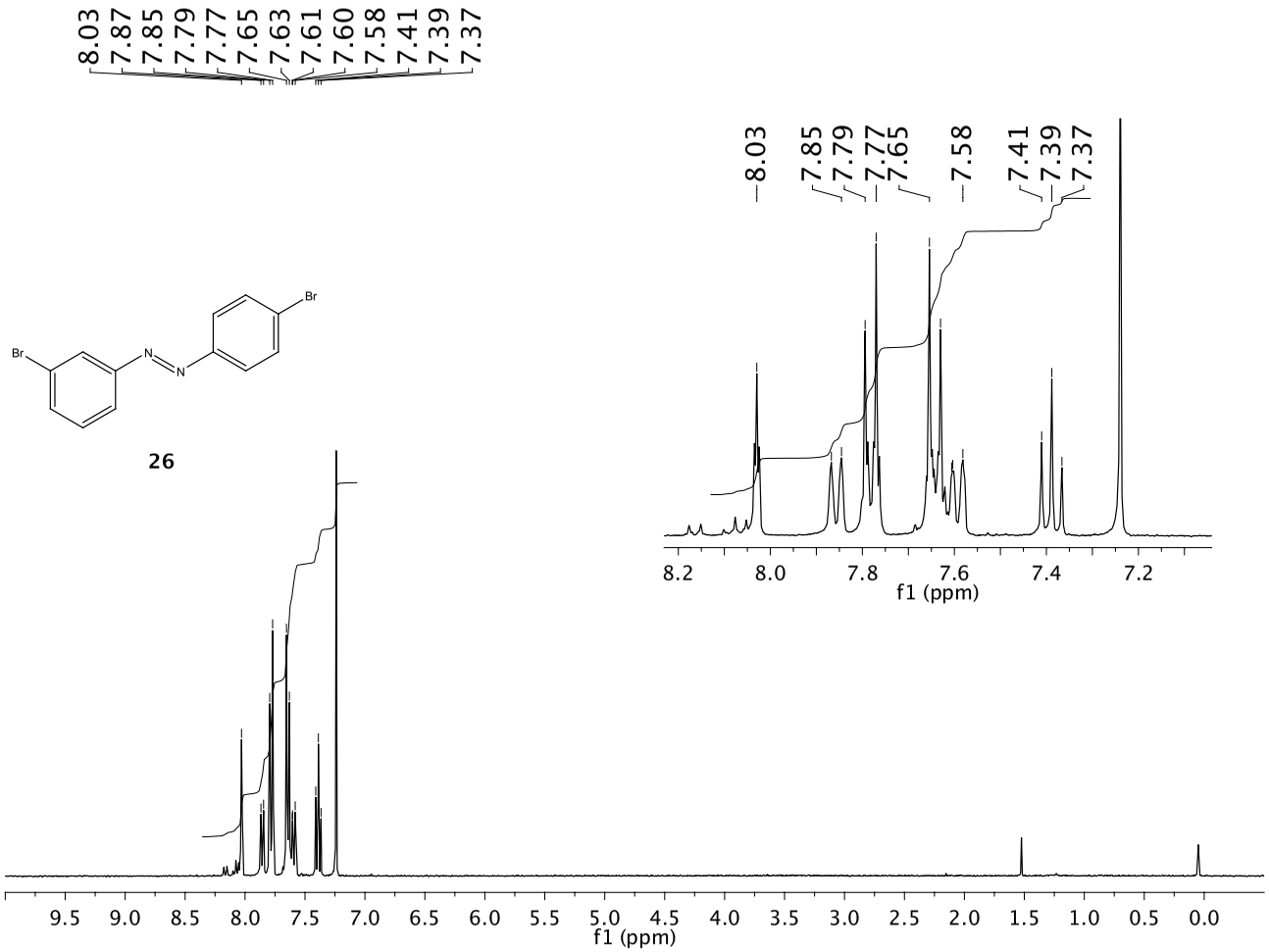

Figure A1.32. ^{1}H NMR spectrum (360 MHz) of **26** in $CDCl_3$

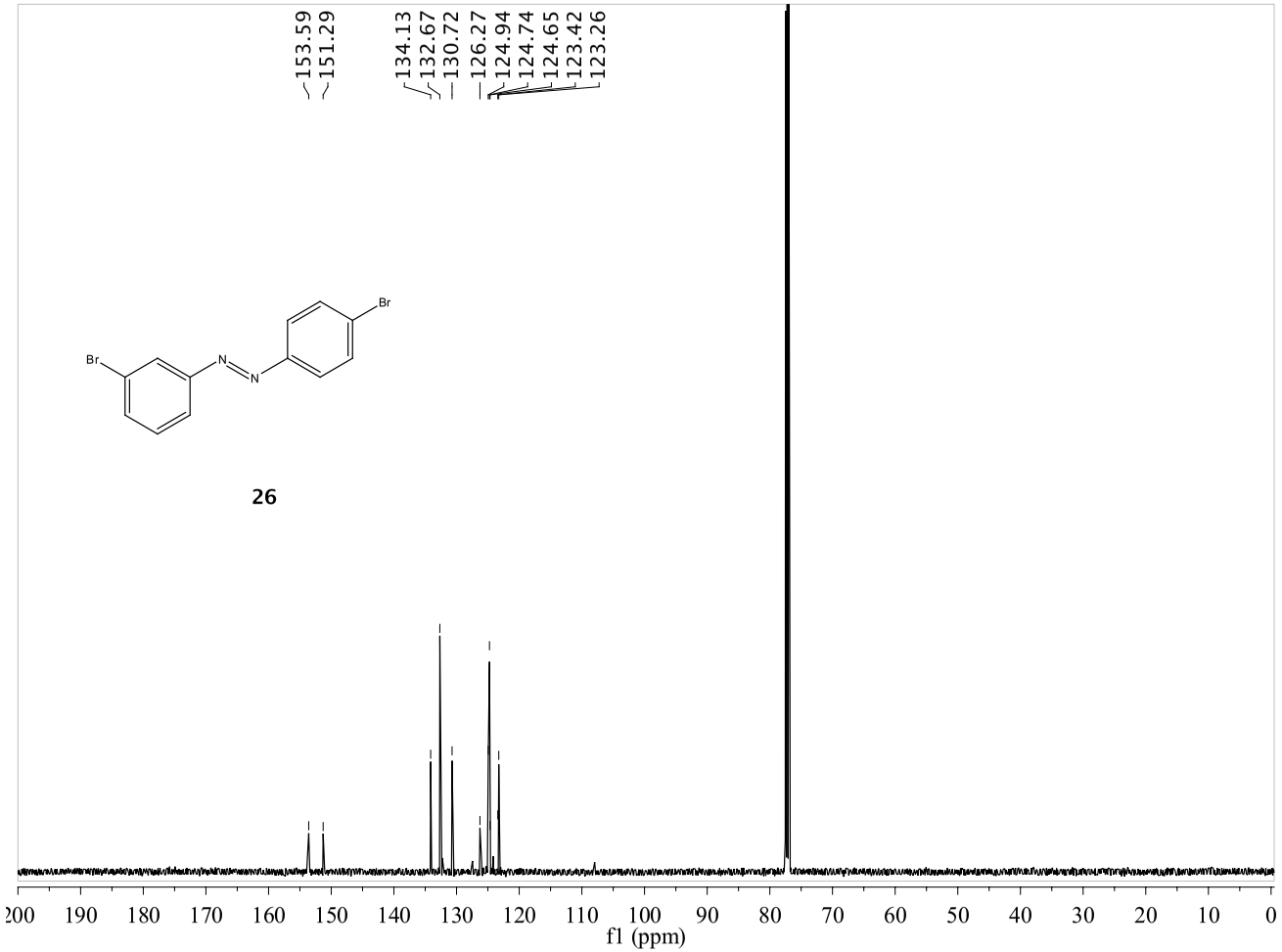

Figure A1.33. ^{13}C NMR spectrum (125 MHz) of **26** in $CDCl_3$

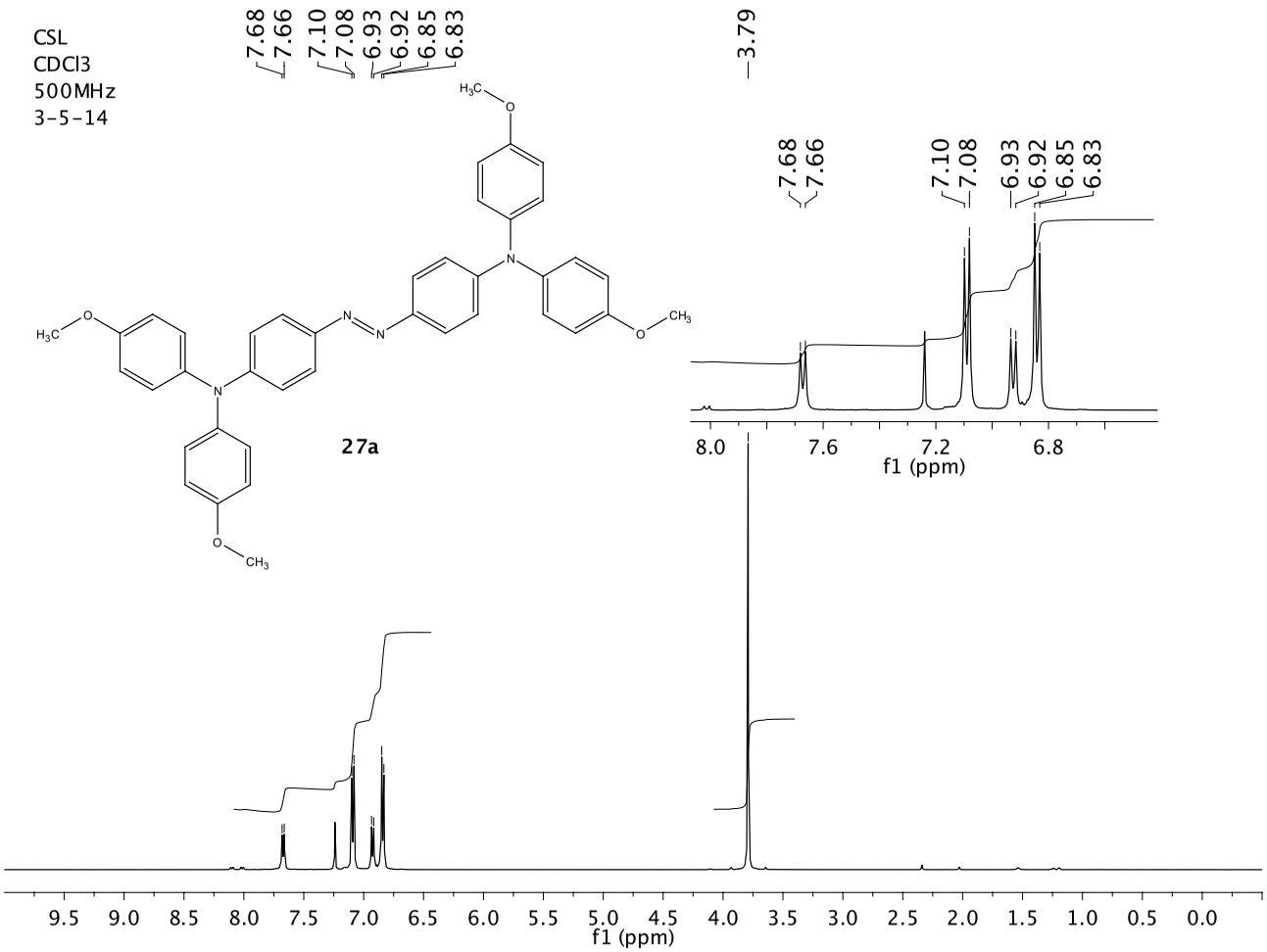

Figure A1.34. ^{1}H NMR spectrum (500 MHz) of **27a** in $CDCl_3$

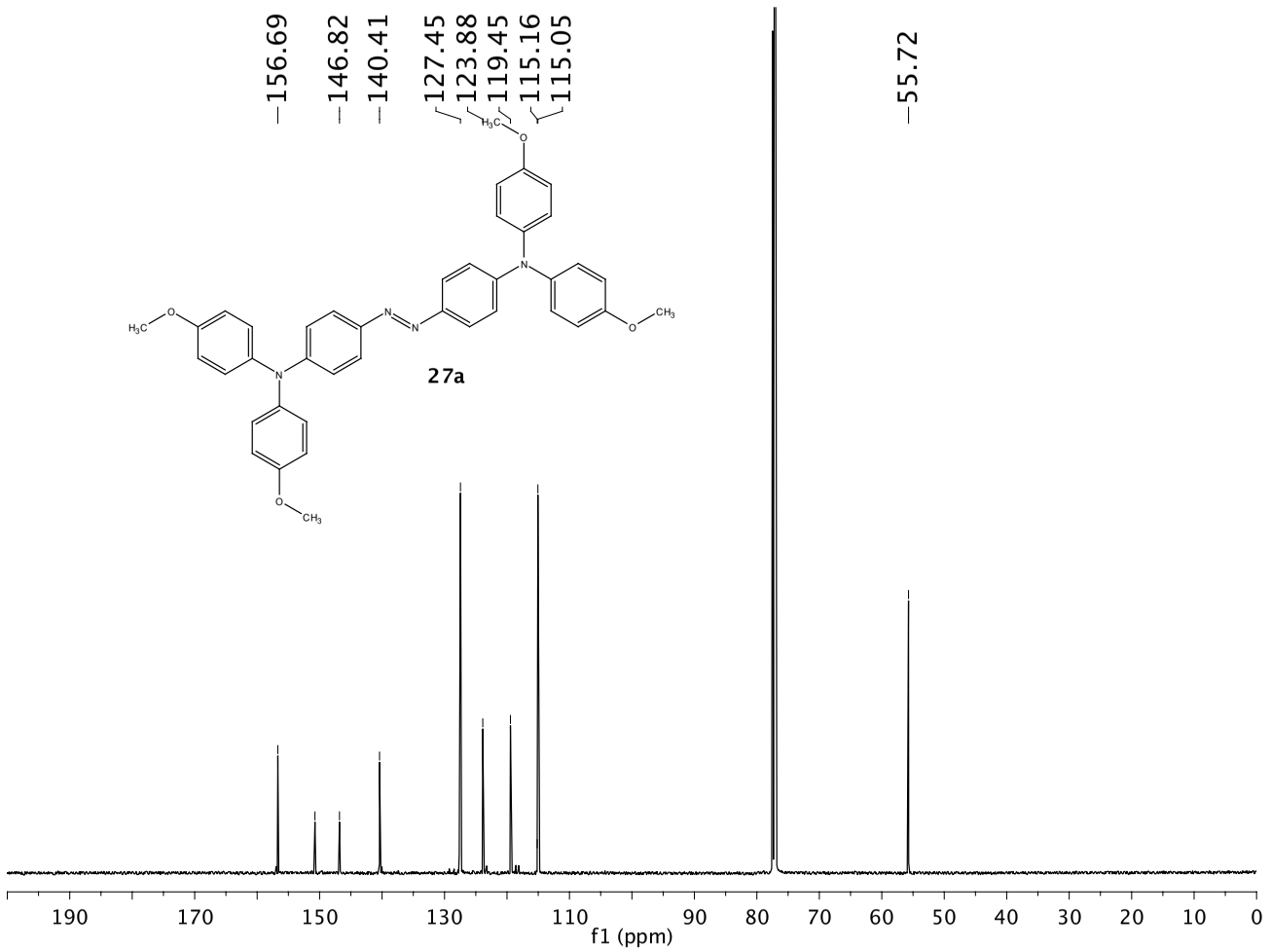

Figure A1.35. ^{13}C NMR spectrum (125 MHz) of **27a** in $CDCl_3$

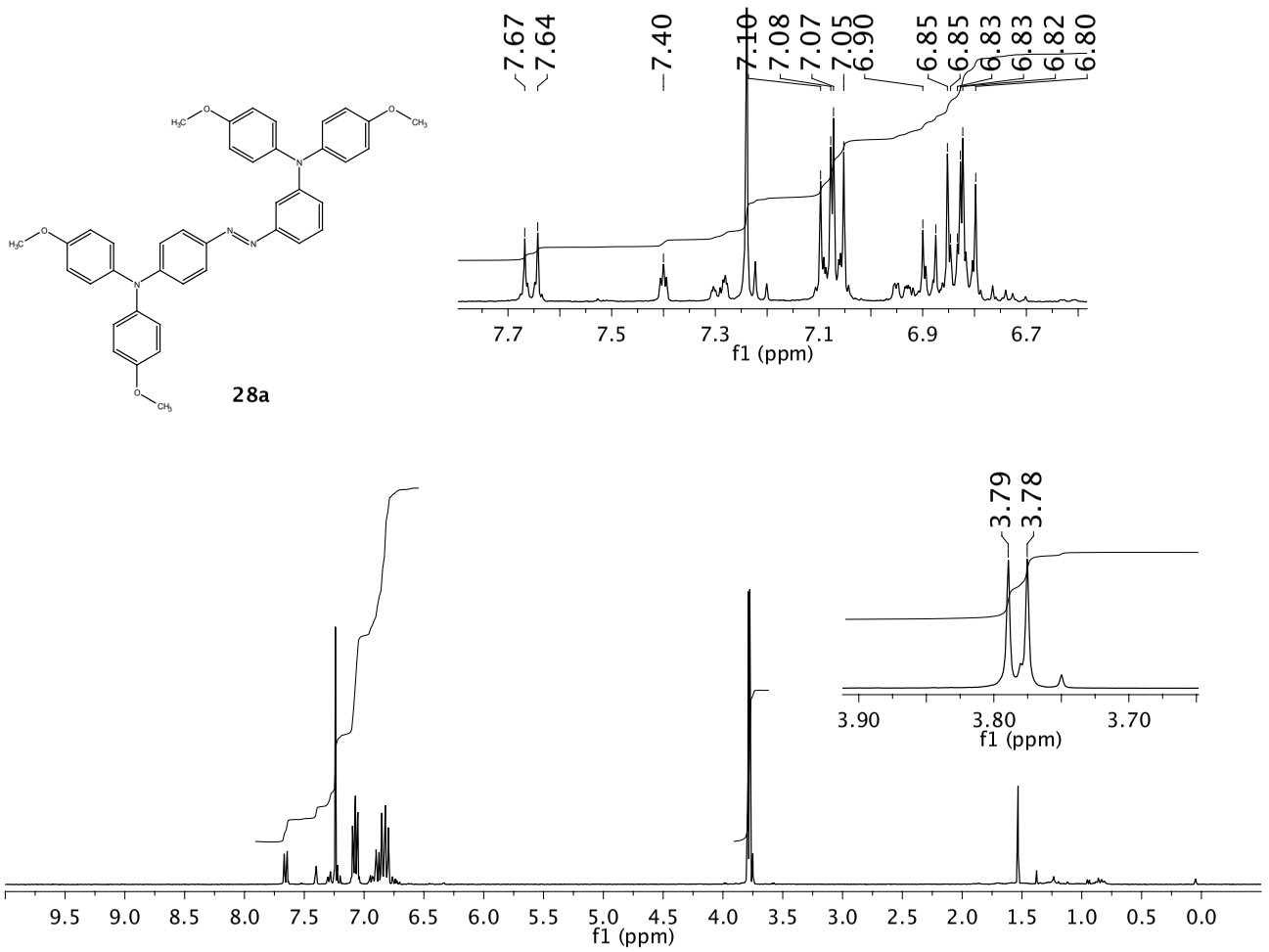

Figure A1.36. ^{1}H NMR spectrum (360 MHz) of **28a** in $CDCl_3$

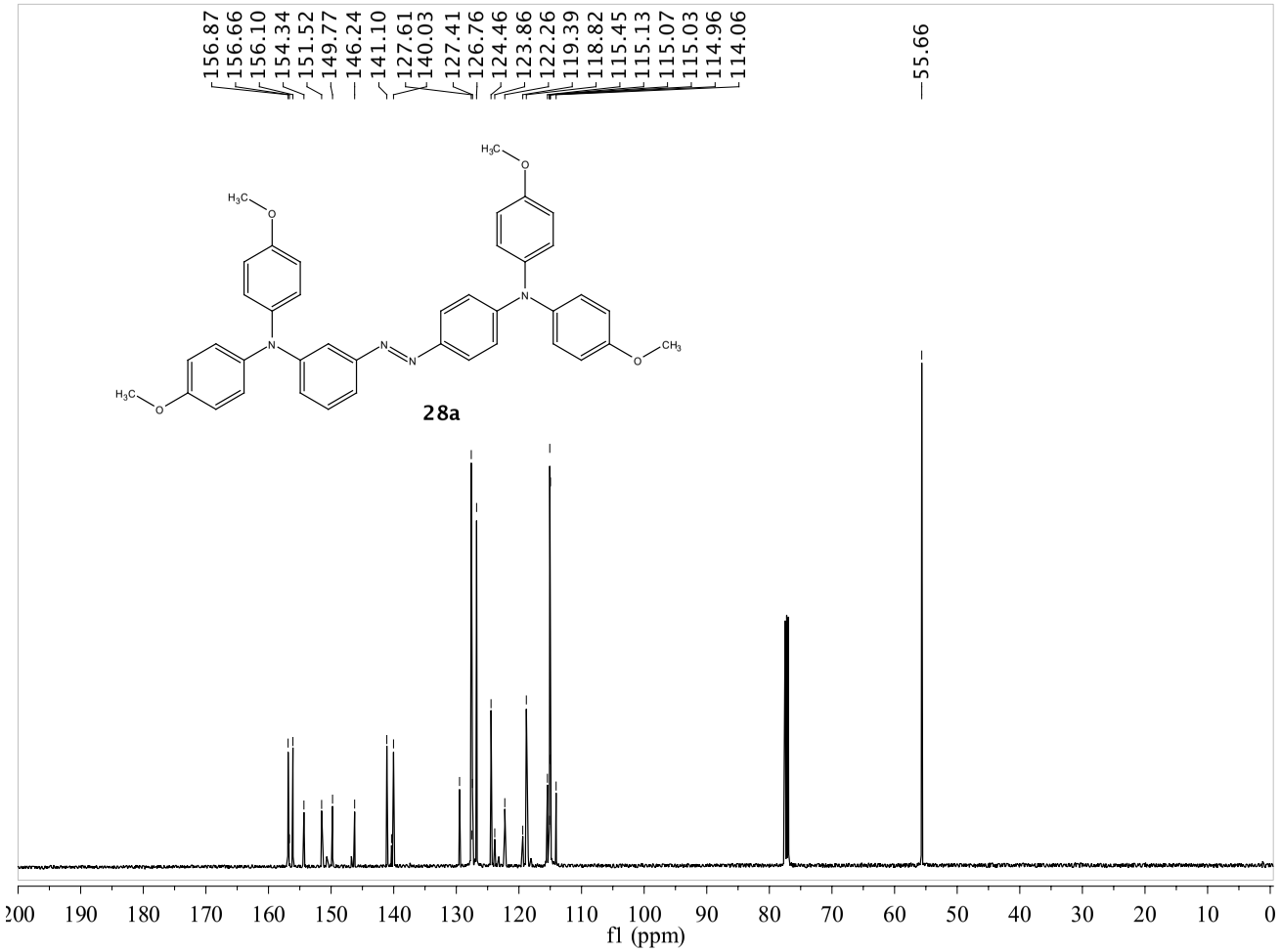

Figure A1.37. ^{13}C NMR spectrum (125 MHz) of **28a** in $CDCl_3$

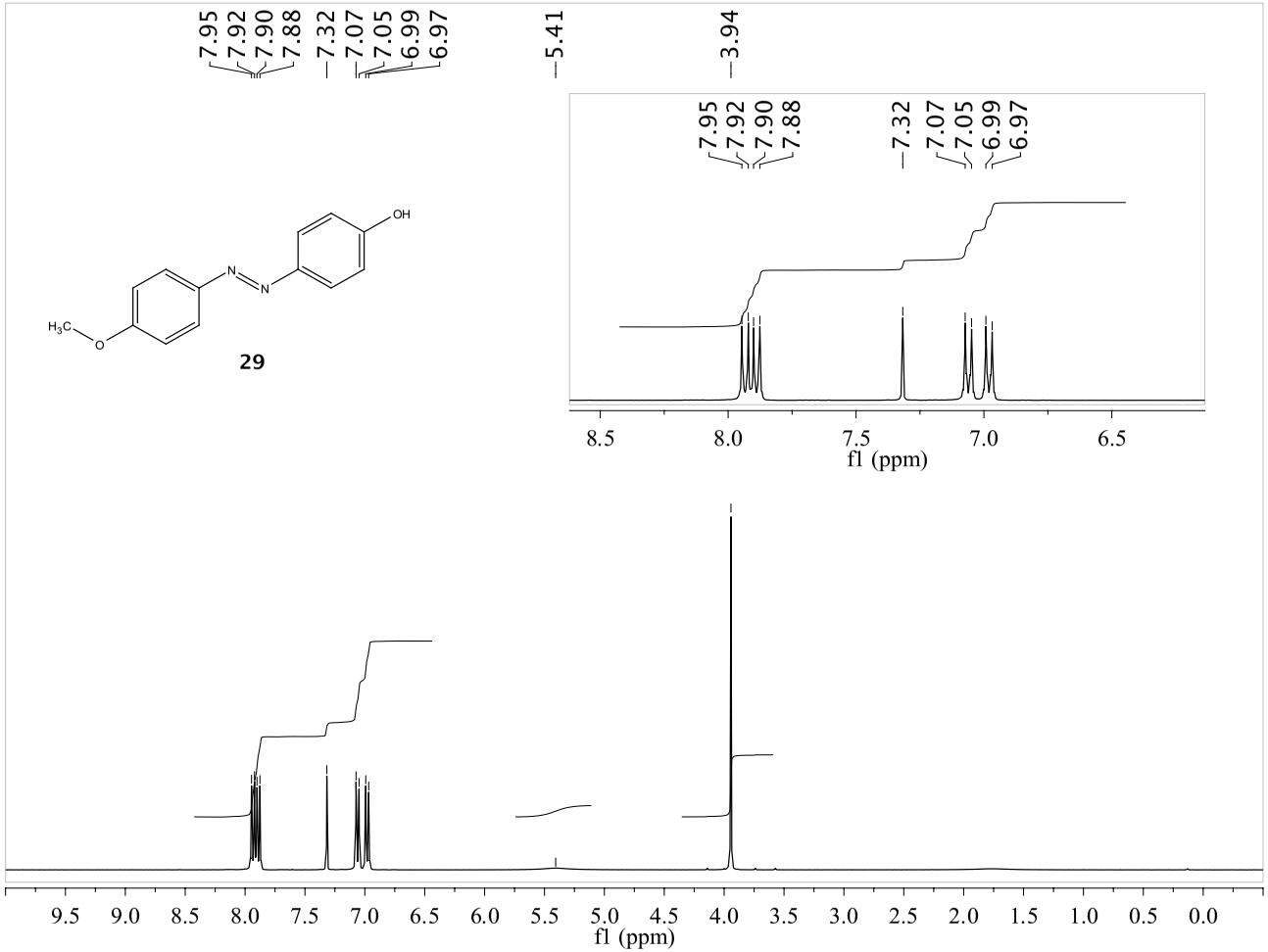

Figure A1.38. ^{1}H NMR spectrum (360 MHz) of **29** in $CDCl_3$

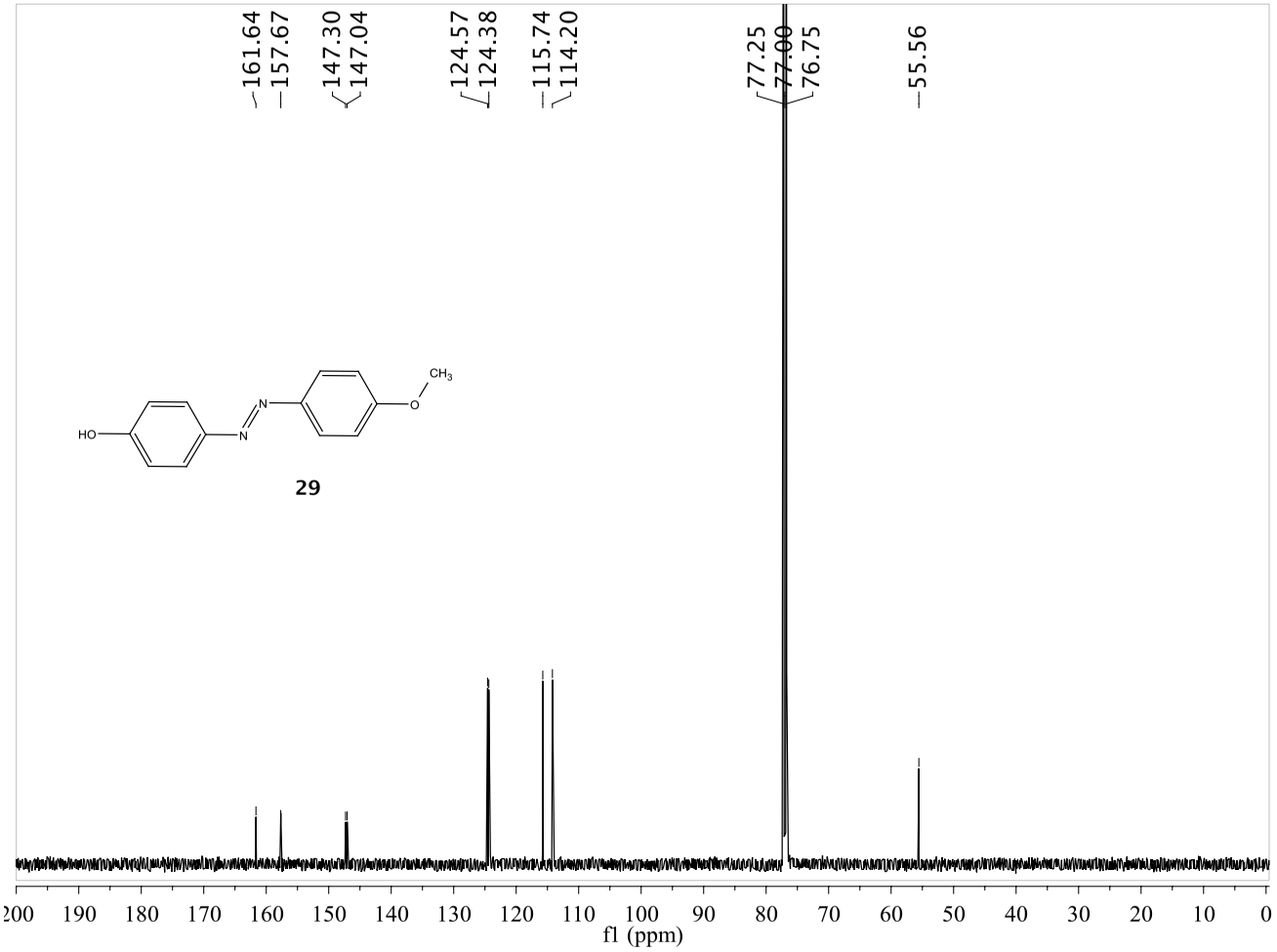

Figure A1.39. ^{13}C NMR spectrum (125 MHz) of **29** in $CDCl_3$

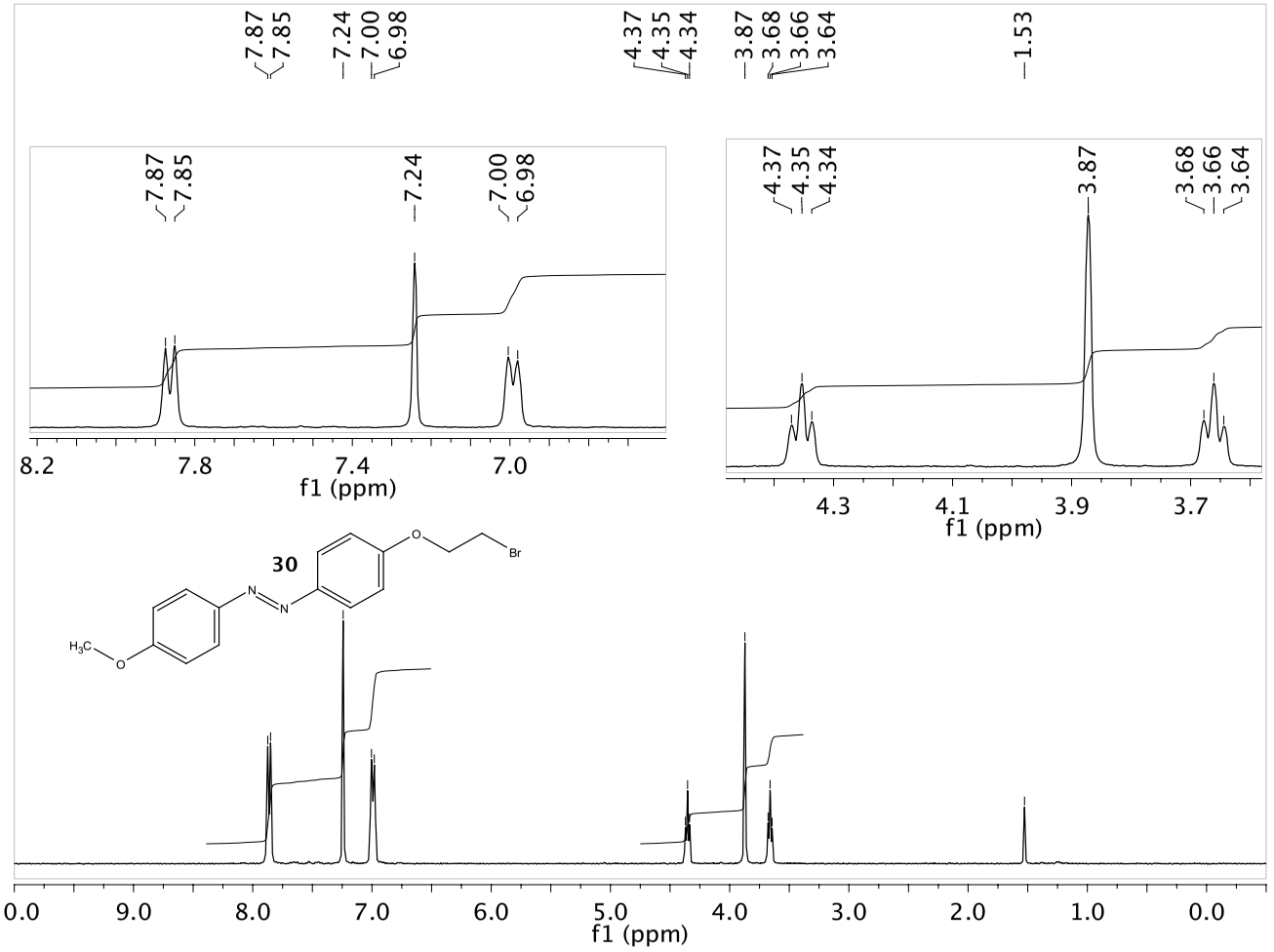

Figure A1.40. ^{1}H NMR spectrum (360 MHz) of **30** in $CDCl_3$

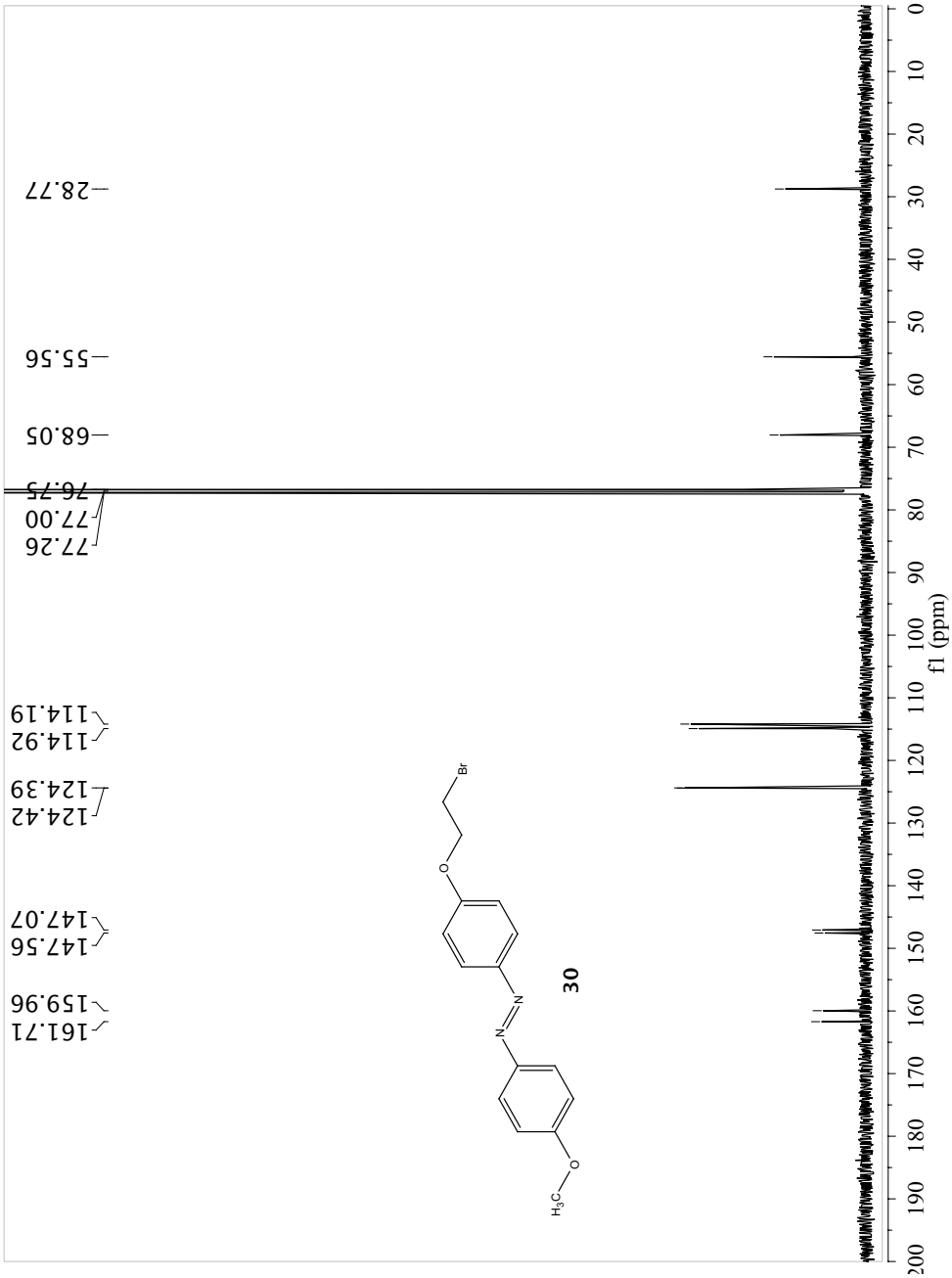

Figure A1.41. ^{13}C NMR spectrum (125 MHz) of **30** in $CDCl_3$

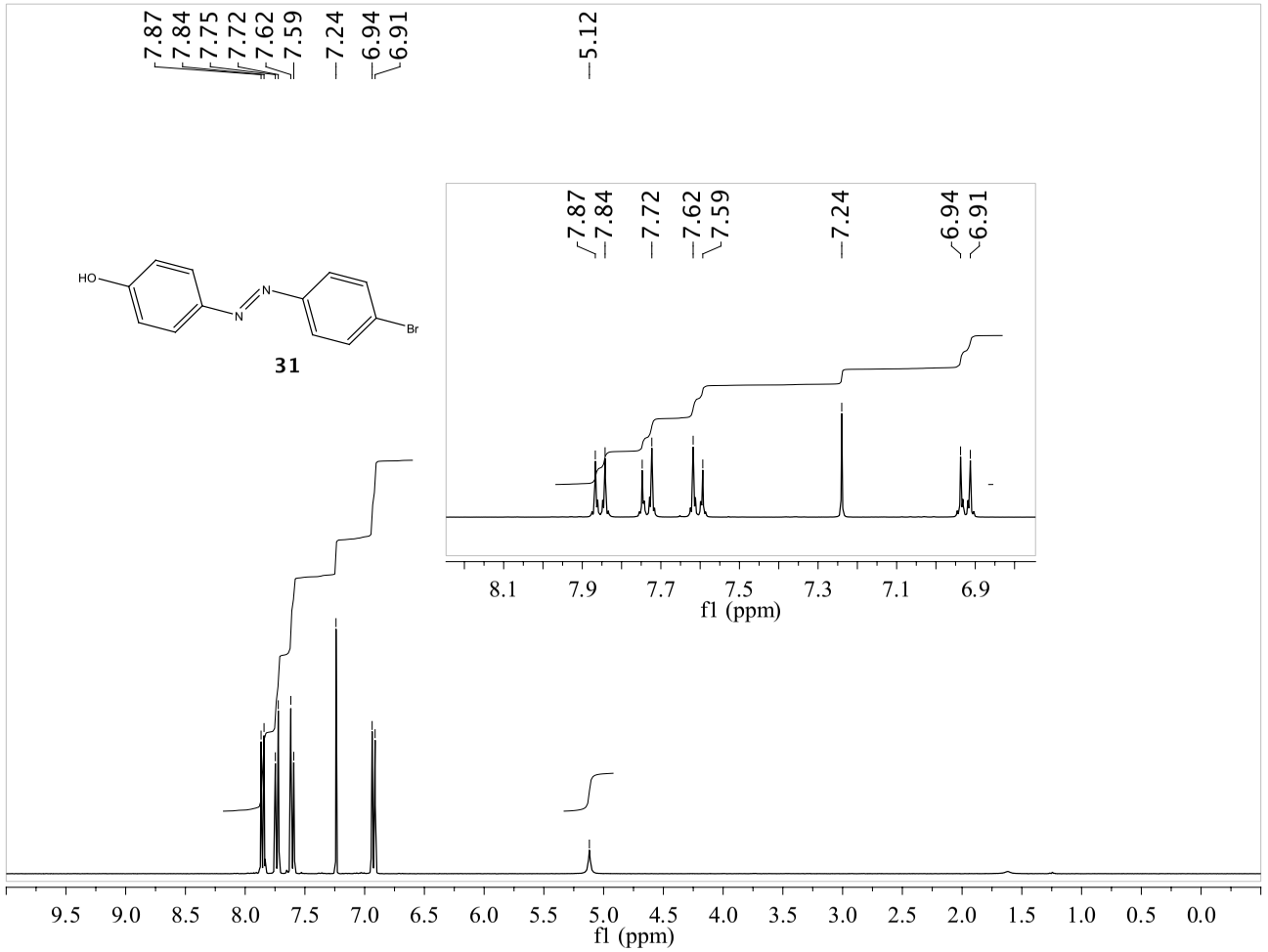

Figure A1.42. ^{1}H NMR spectrum (360 MHz) of **31** in $CDCl_3$

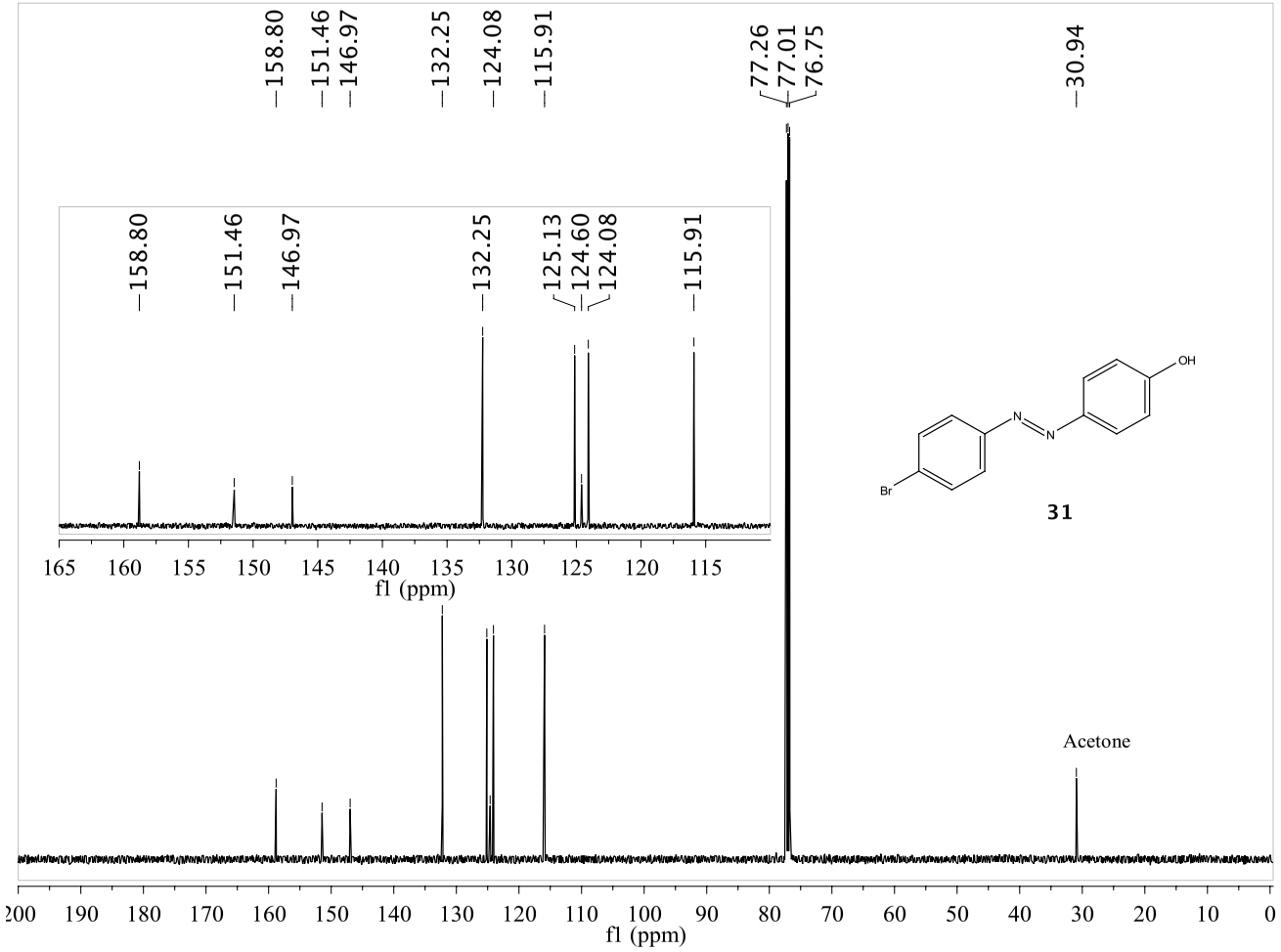

Figure A1.43. ^{13}C NMR spectrum (125 MHz) of **31** in $CDCl_3$

APPENDIX B

X-RAY CRYSTALLOGRAPHY DATA FOR *p*AA-Ph-N=N-Ph **4a**

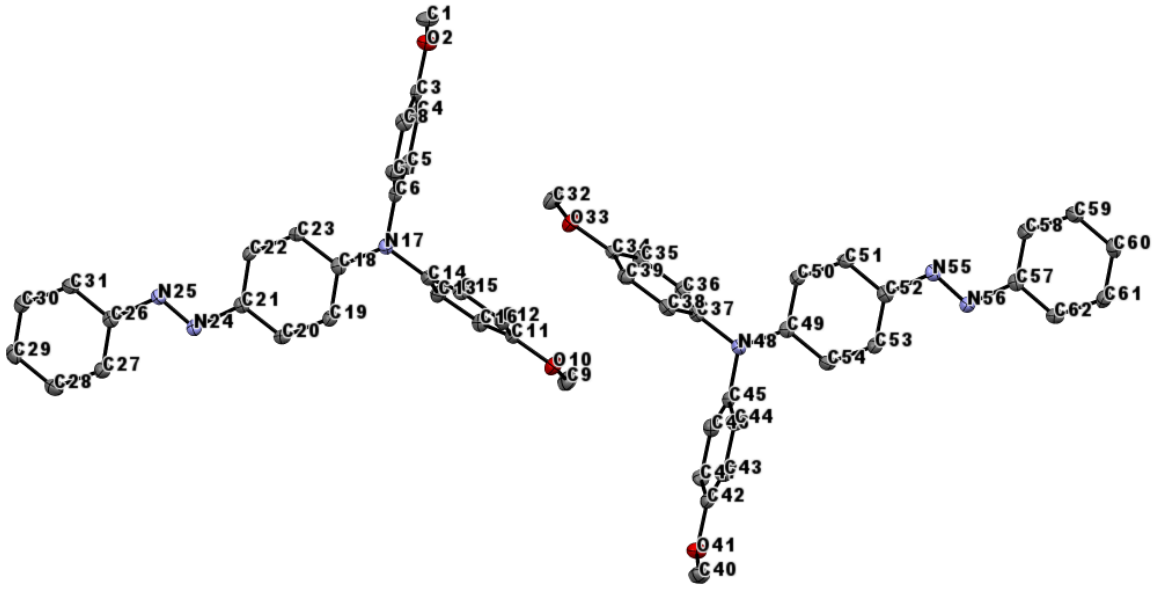

Table B1. Positional Parameters and U(eq) for *p*AA-Ph-N=N-Ph

atom	x	y	z	U(eq)
C(1)	8886(3)	10737(3)	-3318(2)	28(1)
C(3)	10519(3)	9100(2)	-3545(2)	18(1)
C(4)	11667(3)	8462(2)	-3344(2)	21(1)
C(5)	12195(3)	7468(2)	-3703(2)	21(1)
C(6)	11590(3)	7089(2)	-4270(2)	19(1)
C(7)	10452(3)	7720(2)	-4468(2)	21(1)
C(8)	9912(3)	8727(2)	-4112(2)	22(1)
C(9)	11864(4)	1741(3)	-2466(2)	30(1)
C(11)	11281(3)	3227(2)	-3283(2)	18(1)
C(12)	10260(3)	3810(2)	-3628(2)	22(1)
C(13)	12871(3)	4493(2)	-3841(2)	20(1)
C(14)	11859(3)	5069(2)	-4183(2)	18(1)
C(15)	10544(3)	4723(2)	-4067(2)	20(1)
C(16)	12585(3)	3579(2)	-3385(2)	21(1)
C(18)	12782(3)	5974(2)	-5395(2)	18(1)
C(19)	13122(3)	4954(2)	-5788(2)	19(1)
C(20)	13766(3)	4915(2)	-6556(2)	19(1)
C(21)	14099(3)	5866(2)	-6955(2)	17(1)
C(22)	13760(3)	6884(2)	-6568(2)	18(1)
C(23)	13127(3)	6936(2)	-5809(2)	19(1)
C(26)	15803(3)	6505(2)	-8833(2)	19(1)
C(27)	15987(3)	5532(2)	-9259(2)	22(1)
C(28)	16685(3)	5516(3)	-10013(2)	26(1)
C(29)	17184(3)	6458(3)	-10353(2)	25(1)
C(30)	16969(3)	7430(3)	-9936(2)	26(1)
C(31)	16278(3)	7454(2)	-9180(2)	22(1)
C(32)	11146(3)	5611(3)	-1720(2)	30(1)
C(34)	9533(3)	4281(2)	-1479(2)	18(1)
C(35)	10097(3)	3801(2)	-882(2)	21(1)
C(36)	9557(3)	2883(2)	-512(2)	22(1)
C(37)	8478(3)	2452(2)	-733(2)	19(1)
C(38)	7924(3)	2938(2)	-1336(2)	20(1)
C(39)	8439(3)	3849(2)	-1705(2)	21(1)
C(40)	8050(3)	-2719(3)	-2501(2)	27(1)
C(42)	8686(3)	-1411(2)	-1700(2)	19(1)
C(43)	7394(3)	-791(2)	-1584(2)	22(1)
C(44)	7141(3)	161(2)	-1134(2)	23(1)
C(45)	8174(3)	497(2)	-816(2)	18(1)
C(46)	9481(3)	-124(2)	-945(2)	20(1)
C(47)	9741(3)	-1070(2)	-1382(2)	20(1)
C(49)	7256(3)	1517(2)	392(2)	17(1)
C(50)	6881(3)	2515(2)	810(2)	21(1)
C(51)	6232(3)	2519(2)	1567(2)	20(1)

C(52)	5927(3)	1545(2)	1949(2)	19(1)
C(53)	6286(3)	549(2)	1539(2)	19(1)
C(54)	6929(3)	535(2)	780(2)	20(1)
C(57)	4274(3)	852(2)	3824(2)	19(1)
C(58)	3837(3)	1859(3)	4209(2)	26(1)
C(59)	3099(3)	1865(3)	4952(2)	27(1)
C(60)	2783(3)	891(3)	5324(2)	25(1)
C(61)	3233(3)	-109(3)	4945(2)	24(1)
C(62)	3980(3)	-127(2)	4196(2)	20(1)
N(17)	12138(3)	6039(2)	-4633(1)	20(1)
N(24)	14790(2)	5737(2)	-7730(1)	18(1)
N(25)	15129(2)	6619(2)	-8049(1)	19(1)
N(48)	7933(3)	1495(2)	-366(1)	20(1)
N(55)	5242(2)	1645(2)	2725(1)	19(1)
N(56)	5004(3)	736(2)	3047(1)	20(1)
O(2)	10082(2)	10073(2)	-3155(1)	24(1)
O(10)	10895(2)	2331(2)	-2868(1)	25(1)
O(33)	9968(2)	5179(2)	-1885(1)	25(1)
O(41)	9049(2)	-2370(2)	-2112(1)	24(1)

Table B2. Intramolecular Bond Distances (Å) for *p*AA-Ph-N=N-Ph

C(11)-C(12)	1.399(4)
C(11)-C(16)	1.387(4)
C(12)-C(15)	1.374(4)
C(14)-C(13)	1.385(4)
C(14)-C(15)	1.393(4)
C(16)-C(13)	1.391(4)
C(18)-C(19)	1.412(4)
C(18)-C(23)	1.415(4)
C(18)-N(17)	1.381(4)
C(20)-C(19)	1.389(4)
C(21)-C(20)	1.389(4)
C(21)-C(22)	1.405(4)
C(23)-C(22)	1.373(4)
C(26)-C(27)	1.398(4)
C(26)-C(31)	1.392(4)
C(28)-C(27)	1.383(4)
C(29)-C(28)	1.389(4)
C(29)-C(30)	1.386(4)
C(3)-C(8)	1.392(4)
C(31)-C(30)	1.384(4)
C(34)-C(35)	1.387(4)
C(34)-C(39)	1.396(4)
C(35)-C(36)	1.398(4)
C(37)-C(36)	1.377(4)
C(37)-C(38)	1.394(4)
C(39)-C(38)	1.381(4)
C(4)-C(3)	1.397(4)
C(4)-C(5)	1.376(4)
C(43)-C(42)	1.378(4)
C(43)-C(44)	1.396(4)
C(45)-C(44)	1.376(4)
C(45)-C(46)	1.390(4)
C(47)-C(42)	1.397(4)
C(47)-C(46)	1.377(4)

C(49)-C(50)	1.411(4)
C(49)-C(54)	1.412(4)
C(51)-C(50)	1.375(4)
C(52)-C(51)	1.394(4)
C(52)-C(53)	1.403(4)
C(53)-C(54)	1.374(4)
C(57)-C(58)	1.397(4)
C(57)-C(62)	1.389(4)
C(59)-C(58)	1.379(4)
C(6)-C(5)	1.394(4)
C(6)-C(7)	1.383(4)
C(60)-C(59)	1.388(4)
C(60)-C(61)	1.386(4)
C(62)-C(61)	1.390(4)
C(7)-C(8)	1.389(4)
N(17)-C(14)	1.440(4)
N(17)-C(6)	1.440(4)
N(24)-C(21)	1.417(4)
N(24)-N(25)	1.258(3)
N(25)-C(26)	1.425(4)
N(48)-C(37)	1.439(4)
N(48)-C(45)	1.444(4)
N(48)-C(49)	1.383(4)
N(55)-C(52)	1.414(4)
N(56)-C(57)	1.429(4)
O(10)-C(11)	1.358(3)
O(10)-C(9)	1.426(4)
O(2)-C(1)	1.423(4)
O(2)-C(3)	1.367(3)
O(33)-C(32)	1.425(4)
O(33)-C(34)	1.368(3)
O(41)-C(40)	1.430(3)
O(41)-C(42)	1.366(3)
N(55)-N(56)	1.266(3)

Table B3. Intramolecular Bond Angles (degrees) for *p*AA-Ph-N=N-Ph

C(11)-C(16)-C(13)	119.7(3)
C(11)-O(10)-C(9)	118.1(2)
C(12)-C(15)-C(14)	120.4(3)
C(13)-C(14)-C(15)	119.3(3)
C(13)-C(14)-N(17)	120.8(3)
C(14)-C(13)-C(16)	120.7(3)
C(14)-N(17)-C(6)	116.5(2)
C(15)-C(12)-C(11)	120.4(3)
C(15)-C(14)-N(17)	119.9(3)
C(16)-C(11)-C(12)	119.5(3)
C(18)-N(17)-C(14)	122.0(2)
C(18)-N(17)-C(6)	121.1(2)
C(19)-C(18)-C(23)	117.7(3)
C(19)-C(20)-C(21)	121.4(3)
C(20)-C(19)-C(18)	120.3(3)
C(20)-C(21)-C(22)	118.6(3)
C(20)-C(21)-N(24)	117.2(2)
C(22)-C(21)-N(24)	124.1(2)
C(22)-C(23)-C(18)	121.4(3)
C(23)-C(22)-C(21)	120.6(3)
C(27)-C(26)-N(25)	124.8(3)
C(27)-C(28)-C(29)	120.7(3)
C(28)-C(27)-C(26)	119.5(3)
C(3)-C(8)-C(7)	119.5(3)
C(3)-O(2)-C(1)	117.8(2)
C(30)-C(29)-C(28)	119.7(3)
C(30)-C(31)-C(26)	120.4(3)
C(31)-C(26)-C(27)	119.6(3)
C(31)-C(26)-N(25)	115.6(3)
C(31)-C(30)-C(29)	120.0(3)
C(34)-C(35)-C(36)	119.2(3)
C(34)-O(33)-C(32)	117.8(2)
C(35)-C(34)-C(39)	120.2(3)
C(36)-C(37)-C(38)	119.4(3)

C(36)-C(37)-N(48)	121.3(3)
C(37)-C(36)-C(35)	120.9(3)
C(37)-N(48)-C(45)	116.9(2)
C(38)-C(37)-N(48)	119.3(3)
C(38)-C(39)-C(34)	119.8(3)
C(39)-C(38)-C(37)	120.5(3)
C(4)-C(5)-C(6)	120.3(3)
C(42)-C(43)-C(44)	119.6(3)
C(42)-O(41)-C(40)	117.8(2)
C(43)-C(42)-C(47)	119.9(3)
C(44)-C(45)-C(46)	119.4(3)
C(44)-C(45)-N(48)	121.1(3)
C(45)-C(44)-C(43)	120.7(3)
C(46)-C(45)-N(48)	119.4(2)
C(46)-C(47)-C(42)	119.9(3)
C(47)-C(46)-C(45)	120.4(3)
C(49)-N(48)-C(37)	121.6(2)
C(49)-N(48)-C(45)	121.4(2)
C(5)-C(4)-C(3)	120.2(3)
C(5)-C(6)-N(17)	119.8(3)
C(50)-C(51)-C(52)	121.5(3)
C(51)-C(50)-C(49)	120.7(3)
C(51)-C(52)-C(53)	118.2(3)
C(51)-C(52)-N(55)	116.8(3)
C(53)-C(52)-N(55)	124.9(3)
C(53)-C(54)-C(49)	121.2(3)
C(54)-C(49)-C(50)	117.5(3)
C(54)-C(53)-C(52)	120.8(3)
C(58)-C(57)-N(56)	124.8(3)
C(58)-C(59)-C(60)	121.2(3)
C(59)-C(58)-C(57)	119.3(3)
C(59)-C(60)-C(61)	119.5(3)
C(6)-C(7)-C(8)	120.9(3)
C(61)-C(62)-C(57)	120.3(3)
C(62)-C(57)-C(58)	119.8(3)
C(62)-C(57)-N(56)	115.4(3)

C(62)-C(61)-C(60)	119.9(3)
C(7)-C(6)-C(5)	119.4(3)
C(7)-C(6)-N(17)	120.7(2)
C(8)-C(3)-C(4)	119.7(3)
N(17)-C(18)-C(19)	121.6(3)
N(17)-C(18)-C(23)	120.7(3)
N(24)-N(25)-C(26)	114.7(2)
N(25)-N(24)-C(21)	114.2(2)
N(48)-C(49)-C(50)	121.5(3)
N(48)-C(49)-C(54)	121.0(3)
N(55)-N(56)-C(57)	113.6(2)
N(56)-N(55)-C(52)	114.3(2)
O(10)-C(11)-C(12)	115.6(3)
O(10)-C(11)-C(16)	125.0(3)
O(2)-C(3)-C(4)	115.4(2)
O(2)-C(3)-C(8)	124.9(3)
O(33)-C(34)-C(35)	124.8(3)
O(33)-C(34)-C(39)	115.0(2)
O(41)-C(42)-C(43)	125.0(3)
O(41)-C(42)-C(47)	115.1(3)

APPENDIX C

X-RAY CRYSTALLOGRAPHY DATA FOR *p*AA-Ph-N=N-An **5a**

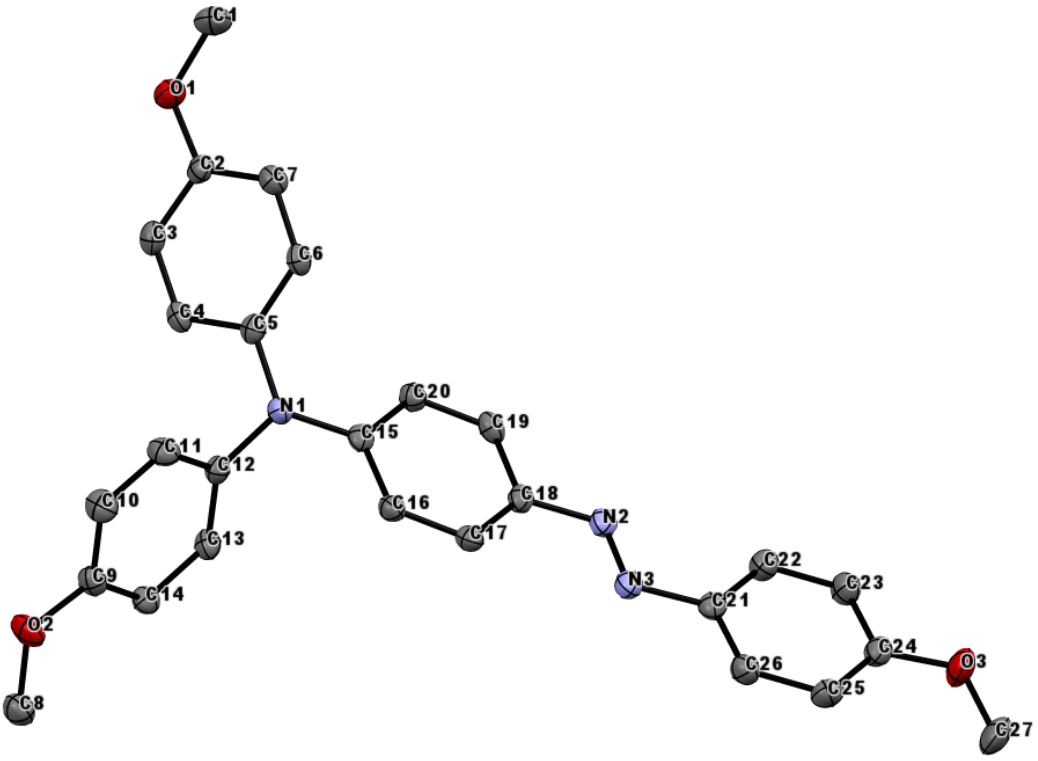

Table C1. Positional Parameters and U(eq) for *p*AA-Ph-N=N-An

atom	x	y	z	U(eq)
C(1)	2362(2)	4868(4)	115(1)	38(1)
C(2)	1919(1)	4429(3)	931(1)	22(1)
C(3)	1476(1)	3582(3)	1224(1)	24(1)
C(4)	1422(1)	3921(3)	1728(1)	22(1)
C(5)	1798(1)	5125(3)	1949(1)	20(1)
C(6)	2221(1)	5998(3)	1650(1)	22(1)
C(7)	2287(1)	5649(3)	1145(1)	23(1)
C(8)	-933(1)	4205(4)	3652(1)	31(1)
C(9)	-149(1)	5195(3)	3071(1)	23(1)
C(10)	-13(1)	6210(3)	2669(1)	27(1)
C(11)	604(1)	6314(3)	2482(1)	25(1)
C(12)	1100(1)	5380(3)	2683(1)	19(1)
C(13)	961(1)	4373(3)	3081(1)	22(1)
C(14)	343(1)	4274(3)	3277(1)	21(1)
C(15)	2281(1)	5542(3)	2782(1)	20(1)
C(16)	2224(1)	6301(3)	3250(1)	21(1)
C(17)	2734(1)	6388(3)	3573(1)	22(1)
C(18)	3334(1)	5719(3)	3441(1)	21(1)
C(19)	3398(1)	5002(3)	2975(1)	23(1)
C(20)	2883(1)	4905(3)	2647(1)	22(1)
C(21)	4395(1)	6707(3)	4434(1)	22(1)
C(22)	4996(1)	6062(3)	4297(1)	26(1)
C(23	5527(1)	6353(4)	4593(1)	29(1)
C(24)	5480(1)	7287(4)	5021(1)	26(1)
C(25)	4884(2)	7914(4)	5164(1)	28(1)
C(26)	4350(1)	7610(4)	4867(1)	27(1)
C(27)	6016(2)	8346(5)	5737(1)	42(1)
N(1)	1737(1)	5459(3)	2469(1)	21(1)
N(2)	3899(1)	5793(3)	3740(1)	23(1)
N(3)	3823(1)	6545(3)	4148(1)	24(1)
O(1)	1951(1)	3963(3)	440(1)	30(1)
O(2)	-781(1)	5164(3)	3226(1)	30(1)
O(3)	6045(1)	7519(3)	5274(1)	38(1)

Table C2. Intramolecular Bond Distances (Å) for *p*AA-Ph-N=N-An

C(11)-C(10)	1.373(4)
C(12)-C(11)	1.394(4)
C(13)-C(12)	1.383(4)
C(13)-C(14)	1.385(4)
C(14)-C(9)	1.386(4)
C(15)-C(16)	1.406(4)
C(15)-C(20)	1.400(4)
C(17)-C(16)	1.367(4)
C(18)-C(17)	1.406(4)
C(18)-C(19)	1.389(4)
C(2)-C(3)	1.396(4)
C(20)-C(19)	1.385(4)
C(21)-C(22)	1.403(4)
C(21)-C(26)	1.383(4)
C(23)-C(22)	1.376(4)
C(24)-C(23)	1.385(4)
C(24)-C(25)	1.391(4)
C(25)-C(26)	1.386(4)
C(4)-C(3)	1.382(4)
C(4)-C(5)	1.395(4)
C(6)-C(5)	1.390(4)
C(7)-C(2)	1.387(4)
C(7)-C(6)	1.389(4)
C(9)-C(10)	1.395(4)
N(1)-C(12)	1.440(3)
N(1)-C(5)	1.424(3)
N(2)-C(18)	1.417(3)
N(2)-N(3)	1.266(3)
N(3)-C(21)	1.415(4)
O(1)-C(1)	1.428(4)
O(1)-C(2)	1.372(3)
O(2)-C(8)	1.423(3)
O(2)-C(9)	1.374(3)
O(3)-C(24)	1.365(3)

O(3)-C(27)	1.417(4)
N(1)-C(15)	1.406(3)

Table C3. Intramolecular Bond Angles (degrees) for *p*AA-Ph-N=N-An

C(10)-C(11)-C(12)	120.6(3)
C(11)-C(10)-C(9)	120.5(3)
C(11)-C(12)-N(1)	119.7(2)
C(12)-C(13)-C(14)	121.3(3)
C(13)-C(12)-C(11)	118.6(2)
C(13)-C(12)-N(1)	121.6(2)
C(14)-C(9)-C(10)	119.3(3)
C(15)-N(1)-C(12)	119.9(2)
C(16)-C(15)-C(20)	118.3(2)
C(16)-C(17)-C(18)	120.2(3)
C(17)-C(16)-C(15)	121.5(3)
C(17)-C(18)-N(2)	124.8(2)
C(18)-C(19)-C(20)	121.4(3)
C(19)-C(18)-C(17)	118.6(2)
C(19)-C(18)-N(2)	116.5(2)
C(19)-C(20)-C(15)	120.0(3)
C(2)-C(3)-C(4)	120.0(3)
C(2)-C(7)-C(6)	119.9(3)
C(2)-O(1)-C(1)	117.7(2)
C(21)-C(26)-C(25)	121.8(3)
C(22)-C(23)-C(24)	121.1(3)
C(23)-C(22)-C(21)	119.5(3)
C(24)-C(25)-C(26)	118.8(3)
C(24)-O(3)-C(27)	117.7(2)
C(25)-C(24)-C(23)	120.0(3)
C(26)-C(21)-C(22)	118.9(3)
C(26)-C(21)-N(3)	116.7(2)
C(4)-C(5)-N(1)	120.2(2)
C(5)-C(4)-C(3)	120.9(3)

C(5)-C(6)-C(7)	121.0(2)
C(5)-N(1)-C(12)	117.5(2)
C(6)-C(5)-C(4)	118.5(3)
C(6)-C(5)-N(1)	121.2(2)
C(7)-C(2)-C(3)	119.6(3)
C(9)-C(14)-C(13)	119.7(3)
C(9)-O(2)-C(8)	117.5(2)
N(1)-C(15)-C(16)	119.1(2)
N(1)-C(15)-C(20)	122.7(2)
N(2)-N(3)-C(21)	114.2(2)
N(3)-C(21)-C(22)	124.4(3)
N(3)-N(2)-C(18)	114.0(2)
O(1)-C(2)-C(3)	115.5(2)
O(1)-C(2)-C(7)	125.0(3)
O(2)-C(9)-C(10)	115.9(2)
O(2)-C(9)-C(14)	124.8(3)
O(3)-C(24)-C(23)	115.3(3)
O(3)-C(24)-C(25)	124.8(3)
C(15)-N(1)-C(5)	121.4(2)

APPENDIX D

X-RAY CRYSTALLOGRAPHY DATA FOR *m*AA-Ph-N=N-An **19a**

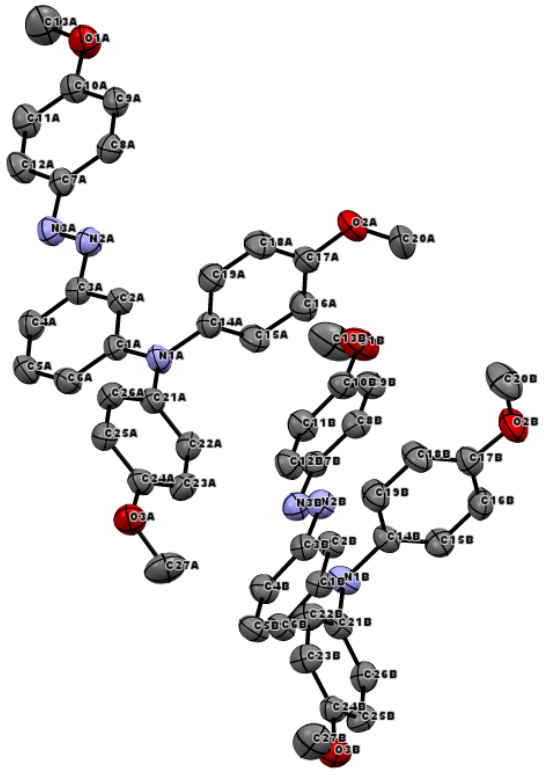

Table D1. Positional Parameters and U(eq) for *m*AA-Ph-N=N-An

atom	x	y	z	Ueq)
C(1A)	8191(3)	7492(2)	3251(2)	42(1)
C(1B)	3480(3)	2792(2)	3115(2)	41(1)
C(2A)	8217(3)	8236(2)	2817(2)	44(1)
C(2B)	3235(3)	3513(2)	2676(2)	43(1)
C(3A)	8585(3)	9090(2)	3244(2)	43(1)
C(3B)	3025(3)	4343(2)	3097(2)	41(1)
C(4A)	8941(3)	9237(2)	4110(2)	50(1)
C(4B)	3073(3)	4486(2)	3971(2)	50(1)
C(5A)	8949(3)	8507(2)	4537(2)	54(1)
C(5B)	3288(3)	3774(2)	4405(2)	53(1)
C(6A)	8584(3)	7643(2)	4122(2)	49(1)
C(6B)	3480(3)	2934(2)	3989(2)	47(1)
C(7A)	8918(3)	11212(2)	2535(2)	43(1)
C(7B)	2283(3)	6408(2)	2386(2)	41(1)
C(8A)	8541(3)	11046(2)	1661(2)	46(1)
C(8B)	2176(3)	6245(2)	1510(2)	46(1)
C(9A)	8578(3)	11743(2)	1196(2)	49(1)
C(9B)	1900(3)	6925(2)	1042(2)	50(1)
C(10A)	8978(3)	12615(2)	1591(2)	47(1)
C(10B)	1724(3)	7775(2)	1446(2)	48(1)
C(11A)	9366(3)	12784(2)	2452(2)	53(1)
C(11B)	1796(3)	7939(2)	2315(2)	54(1)
C(12A)	9336(3)	12077(2)	2913(2)	53(1)
C(12B)	2080(3)	7251(2)	2773(2)	51(1)
C(13A)	9380(4)	14162(2)	1434(2)	87(1)
C(13B)	1308(4)	9297(2)	1301(2)	94(1)
C(14A)	7301(3)	6510(2)	1925(2)	43(1)
C(14B)	3668(3)	1787(2)	1797(2)	43(1)
C(15A)	5929(3)	6539(2)	1626(2)	59(1)
C(15B)	2401(3)	1707(2)	1298(2)	53(1)
C(16A)	5477(3)	6405(2)	764(2)	60(1)
C(16B)	2313(3)	1515(2)	434(2)	56(1)
C(17A)	6420(3)	6245(2)	203(2)	50(1)
C(17B)	3502(3)	1379(2)	55(2)	48(1)
C(18A)	7809(3)	6244(2)	499(2)	58(1)
C(18B)	4773(3)	1456(2)	542(2)	60(1)
C(19A)	8243(3)	6370(2)	1358(2)	51(1)
C(19B)	4852(3)	1673(2)	1413(2)	58(1)
C(20A)	4642(4)	6021(2)	-982(2)	82(1)
C(20B)	4498(4)	1004(2)	-1223(2)	83(1)
C(21A)	7916(3)	5847(2)	3221(2)	43(1)
C(21B)	3826(3)	1189(2)	3137(2)	43(1)
C(22A)	6761(3)	5279(2)	3278(2)	49(1)

C(22B)	5067(3)	802(2)	3277(2)	51(1)
C(23A)	6885(3)	4513(2)	3659(2)	52(1)
C(23B)	5118(3)	24(2)	3643(2)	53(1)
C(24A)	8182(3)	4329(2)	4000(2)	45(1)
C(24B)	3919(3)	-363(2)	3878(2)	44(1)
C(25A)	9349(3)	4891(2)	3945(2)	48(1)
C(25B)	2683(3)	32(2)	3758(2)	50(1)
C(26A)	9214(3)	5641(2)	3554(2)	49(1)
C(26B)	2636(3)	794(2)	3386(2)	48(1)
C(27A)	7297(4)	3005(2)	4506(2)	81(1)
C(27B)	5059(3)	-1629(2)	4243(2)	78(1)
N(1A)	7758(2)	6640(1)	2822(1)	50(1)
N(1B)	3768(2)	1965(1)	2703(1)	48(1)
N(2A)	8568(2)	9769(2)	2706(1)	49(1)
N(2B)	2761(2)	5007(1)	2556(1)	47(1)
N(3A)	8930(2)	10540(2)	3079(1)	49(1)
N(3B)	2577(2)	5756(1)	2933(1)	48(1)
O(1A)	8967(2)	13255(1)	1071(1)	65(1)
O(1B)	1477(2)	8406(1)	928(1)	71(1)
O(2A)	6085(2)	6088(1)	-653(1)	71(1)
O(2B)	3307(2)	1170(1)	-807(1)	69(1)
O(3A)	8452(2)	3607(1)	4414(1)	62(1)
O(3B)	3846(2)	-1147(1)	4221(1)	58(1)

Table D2. Intramolecular Bond Distances (Å) for *m*AA-Ph-N=N-An

C(10A)-C(11A)	1.378(3)
C(10B)-C(11B)	1.379(3)
C(11A)-C(12A)	1.381(3)
C(11B)-C(12B)	1.380(3)
C(14A)-C(15A)	1.362(4)
C(14A)-C(19A)	1.366(3)
C(14B)-C(15B)	1.372(3)
C(14B)-C(19B)	1.370(3)
C(15A)-C(16A)	1.388(4)
C(15B)-C(16B)	1.374(3)
C(16A)-C(17A)	1.364(4)
C(16B)-C(17B)	1.374(4)
C(17A)-C(18A)	1.371(4)
C(17B)-C(18B)	1.367(4)
C(18A)-C(19A)	1.381(4)
C(18B)-C(19B)	1.388(3)
C(1A)-C(2A)	1.403(3)
C(1A)-C(6A)	1.393(3)
C(1B)-C(2B)	1.397(3)
C(1B)-C(6B)	1.394(3)
C(21A)-C(22A)	1.377(3)
C(21A)-C(26A)	1.378(3)
C(21B)-C(22B)	1.378(3)
C(21B)-C(26B)	1.381(3)
C(22A)-C(23A)	1.388(3)
C(22B)-C(23B)	1.387(3)
C(23A)-C(24A)	1.370(4)
C(23B)-C(24B)	1.375(3)
C(24A)-C(25A)	1.381(3)
C(24B)-C(25B)	1.377(3)
C(25A)-C(26A)	1.377(3)
C(25B)-C(26B)	1.370(3)
C(2A)-C(3A)	1.382(3)
C(2B)-C(3B)	1.383(3)
C(3A)-C(4A)	1.380(3)
C(3B)-C(4B)	1.389(3)
C(4A)-C(5A)	1.378(3)
C(4B)-C(5B)	1.374(3)
C(5A)-C(6A)	1.387(3)
C(5B)-C(6B)	1.389(3)
C(7A)-C(12A)	1.378(3)
C(7A)-C(8A)	1.396(3)
C(7B)-C(12B)	1.378(3)
C(7B)-C(8B)	1.388(3)

C(8A)-C(9A)	1.372(3)
C(8B)-C(9B)	1.377(3)
C(9A)-C(10A)	1.392(3)
C(9B)-C(10B)	1.391(3)
N(1A)-C(14A)	1.443(3)
N(1A)-C(1A)	1.390(3)
N(1A)-C(21A)	1.444(3)
N(1B)-C(14B)	1.438(3)
N(1B)-C(1B)	1.396(3)
N(1B)-C(21B)	1.446(3)
N(2A)-C(3A)	1.430(3)
N(2A)-N(3A)	1.244(3)
N(2B)-C(3B)	1.432(3)
N(2B)-N(3B)	1.245(3)
N(3A)-C(7A)	1.429(3)
N(3B)-C(7B)	1.432(3)
O(1A)-C(10A)	1.363(3)
O(1A)-C(13A)	1.426(3)
O(1B)-C(13B)	1.428(3)
O(2A)-C(17A)	1.363(3)
O(2A)-C(20A)	1.424(3)
O(2B)-C(17B)	1.370(3)
O(2B)-C(20B)	1.415(3)
O(3A)-C(24A)	1.379(3)
O(3A)-C(27A)	1.423(3)
O(3B)-C(24B)	1.373(3)
O(3B)-C(27B)	1.422(3)
O(1B)-C(10B)	1.366(3)

Table D3. Intramolecular Bond Angles (degrees) for *m*AA-Ph-N=N-An

C(10A)-C(11A)-C(12A)	118.9(3)
C(10A)-O(1A)-C(13A)	118.4(2)
C(10B)-C(11B)-C(12B)	118.7(3)
C(11A)-C(10A)-C(9A)	120.1(2)
C(11B)-C(10B)-C(9B)	120.4(2)
C(12A)-C(7A)-C(8A)	118.9(2)
C(12A)-C(7A)-N(3A)	116.4(2)
C(12B)-C(7B)-C(8B)	119.0(2)
C(12B)-C(7B)-N(3B)	116.2(2)
C(14A)-C(15A)-C(16A)	121.2(3)
C(14A)-C(19A)-C(18A)	120.7(3)
C(14A)-N(1A)-C(21A)	117.2(2)
C(14B)-C(15B)-C(16B)	121.1(3)
C(14B)-C(19B)-C(18B)	121.0(3)
C(14B)-N(1B)-C(21B)	115.8(2)
C(15A)-C(14A)-C(19A)	118.7(3)
C(15A)-C(14A)-N(1A)	120.8(3)
C(15B)-C(14B)-N(1B)	121.6(3)
C(16A)-C(17A)-C(18A)	119.4(3)
C(17A)-C(16A)-C(15A)	119.7(3)
C(17A)-C(18A)-C(19A)	120.3(3)
C(17A)-O(2A)-C(20A)	117.7(2)
C(17B)-C(16B)-C(15B)	120.0(3)
C(17B)-C(18B)-C(19B)	119.7(3)
C(17B)-O(2B)-C(20B)	117.9(2)
C(18B)-C(17B)-C(16B)	119.6(3)
C(18B)-C(17B)-O(2B)	124.4(3)
C(19A)-C(14A)-N(1A)	120.5(3)
C(19B)-C(14B)-C(15B)	118.4(3)
C(19B)-C(14B)-N(1B)	120.0(2)
C(1A)-N(1A)-C(14A)	120.5(2)
C(1A)-N(1A)-C(21A)	121.8(2)
C(1B)-N(1B)-C(14B)	121.2(2)
C(1B)-N(1B)-C(21B)	121.2(2)
C(21A)-C(22A)-C(23A)	121.4(3)
C(21B)-C(22B)-C(23B)	120.9(3)
C(22A)-C(21A)-C(26A)	118.5(2)
C(22A)-C(21A)-N(1A)	120.3(2)
C(22B)-C(21B)-C(26B)	118.5(2)
C(22B)-C(21B)-N(1B)	120.3(2)
C(23A)-C(24A)-C(25A)	120.0(2)
C(23A)-C(24A)-O(3A)	125.3(3)
C(23B)-C(24B)-C(25B)	119.6(2)
C(24A)-C(23A)-C(22A)	119.2(3)

C(24A)-O(3A)-C(27A)	117.8(2)
C(24B)-C(23B)-C(22B)	119.7(2)
C(24B)-O(3B)-C(27B)	116.9(2)
C(25A)-C(26A)-C(21A)	120.6(3)
C(25B)-C(26B)-C(21B)	120.9(3)
C(26A)-C(21A)-N(1A)	121.2(3)
C(26A)-C(25A)-C(24A)	120.2(3)
C(26B)-C(21B)-N(1B)	121.2(2)
C(26B)-C(25B)-C(24B)	120.4(3)
C(2A)-C(3A)-N(2A)	113.7(2)
C(2B)-C(3B)-C(4B)	120.8(2)
C(2B)-C(3B)-N(2B)	114.2(2)
C(3A)-C(2A)-C(1A)	120.9(2)
C(3B)-C(2B)-C(1B)	121.0(2)
C(4A)-C(3A)-C(2A)	121.0(2)
C(4A)-C(3A)-N(2A)	125.3(2)
C(4A)-C(5A)-C(6A)	121.7(3)
C(4B)-C(3B)-N(2B)	125.0(2)
C(4B)-C(5B)-C(6B)	121.4(3)
C(5A)-C(4A)-C(3A)	118.3(3)
C(5A)-C(6A)-C(1A)	120.3(2)
C(5B)-C(4B)-C(3B)	118.4(3)
C(5B)-C(6B)-C(1B)	120.5(2)
C(6A)-C(1A)-C(2A)	117.8(3)
C(6B)-C(1B)-C(2B)	117.8(2)
C(6B)-C(1B)-N(1B)	120.6(2)
C(7A)-C(12A)-C(11A)	121.7(3)
C(7B)-C(12B)-C(11B)	121.8(3)
C(8A)-C(7A)-N(3A)	124.6(2)
C(8A)-C(9A)-C(10A)	120.6(3)
C(8B)-C(7B)-N(3B)	124.7(2)
C(8B)-C(9B)-C(10B)	120.1(3)
C(9A)-C(8A)-C(7A)	119.7(3)
C(9B)-C(8B)-C(7B)	120.0(3)
N(1A)-C(1A)-C(2A)	120.5(2)
N(1A)-C(1A)-C(6A)	121.7(2)
N(1B)-C(1B)-C(2B)	121.6(2)
N(2A)-N(3A)-C(7A)	114.0(2)
N(2B)-N(3B)-C(7B)	113.9(2)
N(3A)-N(2A)-C(3A)	114.4(2)
N(3B)-N(2B)-C(3B)	114.4(2)
O(1A)-C(10A)-C(11A)	124.3(3)
O(1A)-C(10A)-C(9A)	115.6(3)
O(1B)-C(10B)-C(11B)	124.0(3)
O(1B)-C(10B)-C(9B)	115.6(3)
O(2A)-C(17A)-C(16A)	124.5(3)

O(2A)-C(17A)-C(18A)	116.1(3)
O(2B)-C(17B)-C(16B)	115.9(3)
O(3A)-C(24A)-C(25A)	114.7(2)
O(3B)-C(24B)-C(23B)	124.4(2)
O(3B)-C(24B)-C(25B)	116.0(3)
C(10B)-O(1B)-C(13B)	118.6(2)

APPENDIX E

X-RAY CRYSTALLOGRAPHY DATA FOR *m*AA-Ph-N=N-Ph **18a**

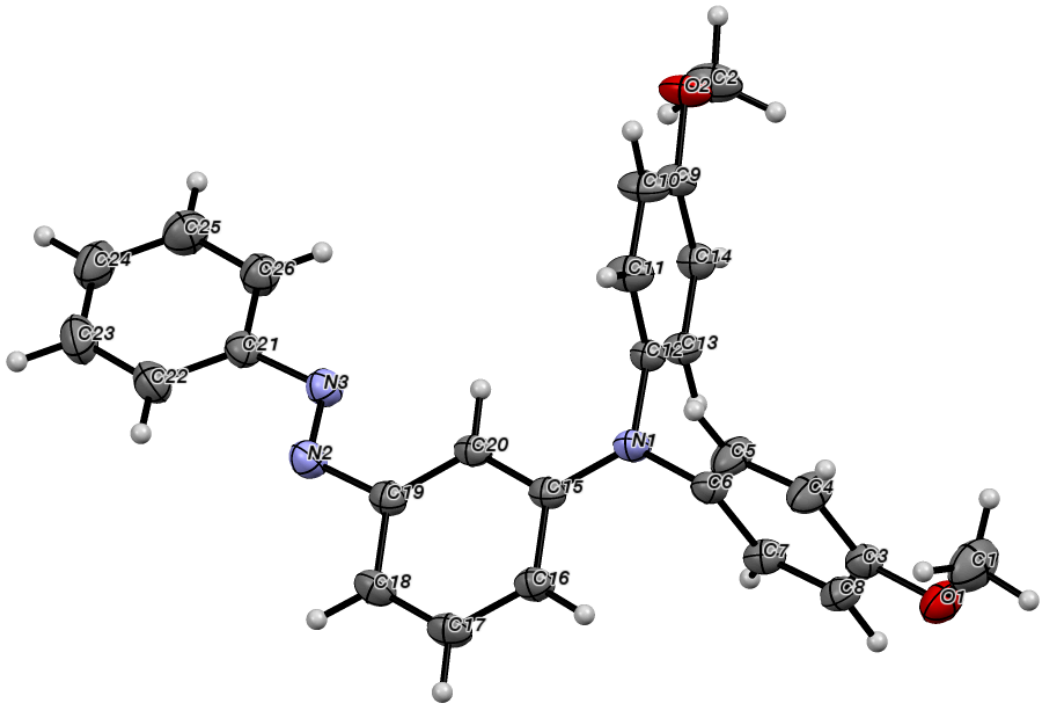

Table E1. Positional Parameters and U(eq) for *m*AA-Ph-N=N-Ph

atom	x	y	z	Ueq)
N(1)	800(1)	1933(1)	754(1)	29(1)
O(1)	3525(1)	216(1)	4468(1)	41(1)
C(1)	3177(2)	-923(2)	5166(2)	56(1)
O(2)	-5342(1)	4749(1)	1434(1)	40(1)
N(2)	966(1)	2497(1)	-3201(1)	33(1)
C(2)	-5792(2)	6261(2)	1442(2)	46(1)
N(3)	-327(1)	3315(1)	-3054(1)	30(1)
C(3)	2838(1)	557(1)	3563(1)	30(1)
C(4)	1927(2)	-202(2)	3228(1)	39(1)
C(5)	1295(2)	250(2)	2285(1)	37(1)
C(6)	1534(1)	1450(1)	1688(1)	27(1)
C(7)	2445(1)	2205(1)	2033(1)	30(1)
C(8)	3100(1)	1753(1)	2954(1)	31(1)
C(9)	-3816(1)	4130(1)	1293(1)	29(1)
C(10)	-3409(1)	2662(1)	1233(1)	38(1)
C(11)	-1896(1)	1940(1)	1054(1)	36(1)
C(12)	-771(1)	2675(1)	946(1)	26(1)
C(13)	-1188(1)	4131(1)	1037(1)	28(1)
C(14)	-2705(1)	4870(1)	1205(1)	29(1)
C(15)	1584(1)	1785(1)	-295(1)	25(1)
C(16)	3150(1)	1136(1)	-481(1)	29(1)

C(17)	3926(1)	961(1)	-1526(1)	34(1)
C(18)	3187(1)	1409(1)	-2418(1)	34(1)
C(19)	1645(1)	2068(1)	-2240(1)	28(1)
C(20)	840(1)	2263(1)	-1195(1)	26(1)
C(21)	-992(1)	3721(1)	-4025(1)	30(1)
C(22)	-344(2)	3173(2)	-5033(1)	39(1)
C(23)	-1091(2)	3635(2)	-5915(1)	47(1)
C(24)	-2463(2)	4634(2)	-5807(1)	47(1)
C(25)	-3104(2)	5187(2)	-4808(1)	46(1)
C(26)	-2369(2)	4724(2)	-3914(1)	37(1)

Table E2. Intramolecular Bond Distances (Å) for *m*AA-Ph-N=N-Ph

N(1)-C(15)	1.3884(15)
N(1)-C(6)	1.4320(15)
N(1)-C(12)	1.4349(14)
O(1)-C(3)	1.3645(15)
O(1)-C(1)	1.4234(19)
O(2)-C(9)	1.3700(14)
O(2)-C(2)	1.4282(17)
N(2)-N(3)	1.2480(14)
N(2)-C(19)	1.4298(16)
N(3)-C(21)	1.4316(16)
C(3)-C(4)	1.3894(18)
C(3)-C(8)	1.3902(18)
C(4)-C(5)	1.3908(19)
C(5)-C(6)	1.3808(18)
C(6)-C(7)	1.3927(16)
C(7)-C(8)	1.3769(18)
C(9)-C(14)	1.3854(16)
C(9)-C(10)	1.3913(18)
C(10)-C(11)	1.3840(18)
C(11)-C(12)	1.3913(17)
C(12)-C(13)	1.3845(16)
C(13)-C(14)	1.3908(16)

C(15)-C(20)	1.3997(17)
C(15)-C(16)	1.4096(15)
C(16)-C(17)	1.3834(18)
C(17)-C(18)	1.3851(19)
C(18)-C(19)	1.3920(17)
C(19)-C(20)	1.3932(17)
C(21)-C(26)	1.3852(18)
C(21)-C(22)	1.3913(18)
C(22)-C(23)	1.379(2)
C(23)-C(24)	1.380(2)
C(24)-C(25)	1.382(2)
C(25)-C(26)	1.387(2)

Table E3. Intramolecular Bond Angles (degrees) for *m*AA-Ph-N=N-Ph

C(15)-N(1)-C(6)	122.05(9)
C(15)-N(1)-C(12)	120.72(10)
C(6)-N(1)-C(12)	117.08(10)
C(3)-O(1)-C(1)	117.52(11)
C(9)-O(2)-C(2)	116.96(10)
N(3)-N(2)-C(19)	114.82(10)
N(2)-N(3)-C(21)	113.92(10)
O(1)-C(3)-C(4)	124.63(12)
O(1)-C(3)-C(8)	115.72(11)
C(4)-C(3)-C(8)	119.66(12)
C(3)-C(4)-C(5)	119.22(12)
C(6)-C(5)-C(4)	121.28(12)
C(5)-C(6)-C(7)	118.99(11)
C(5)-C(6)-N(1)	119.99(11)
C(7)-C(6)-N(1)	120.97(11)
C(8)-C(7)-C(6)	120.28(11)
C(7)-C(8)-C(3)	120.56(11)
O(2)-C(9)-C(14)	124.30(11)
O(2)-C(9)-C(10)	115.70(10)
C(14)-C(9)-C(10)	120.00(11)
C(11)-C(10)-C(9)	120.22(11)
C(10)-C(11)-C(12)	120.20(11)

C(13)-C(12)-C(11)	119.13(11)
C(13)-C(12)-N(1)	120.37(10)
C(11)-C(12)-N(1)	120.50(11)
C(12)-C(13)-C(14)	121.12(10)
C(9)-C(14)-C(13)	119.29(11)
N(1)-C(15)-C(20)	120.98(10)
N(1)-C(15)-C(16)	120.69(11)
C(20)-C(15)-C(16)	118.32(11)
C(17)-C(16)-C(15)	120.74(12)
C(16)-C(17)-C(18)	121.06(11)
C(17)-C(18)-C(19)	118.44(12)
C(18)-C(19)-C(20)	121.57(11)
C(18)-C(19)-N(2)	115.04(11)
C(20)-C(19)-N(2)	123.39(10)
C(19)-C(20)-C(15)	119.85(10)
C(26)-C(21)-C(22)	120.02(12)
C(26)-C(21)-N(3)	115.75(11)
C(22)-C(21)-N(3)	124.22(12)
C(23)-C(22)-C(21)	119.34(14)
C(22)-C(23)-C(24)	120.78(14)
C(23)-C(24)-C(25)	120.00(14)
C(24)-C(25)-C(26)	119.76(14)
C(21)-C(26)-C(25)	120.09(13)

APPENDIX F

X-RAY CRYSTALLOGRAPHY DATA FOR *p*AA-Ph-N=N-Ph-*p*AA

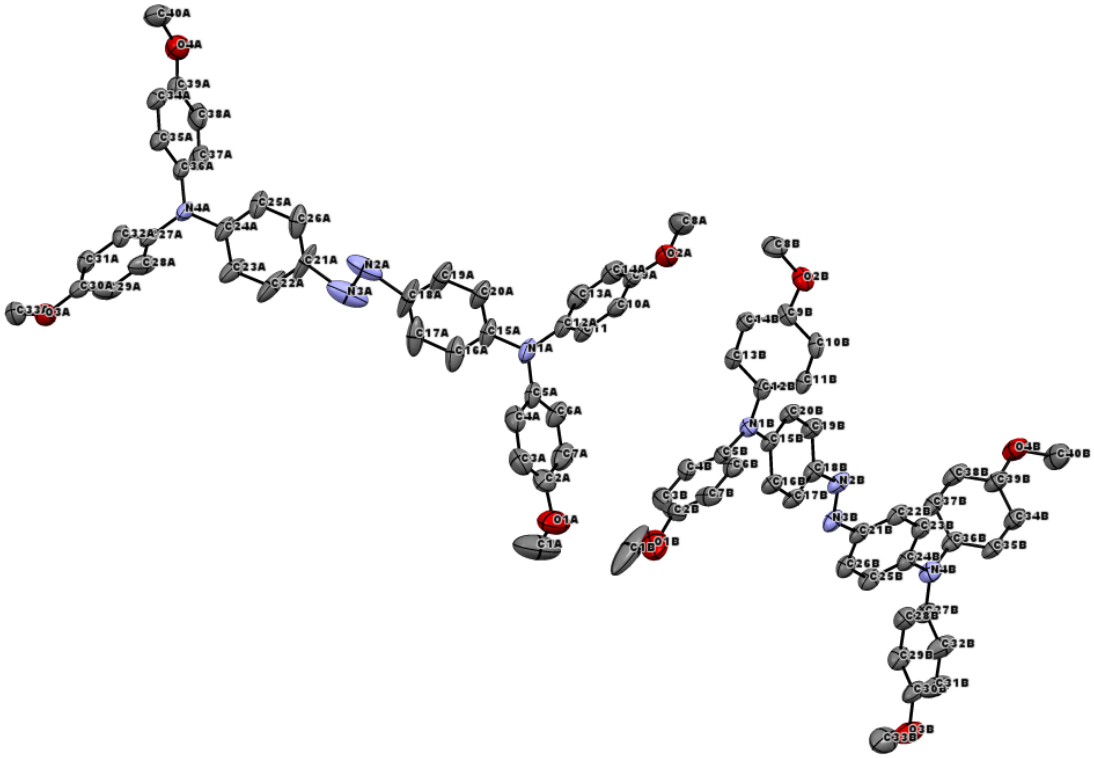

Table F1. Positional Parameters and U(eq) for *p*AA-Ph-N=N-Ph-*p*AA

atom	x	y	z	U(eq)
C(1A)	4630(3)	9286(8)	-599(2)	155(3)
C(1B)	6933(5)	8433(6)	1640(2)	197(5)
C(2A)	3497(2)	8927(5)	-600(1)	70(1)
C(2B)	6281(3)	9165(4)	1903(2)	84(2)
C(3A)	3609(2)	7609(5)	-462(1)	73(1)
C(3B)	5725(3)	9231(4)	1573(2)	82(2)
C(4A)	3081(2)	6863(4)	-391(1)	66(1)
C(4B)	5126(2)	9724(3)	1632(1)	58(1)
C(5A)	2446(2)	7396(3)	-460(1)	51(1)
C(5B)	5083(2)	10158(3)	2010(1)	41(1)
C(6A)	2341(2)	8702(4)	-599(1)	58(1)
C(6B)	5637(2)	10052(3)	2333(1)	47(1)
C(7A)	2853(2)	9479(4)	-674(1)	68(1)
C(7B)	6239(2)	9558(3)	2277(2)	64(1)
C(8A)	326(2)	8422(4)	952(1)	73(1)
C(8B)	3120(2)	7553(4)	3312(1)	66(1)
C(9A)	1187(2)	7794(3)	629(1)	48(1)
C(9B)	3644(2)	9264(3)	2996(1)	40(1)
C(10A)	1852(2)	7455(3)	674(1)	48(1)
C(10B)	3883(2)	10582(3)	3009(1)	47(1)
C(11)	2090(2)	7080(3)	347(1)	47(1)
C(11B)	4158(2)	11067(3)	2705(1)	43(1)
C(12A)	1660(2)	7025(3)	-36(1)	47(1)
C(12B)	4198(2)	10243(3)	2380(1)	37(1)
C(13A)	997(2)	7368(4)	-80(1)	58(1)
C(13B)	3971(2)	8917(3)	2377(1)	39(1)
C(14A)	759(2)	7748(4)	254(1)	58(1)
C(14B)	3696(2)	8422(3)	2680(1)	38(1)
C(15A)	1740(2)	5352(3)	-557(1)	56(1)
C(15B)	4256(2)	12002(3)	1877(1)	37(1)
C(16A)	1846(2)	5076(4)	-936(1)	78(1)
C(16B)	4685(2)	12806(3)	1712(1)	44(1)
C(17A)	1681(2)	3805(5)	-1111(1)	87(2)
C(17B)	4478(2)	14052(3)	1542(1)	43(1)
C(18A)	1419(2)	2798(4)	-914(2)	87(2)
C(18B)	3841(2)	14541(3)	1529(1)	43(1)
C(19A)	1307(2)	3094(4)	-546(2)	77(1)
C(19B)	3407(2)	13745(3)	1691(1)	45(1)
C(20A)	1459(2)	4334(3)	-367(1)	60(1)
C(20B)	3608(2)	12488(3)	1860(1)	42(1)
C(21A)	1059(2)	-282(4)	-1446(2)	83(2)
C(21B)	3716(2)	17739(3)	1028(1)	41(1)
C(22A)	1272(2)	-615(4)	-1785(1)	84(2)

C(22B)	3350(2)	18578(3)	1226(1)	44(1)
C(23A)	1114(2)	-1827(4)	-1972(1)	67(1)
C(23B)	3141(2)	19834(3)	1076(1)	44(1)
C(24A)	723(2)	-2773(3)	-1829(1)	55(1)
C(24B)	3282(2)	20311(3)	718(1)	44(1)
C(25A)	511(2)	-2446(3)	-1482(1)	58(1)
C(25B)	3666(2)	19493(3)	530(1)	48(1)
C(26A)	680(2)	-1219(4)	-1295(1)	68(1)
C(26B)	3891(2)	18231(3)	687(1)	48(1)
C(27A)	900(2)	-4543(3)	-2300(1)	52(1)
C(27B)	3358(2)	22304(3)	297(1)	45(1)
C(28A)	1582(2)	-4782(5)	-2168(1)	74(1)
C(28B)	3068(2)	22399(3)	-110(1)	52(1)
C(29A)	1940(2)	-5297(4)	-2428(1)	66(1)
C(29B)	3397(2)	23059(3)	-368(1)	54(1)
C(30A)	1625(2)	-5577(3)	-2822(1)	45(1)
C(30B)	4010(2)	23626(3)	-216(1)	55(1)
C(31A)	942(2)	-5336(3)	-2959(1)	45(1)
C(31B)	4295(2)	23578(4)	192(1)	78(1)
C(32A)	585(2)	-4815(3)	-2694(1)	47(1)
C(32B)	3974(2)	22916(4)	449(1)	71(1)
C(33A)	1707(2)	-6421(4)	-3463(1)	63(1)
C(33B)	4141(3)	24251(5)	-871(1)	97(2)
C(34A)	-853(2)	-6307(3)	-1922(1)	50(1)
C(34B)	1668(2)	23794(3)	740(1)	52(1)
C(35A)	-210(2)	-5829(3)	-1914(1)	50(1)
C(35B)	2292(2)	23346(3)	707(1)	48(1)
C(36A)	-118(2)	-4541(3)	-2040(1)	51(1)
C(36B)	2387(2)	22035(3)	588(1)	43(1)
C(37A)	-669(2)	-3725(4)	-2184(1)	67(1)
C(37B)	1835(2)	21166(3)	488(1)	50(1)
C(38A)	-1308(2)	-4168(4)	-2190(1)	69(1)
C(38B)	1215(2)	21611(3)	523(1)	54(1)
C(39A)	-1395(2)	-5457(4)	-2055(1)	52(1)
C(39B)	1126(2)	22918(3)	653(1)	51(1)
C(40A)	-2170(2)	-7107(5)	-1918(1)	76(1)
C(40B)	383(2)	24594(4)	806(2)	83(1)
N(1A)	1907(2)	6617(3)	-376(1)	58(1)
N(1B)	4472(1)	10749(2)	2060(1)	40(1)
N(2A)	1143(2)	1183(4)	-1050(1)	85(1)
N(2B)	3593(1)	15843(3)	1378(1)	47(1)
N(3A)	1350(2)	1315(5)	-1313(1)	101(2)
N(3B)	3943(1)	16411(3)	1159(1)	46(1)
N(4A)	538(2)	-4017(3)	-2023(1)	62(1)
N(4B)	3034(1)	21588(3)	562(1)	50(1)
O(1A)	3971(2)	9803(4)	-677(1)	103(1)

O(1B)	7076(3)	8661(4)	1964(2)	146(2)
O(2A)	1009(1)	8163(3)	980(1)	63(1)
O(2B)	3365(1)	8898(2)	3307(1)	57(1)
O(3A)	2022(1)	-6108(3)	-3055(1)	59(1)
O(3B)	4383(2)	24278(3)	-444(1)	80(1)
O(4A)	-2051(1)	-5807(3)	-2067(1)	70(1)
O(4B)	493(1)	23231(2)	693(1)	68(1)

Table F2. Intramolecular Bond Distances (Å) for *p*AA-Ph-N=N-Ph-*p*AA

C(10A)-C(11)	1.372(4)
C(10B)-C(11B)	1.378(4)
C(11)-C(12A)	1.387(5)
C(11B)-C(12B)	1.392(4)
C(12A)-C(13A)	1.375(5)
C(12A)-N(1A)	1.431(4)
C(12B)-C(13B)	1.383(4)
C(13A)-C(14A)	1.394(5)
C(13B)-C(14B)	1.381(4)
C(15A)-C(16A)	1.386(5)
C(15A)-C(20A)	1.391(5)
C(15A)-N(1A)	1.392(4)
C(15B)-C(16B)	1.400(4)
C(15B)-C(20B)	1.401(4)
C(16A)-C(17A)	1.391(6)
C(17A)-C(18A)	1.378(7)
C(17B)-C(16B)	1.376(4)
C(18A)-C(19A)	1.360(7)
C(18A)-N(2A)	1.711(6)
C(18B)-C(17B)	1.384(4)
C(18B)-C(19B)	1.397(4)
C(19A)-C(20A)	1.364(5)
C(20B)-C(19B)	1.382(4)
C(21A)-C(22A)	1.371(7)
C(21A)-C(26A)	1.383(6)
C(21A)-N(2A)	1.953(6)
C(21A)-N(3A)	1.701(6)
C(22A)-C(23A)	1.352(5)
C(22B)-C(21B)	1.395(4)
C(22B)-C(23B)	1.364(4)
C(23A)-C(24A)	1.392(5)
C(23B)-C(24B)	1.400(4)
C(24A)-C(25A)	1.393(5)
C(24A)-N(4A)	1.398(4)
C(25A)-C(26A)	1.369(5)
C(25B)-C(24B)	1.388(4)
C(26B)-C(21B)	1.385(4)
C(26B)-C(25B)	1.385(4)
C(27A)-C(28A)	1.382(5)
C(27A)-C(32A)	1.369(4)
C(27A)-N(4A)	1.432(4)
C(27B)-C(28B)	1.375(4)
C(27B)-C(32B)	1.381(5)
C(28A)-C(29A)	1.378(5)

C(28B)-C(29B)	1.391(5)
C(29A)-C(30A)	1.370(5)
C(29B)-C(30B)	1.359(5)
C(2A)-C(3A)	1.379(6)
C(2A)-C(7A)	1.394(6)
C(2A)-O(1A)	1.372(5)
C(2B)-C(3B)	1.396(7)
C(2B)-C(7B)	1.351(7)
C(2B)-O(1B)	1.670(7)
C(30A)-C(31A)	1.386(4)
C(30A)-O(3A)	1.370(4)
C(30B)-C(31B)	1.371(5)
C(31A)-C(32A)	1.393(4)
C(31B)-C(32B)	1.381(5)
C(33A)-O(3A)	1.418(4)
C(34A)-C(35A)	1.397(5)
C(34A)-C(39A)	1.377(5)
C(34B)-C(35B)	1.385(5)
C(34B)-C(39B)	1.381(4)
C(35A)-C(36A)	1.364(5)
C(35B)-C(36B)	1.379(4)
C(36A)-C(37A)	1.378(5)
C(36A)-N(4A)	1.431(4)
C(36B)-C(37B)	1.392(4)
C(37A)-C(38A)	1.377(5)
C(37B)-C(38B)	1.378(5)
C(38A)-C(39A)	1.374(5)
C(38B)-C(39B)	1.386(5)
C(39A)-O(4A)	1.380(4)
C(3A)-C(4A)	1.379(5)
C(3B)-C(4B)	1.382(6)
C(40A)-O(4A)	1.419(5)
C(4A)-C(5A)	1.371(5)
C(4B)-C(5B)	1.380(5)
C(5A)-C(6A)	1.367(5)
C(5A)-N(1A)	1.431(4)
C(5B)-C(6B)	1.382(5)
C(6A)-C(7A)	1.372(5)
C(6B)-C(7B)	1.384(5)
C(8A)-O(2A)	1.406(4)
C(9A)-C(10A)	1.378(5)
C(9A)-C(14A)	1.364(5)
C(9A)-O(2A)	1.381(4)
C(9B)-C(10B)	1.382(4)
C(9B)-C(14B)	1.383(4)
N(1B)-C(12B)	1.431(4)

N(1B)-C(15B)	1.403(4)
N(1B)-C(5B)	1.430(4)
N(2A)-N(3A)	1.088(4)
N(2B)-C(18B)	1.426(4)
N(2B)-N(3B)	1.282(4)
N(3B)-C(21B)	1.421(4)
N(4B)-C(24B)	1.409(4)
N(4B)-C(27B)	1.428(4)
N(4B)-C(36B)	1.424(4)
O(1B)-C(1B)	1.095(6)
O(2B)-C(8B)	1.415(4)
O(2B)-C(9B)	1.370(4)
O(3B)-C(30B)	1.377(4)
O(3B)-C(33B)	1.419(5)
O(4B)-C(39B)	1.373(4)
O(4B)-C(40B)	1.427(4)
C(1A)-O(1A)	1.408(7)

Table F3. Intramolecular Bond Angles (degrees) for *p*AA-Ph-N=N-Ph-*p*AA

C(10A)-C(11)-C(12A)	120.2(3)
C(10B)-C(11B)-C(12B)	120.7(3)
C(10B)-C(9B)-C(14B)	119.4(3)
C(11)-C(10A)-C(9A)	121.0(3)
C(11)-C(12A)-N(1A)	120.2(3)
C(11B)-C(12B)-N(1B)	121.0(3)
C(12A)-C(13A)-C(14A)	120.8(3)
C(12B)-N(1B)-C(5B)	118.0(2)
C(13A)-C(12A)-C(11)	118.7(3)
C(13A)-C(12A)-N(1A)	121.1(3)
C(13B)-C(12B)-C(11B)	118.0(3)
C(13B)-C(12B)-N(1B)	121.0(3)
C(13B)-C(14B)-C(9B)	119.7(3)
C(14A)-C(9A)-C(10A)	119.5(3)
C(14A)-C(9A)-O(2A)	125.0(3)
C(14B)-C(13B)-C(12B)	121.6(3)
C(15A)-C(16A)-C(17A)	119.9(4)
C(15A)-N(1A)-C(12A)	120.8(3)
C(15A)-N(1A)-C(5A)	120.6(3)
C(15B)-N(1B)-C(12B)	120.1(2)
C(15B)-N(1B)-C(5B)	119.7(2)
C(16A)-C(15A)-C(20A)	118.0(3)
C(16A)-C(15A)-N(1A)	120.6(4)
C(16B)-C(17B)-C(18B)	121.0(3)
C(17A)-C(18A)-N(2A)	132.6(5)
C(17B)-C(16B)-C(15B)	120.7(3)
C(17B)-C(18B)-C(19B)	118.8(3)
C(17B)-C(18B)-N(2B)	125.2(3)
C(18A)-C(17A)-C(16A)	121.2(4)
C(18A)-C(19A)-C(20A)	122.1(5)
C(18A)-N(2A)-C(21A)	147.0(4)
C(19A)-C(18A)-C(17A)	118.0(4)
C(19A)-C(18A)-N(2A)	109.2(4)
C(19A)-C(20A)-C(15A)	120.7(4)
C(19B)-C(18B)-N(2B)	115.9(3)
C(19B)-C(20B)-C(15B)	120.4(3)
C(1B)-O(1B)-C(2B)	85.5(8)
C(20A)-C(15A)-N(1A)	121.4(3)
C(20B)-C(15B)-C(16B)	118.4(3)
C(20B)-C(15B)-N(1B)	120.9(3)
C(20B)-C(19B)-C(18B)	120.6(3)
C(21B)-C(26B)-C(25B)	120.4(3)
C(22A)-C(21A)-C(26A)	118.6(3)
C(22A)-C(21A)-N(2A)	140.0(4)

C(22A)-C(21A)-N(3A)	106.4(4)
C(22A)-C(23A)-C(24A)	121.1(4)
C(22B)-C(21B)-N(3B)	124.4(3)
C(22B)-C(23B)-C(24B)	121.1(3)
C(23A)-C(22A)-C(21A)	121.2(4)
C(23A)-C(24A)-C(25A)	118.0(3)
C(23A)-C(24A)-N(4A)	122.1(3)
C(23B)-C(22B)-C(21B)	120.8(3)
C(23B)-C(24B)-N(4B)	119.7(3)
C(24A)-N(4A)-C(27A)	120.2(3)
C(24A)-N(4A)-C(36A)	118.6(3)
C(24B)-N(4B)-C(27B)	119.8(3)
C(24B)-N(4B)-C(36B)	120.5(3)
C(25A)-C(24A)-N(4A)	119.9(3)
C(25A)-C(26A)-C(21A)	121.1(4)
C(25B)-C(24B)-C(23B)	118.0(3)
C(25B)-C(24B)-N(4B)	122.3(3)
C(26A)-C(21A)-N(2A)	101.3(4)
C(26A)-C(21A)-N(3A)	135.0(5)
C(26A)-C(25A)-C(24A)	120.1(4)
C(26B)-C(21B)-C(22B)	118.7(3)
C(26B)-C(21B)-N(3B)	116.9(3)
C(26B)-C(25B)-C(24B)	121.0(3)
C(27A)-C(32A)-C(31A)	120.7(3)
C(27A)-N(4A)-C(36A)	118.6(3)
C(27B)-C(28B)-C(29B)	120.7(3)
C(27B)-C(32B)-C(31B)	120.1(3)
C(28A)-C(27A)-N(4A)	119.7(3)
C(28B)-C(27B)-C(32B)	118.8(3)
C(28B)-C(27B)-N(4B)	121.1(3)
C(29A)-C(28A)-C(27A)	120.7(3)
C(29A)-C(30A)-C(31A)	119.6(3)
C(29B)-C(30B)-C(31B)	120.0(3)
C(29B)-C(30B)-O(3B)	124.5(3)
C(2A)-O(1A)-C(1A)	115.6(4)
C(2B)-C(3B)-C(4B)	118.8(4)
C(2B)-C(7B)-C(6B)	119.7(4)
C(30A)-C(29A)-C(28A)	120.4(4)
C(30A)-C(31A)-C(32A)	119.6(3)
C(30A)-O(3A)-C(33A)	117.2(3)
C(30B)-C(29B)-C(28B)	119.8(3)
C(30B)-C(31B)-C(32B)	120.5(4)
C(30B)-O(3B)-C(33B)	117.9(3)
C(31B)-C(30B)-O(3B)	115.5(3)
C(32A)-C(27A)-C(28A)	119.1(3)
C(32A)-C(27A)-N(4A)	121.2(4)

C(32B)-C(27B)-N(4B)	120.1(3)
C(34A)-C(39A)-O(4A)	124.3(3)
C(34B)-C(39B)-C(38B)	118.9(3)
C(35A)-C(36A)-C(37A)	119.2(4)
C(35A)-C(36A)-N(4A)	121.5(4)
C(35B)-C(34B)-C(39B)	119.8(3)
C(35B)-C(36B)-C(37B)	118.7(3)
C(35B)-C(36B)-N(4B)	120.5(3)
C(36A)-C(35A)-C(34A)	120.5(4)
C(36A)-C(37A)-C(38A)	121.2(4)
C(36B)-C(35B)-C(34B)	121.4(3)
C(36B)-N(4B)-C(27B)	118.3(2)
C(37A)-C(36A)-N(4A)	119.3(3)
C(37B)-C(36B)-N(4B)	120.8(3)
C(37B)-C(38B)-C(39B)	121.3(3)
C(38A)-C(39A)-C(34A)	120.5(4)
C(38A)-C(39A)-O(4A)	115.2(3)
C(38B)-C(37B)-C(36B)	119.9(3)
C(39A)-C(34A)-C(35A)	119.2(3)
C(39A)-C(38A)-C(37A)	119.3(4)
C(39A)-O(4A)-C(40A)	117.7(3)
C(39B)-O(4B)-C(40B)	116.9(3)
C(3A)-C(2A)-C(7A)	119.9(4)
C(3B)-C(2B)-C(7B)	121.2(4)
C(3B)-C(2B)-O(1B)	134.1(5)
C(4A)-C(3A)-C(2A)	119.1(4)
C(4A)-C(5A)-C(6A)	118.8(4)
C(4A)-C(5A)-N(1A)	120.7(3)
C(4B)-C(5B)-C(6B)	119.6(3)
C(4B)-C(5B)-N(1B)	119.5(3)
C(5A)-C(4A)-C(3A)	121.5(4)
C(5A)-N(1A)-C(12A)	117.0(3)
C(5B)-C(4B)-C(3B)	120.3(4)
C(5B)-C(6B)-C(7B)	120.3(4)
C(6A)-C(5A)-N(1A)	120.5(4)
C(6A)-C(7A)-C(2A)	119.1(4)
C(6B)-C(5B)-N(1B)	120.8(3)
C(7A)-C(6A)-C(5A)	121.6(4)
C(7B)-C(2B)-O(1B)	104.6(5)
C(9A)-C(14A)-C(13A)	119.9(4)
C(9A)-O(2A)-C(8A)	117.4(3)
C(9B)-C(10B)-C(11B)	120.5(3)
C(9B)-O(2B)-C(8B)	118.0(3)
N(1B)-C(15B)-C(16B)	120.8(3)
N(2A)-N(3A)-C(21A)	85.9(4)
N(2B)-N(3B)-C(21B)	113.3(3)

N(3A)-C(21A)-N(2A)	33.77(16)
N(3A)-N(2A)-C(18A)	86.7(4)
N(3A)-N(2A)-C(21A)	60.3(4)
N(3B)-N(2B)-C(18B)	113.4(3)
O(1A)-C(2A)-C(7A)	114.2(4)
O(2A)-C(9A)-C(10A)	115.5(3)
O(2B)-C(9B)-C(10B)	115.7(3)
O(2B)-C(9B)-C(14B)	124.9(3)
O(3A)-C(30A)-C(29A)	115.9(3)
O(3A)-C(30A)-C(31A)	124.5(3)
O(4B)-C(39B)-C(34B)	124.9(3)
O(4B)-C(39B)-C(38B)	116.2(3)
O(1A)-C(2A)-C(3A)	125.9(5)

APPENDIX G

X-RAY CRYSTALLOGRAPHY DATA FOR TRIS(AZOBENZENE) DERIVATIVE

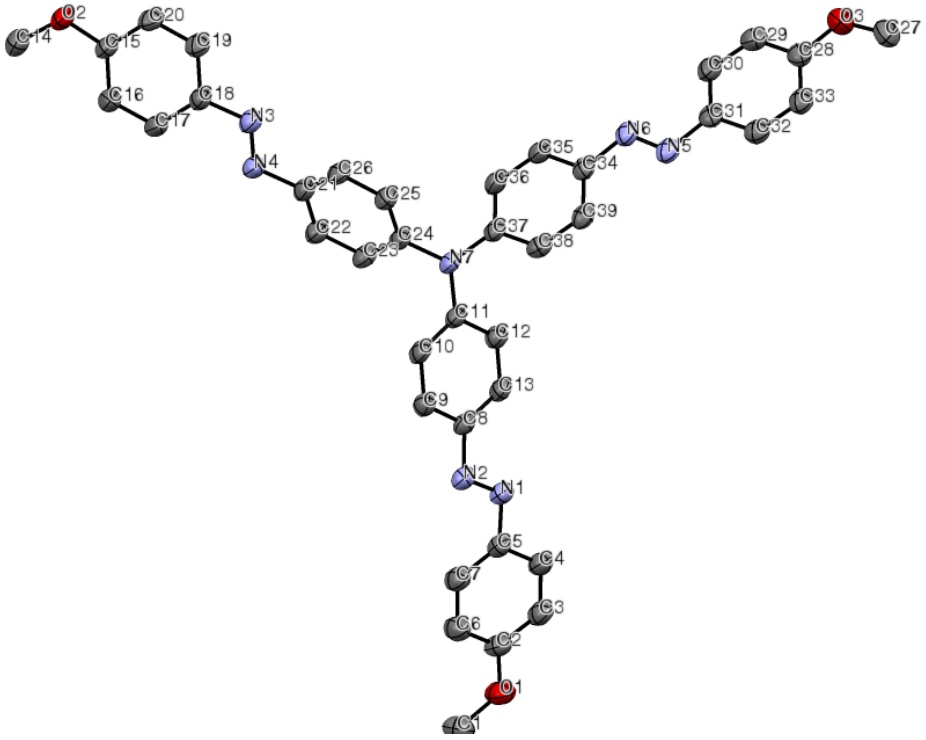

Table G1. Positional Parameters and U(eq) for Tris(azobenzene) derivative

atom	x	y	z	U(eq)
N(7)	8760(1)	5905(1)	2318(1)	40(1)
O(2)	2304(1)	946(1)	-731(1)	48(1)
N(6)	10512(2)	10353(1)	1741(1)	42(1)
N(1)	12156(2)	3943(1)	4099(1)	41(1)
O(1)	14958(1)	1128(2)	5436(1)	61(1)
O(3)	12826(2)	15339(1)	1401(1)	65(1)
N(2)	10998(2)	3678(1)	3962(1)	40(1)
N(5)	10804(2)	11139(1)	2043(1)	42(1)
N(4)	5812(2)	3047(1)	977(1)	42(1)
N(3)	5154(2)	3603(2)	654(1)	44(1)
C(8)	10458(2)	4334(2)	3564(1)	35(1)
C(12)	10608(2)	5635(2)	2915(1)	39(1)
C(24)	7987(2)	5178(2)	1987(1)	37(1)
C(36)	9392(2)	7254(2)	1721(1)	43(1)
C(34)	10055(2)	9263(2)	1916(1)	37(1)
C(37)	9187(2)	7033(2)	2180(1)	36(1)
C(11)	9323(2)	5401(2)	2747(1)	36(1)
C(10)	8604(2)	4651(2)	2999(1)	42(1)
C(5)	12765(2)	3214(2)	4463(1)	40(1)
C(26)	6172(2)	4997(2)	1389(1)	43(1)
C(38)	9415(2)	7954(2)	2505(1)	38(1)

C(39)	9844(2)	9051(2)	2376(1)	39(1)
C(15)	3019(2)	1513(2)	-371(1)	39(1)
C(2)	14168(2)	1797(2)	5128(1)	46(1)
C(21)	6509(2)	3816(2)	1313(1)	40(1)
C(31)	11308(2)	12203(2)	1863(1)	39(1)
C(28)	12340(2)	14327(2)	1580(1)	47(1)
C(13)	11171(2)	5106(2)	3318(1)	40(1)
C(19)	3909(2)	3384(2)	-89(1)	45(1)
C(18)	4429(2)	2844(2)	323(1)	39(1)
C(30)	11534(2)	12354(2)	1399(1)	49(1)
C(32)	11624(2)	13115(2)	2177(1)	44(1)
C(33)	12123(2)	14186(2)	2038(1)	45(1)
C(22)	7556(2)	3319(2)	1586(1)	43(1)
C(25)	6899(2)	5669(2)	1727(1)	43(1)
C(35)	9816(2)	8356(2)	1594(1)	43(1)
C(9)	9172(2)	4116(2)	3403(1)	40(1)
C(23)	8305(2)	3998(2)	1916(1)	42(1)
C(3)	14746(2)	2788(2)	4950(1)	48(1)
C(7)	12189(2)	2238(2)	4648(1)	50(1)
C(17)	4226(2)	1639(2)	385(1)	52(1)
C(29)	12058(2)	13405(2)	1261(1)	53(1)
C(20)	3214(2)	2726(2)	-434(1)	45(1)
C(27)	13040(3)	16335(2)	1697(1)	67(1)

C(4)	14044(2)	3486(2)	4619(1)	46(1)
C(16)	3535(2)	970(2)	38(1)	52(1)
C(6)	12886(2)	1536(2)	4982(1)	53(1)
C(14)	2187(2)	-315(2)	-715(1)	63(1)
C(1)	14419(2)	115(2)	5640(1)	62(1)

Table G2. Intramolecular Bond Distances (Å) for *Tris(azobenzene) derivative*

N(7)-C(37)	1.412(2)
N(7)-C(11)	1.424(2)
N(7)-C(24)	1.428(2)
O(2)-C(15)	1.361(2)
O(2)-C(14)	1.419(2)
N(6)-N(5)	1.252(2)
N(6)-C(34)	1.424(2)
N(1)-N(2)	1.255(2)
N(1)-C(5)	1.420(2)
O(1)-C(2)	1.362(2)
O(1)-C(1)	1.424(3)
O(3)-C(28)	1.367(2)
O(3)-C(27)	1.408(3)
N(2)-C(8)	1.424(2)
N(5)-C(31)	1.426(2)
N(4)-N(3)	1.255(2)
N(4)-C(21)	1.430(2)
N(3)-C(18)	1.426(2)
C(8)-C(9)	1.381(3)
C(8)-C(13)	1.387(3)
C(12)-C(13)	1.373(3)
C(12)-C(11)	1.389(2)

C(24)-C(23)	1.384(3)
C(24)-C(25)	1.392(3)
C(36)-C(35)	1.375(3)
C(36)-C(37)	1.392(3)
C(34)-C(35)	1.380(3)
C(34)-C(39)	1.395(3)
C(37)-C(38)	1.395(2)
C(11)-C(10)	1.386(3)
C(10)-C(9)	1.382(3)
C(5)-C(4)	1.383(3)
C(5)-C(7)	1.384(3)
C(26)-C(25)	1.384(3)
C(26)-C(21)	1.392(3)
C(38)-C(39)	1.373(3)
C(15)-C(16)	1.380(3)
C(15)-C(20)	1.389(3)
C(2)-C(6)	1.378(3)
C(2)-C(3)	1.389(3)
C(21)-C(22)	1.380(3)
C(31)-C(32)	1.380(3)
C(31)-C(30)	1.399(3)
C(28)-C(33)	1.379(3)
C(28)-C(29)	1.392(3)

C(19)-C(20)	1.374(3)
C(19)-C(18)	1.385(3)
C(18)-C(17)	1.382(3)
C(30)-C(29)	1.375(3)
C(32)-C(33)	1.385(3)
C(22)-C(23)	1.385(3)
C(3)-C(4)	1.374(3)
C(7)-C(6)	1.381(3)
C(17)-C(16)	1.381(3)

Table G3. Intramolecular Bond Angles (degrees) for Tris(azobenzene) derivative

C(37)-N(7)-C(11)	119.35(14)
C(37)-N(7)-C(24)	119.46(15)
C(11)-N(7)-C(24)	119.83(15)
C(15)-O(2)-C(14)	118.72(16)
N(5)-N(6)-C(34)	114.77(16)
N(2)-N(1)-C(5)	114.96(16)
C(2)-O(1)-C(1)	118.39(17)
C(28)-O(3)-C(27)	117.71(18)
N(1)-N(2)-C(8)	113.71(16)
N(6)-N(5)-C(31)	113.65(16)
N(3)-N(4)-C(21)	113.21(16)
N(4)-N(3)-C(18)	113.67(16)
C(9)-C(8)-C(13)	119.43(17)
C(9)-C(8)-N(2)	116.82(17)
C(13)-C(8)-N(2)	123.61(16)
C(13)-C(12)-C(11)	120.59(18)
C(23)-C(24)-C(25)	119.32(17)
C(23)-C(24)-N(7)	121.27(16)
C(25)-C(24)-N(7)	119.41(17)
C(35)-C(36)-C(37)	120.35(18)
C(35)-C(34)-C(39)	118.90(17)
C(35)-C(34)-N(6)	115.61(17)

C(39)-C(34)-N(6)	125.49(17)
C(36)-C(37)-C(38)	118.46(17)
C(36)-C(37)-N(7)	121.10(16)
C(38)-C(37)-N(7)	120.44(16)
C(12)-C(11)-C(10)	118.96(17)
C(12)-C(11)-N(7)	120.49(17)
C(10)-C(11)-N(7)	120.54(16)
C(9)-C(10)-C(11)	120.40(17)
C(4)-C(5)-C(7)	119.27(18)
C(4)-C(5)-N(1)	116.13(18)
C(7)-C(5)-N(1)	124.53(17)
C(25)-C(26)-C(21)	120.04(18)
C(39)-C(38)-C(37)	120.98(18)
C(38)-C(39)-C(34)	120.16(17)
O(2)-C(15)-C(16)	124.75(18)
O(2)-C(15)-C(20)	115.50(17)
C(16)-C(15)-C(20)	119.75(17)
O(1)-C(2)-C(6)	124.50(19)
O(1)-C(2)-C(3)	115.49(18)
C(6)-C(2)-C(3)	119.99(19)
C(22)-C(21)-C(26)	119.35(17)
C(22)-C(21)-N(4)	116.39(17)
C(26)-C(21)-N(4)	124.22(17)

C(32)-C(31)-C(30)	119.15(18)
C(32)-C(31)-N(5)	116.53(17)
C(30)-C(31)-N(5)	124.28(18)
O(3)-C(28)-C(33)	124.65(19)
O(3)-C(28)-C(29)	115.04(19)
C(33)-C(28)-C(29)	120.30(19)
C(12)-C(13)-C(8)	120.30(17)
C(20)-C(19)-C(18)	120.39(19)
C(17)-C(18)-C(19)	119.27(18)
C(17)-C(18)-N(3)	124.86(18)
C(19)-C(18)-N(3)	115.87(17)
C(29)-C(30)-C(31)	119.83(19)
C(31)-C(32)-C(33)	121.26(19)
C(28)-C(33)-C(32)	119.13(19)
C(21)-C(22)-C(23)	120.65(19)
C(26)-C(25)-C(24)	120.35(19)
C(36)-C(35)-C(34)	121.14(18)
C(8)-C(9)-C(10)	120.28(18)
C(22)-C(23)-C(24)	120.19(18)
C(4)-C(3)-C(2)	119.72(19)
C(6)-C(7)-C(5)	120.41(19)
C(16)-C(17)-C(18)	120.64(19)
C(30)-C(29)-C(28)	120.3(2)

C(19)-C(20)-C(15)	120.12(18)
C(3)-C(4)-C(5)	120.7(2)
C(17)-C(16)-C(15)	119.81(19)
C(2)-C(6)-C(7)	119.9(2)